The deformations of thin nematic elastomer sheets

Thesis by
Paul Plucinsky

In Partial Fulfillment of the Requirements for the
degree of
Doctor of Philosophy

CALIFORNIA INSTITUTE OF TECHNOLOGY
Pasadena, California

2017
Defended May 10, 2017

Paul Plucinsky
ORCID: 0000-0003-2060-8657

ACKNOWLEDGEMENTS

Kaushik Bhattacharya. I can say a lot about Kaushik as a PhD advisor, but perhaps it is best not to overdo it. Academic and research qualities aside, I find Kaushik to be a genuinely good person, and especially a person who cares deeply for his responsibility as a mentor. I am so glad to have had the privilege to learn from him these past five years.

Kaushik's research group: Lincoln, Chun-Jen, Tori, Paul, Dingyi, Ying Shi, Jin, Kevin, Sharan, Noy, Swarnava, Stella, Vinamra, Xian, Sri, Cindy, Mauricio, Gal, Linkun, Zubaer, Pierluigi, Bharat, Andy, and Ha. Many of them have had to endure ongoing pesering in the form of questions from me during the Kaushik-Ravi group meetings over the years, but I have learned a great deal during these interactions. I hope they can say the same. I also want to acknowledge Jenni and Leslie (Kaushik's current and former assistant). They have proven very helpful over the years.

My thesis committee: Ravi Ravichandran, Sergio Pellegrino and Chiara Daraio. Ravi is perhaps the nicest and most approachable professor I have met during my time at Caltech. I really appreciate all his useful edits on drafts and presentations, especially this past year with applications, as well as his words of encouragement. Sergio has done excellent work on the wrinkling of membranes, and Chiara is now working on clever strategies for actuation. I am grateful for their comments and insights on this thesis, and I think we have much common ground for work in the future.

My collaborators. Marius Lemm for helping me pin down the mathematics of actuation; Pierluigi Cesana for the effective membrane theory for nematic elastomers; Jay Warren for seeing the potential in exploiting novel material behavior to suppress wrinkling in membranes; Tim White and Ben Kowalski for experiments on actuating nematic elastomers.

My friends. A shoutout to the "Ballers", the "Goat/Sheep/GIF" group, the "MCEers", and the "Pincones and Physicist" for all the good times.

My family. For their love and support, especially in the times it was most needed.

Funding. This research was supported by the NASA Space Technology Research Fellowship.

ABSTRACT

Thin structures exhibit a broad range of mechanical responses as the competition between stretching and bending in these structures can result in buckling and localized deformations like folding and tension wrinkling. Active materials also exhibit a broad range of mechanical responses as features that manifest themselves at the microscale in these materials result in mechanical couplings at the engineering scale (thermal/electrical/dissipative) and novel function (e.g., the shape memory effect and piezoelectricity in select metal alloys and the immense fracture toughness of hydrogels). Given this richness in behaviors, my research broadly aims to address the following questions: What happens when active materials are incorporated into thin structures? Do phenomena inherent to these materials compete with or enhance those inherent to thin structures? Does this interplay result in entirely new and unexpected phenomena? And can all this be exploited to design new functions in engineering systems?

In this thesis, we explore these questions in the context of a theoretical study of thin sheets of nematic liquid crystal elastomer. These materials are active rubbery solids made of cross-linked polymer chains that have liquid crystals either incorporated into the main chain or pendent from them. Their structure enables a coupling between the mechanical elasticity of the polymer network and the ordering of the liquid crystals, and this in turn results in fairly complex mechanical behavior including large spontaneous distortion due to temperature change, soft-elasticity and fine-scale microstructure.

We study thin sheets of nematic elastomer. First, we show that thin of sheets of a particular class of nematic elastomer can resist wrinkling when stretched. Second, we show that thin sheets of another class of nematic elastomer can be actuated into a multitude of complex shapes. In order to obtain these results, we systematically develop two dimensional theories for thin sheets starting from a well-accepted first principles theory for nematic elastomers. These characterize (i) the mechanical response due to instabilities such as structural wrinkling and fine-scale material microstructure, and (ii) thermal actuation of heterogeneously patterned sheets. For the latter, we show that the theory, which comes in the form of a two dimensional metric constraint, admits two broad classes of designable actuation in nonisometric origami and lifted surface. For the former, we show that taut and appreciably stressed sheets of nematic elastomer are capable of suppressing wrinkling by modifying the

expected state of stress through the formation of microstructure.

PUBLISHED CONTENT AND CONTRIBUTIONS

[1] Pierluigi Cesana, Paul Plucinsky, and Kaushik Bhattacharya. "Effective Behavior of Nematic Elastomer Membranes". In: *Archive for Rational Mechanics and Analysis* 218.2 (2015), pp. 863–905. ISSN: 1432-0673. DOI: 10.1007/s00205-015-0871-0. URL: http://dx.doi.org/10.1007/s00205-015-0871-0.
This work was a collaborative effort for which each author made substantial contributions to all aspects.

[2] Paul Plucinsky and Kaushik Bhattacharya. "Microstructure-enabled control of wrinkling in nematic elastomer sheets". In: *Journal of the Mechanics and Physics of Solids* 102 (2017), pp. 125–150. ISSN: 0022-5096. DOI: http://dx.doi.org/10.1016/j.jmps.2017.02.009. URL: http://www.sciencedirect.com/science/article/pii/S0022509616308572.
This work was a collaborative effort for which each author made substantial contributions to all aspects.

[3] Paul Plucinsky, Marius Lemm, and Kaushik Bhattacharya. "Actuation of thin nematic elastomer sheets with controlled heterogeneity". In: *arXiv preprint arXiv:1611.00729 (and to be submitted)* (2017).
This work was a collaborative effort for which each author made substantial contributions to all aspects.

[4] Paul Plucinsky, Marius Lemm, and Kaushik Bhattacharya. "Programming complex shapes in thin nematic elastomer and glass sheets". In: *Phys. Rev. E* 94 (1 July 2016), p. 010701. DOI: 10.1103/PhysRevE.94.010701. URL: http://link.aps.org/doi/10.1103/PhysRevE.94.010701.
This work was a collaborative effort for which each author made substantial contributions to all aspects.

TABLE OF CONTENTS

LIST OF ILLUSTRATIONS

LIST OF TABLES

Number *Page*

Chapter 1

INTRODUCTION

1.1 What is a nematic elastomer?

Nematic elastomers are rubbery solids made of cross-linked polymer chains that have nematic mesogens (rod-like liquid crystal molecules) either incorporated into the main chain or pendent from them. Their structure enables a coupling between the entropic (mechanical) elasticity of the polymer network and the ordering of the liquid crystals, and this in turn results in a fairly complex mechanical behavior and thermo-mechanical coupling (see Warner and Terentjev [105] for a comprehensive introduction and review).

The liquid crystals within the nematic elastomer have a temperature-dependent interaction. This underlies a host of phases of orientational and positional order within the solid (see, for instance, de Gennes and Prost [49]). At low temperatures, the rod-like liquid crystals tend to align themselves, giving rise to a local nematic orientational order described by a director (a unit vector on $\mathbb{R}^3$). As the temperature is increased, thermal fluctuations thwart the attempt to order, driving a nematic to isotropic transition in the solid whereby the liquid crystals become randomly oriented. Due to the intrinsic coupling of the liquid crystals to the soft polymer network, the solid distorts to accommodate this temperature driven transition—typically by a large spontaneous contraction along the director and expansion transverse to it. Mechanistically, one can idealize this coupling and local distortion as in the sketch in Figure 1.1(a). We note, though, the coupling is in the molecular structure (b).

Throughout this thesis, we refer to two phases of this material: the low temperature *nematic* phase and a high temperature *isotropic* phase. Other phases are possible. These include a cholesteric or twisted nematic phase—where the liquid crystal units posses a certain handedness in their shape or polarizability—and a smectic phase—where the liquid crystals posses positional ordering in addition to the orientational ordering akin to nematics [49, 105]. Our focus here is restricted to *nematic* elastomers (as opposed to smectic or cholesteric elastomers), and specifically the rich mechanical behavior and thermo-mechanical coupling in sheets of this material.

On this topic, there are, broadly speaking, two types of nematic elastomers: there

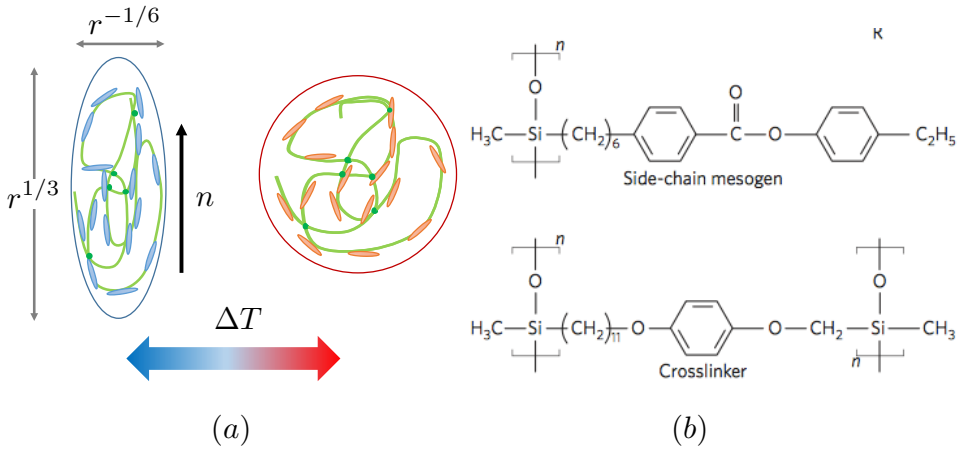

Figure 1.1: (a) At low temperatures, the rod-like liquid crystals are (on average) aligned, and this alignment is modeled by a director $n \in \mathbb{S}^2$. This influences the distribution of the long-chain polymers in the network, with the chains elongated along the director and contracted transverse to the director. At high temperatures, the alignment is suppressed and the long-chains have no preferential direction, and thus are spheroidal in shape on average. The transition from the nematic to the isotropic phase leads to a distortion of the network as depicted. One can model the preferred shape change induced by nematic alignment through an order parameter $r(T) \geq 1$. For $r(T) = 1$, the shape is spheroidal and the material is isotropic. However, on increasing $r(T)$, the preferred shape change is expansion along the director $r^{1/3}$ and contraction $r^{-1/6}$ transversely, as depicted. (b) The coupling is in the molecular structure: The liquid crystals (rods in (a)) are side-chain mesogens with a representative chemical formula given in the top figure in (b). These are connected to a polymer backbone, commonly polysiloxane. In nematic elastomers, the chains are lightly cross-linked (the green dots in (a)) with the cross-linkers as depicted in the bottom in (b). For more details on the chemistry, we refer to White and Broer [106].

are nematic elastomers cross-linked[1] in high-temperature isotropic phase, and there are those cross-linked in the low temperature nematic phase. The distinction is important. If the network is cross-linked in the nematic phase, then (at least heuristically) the cross-linkers couple to the polymer network in a way to accommodate that *particular* nematic orientation. This means the nematic orientation at the time of cross-linking is preferred over the rest even after deformation from this state, i.e, that the director has *memory* of its cross-linking orientation. On the other hand, nematic elastomers cross-linked in the isotropic phase have no preferential orientation for the director. That is, these nematic elastomers are ideally without memory, and

[1]Crosslinking describes the point at which the free-flowing chains are turned into a *solid* by, for instance, the introduction of crosslinking reagents to the melt. These induce a chemical reaction that forms cross-links to link the chains together; see Figure 1.1(b).

so the director is free to reorient with respect to coupled long chain polymer network upon deformation. This destinction will be reflected in the forthcoming modeling of these materials (discussed in detail in Chapter 2).

1.2 Examples of nematic elastomers

Nematic-elastic coupling is a key feature of these materials. The isotropic to nematic phase transformation is accompanied by a very significant distortion of the solid, which is coupled to the alignment of the director. Additionally, in some nematic elastomers the material is isotropic in the high temperature state, and so there is no preferential orientation for the director. In these materials, the director may rotate freely with respect to the material frame and the solid may form domains where the director varies spatially. Both these features manifest themselves in a very rich range of phenomena.

Monodomain samples and thermo-mechanical shape change

The earliest question pertaining to "nematic elastomers" was posed by de Gennes in 1969 [48]. He asked: if one cross-links conventional polymers into a network in the presence of a liquid crystalline solvent, do the intrinsically isotropic chains remember the nematic anisotropy upon solvent removal? The answer (for ideal chains) turns out to be NO! This *suggested* that dramatic shape change could be realized if one were able to synthesis a polymer with nematic order, and for which nematic order could be thwarted (by heating for example), as the chains ideally would not longer remember the ordering.

The first breakthrough in experimentally realizing dramatic thermo-mechanical shape change in nematic elastomers came in the early 90s, when Küpfer and Finkelmann [60] developed a technique to fabricate large samples of perfectly monodomain nematic elastomer[2]. (By monodomain, we mean that the director is uniform throughout the undeformed sample.)

An example of such a sheet is highlighted in Figure 1.2. Here, the monodomain nematic elastomer is supported from the top and a dark paper clip is appended to the bottom of the sample (simply to use gravity to keep it from curling up out-of-plane). Further, the director is aligned vertically throughout the sample when in the in the low

[2]Without careful control of the synthesis of nematic elastomers, large samples are always polydomain [105] (where there are several regions of different director alignment) and there are often topological defects (singularities in the director profile). From personal experience, heating a sheet of a polydomain sample results in an actuation akin to crumpling.

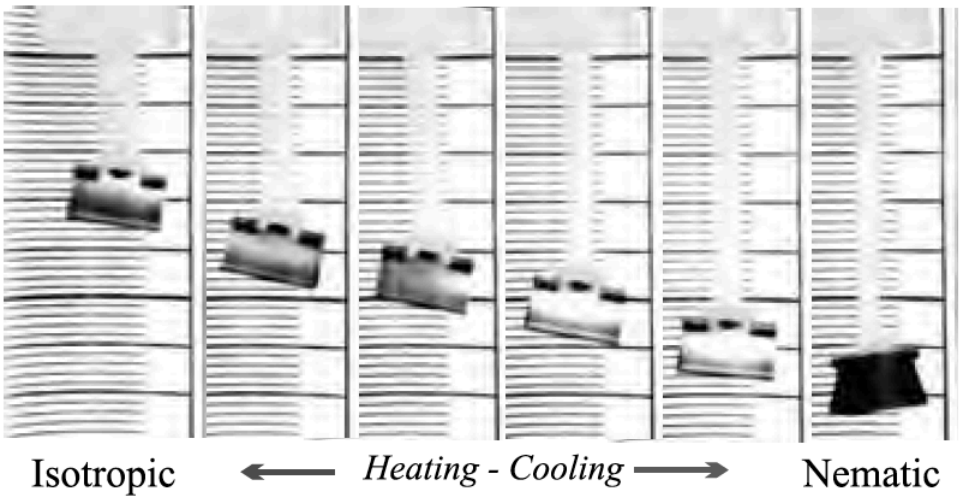

Figure 1.2: Shape change in a monodomain sample of nematic elastomer upon temperature change (figure reproduced from Warner and Terentjev [105]).

temperature nematic phase. Heating the sample results in large spontaneous shape change: the full sample contracts along the vertical direction—eventually to more than half of its original length—and expands uniformly transverse to this contraction (i.e., the sample widens upon heating). Note that the macroscopic behavior here is completely analogous to the local picture in Figure 1.1(a), where the nematic alignment of the liquid crystals is being thwarted upon heating, and this results in a distortion of the coupled long-chain network. Further, this macroscopic response is distinct from the thermo-mechanical behavior of conventional solids, where one expects volumetric expansion due to heating. Thus, the local microscopic physics of this monodomain nematic elastomer (i.e., a nematic-isotropic phase transition) is driving dramatic and novel macroscopic thermo-mechanical shape change.

Director reorientation and soft deformation

In some nematic elastomers (i.e., those cross-linked in the isotropic phase), the director may freely reorient with respect to the coupled long-chain network, with this reorientation typically accompanied by a distortion of the network. Thus macroscopically, this feature can lead to shape change absent any (or nearly any) stress; this is called *soft deformation*. In its simplest manifestation, this soft deformation and director reorientation is, perhaps, best captured by a series of experimental studies due to Urayama et al. [97, 98] (see also Urayama [96]).

We highlight this in Figure 1.3. Here, a thin swollen nematic gel is synthesized with a dielectrically positive nematic director aligned initially along the “x" direction in

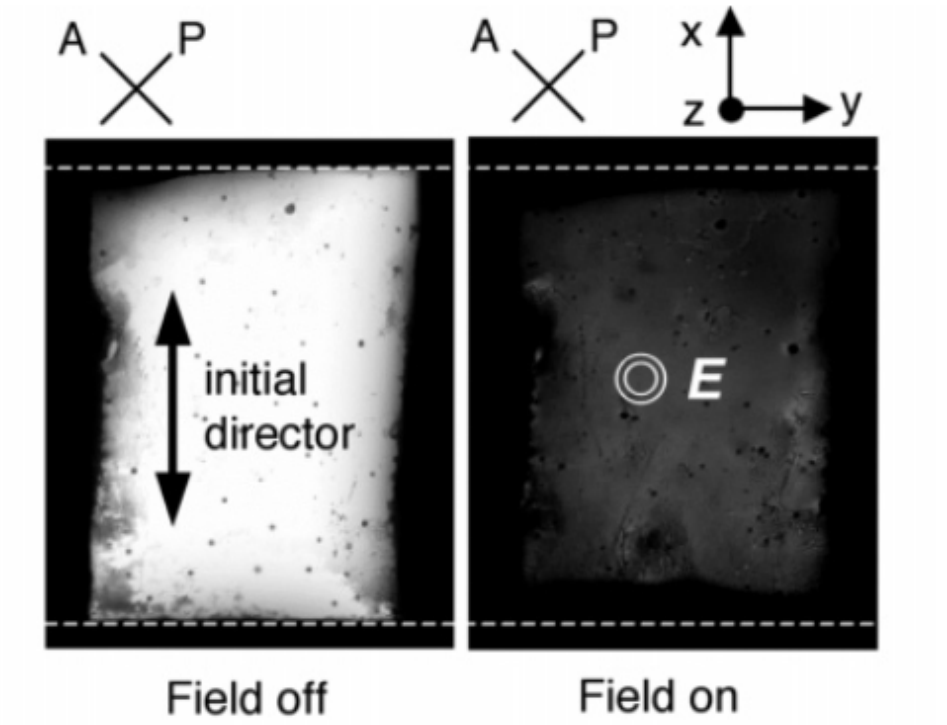

Figure 1.3: Swollen nematic gel subject to an electric field. The director reorients and this induces soft deformation (figure reproduced from Urayama [96]).

the figure. This director profile is illuminated under polarization as depicted. Upon application of an electric field in the “z" direction (out-of-plane), the polarization no longer illuminates the sample as the director reorients to align with the electric field through the thickness. The sample is unconstrained and free to deform to accommodate the director reorientation. And indeed, it contracts along the “x" direction with an engineering strain of roughly 10%, and without appreciable strain in the “y" direction. Note that the nematic anisotropy in applying the electric field is unchanged along the “y" direction, and so this observation regarding the deformation is exactly consistent with the notion that the director reorientation influences the macroscopic shape change.

Consequently, a nematic elastomer can finitely deform through director reorientation at little to no stress[3]. Hence, nematic elastomers can exhibit soft deformation.

[3]In this experiment, the only possible stress is related to application of the electric field, and this is certainly small when considering the relatively large strains observed.

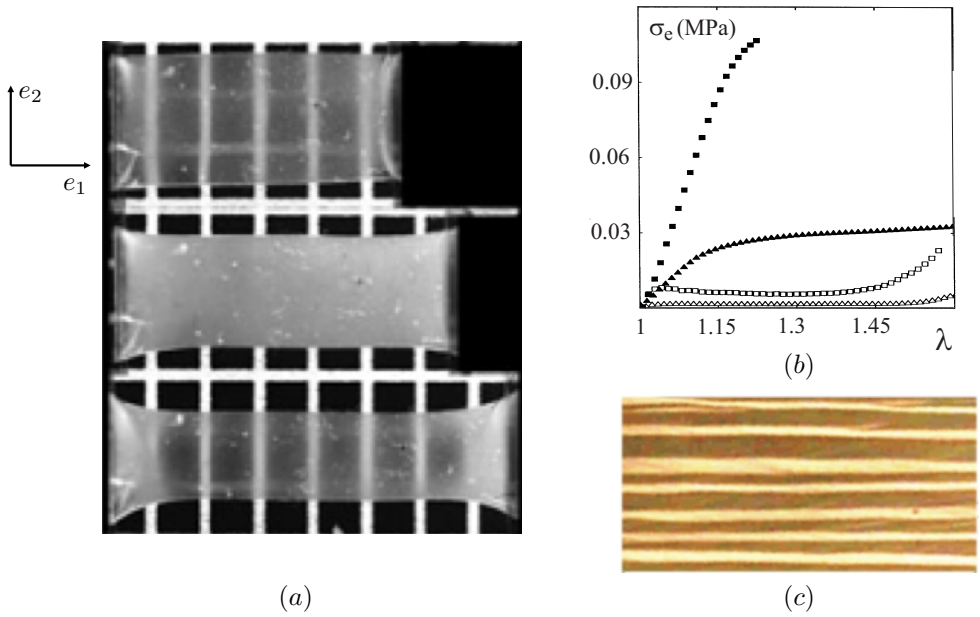

Figure 1.4: The clamped-stretch experiments of Kundler and Finkelmann [58] showing soft elasticity and fine scale microstructure, but no wrinkling. (a) Snapshots of the sheet. The nematic director is oriented vertically when undeformed (top), develops stripe domains of alternating rotated directors depicted in (c) for moderate deformation (middle) and eventually is uniform and oriented horizontally (bottom). (b) Stress-strain curves of Küpfer and Finkelmann [59] for elastomers of different preparation histories – the lowest curve is akin to the clamped-stretch sheet in part (a) and describes a sheet with significant soft elasticity. (c) Fine-scale strip domain microstructure. (These figures are reproduced from Warner and Terentjev [105].)

Soft elasticity and fine-scale material microstructure

So far, we have highlighted examples of nematic elastomers in which the microscopic picture was representative of the macroscopic picture. That is, the local shape change—corresponding to either the temperature driven nematic to isotropic phase transition or the electrically driven director reorientation—was identical to the observed macroscopic deformation of the monodomain nematic elastomer. This need not be the case.

Of particular note is the soft elasticity and fine scale microstructure (textured deformation or striped domains) observed in the clamped-stretch experiments of Kundler and Finkelmann [58]. Some of their key observations are reproduced in Figure 1.4. They begin with a thin rectangular sheet where the director is uniformly oriented tangential to the sheet but in the short direction (top of Figure 1.4(a)). The fact that the director is uniform is evident from the fact that the sheet is transparent.

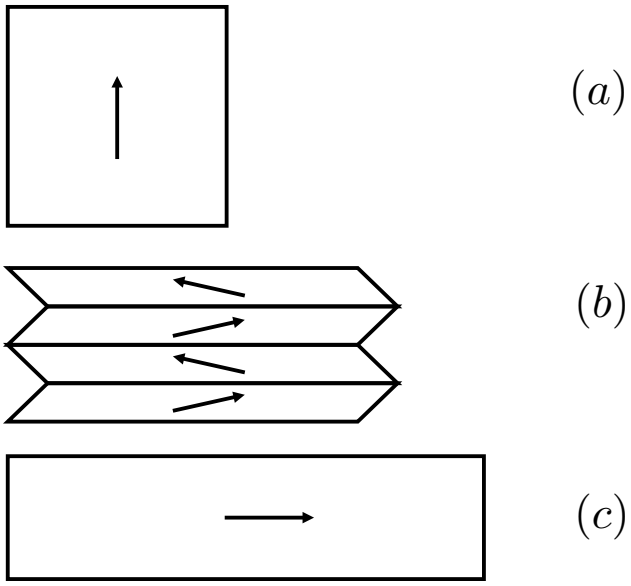

Figure 1.5: Consider a nematic elastomer in which the director is free to rotate through the material. (a) Here, the initial director aligns vertically in the sample, and the sample is stretched horizontally. (b)To avoid large shear, the director reorientation occurs in strip domain to accommodate the stretch. (c) Eventually (i.e., at large enough stretch), the director full rotates to the horizontal.

They clamp the short edges and pull it along the long edge. The nominal stretch vs. nominal stress behavior for this sheet is akin the bottom-most curve in Figure 1.4(b). Notice that nematic sheets display essentially zero stress for very significant values of stretch: this is known as the *soft elasticity*. The center and bottom images of Figure 1.4(a) capture stretch midway through the soft behavior and at the end of the soft behavior respectively. During the soft stage of stretch, the entire sheet is strongly scattering light and so visibly cloudy, an optical indication that the director is no longer uniform. Beyond the soft plateau (i.e., the bottom image), the sheet becomes transparent again in its central region, indicating uniform director arrangement in this region. However, it remains cloudy near the clamped edges.

The cloudy regions indicate material *microstructure* in the form of strip domains of oscillating director as shown in Figure 1.4(c). The heuristic is as follows (see also Figure 1.5): A nematic elastomer features a director that can rotate through the material, and this rotation is accommodated by spontaneous elongation along the director. Thus, the sheet can elongate along the direction of stretch with little stress by having its director rotate from vertical to horizontal. Doing so uniformly, however, results in a shear at intermediate orientations, but this shear can be avoided on average by breaking up the cross-section into domains where one half the directors

rotate one way (say through θ) while the other half rotates the other way (through $-\theta$). This is exactly what happens in the clamped stretched sheet at a very fine scale (microns), manifesting in stripe domains. Finally, when the director has fully rotated to the horizontal, it becomes uniform again (since the material is invariant under the change of sign of the director).

Hence, the mechanically induced director reorientation—which is spurred on by the unique microscopic physics of nematic elastomers—is driving textured deformation and material microstructure which enables a (semi-)soft macroscopic response to stretch. In particular, here the "effective" macroscopic behavior of the nematic elastomer is being driven by the microscopic physics, but in a way such that the picture changes dramatically going from the micro (the material microstructure in Figure 1.4(c)) to the macro (the clamped-stretched sheet in Figure 1.4(a)) .

What is the origin of this microstructure, and how does it precisely influence the macroscopic behavior of these elastomers? These questions are part of a major theme of this thesis.

Heterogeneously patterned thin sheets

We have seen, by example, some of the rich mechanical behavior and thermo-mechanical coupling exhibited by monodomain nematic elastomers. This begs the question: what new phenomena emerge when we go beyond the restrictions of a *monodomain*? For one[4], recent advances in the synthesis of sheets with controlled heterogeneities—where the director is programmed in a nonuniform but controlled manner throughout the sheet—have enabled their actuation into nontrivial shapes with unprecedented energy density.

Modes et al. [66, 67] predicted that if one could program azimuthal or radial heterogeneity in the anisotropy of a thin nematic glass sheet, then a uniform temperature change would actuate a conical or saddlelike three-dimensional shape. The first experimental realization of this came in nematic glass sheets with the work of de Haan et al. [51]; they programmed such heterogeneity in a thin nematic glass sheet,

[4]We are going to focus here on sheets with "controlled" heterogeneity. There are other examples beyond these and monodomain samples such as polydomain samples, where the sample is allowed to freely form many different domains of nematic anisotropy. Typically these domains have a characteristic mesoscopic length scale which is small compared to the overall sample, but large compared to length scale on which the anisotropy can be approximated by a director. Such samples can (if cross-linked in the isotropic phase) display soft elasticity akin to the monodomain sample in Figure 1.4. We refer the interested reader to Biggins et al. [17, 18] for the theoretical underpinning of this, and Urayama [99] for an experimental realization.

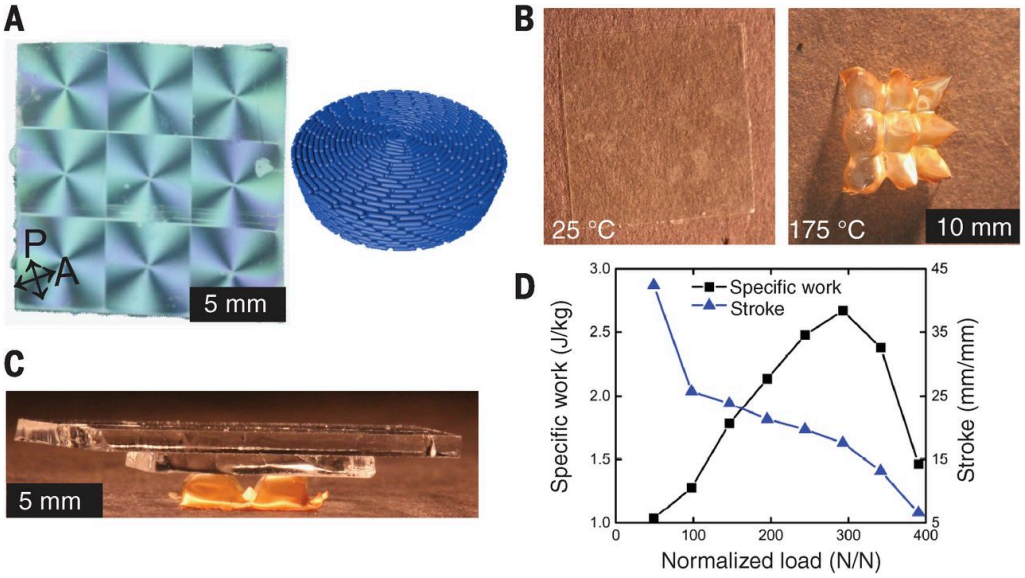

Figure 1.6: Programmed azimuthal heterogeneity in a nematic elastomer sheet “A". “B" Upon heating, the sheet actuates into a series of conical shapes “B". The actuated sheet can support in excess of 10 times its weight “C", and it has tremendous work density “D" . (This figure is reproduced from Ware et al. [102].)

and observed the predicted three-dimensional shape by thermal actuation. However, nematic *glass* is more densely cross-linked then nematic elastomer (recall Figure 1.1), and so the response of these sheets was muted in light of the small strains and high stiffness of glasses. More recently, Ware et al. [102] developed so-called *voxelated* nematic elastomers, and with these they were able to realize dramatic shape change upon heating a sample with azimuthal heterogeneity.

Some of their key results are reproduced in Figure 1.6. The sheet is programmed with nine unit cells each incorporating an azimuthal pattern around a central defect (i.e., where the direct field aligns parallel to the circumference of a circle whose center is at each of the defects as in the cartoon in “A"). Upon heating, each of the unit cells actuates into a conical shape. The heuristic is a follows: Recall that in the temperature-driven nematic to isotropic transformation (Figure 1.1(a)), the polymer network wants to contract along the director and expand transverse to this direction. Thus, consider one of the unit cells, and in particular, fix a radius r_0 from the defect of the cell and the corresponding circumference C_0 in the initially flat sheet. Since the radius is everywhere perpendicular to the director, it wants to expand under heating (i.e., $r_0 \mapsto r$ where $r > r_0$). Alternatively, since the circumference is everywhere parallel to the directer, it wants to contract under heating (i.e., $C_0 \mapsto C$ where $C < C_0$). The desired expansion and contraction in this setting is uniform,

and thus, the only configuration which can attain this state everywhere in the sample (up to a defect at each origin) is a cone. This is precisely what is observed in the actuation of this sample (i.e., “B" in the figure). Further, since the entire sheet is participating in the actuation, this soft elastomer is robust to added forcing as seen in “C", and it has an energy density (i.e.,“D" in the figure) comparable to some of the best actuator materials[5].

Hence, we see that azimuthal heterogeneity causes a *buckling* of the sheet to a cone upon thermal actuation. Beyond this, we note that in voxelated nematic elastomers (e.g., Ware et al. [102]), the director field is prescribed in voxels or cubes whose characteristic length is $\sim 50\mu m$, which is on the order of the thickness of the sheet. Moreover, any planar director profile (where the director is in the plane of the initially flat sheet) can be prescribed within each voxel. Thus, there is an enormous design landscape to explore given this capability.

Questions of how properties of thin sheets (i.e., buckling and localized deformation) couple with the shape change induced by controlled heterogeneity in actuation are another major theme of this thesis.

1.3 Theoretical background and an overview of our results

We have highlighted examples of nematic elastomers (i) undergoing large spontaneous distortion under temperature change, (ii) deforming without stress, (iii) exhibiting fine-scale material microstructure and soft elasticity and (iv) actuating into complex three dimensional shapes. We have also intimated that these behaviors emerge essentially as consequences of a coupling of the deformation (or the elasticity) of nematic elastomers to (I) a nematic to isotropic phase transition and (II) director reorientation. In fact, we will show that a careful accounting of the elasticity of thin sheets incorporating these properties will lead naturally to the macroscopic behaviors seen in the examples (i-iv). To do this, we build from well-established theories in the physics literature which capture the *three dimensional* picture of the microscopic physics (i.e., properties (I) and (II)), and we derive *two dimensional* theories from them based on sound (and in most cases rigorous) mathematical arguments. These two dimensional theories capture the macroscopic behaviors seen in (i-iv) and much more.

To introduce our results, we find it most natural to progress in the context of the relevant theoretical background upon which they are built:

[5]See Krulevitch et al. [57] Figure 10 for the work density of actuator materials.

On the mechanical response and instabilities in thin sheets

A theory to describe the elasticity of nematic elastomers was formulated by Bladon et al. [19]. It is derived from the statistical mechanics point of view by capturing entropic elasticity of the chains in the presence of nematic order. In this framework, the material is isotropic in the high temperature state, and there is no preferential orientation for the director. Thus, the director may rotate freely with respect to the material frame. This novelty results in a degeneracy in the low energy states associated to the entropic elasticity, whereby the material has a non-trivial set of stress-free shape-changing configurations. Hence, Warner et al. [103] predicted that these features should give rise to soft elasticity under the application of an electric field or mechanical deformation.

This prediction came to fruition, as highlighted above with the electro-mechanical experiments of Urayama et al. [97, 98] and the clamped-stretch experiments of Kundler and Finkelmann [58]. Strikingly though, the soft elasticity in the Finkelmann experiment corresponds to the formation of fine-scale material microstructure or strip domains (where the director alternates between two orientations in stripes). Such domains would appear to run counter to conventional wisdom on the modeling of liquid crystals. In particular, liquid crystals desire uniform alignment, and therefore, deviations from the preferred uniform alignment are often said to incur an elastic penalty. Following Frank [44] (see also de Gennes and Prost [49]), this elastic contribution is widely modeled by a phenomenological description termed *Frank elasticity*. It is an energetic penalty on the most general quadratic form in n and ∇n (the director and its gradient). In the context of nematic elastomers, this contribution would appear to penalize domain walls (i.e., the narrow regions that separate strip domains of uniform director seen in the microstructure in Figure 1.4(c)).

In contrast to the conventional wisdom, Verwey et al. [101] explained how stripe domains can arise as a means of minimizing this combined free energy. Specifically, they recognized that the competition between entropic elasticity and Frank elasticity—precisely the square-root of the ratio of the moduli κ of the Frank elasticity to μ of the entropic elasticity—introduces a small length-scale. Roughly, $\sqrt{\kappa/\mu} \sim 10 - 100\ nm$ (see, for instance, chapter 3 of Warner and Terentjev [105]), and they argued that stripe domains with alternating directors can emerge as minimizers of this combined energy with transition zones proportional to this small length-scale.

DeSimone and Dolzmann [37] noted that the entropic energy density proposed by Bladon et al. [19] is not quasiconvex, and thus fine-scale microstructure can arise naturally in these materials. Mathematically, the energy functional is not weakly lower-semicontinuous, resulting in possible non-existence of minimizers: briefly, minimizing sequences develop rapid oscillations that result in a lower energy than its weak limit. These rapid oscillations are interpreted as the fine-scale microstructure in the material. DeSimone and Dolzmann [37] also computed the relaxation, wherein the energy density is replaced with an effective energy density that accounts for all possible microstructures. Further, Conti et al. [27, 28] used the planar version of free energy to study the stretching of sheets and were able to explain various details of the experiments described above including the soft elasticity, formation and disappearance of stripe domains, and the persistence of domains near the grips even at high stretches.

Nevertheless, experiments on nematic elastomers, like the ones highlighted, have largely been performed on thin sheets or membranes. These structures are typically unable to sustain compression, having rather a state of stress limited to just uniaxial and biaxial tension. Consequently, sheets are often plagued by instabilities such as wrinkling. To this point, we highlight another surprising observation inherent to the experiments of Kundler and Finklemann [58], one that that has thus far escaped notice and exploration. Even though the thin sheet in Figure 1.4(a) has been stretched significantly with clamped grips, it remains planar and does not wrinkle. In fact, similar experiments have been conducted by a number of researchers, and none of them have reported any wrinkling instability. This is surprising because thin sheets of purely elastic materials wrinkle readily when subjected to either shear (as shown by Wong and Pellegrino [109, 110, 111]) or stretching with clamped grips [24, 75, 93, 113].

The wrinkling of thin elastic membranes has been widely studied, motivated by various applications. Early research was motivated by the use of membranes for aircraft skins where wrinkling altered their aerodynamic performance. More recent interest stems from the use of membranes in light-weight deployable space structures including solar sails, telescopes and antennas [53, 65], and renewed interest in fabric roofs of complex shape [23] (see also [113] and references therein). The underlying mechanism is relatively simple: thin elastic membranes are unable to sustain any compression; instead they accommodate imposed compressive strains by buckling out-of-plane. When a sheet is pulled on clamped edges, the clamps inhibit the

natural lateral contraction, leading to compressive stresses in the lateral direction, which in turn leads to wrinkles or undulations elongated along the direction of stretch. The wavelength of the undulations are large compared to thickness, but small compared to the overall dimensions of the sheet.

Mathematically, any finite deformation theory of membranes is not quasiconvex, and thus suffers from instabilities which can be interpreted as wrinkles (see, for instance, the works of Pipkin and Steigmann [78, 88, 89]). Further, the relaxation of such theories gives rise to tension-field theories like those of Mansfield [64] where membranes can resist tension but not compression. Such theories are zero thickness idealizations of the membrane which account for the consequences of wrinkles at a scale large compared to the wrinkles but do not describe them explicitly. Alternatively, in recognizing that wrinkles cause bending due to the non-zero thickness of the membrane, Koiter-type theories, which capture a sum of bending and membrane energies, lead to an explicit description of wrinkles. Such theories form the basis of the analysis of wrinkling described above [24, 75, 93, 111, 113].

In general, there are two approaches to dealing with instabilities resulting from the failure of (an appropriate notion of) convexity that results in features at a fine scale. The first is relaxation, where one derives an *effective* or *relaxed* theory that describes the overall behavior after accounting for the formation of fine-scale features. The relaxed theory of DeSimone and Dolzmann in the context of liquid crystal elastomers and the tension-field theories for thin membranes are examples of such relaxation. While these theories are extremely useful in describing overall behavior, they are often difficult to compute explicitly and they do not resolve all fine scale details though it is at times possible to *a posteriori* reconstruct them. Further, they are often degenerately convex and therefore lead to extremely stiff numerical problems. The second approach is *regularization* where one recognizes that the source of the nonconvexity is the neglect of some smaller order physics, and adds some higher order term to the energy. The second gradient theories of plasticity, the phase field theories of phase transformations and the theories of Verwey et al. [101] (where the Frank elasticity regularizes the entropic elasticity) are examples. These resolve the fine-scale details, but are computationally extremely expensive as they require a very fine resolution.

In this thesis, we are interested in the potential wrinkling behavior of stretched nematic elastomer sheets. Therefore we have to account for two sources of instability—a material instability that results in the formation of fine-scale microstructure

and a structural instability that results in fine-scale wrinkles. We develop the theory for this on multiple fronts:

Overview of our results (The effective membrane theory)

First, we derive the effective theory of thin sheets of nematic elastomers that accounts not only for the formation of fine-scale material microstructure but also instabilities like wrinkling. An important insight that results from this is the possible states of stress in these materials. We find that like usual elastic sheets, sheets of nematic elastomers are also incapable of sustaining compression, and the state of stress is limited to uniaxial and biaxial tension. Importantly, due to the ability of these materials to form microstructure, there is a large range of deformation gradients involving unequal stretch where the state of stress is purely equibiaxial. Consequently, a membrane of this material has zero shear stress even when subjected to a shear deformation within a certain range.

We start with a three dimensional variational model of nematic elastomers and derive the effective behavior of a membrane—a domain where one dimension is small compared to the other two—as the $\Gamma-$limit of a suitably normalized functional as the ratio of these dimensions goes to zero following LeDret and Raoult [61] and others [14, 31, 87]. Our variational model is based on a Helmholtz free energy density that has two contributions: the first contribution is the entropic elasticity of Bladon et al. [19], and the second is Frank elasticity. We recall that the lengscale of Frank elasticity $\sqrt{\kappa/\mu} \sim 10 - 100\ nm$, and note that the thickness h of a realistic membrane is on the order of $10 - 100\ \mu m$ depending on the application. Thus, one has two small parameters, and one needs to study the joint limit as both $\sqrt{\kappa/\mu}$ and h go to zero, but at possibly different rates. We do so by setting $\kappa = \kappa_h$ and studying the limit $h \to 0$.

We find that the $\Gamma-$limit and thus the resulting theory is independent of the ratio κ_h/h. This is similar to the result of Shu [87] in the context of membranes of materials undergoing martensitic phase transitions. In other words, the length-scale on which the material can form microstructure does not affect the membrane limit as long as it is small compared to the lateral extent of the membrane. Consequently, the $\Gamma-$limit we obtain coincides with the result of Conti and Dolzmann [31] who studied the case $\kappa = 0$. In fact, our proof draws extensively from their work. Specifically, their result provides a lower bound and our recovery sequence is adapted from theirs.

The $\Gamma-$limit is characterized by an energy per unit area that depends only on

the tangential gradient of the deformation. It is obtained from the density of the entropic elasticity by minimizing out the normal component followed by relaxation or quasiconvexification. We compute this by obtaining upper and lower bounds, and provide an explicit formula shown schematically in Figure 3.2. It is characterized by four regions depending on the in-plane stretch: $\mathcal{S}$ a solid region where there is no relaxation, $\mathcal{L}$ a liquid region where wrinkling and microstructure formation drive the effective energy to zero, $\mathcal{W}$ a wrinkling region where wrinkling relaxes the energy, and $\mathcal{M}$ a microstructure region where stripe domains relax the energy. The techniques employed here are in the same spirit as those employed by DeSimone and Dolzmann [37] in three dimensional nematic elastomers.

We also show that the oscillations in the region $\mathcal{M}$ are necessarily planar oscillations of the nematic director and involve no out-of-plane deformation while those in the region $\mathcal{W}$ are characterized by uniform nematic director and wrinkling. Additionally, we show that region $\mathcal{S}$ is without instability. The effective energy we derive proves to be differentiable, and the derivative associated with each region is precisely related to the characterization of instabilities. We use the derivative to define a stress. The Cauchy stress is given in (3.12): it is general biaxial tension in $\mathcal{S}$ where the membrane is without instability, zero in $\mathcal{L}$ where crumpling and microstructure are driving the effective energy and stress to zero, uniaxial tension in $\mathcal{W}$ where wrinkling relaxes compression and equi-biaxial tension in $\mathcal{M}$ where microstructure relaxes shear. As described above, the unique attributes of nematic elastomers give rise to this region of equi-biaxial tension compared to membranes of usual elastic materials.

These results can also be found in Cesana et al. [25].

Overview of our results (The Koiter theory and suppression of wrinkling)

The effective membrane theory for nematic elastomers accounts for the consequences of wrinkling and microstructure on a scale large compared to the instabilities, but it does not describe them explicitly. Physically though, the scale of the microstructure (microns) is small compared to the scale of wrinkles (millimeters). Hence, we take a multiscale view and systematically develop a theory that is a relaxation for microstructure but a regularization for wrinkles. The resulting theory is a Koiter-type theory (3.183) with two terms; the first is the two-dimensional or plane stress reduction of the relaxed energy of DeSimone and Dolzmann [37] and the second is bending.

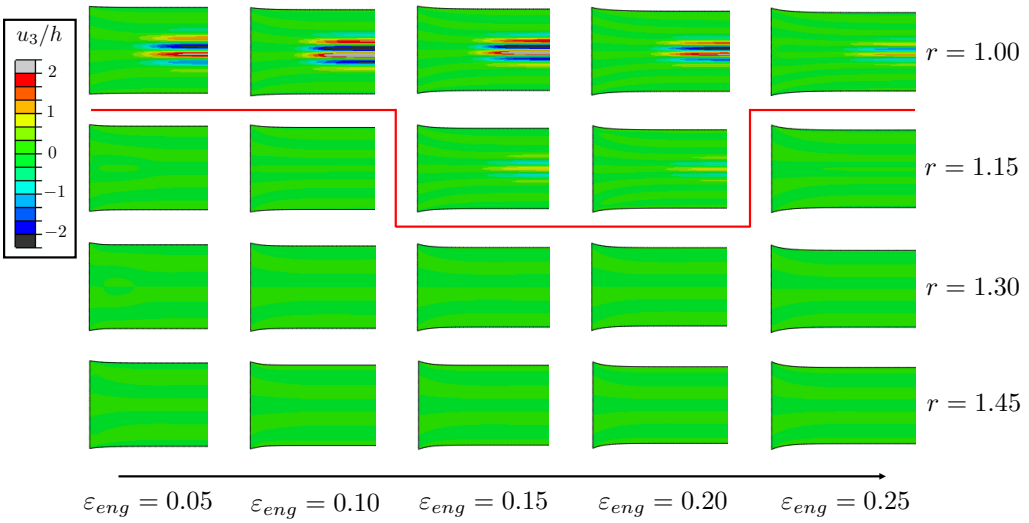

Figure 1.7: The wrinkling of a clamped-stretched sheet is suppressed with the introduction of nematic anisotropy. The strength of nematic ordering is given by $r \geq 1$, with increasing r corresponding to stronger nematic ordering.

To develop this theory, we build on the results of the effective membrane theory: Recall we provided the explicit characterization of the instabilities or oscillations (Young measures) that underly the relaxation. This had two sources—microstructure or stripe domains and wrinkles. Remarkably, for the taut sheets (i.e., regions $\mathcal{M}, \mathcal{S}$ and $\mathcal{W}$), we found that the overall deformation gradients for which microstructure occurs are distinct from the overall deformation gradients for which wrinkling occurs. We show, in addition, that the plane stress reduction of the relaxed entropic elastic energy coincides with the relaxed membrane energy in all regions of interest for taut membranes except the one involving tension wrinkles, where it is the plane stress reduction of the original entropic energy. Consequently, this reduction accurately describes the role of microstructure in the in-plane deformation of nematic elastomer sheets. It does not, however, accurately describe tension wrinkling in these sheets; rather, regularization or relaxation is needed. Taking the regularization approach, we use the Young measure characterization of tension wrinkling oscillations to compute the bending energy for these oscillations systematically from the relaxed entropic elastic energy. This bending together with the plane stress reduction of the relaxed entropic elastic energy gives the appropriate Koiter-type theory for taut sheets of nematic elastomer.

Finally, we use this theory in numerical studies to demonstrate that the ability of the material to form microstructure does indeed suppress wrinkling. Specifically, we study the clamped-stretch experiments of Kundler and Finkelmann [58] and focus

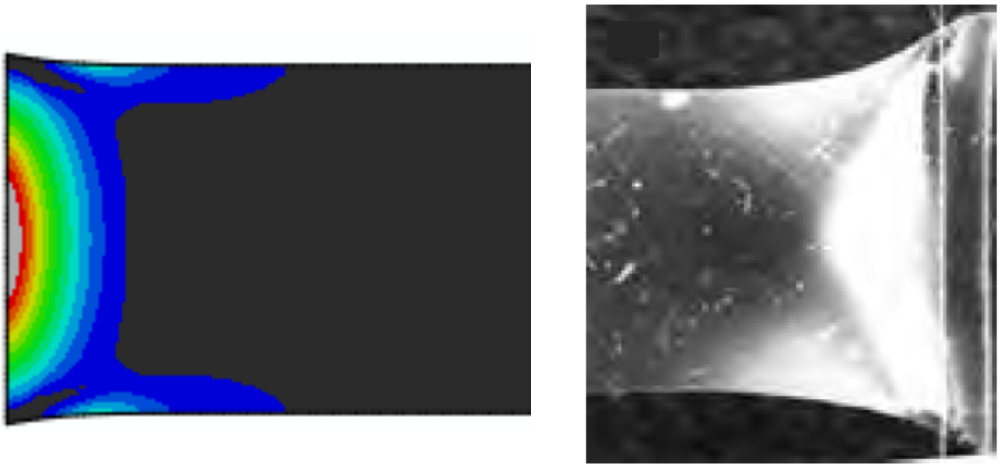

Figure 1.8: Microstructure at the clamps: The simulations and experiments are in striking agreement. This microstructure alters the stress state at the clamps, and as a result, wrinkling is suppressed. (The figure on the right is reproduced from Warner and Terentjev [105].)

on sheets with lateral dimensions for which purely elastic materials readily wrinkle under this stretch. We show that, as a parameter that describes the strength of the nematic order increases, the onset of wrinkling is delayed and the amplitude is decreased, until it is completely suppressed for large enough nematic order (Figure 1.7). We further show that the reason for this is that the ability to form microstructure alters the stress distribution close to the clamps (Figure 1.8). These results open up the possibility of exploiting these materials in applications where one seeks membranes that do not wrinkle.

These results can also be found in Plucinsky and Bhattacharya [80].

On actuation of heterogeneously patterned thin sheets

The free energy or entropic elasticity of nematic elastomers proposed by Bladon et al. [19] has been used by Tajbakhsh and Terentjev [92] to explain the shape-changing response to thermal actuation in mono-domain sheets, i.e., sheets with spatially uniform director. More recently, it has been recognized by Modes et al. [66, 67] and now many others [2, 26, 72, 73, 112, 79] that heterogeneously programing the sheet, so that the director varies spatially in the plane of the sheet, could result in complex three dimensional shapes upon thermal actuation. That is, since sheets are characteristically thin compared to their lateral dimensions, the non-uniform shape-changing response of patterned sheets to thermal actuation could induce out-of-plane *buckling*. Thus, based on a membrane idealization of

the free energy, Modes et al. [66, 67] predicted that a sheet with programmed azimuthal or radial heterogeneity would actuate into a conical or saddle-like three-dimensional shape upon temperature change. Such heterogeneity was later realized experimentally—first by de Haan et al. [51] for nematic glass sheets, and then by Ware et al. [102] in nematic elastomer sheets—and the actuation of these sheets agreed with the prediction.

The underlying mechanism for actuation couples the shape-changing physics of the material to the geometry of the sheet: The heterogeneity encoded into the flat sheet often necessitates internal stresses upon actuation. Indeed, going beyond a uniform prescription of the director, there is likely no stress-free way to accommodate the desired local shape-changing response to actuation to form a compatible deformation of the sheet. This induces stress in two flavors. If the sheet (or a portion of the sheet) remains planar, then it develops internal membrane stresses (i.e., stresses which are essentially uniform through the thickness). Alternatively, the sheets can deform out-of-plane to relieve the membrane stresses, at the cost of bending stresses (i.e., stresses which vary essentially linearly through the thickness). For thin enough sheets, bending and thus out-of-plane deformation is preferred. This is analogous to the classical example of the buckling of a column under axial compressive load: the column remains planar under application of small compressive stress, but on exceeding a critical stress (which depends on thickness/width to length ratio), the column buckles. Here though, we are not dealing with the application of a load, but rather, the *buckling* is induced by incompatible heterogeneity upon actuation.

This phenomenon of incompatible heterogeneity is ubiquitous in the biology of growth; for instance, in the the morphogenesis of growing leaves, in which the leaf forms out-of-plane undulations while growing outwards in a non-uniform manner [35, 40, 86]. It has also been carefully studied in the context of swelling in hydrogels by Klein et al. [56], where the swelling is controlled to induce a desired non-Euclidean metric within the hydrogel sheet, and where strikingly, the actuation is exactly consistent with satisfying this metric. Thus, building off of this work, Efrati et al. [38, 39, 85] developed the general framework of non-Euclidean plate theory to study this phenomenon. Further, this formalism has since been used by Aharoni et al. [2] to propose a metric constraint to govern shape-changing actuation in heterogeneously patterned nematic elastomer sheets.

The successes of non-Euclidean plate theory notwithstanding, there are some limitations: For one, it is often not clear the exact manner by which the microscopic

physics of a complex material gets distilled into a non-Euclidean metric (these are typically proposed in an *ad hoc* manner). In addition, it is possible that the purely geometric picture of active sheets breaks down, say if the formation fine-scale material microstructure competes with shape change driven by programmed heterogeneity. Fortunately, with recent advances in the mathematical treatment of dimension reduction elasticity, these limitations can be addressed.

The derivation of plate theories is old problem with major contributions from Euler, D. Bernoulli, Cauchy, Kirchhoff, Love, E. and F. Cosserat, von Karman, among many others. It is only recently though that such plate theories have been obtained rigorously from three dimensional elasticity. The seminal work along this line is that of Friesecke, James and Müller [46]: They showed that a Kirchhoff type bending theory emerges rigorously as the Γ-limit of three dimensional elasticity at the energy scale proportional to the thickness cubed (and under hypotheses which are natural to conventional solids). The main technical ingredient for this result is geometric rigidity, which allows for a rigorous (i.e., ansatz free) investigation of all possible deformations which have elastic energy proportional thickness cubed, and in particular, is used to deduce that all such deformations with this scaling behave (asymptotically) as isometric immersion of a flat sheet. That is, all pure bending configurations of a flat sheet are developable or ruled surfaces. The techniques to develop this theory are widely applicable to a range of dimension reduction problems in elasticity. Indeed, building on this work, Friesecke et al. [45] also rigorously derived von Karman plate theories as a dimension reduction of three dimensional elasticity (under an appropriate scaling assumption on the plate's boundary conditions). Further, Lewicka and Pakzad [63] generalized key results of geometric rigidity to a setting appropriate for deriving non-Euclidean plate theories from three dimensional elasticity.

In this thesis, we are interested in characterizing designable actuation in heterogeneously patterned sheets of nematic elastomer. Therefore, we have to discern the intimate connection between the microscopic physics of nematic elastomers and the behaviors inherent to thin sheets.

Overview of our results (On actuation)

We start from a variational formulation for the entropic elastic energy of nematic elastomers and we derive the effective two dimensional metric constraint, which links the deformation and the heterogeneous director field. This constraint (equation

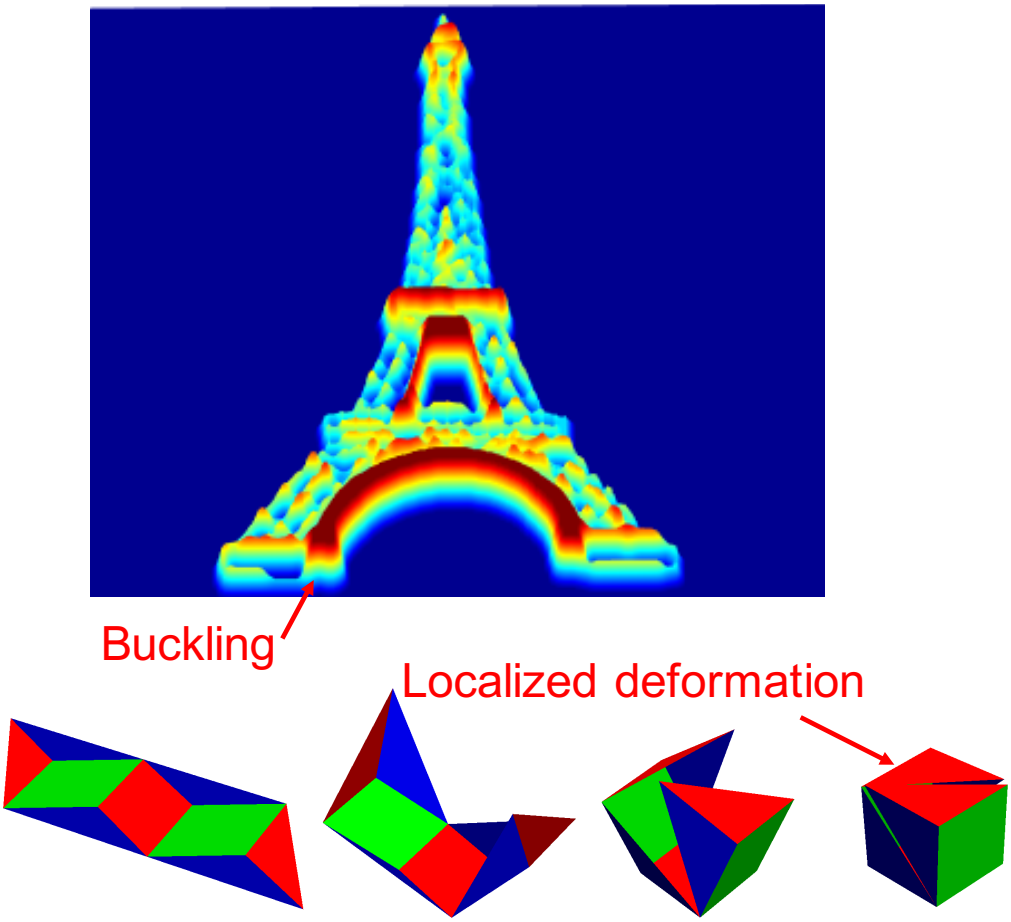

Figure 1.9: One can *lift* the Eiffel Tower out of a sheet through an actuation which exploits buckling. Further, one can actuate a box taking advantage of heterogeneity to induce sharp folds.

(4.17) below) arises in the context of energy minimization due the interplay of stretching, bending and heterogeneity in these sheets. Our main results show that satisfying the metric constraint is both necessary and sufficient for the deformation to be an approximate minimizer of the energy. The metric constraint is also a generalization of the constraint proposed by Aharoni et al. [2] in two directions in that (i) it extends the constraint to three dimensional programming of the director field (where the director can tilt out of the plane of the sheet) and (ii) it relaxes the smoothness requirement asserted there. These generalizations admit a rich class of examples under the metric constraint.

In relaxing the smoothness requirement, we explore *nonisometric origami*—where heterogeneity is programmed in a piecewise constant pattern so that thermal actuation leads to complex folding patterns. We show that if the metric constraint

holds, then the energy of actuation is $O(h^2)$ and this h^2 scaling is optimal. This justifies nonisometric origami as a class of designable actuation. Many examples of nonisometric origami are possible: we highlight this construction that will fold into a box (Figure 1.9) and several other examples. We also develop in some detail an equivalent formulation of the metric constraint (4.20) for nonisometric origami in terms of *compatibility conditions*. These are akin to the rank-one condition studied in the context of fine-scale twinning during the austenite martensite phase transition (also actuation of active martensitic sheets)[4, 13, 14, 15] and to the recently studied compatibility conditions for the actuation for nematic elastomer and glass sheets using planar programming of the director [68, 69]. We also highlight the rich potential of this class of designable actuation by showing that the case of three sectors with fixed distinct planar directors $n_{0i} \equiv \tilde{n}_{0i}$ for $i = 1, 2, 3$ can have up to 32 non-trivial compatible junctions for various $\bar{r}$ and n_{0i}.

For three dimensional programing (where the director can tilt out-of-plane), we explore *lifted surfaces*—where three dimensional heterogeneity is programmed so that thermal actuation leads to a prescribed surface of arbitrary complexity as long as it is smooth and has limited slope. We show that these (and all other sufficiently smooth surfaces satisfying the metric constraint) are bending configurations of the sheet. We also show that any bending configuration of the sheet is necessarily a sufficiently smooth surface satisfying the metric constraint. This establishes a rigorous underpinning to the assertion that the metric constraint governs shape-changing actuation in these sheets. Thus, it can be used as a means of classifying the design landscape for actuation in these sheets. We highlight the rich landscape for the lifted surfaces design through two examples: one where *Caltech* lifts out of the sheet, and another where the *Eiffel Tower* does (Figure 1.9). These are but a small sample of designs amenable to this framework.

This metric constraint first appeared in our earlier short paper [82] with a view towards applications. The justification of this constraint for designable actuation can be found in Plucinsky et al. [81].

Chapter 2

THEORY FOR THE ELASTICITY OF NEMATIC ELASTOMERS

2.1 A first principles theory

The entropic elastic energy density

A widely accepted theory for the free energy or entropic elasticity of nematic elastomers is due to Bladon et al. [19] (see also Warner and Terentjev [105]). As with the classical neo-Hookean model for rubbery solids, this formulation emerges from the statistics of polymer chain conformations, with the caveat being that the distribution properly accounts for nematic anisotropy associated with the liquid crystal rod-like molecules. The free energy $W^e\colon \mathbb{R}^{3\times3}\times\mathbb{R}^3\times\mathbb{R}^3 \to \mathbb{R}\cup\{+\infty\}$ has the form

$$W^e(F,n,n_0) := \frac{\mu}{2}\begin{cases} \operatorname{Tr}\left(F^T(\ell^f_n)^{-1}F(\ell^0_{n_0})\right)-3 & \text{if } n,n_0\in\mathbb{S}^2, \det F=1\\ +\infty & \text{otherwise,}\end{cases} \tag{2.1}$$

where $F\in\mathbb{R}^{3\times3}$ is the deformation gradient,

$$\begin{aligned}\ell^f_n &:= r_f^{-1/3}(I_{3\times3}+(r_f-1)n\otimes n),\\ \ell^0_{n_0} &:= r_0^{-1/3}(I_{3\times3}+(r_0-1)n_0\otimes n_0)\end{aligned} \tag{2.2}$$

are the step-length tensors in the deformed and undeformed configurations, respectively, which incorporate the nematic anisotropy, n and n_0 are the directors (in the deformed and undeformed configurations respectively) and r_f and $r_0 \geq 1$ are order parameters (in the deformed and undeformed configuration, respectively) characterizing the shape-changing response due to the local alignment of liquid crystal molecules. The energy is frame indifferent; specifically, $W^e(RF,Rn,n_0) = W^e(F,n,n_0)$ for all $R\in SO(3)$ (Proposition A.1.1).

As the average alignment of the liquid crystals within the polymer (and thus, the shape-changing response) depends on temperature, the order parameters r_f and r_0 are temperature dependent. Specifically, r_f and r_0 arise from evaluating some underlying monotone decreasing order parameter $r(T)$ at the final temperature T_f and initial temperature T_0, respectively (i.e., $r_f := r(T_f)$ and $r_0 := r(T_0)$). At high temperatures, thermal fluctuations suppress nematic ordering, leading to an isotropic polymer. This is characterized by $r(T) = 1$ for temperatures T larger than

T_{iso}—the temperature inducing a nematic-to-isotropic phase transition within the solid. One can model this state by setting $r_f = r_0 = 1$ in the energy above, in which case $\ell_n^f = \ell_{n_0}^0 = I_{3\times3}$ and W^e reduces to the incompressible neo-Hookean model. (Here, $I_{3\times3} \in \mathbb{R}^{3\times3}$ represents the identity matrix.) More generally, the entropic elasticity is simply an extension of the incompressible neo-Hookean model to account for nematic anisotropy, i.e.,

$$W^e(F, n, n_0) = \begin{cases} W_{nH}\Big((\ell_n^f)^{-1/2} F (\ell_{n_0}^0)^{1/2}\Big) & \text{if } n, n_0 \in \mathbb{S}^2, \\ +\infty & \text{otherwise.} \end{cases} \tag{2.3}$$

Here for definiteness, we note

$$\begin{aligned} (\ell_n^f)^{1/2} &= r_f^{1/6}(I_{3\times3} + (r_f^{1/2} - 1) n \otimes n), \\ (\ell_{n_0}^0)^{-1/2} &= r_0^{-1/6}(I_{3\times3} + (r_0^{-1/2} - 1) n_0 \otimes n_0), \end{aligned} \tag{2.4}$$

and $W_{nH} \colon \mathbb{R}^{3\times3} \to \mathbb{R} \cup \{+\infty\}$ denotes the incompressible neo-Hookean model:

$$W_{nH}(F) := \frac{\mu}{2} \begin{cases} |F|^2 - 3 & \text{if } \det F = 1, \\ +\infty & \text{otherwise.} \end{cases} \tag{2.5}$$

(The equality (2.3) holds since $\det(\ell_n^f), \det(\ell_{n_0}^0) = 1$ for n and $n_0 \in \mathbb{S}^2$.)

An important insight regarding this model for nematic elastomers is that the deformed director n is treated as a variable independent of the deformation gradient F. Physically, this implies that the director can reorient relative to the deformation gradient of the surrounding polymer network. As a result, there is a degenerate set of stress-free shape-changing configurations associated with the entropic elastic energy density W^e. Indeed, W_{nH} is minimized (and equal to zero) strictly on the space of rotation matrices (an implication of Proposition A.1.4). Thus we have that, for a given director $n_0 \in \mathbb{S}^2$ in the undeformed configuration, W^e is minimized (and equal to zero) if and only if the deformation gradient $F \equiv F_{soft}$ satisfies

$$F_{soft} = (\ell_n^f)^{1/2} R (\ell_{n_0}^0)^{-1/2} \quad \text{for any } n \in \mathbb{S}^2 \text{ and } R \in SO(3). \tag{2.6}$$

Some intuition: Consider a (or perhaps the simplest) non-trivial example of this soft deformation. Let $n_0 = e_2$, $R = I_{3\times3}$, $r_f = r_0 = 9$, and parameterize n as $n = \sin(\theta)e_1 + \cos(\theta)e_2$. We find that

$$\begin{aligned} F_{soft} e_1 &= (2 - \cos(2\theta)) e_1 + \sin(2\theta) e_2, \\ F_{soft} e_2 &= \frac{1}{3}\Big(\sin(2\theta) e_1 + (2 + \cos(2\theta)) e_2\Big). \end{aligned} \tag{2.7}$$

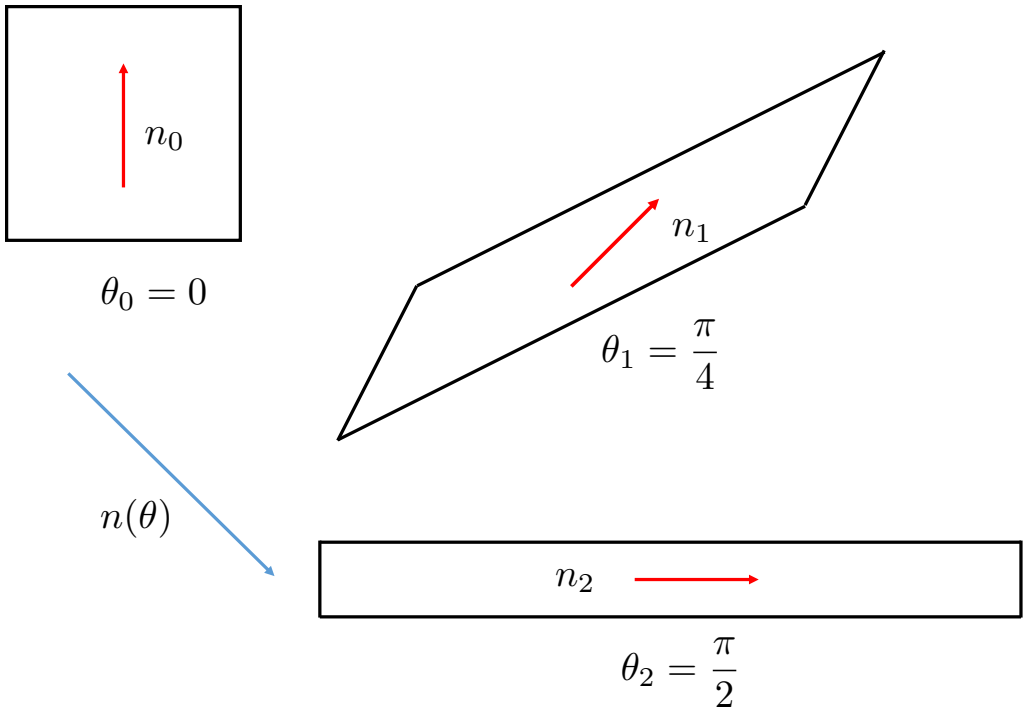

Figure 2.1: An example of a soft deformation mode of a unit cube of nematic elastomer parameterized by an angle θ. Here, we have set $r_f = r_0 = 9$, $R = I_{3\times3}$. By varying $R \in SO(3)$, we can obtain even more soft modes for a given n.

A depiction of F_{soft} in this case is provided in Figure 2.1 for the deformation of a unit cube[1]. Notice that as the director n rotates from vertical to horizontal here, the deformation gradient F_{soft} is accommodating this rotation by a stress-free shape-changing distortion. This is in stark contrast to conventional solids, where the only stress-free shape-changing deformation gradients are rigid rotations.

A non-ideal energy density

Nematic elastomers are never completely soft: Intuitively, reorientation of the liquid crystal molecules can be inhibited by the polymer network (say, if network is densely cross-linked). However, as the example in the figure shows, there is nothing in the above ideal model for the entropic elasticity to suggest such reorientation can be at all suppressed, even in the slightest of ways (i.e., the director is going from vertical to horizontal and the solid is changing its shape *without stress*). This motivates the introduction of a non-ideal energy density which penalizes stress-free reorientation of the director field. Following Biggins et al. [17, 18] and others [27, 76, 101, 100],

[1]Note, an anisotropy parameter of 9 is not physically realistic as this is far more distortion than the typical sample, but it does yield nice formulas in (2.7).

we take $W^{ni}\colon \mathbb{R}^{3\times3}\times\mathbb{R}^3\times\mathbb{R}^3 \to \mathbb{R}\cup\{+\infty\}$ to be

$$W^{ni}(F,n,n_0) := \frac{\mu\alpha}{2}\begin{cases}\mathrm{Tr}\left(F(I_{3\times3}-n_0\otimes n_0)F^T(n\otimes n)\right) & \text{if } n,n_0\in\mathbb{S}^2\\ +\infty & \text{otherwise}\,,\end{cases} \tag{2.8}$$

or equivalently[2] as

$$W^{ni}(F,n,n_0) \equiv \frac{\mu\alpha}{2}\begin{cases}|(I_{3\times3}-n_0\otimes n_0)F^Tn|^2 & \text{if } n,n_0\in\mathbb{S}^2\\ +\infty & \text{otherwise}\,.\end{cases} \tag{2.9}$$

Here, $\alpha \geq 0$ is a material parameter characterizing the influence of non-ideality for the nematic elastomer, and it depends on the cross-linking state (cf. [17, 18])—with α appreciable for nematic elastomers cross-linked in the nematic phase, and quite small for those cross-linked in the isotropic phase. This non-ideal energy density has microscopic origins as detailed by Verwey and Warner [100], and a slight variant of this density has been used to explain the semi-soft behavior[3] of clamped-stretched nematic elastomer sheets [27, 101]. It is frame indifferent (i.e., $W^{ni}(RF,Rn,n_0) = W^{ni}(F,n,n_0)$ for all $R\in SO(3)$).

In introducing this non-ideal energy density, the stress-free shape-changing modes of deformation inherent to the ideal entropic energy density disappear (though for small α, these deformations are still nearly stress-free). To see this, for a given n_0, we note that the sum $W^e + W^{ni}$ is minimized (and equal to zero) if and only if $F\equiv F_{soft}$ and $n\equiv n_{soft}$ satisfy

$$\begin{aligned} &F_{soft} = R(\ell^f_{n_0})^{1/2}(\ell^0_{n_0})^{-1/2},\\ &n_{soft} = Rn_0 \quad \text{or} \quad n_{soft} = -Rn_0\end{aligned} \tag{2.10}$$

for some $R\in SO(3)$. (This can be deduce from the argument of Proposition A.1.8.) That is, the deformed director n is no longer a free parameter. It is instead obtained via a rotation of the reference director which is exactly the rotation associated with the polar decomposition of the deformation gradient[4]. In fact, without thermal

[2] W^{ni} as defined with the trace is the common writing of this energy density in the physics literature (e.g., [17, 18, 76]). However, the latter way of writing the energy makes obvious the fact that it is simply penalizing deviations of $F^Tn/|F^Tn|$ away from n_0 or $-n_0$. The two formulations are equivalent since $(I_{3\times3}-n_0\otimes n_0)^2 = (I_{3\times3}-n_0\otimes n_0)$.

[3] Semi-soft behavior describes, for instance, the initial stressed response to stretch exhibited in some of the clamped-stretched samples of Küpfer and Finkelmann [59] before the plateau and large strain soft-elasticity; see Figure 1.4(b).

[4] Note, that the energy densities, both W^e and W^{ni}, are invariant under a change in sign of the directors. Physically, the alignment of liquid crystal molecules does not "point" in a specific direction in the sense that replacing n (or n_0) with $-n$ (or $-n_0$) yields the same accounting of nematic anisotropy; recall the cartoon in Figure 1.1(a). Therefore, one cannot distinguish between the director n_0 rotating to n via the rotation associated with the deformation gradient or rotating to $-n$; hence the "or" in (2.10).

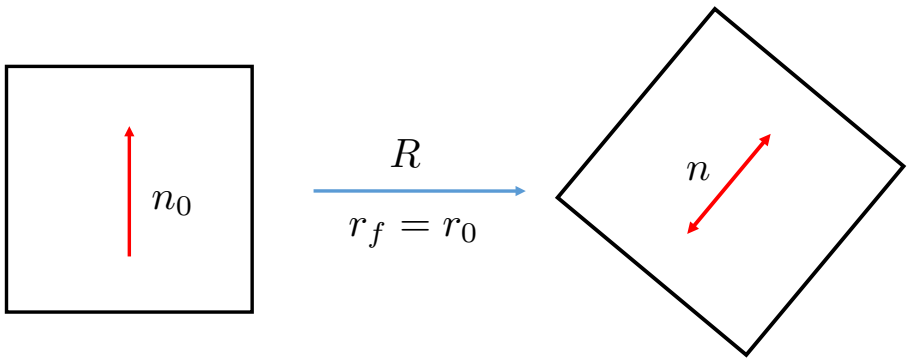

Figure 2.2: In introducing non-ideality, stress-free states are only rigid body rotations if the system is not being thermally actuated.

actuation, the soft-modes are completely classical with the introduction of non-ideality: in setting $r_f = r_0$ (which is equivalent to fixing the temperature), we see that $(\ell^f_{n_0})^{1/2}(\ell^0_{n_0})^{-1/2} = I_{3\times 3}$, and so the soft-modes are simply rigid-body rotations as depicted in Figure 2.2.

Alternatively, for actuation by heating, thermal fluctuations suppress the ordering of the liquid crystal molecules, and this transition is accommodated by shape-changing distortion of the solid. Indeed, consider the experiment in Figure 1.2 in the context of this model for nematic elastomers: $W^e + W^{ni}$. By heating, the anisotropy parameters satisfy $r_0 > r_f \geq 1$ since $T_0 < T_f$ (recall that $r(T) = 1$ for sufficiently high temperature, and this describes the isotropic case). Thus, for actuation without stress, the elastomer needs to satisfy (2.10) for some $R \in SO(3)$. If, as in the experiment, the initial director is $n_0 = e_2$ and we support the sample so that the rigid body rotation satisfies $R = I_{3\times 3}$ (by say exploiting gravity in adding a paper clip to the end of the sample), we obtain

$$F_{soft} = (\ell^f_{n_0})^{1/2}(\ell^0_{n_0})^{-1/2} = \bar{r}^{-1/6}(I_{3\times 3} + (\bar{r}^{1/2} - 1)e_2 \otimes e_2) \tag{2.11}$$

for this case. Here $\bar{r} = (r_f/r_0)$ which, since we are heating the sample, satisfies $\bar{r} \in (0, 1)$ (for cooling $\bar{r} > 1$). We plot a sample of initial dimensions $\frac{1}{3}L \times L$ under this deformation gradient in Figure 2.3. Notice that this model is (at least qualitatively) capturing the behavior of the thermally actuated monodomian nematic elastomer shown in Figure 1.2. For a more detailed understanding of the experiment in the figure and its characterization under this theory, we refer to Tajbakhsh and Terentjev [92].

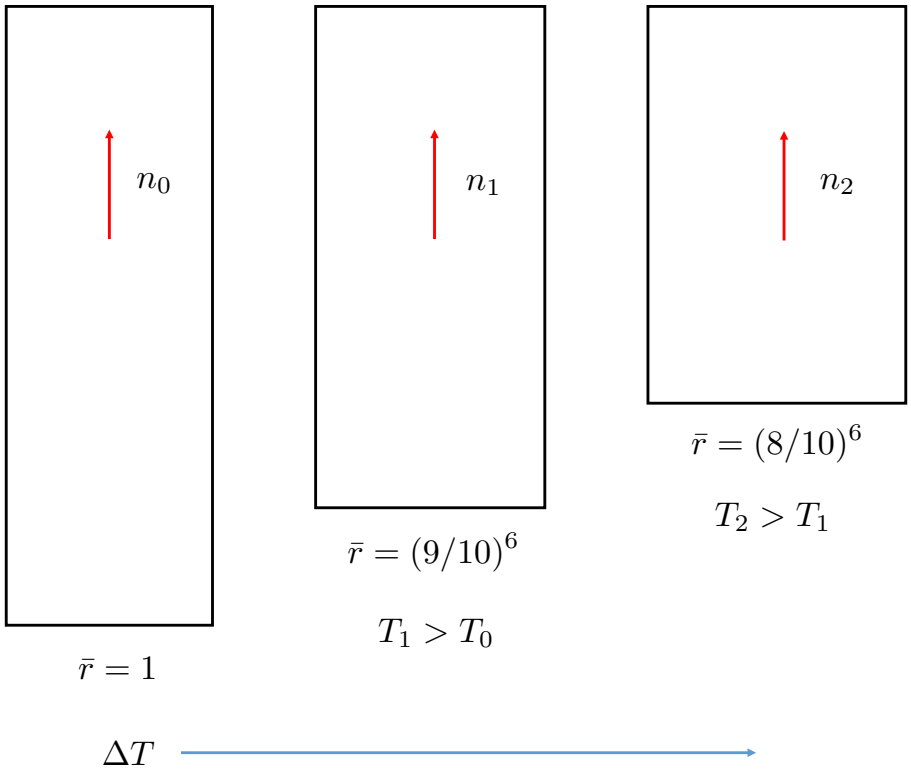

Figure 2.3: Upon actuation, the nematic elastomer contracts along the director and expands in the transverse directions, resulting in shape-changing distortion.

Frank elasticity and the total free energy

Thus far, we have examined how nematic anisotropy couples to deformation in both the ideal setting of the entropic elasticity W^e in (2.1) and when that ideality breaks down via W^{ni} in (2.8). There can be other contributions to the elasticity of nematic elastomers, which are largely independent of this coupling. For instance, the liquid crystal molecules desire alignment at low enough temperatures, and so deviation from uniform alignments should incur an energetic penalty. Hence, we introduce an energetic contribution termed Frank elasticity which reflects an elastic resistance due to such deviations. It is given by (see for example De Gennes and Prost [49])

$$W_{Fr} = \frac{1}{2}\kappa_1(\text{div } n)^2 + \frac{1}{2}\kappa_2(n \cdot \text{curl } n)^2 + \frac{1}{2}\kappa_3(n \times \text{curl } n)^2, \tag{2.12}$$

where all the derivatives are spatial. Here, the three terms physically represent splay, twist and bend of the director field with respective moduli $\kappa_1, \kappa_2, \kappa_3 > 0$. Further, these moduli $\kappa_1, \kappa_2, \kappa_3$ are typically close to each other, and so we can approximate this energy (and bound it from above and below) as:

$$W_{Fr} \approx \frac{1}{2}\kappa|\nabla_y n|^2 = \frac{1}{2}\kappa|(\nabla n)F^{-1}|^2 = \frac{1}{2}\kappa|(\nabla n)(\text{cof}F)^T|^2, \tag{2.13}$$

where the final equality holds when $\det F = 1$ as $\mathrm{cof} F \in \mathbb{R}^{3\times 3}$ denotes the cofactor matrix of F.

Hence, the free energy of a specimen of nematic elastomer occupying a region Ω when it is undeformed and under the deformation $y\colon \Omega \to \mathbb{R}^3$ and with undeformed and deformed director fields $n_0, n\colon \Omega \to \mathbb{S}^2$ is written as

$$\mathcal{E}_{n_0}(y,n) := \int_\Omega \left\{ \widehat{W}(\nabla y, n, n_0) + \frac{\kappa}{\mu} |(\nabla n)(\mathrm{cof}\nabla y)^T|^2 \right\} dx, \tag{2.14}$$

where we have normalized the energy by the shear modulus via $\mu/2$ as the energy density $\widehat{W}\colon \mathbb{R}^{3\times 3}\colon \mathbb{R}^3\colon \mathbb{R}^3 \to \mathbb{R}\cup\{+\infty\}$ is defined by

$$\widehat{W}(F,n,n_0) := (\mu/2)^{-1}\Big(W^e(F,n,n_0) + W^{ni}(F,n,n_0)\Big). \tag{2.15}$$

The parameter $\varepsilon = \sqrt{\kappa/\mu}$ is likely quite small in nematic elastomers. Specifically, in liquid crystal fluids, the moduli κ_i (which bound κ) have been measured in detail, and these moduli are likely similar for nematic elastomers (see, for instance, the discussion in Chapter 3 [105]). Further, the shear modulus μ of the rubbery network, which is distinct to elastomers, is much larger. Substituting the typical values for these parameters, we find $\varepsilon \sim 10 - 100nm$. Thus, entropic elasticity will often dominate Frank elasticity in these elastomers. This observation is a key point in many of the results developed herein.

2.2 Preliminaries: Mechanical response and instabilities

Monodomain samples and the isotropic reference configuration

In the experiments of Kundler and Finkelmann [58] depicted in Figure 1.4, the undeformed state is a monodomain sample with director alignment in the vertical direction. This monodomain synthesis is quite common for nematic elastomers, and it will be the main focus of our results on the mechanical response and instabilities in thin sheets detailed in Chapter 3. We will also only consider the mechanical response keeping the temperature fixed in this chapter, and so $r_f = r_0 =: r$ is simply a fixed constant greater than or equal to 1.

In this setting, it is natural to introduce an *isotropic reference configuration* as opposed to using the undeformed monodomain configuration as the reference. To do this, we let $y_m\colon \Omega_m \to \mathbb{R}^3$ and $n_m\colon \Omega \to \mathbb{S}^2$ be the deformation and deformed director of the monodomain sample (from the undeformed monodomain configuration $\Omega_m \subset \mathbb{R}^3$). We set

$$\Omega := (\ell^*_{n_0})^{-1/2}\Omega_m, \quad \text{for} \quad (\ell^*_{n_0})^{-1/2} := r^{1/6}(I_{3\times 3} + (r^{-1/2}-1)n_0\otimes n_0), \tag{2.16}$$

where $n_0 \in \mathbb{S}^2$ denotes the undeformed uniform director of the monodomain sample[5]. This is the *isotropic reference configuration*. Indeed, we can relate the deformation and deformed director from the monodomain sample to a deformation and deformed director as mapped from the isotropic reference configuration via

$$y(x) := y_m((\ell^*_{n_0})^{1/2}x) \quad \text{and} \quad n(x) := n_m((\ell^*_{n_0})^{1/2}x), \quad x \in \Omega. \tag{2.17}$$

In doing this, we find that

$$\begin{aligned}\mathcal{E}^m_{n_0}(y_m, n_m) &= \int_{\Omega_m} \left(\widehat{W}(\nabla y_m, n_m, n_0) + \frac{\kappa}{\mu}|(\nabla n_m)(\operatorname{cof}\nabla y_m)^T|^2\right)dx_m \\ &= \int_{\Omega} \Big(\widehat{W}^e_{iso}(\nabla y, n) + \widehat{W}^{ni}((\nabla y)(\ell^*_{n_0})^{-1/2}, n, n_0) \\ &\qquad + \frac{\kappa}{\mu}|(\nabla n)(\operatorname{cof}\nabla y)^T|^2\Big)dx.\end{aligned} \tag{2.18}$$

Here, $x_m := (\ell^*_{n_0})^{1/2}x$ for $x \in \Omega$, $\widehat{(\cdot)} := (\mu/2)^{-1}(\cdot)$, and the identity uses the fact that $\det(\ell^*_{n_0}) = 1$. Further, $W^e_{iso}\colon \mathbb{R}^{3\times3} \times \mathbb{R}^3 \to \mathbb{R} \cup \{+\infty\}$ is given by

$$W^e_{iso}(F, n) := \frac{\mu}{2}\begin{cases}\operatorname{Tr}(F^T(\ell^*_n)^{-1}F) - 3, & \text{if } n \in \mathbb{S}^2, \det F = 1\\ +\infty & \text{otherwise,}\end{cases} \tag{2.19}$$

where $F \in \mathbb{R}^{3\times3}$ now denotes the deformation gradient from the isotropic reference Ω, and the anisotropy is all encoded in the deformed configuration through the step-length tensor [6]

$$\ell^*_n := r^{1/3}(I_{3\times3} + (r-1)n \otimes n). \tag{2.20}$$

This energy density is frame indifferent and isotropic (i.e., $W^e_{iso}(RFQ, Rn) = W^e_{iso}(F, n)$ for all $R, Q \in SO(3)$; see Proposition A.1.1).

Now, the Finkelmann samples exhibiting soft elasticity and fine-scale material microstructure, as in the sample highlighted in Figure 1.4, are cross-linked in the high temperature isotropic phase. In this case, the parameter α is likely quite small, i.e., $\alpha \ll 1$ (cf. [17, 18, 105]). In Chapter 3, we are interested in the competition between instabilities inherent to thin sheets and the fine-scale material microstructure associated to (some) nematic elastomers. At a high level, the reason for soft elasticity and fine-scale material microstructure is the existence of soft modes of deformation

[5]Note, $(\ell^*_{n_0})^{1/2}$ is equal to $(\ell^0_{n_0})^{1/2}$ for $r_0 = r$. We introduce the notation $(\cdot)^*$ so as to distinguish this step-length tensor from a step-length tensor defined later for actuation.

[6]Again, this step-length tensor is simply ℓ^f_n evaluated for $r_f = r$.

inherent to the ideal entropic elastic energy (i.e., the deformations depicted in Figure 2.1). This behavior would be suppressed for large α, but it is well-established (cf. [17, 27, 101]) that for small α, semi-soft behavior and fine-scale material microstructure are still pervasive in these nematic elastomers. Thus, we study the case $\alpha = 0$, for which the free energy from an isotropic reference (2.18) reduces to

$$\mathcal{E}_{iso}(y, n) := \int_\Omega \left(\widehat{W}^e_{iso}(\nabla y, n)dx + \frac{\kappa}{\mu}|(\nabla n)(\operatorname{cof} \nabla y)^T|^2 \right) dx, \tag{2.21}$$

as this is likely not a far departure from reality for samples cross-linked in the isotropic phase. (We refer the interested reader to Conti and Dolzmann [29] for a recent numerical approach to deriving effective theories for the mechanical behavior of nematic elastomers in the case $\alpha > 0$.)

Notice that this energy (i.e., (2.21)) now has no dependence on the initial reference director of the undeformed monodomain sample (hence, the terminology: isotropic reference configuration). In Chapter 3, we introduce effective and two dimensional theories for nematic elastomers which are systematically derived from this free energy. That is, the deformations in these theories are all mappings from the isotropic reference configuration, rather than the physical undeformed monodomain sample. Nevertheless, for a monodomain sheet in which the initial director n_0 is in the plane of the sheet, one can properly account for the distinction between the isotropic reference state and monodomain reference state via the change of variables (2.17), and thus derive the corresponding theories as energies from the undeformed monodomain state. For clarity, we develop this in Appendix A.2.

As a final remark regarding this energy, we note that Verwey et al. [101] argued that stripe domains with alternating directors can emerge as minimizers of this energy functional, with transition zones proportional to the length-scale $\sqrt{\kappa/\mu}$ (recall that this length-scale is on the order of $1 - 100nm$). Thus, Frank elasticity need not inhibit very fine material microstructure in nematic elastomers.

A macroscopic three dimensional description via relaxation

In this section, we recall the results of DeSimone and Dolzmann [37] concerning the macroscopic behavior of nematic elastomers. Since the Frank energy is small, we can neglect it while studying the behavior of specimens that are large compared to $\sqrt{\kappa/\mu}$. Thus, we can define a purely mechanical energy density by minimizing

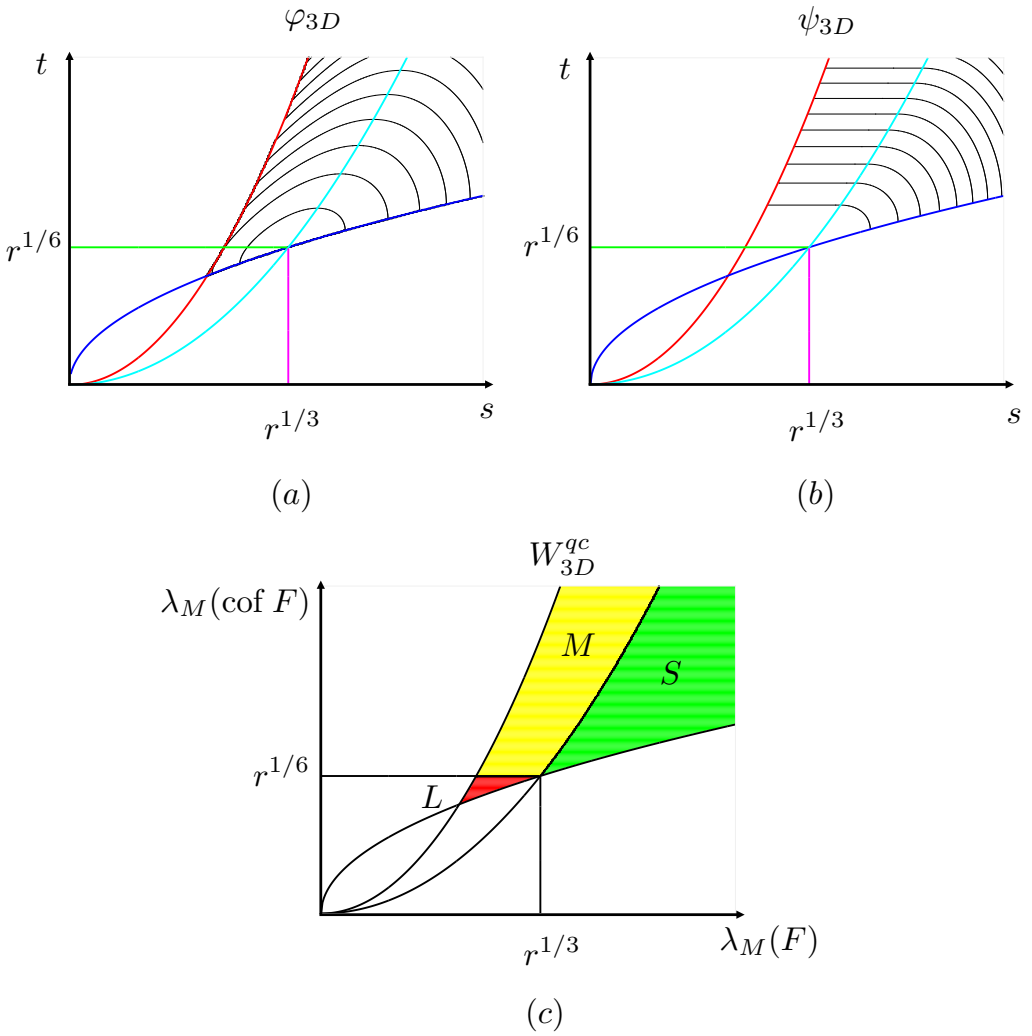

Figure 2.4: Macroscopic three-dimensional energy of nematic elastomers following DeSimone and Dolzmann [37]. (a) Contour plots of the function φ_{3D} that describes the entropic elastic energy W_{3D}, (b) contour plots of the function ψ_{3D} that describes the relaxed elastic energy W_{3D}^{qc} (i.e., one that implicitly accounts for microstructure and (c) Identification of the regions L, M and S.

out the effect of the director n in W^e_{iso}. This is given by

$$W_{3D}(F) := \inf_{n\in\mathbb{S}^2} W^e_{iso}(F,n) = \begin{cases} \varphi_{3D}(\lambda_M(F), \lambda_M(\mathrm{cof}F)) & \text{if } \det F = 1 \\ +\infty & \text{otherwise,} \end{cases} \tag{2.22}$$

where

$$\varphi_{3D}(s,t) := \frac{\mu}{2}\left(r^{1/3}\left(\frac{s^2}{r} + \frac{t^2}{s^2} + \frac{1}{t^2}\right) - 3\right), \tag{2.23}$$

$\lambda_M(F)$ is the maximum singular value of F (i.e., the largest principal stretch or the square-root of the maximum eigenvalue of F^TF and FF^T) and $\lambda_M(\mathrm{cof}F)$ is the maximum singular value of $\mathrm{cof}F \in \mathbb{R}^{3\times3}$ (it is easy to show that the this is also equal to the product of the largest two principal values of F). A contour plot of φ_{3D} is given in Figure 2.4(a).

This energy density is not quasiconvex. Thus, fine-scale microstructure can drive energy minimization in the variational formulation of the elastic energy with this strain energy density, and this leads to a possible non-existence of minimizers. We account for this by replacing W_{3D} with its relaxation. Mathematically, this is the quasiconvex envelope of W_{3D} (see Dacorogna [33]),

$$W^{qc}_{3D}(F) = \inf\left\{ \fint_\Omega W_{3D}(F + \nabla\phi)dx \colon \phi \in W^{1,\infty}_0(\Omega, \mathbb{R}^3)\right\}, \tag{2.24}$$

where $W^{1,\infty}_0(\Omega,\mathbb{R}^3)$ is the space of Lipschitz continuous functions $\phi\colon \Omega \to \mathbb{R}^3$ which vanish on the boundary of Ω, and $\fint_\Omega = \frac{1}{|\Omega|}\int_\Omega$ averages the energy density over Ω.

DeSimone and Dolzmann [37] computed the analytical expression for W^{qc}_{3D} for W_{3D} in (2.22),

$$W^{qc}_{3D}(F) = \begin{cases} \psi_{3D}(\lambda_M(F), \lambda_M(\mathrm{cof}F)) & \text{if } \det F = 1 \\ +\infty & \text{otherwise,} \end{cases} \tag{2.25}$$

where

$$\begin{aligned} \psi_{3D}(s,t) &:= \frac{\mu}{2}\begin{cases} 0 & \text{if } (s,t) \in L \\ r^{1/3}\left(\frac{2t}{r^{1/2}} + \frac{1}{t^2}\right) - 3 & \text{if } (s,t) \in M \\ r^{1/3}\left(\frac{s^2}{r} + \frac{t^2}{s^2} + \frac{1}{t^2}\right) - 3 & \text{if } (s,t) \in S, \end{cases} \\ L &:= \{(s,t) \in \mathbb{R}^+\times\mathbb{R}^+ \colon t \le s^2,\ t \le r^{1/6},\ t \ge s^{1/2}\}, \\ M &:= \{(s,t) \in \mathbb{R}^+\times\mathbb{R}^+ \colon t \le s^2,\ t \ge r^{-1/2}s^2,\ t \ge r^{1/6}\}, \\ S &:= \{(s,t) \in \mathbb{R}^+\times\mathbb{R}^+ \colon t \le r^{-1/2}s^2,\ t \ge s^{1/2}\}. \end{aligned} \tag{2.26}$$

A contour plot of W_{3D}^{qc} is given in Figure 2.4(b), and the regions L (of *liquid*-like behavior), M (related to stressed *microstructure*) and S (of normal *solid* behavior) are identified in in Figure 2.4(c). Specifically, note that the relaxation W_{3D}^{qc} deviates from the energy density W_{3D} in regions L and M in Figure 2.4(c). Importantly, these are the regions where macroscopic deformation can be accommodated by fine-scale oscillations in the director field of a nematic elastomer, resulting in the relaxation having lower energy in region M and zero energy in region L. These features were used by Conti et al. [27, 28] to explain soft elasticity and the complex deformation states in the clamped-stretch experiments of Kundler and Finkelmann [58] (Figure 1.4) assuming purely planar deformations.

2.3 Preliminaries: Actuation

We turn now to developing a framework and some heuristics for studying actuation of heterogeneously patterned nematic elastomers. Recall that, for capturing actuation in the simple setting of a monodomain strip depicted in Figure 2.3, we characterized the soft modes associated with the sum of the entropic and non-ideal energy densities via (2.10). We note that this characterization can be written in a somewhat more fundamental way, where the rotation disappears and the result is completely characterized in terms of $F \equiv F_{soft}$ and n_0. That is, (2.10) is equivalent to (cf. Proposition A.1.8)

$$\begin{aligned} &(F_{soft})^T F_{soft} = \bar{r}^{-1/3}(I_{3\times 3} + (\bar{r}-1)n_0 \otimes n_0) =: \ell_{n_0}, \quad \det(F_{soft}) = 1, \\ &n_{soft} = \frac{F_{soft}n_0}{|F_{soft}n_0|} \quad \text{or} \quad n_{soft} = -\frac{F_{soft}n_0}{|F_{soft}n_0|}, \end{aligned} \tag{2.27}$$

where we recall that $\bar{r} \in (0, 1)$ for heating and $\bar{r} > 1$ for cooling. Thus, in the context of stress-free actuation, n_{soft} is simply obtained as a convection of n_0 by the deformation gradient F_{soft}, and the right Cauchy-Green deformation tensor satisfies a compatibility condition which depends only on n_0 and the change in temperature through $\bar{r}$.

Can we have stress-free actuation when the director field $n_0 \equiv n_0(x)$ is not uniform? It turns out that in the context of three dimensional elasticity, compatibility of the right Cauchy-Green tensor is highly restrictive (the components of the Riemann curvature tensor of ℓ_{n_0} must vanish; see Remark 4.2.3). But, what if we are dealing with a very thin sheet? In particular, *suppose due to thinness*, the deformation y can be approximated as a mapping from the two-dimensional midplane $\omega \subset \mathbb{R}^2$ of the flat sheet to $\mathbb{R}^3$. Thus, rather than the full constraint in (2.27) on the deformation

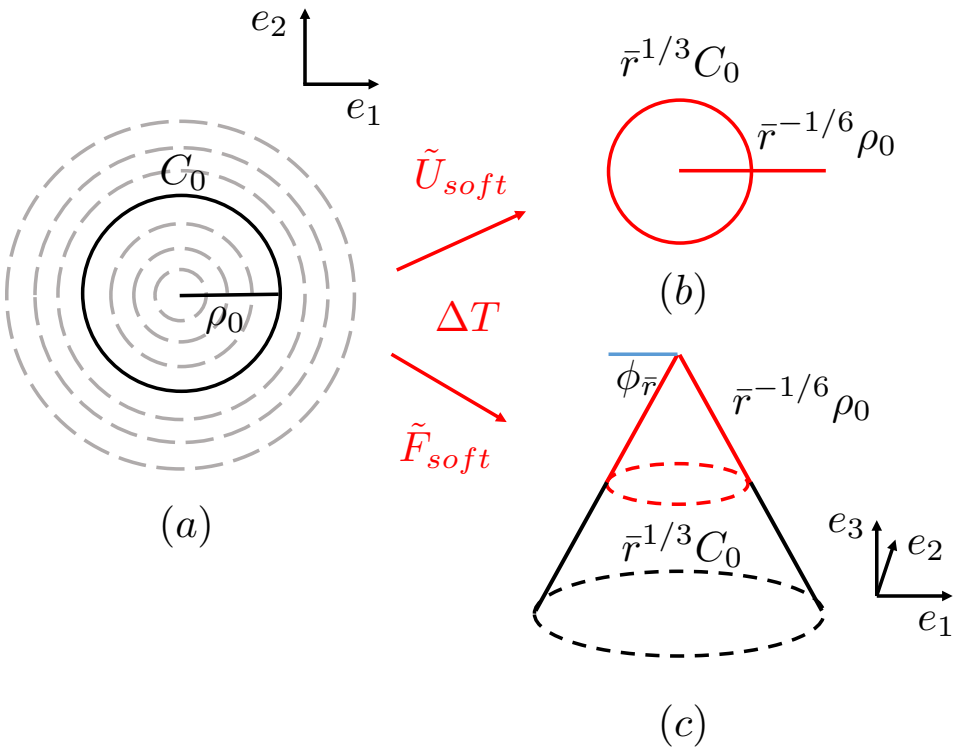

Figure 2.5: (a) An azimuthal programmed director field about a defect. We highlight a radius ρ_0 and circumference C_0. (b) To satisfy the metric constraint in the plane, $\rho_0 \mapsto \bar{r}^{-1/6}\rho_0$ and $C_0 \mapsto \bar{r}^{1/3}C_0$. This is not compatible. (c) We can rotate these stretches to form a compatible cone which satisfies the metric constraint.

gradient $F_{soft} \in \mathbb{R}^{3\times3}$, *suppose* we need only deal with a constraint on the midplane deformation gradient $\tilde{F}_{soft} \in \mathbb{R}^{3\times2}$:

$$(\tilde{F}_{soft})^T\tilde{F}_{soft} = \bar{r}^{-1/3}(I_{3\times3} + (\bar{r}-1)\tilde{n}_0 \otimes \tilde{n}_0) =: \tilde{\ell}_{n_0}, \tag{2.28}$$

where $\tilde{n}_0 \in B_1(0) \subset \mathbb{R}^2$ denotes the projection of the director $n_0 \in \mathbb{S}^2$ onto the tangent plane of ω. This two dimensional *metric constraint* is not all that restrictive.

To highlight this, we consider the example of Modes et al. [66, 67] for actuating the conical defect by heating in the context of this theoretical framework. The heterogeneous director field in this case (see Figure 2.5(a)) is given in polar coordinates (ρ, θ) by

$$n_0 \equiv n_0(\theta) = -\sin(\theta)e_1 + \cos(\theta)e_2 =: e_\theta \tag{2.29}$$

(note, $e_\rho := \cos(\theta)e_1 + \sin(\theta)e_2$). Thus for (2.28), we need $\tilde{F}_{soft}$ to satisfy

$$\begin{aligned}\begin{pmatrix} |\tilde{F}_{soft}\tilde{e}_\rho|^2 & (\tilde{F}_{soft}\tilde{e}_\rho \cdot \tilde{F}_{soft}\tilde{e}_\theta)^2 \\ (\tilde{F}_{soft}\tilde{e}_\rho \cdot \tilde{F}_{soft}\tilde{e}_\theta)^2 & |\tilde{F}_{soft}\tilde{e}_\theta|^2 \end{pmatrix} \\ = (\tilde{F}_{soft})^T\tilde{F}_{soft} = \tilde{\ell}_{n_0} = \begin{pmatrix} \bar{r}^{-1/3} & 0 \\ 0 & \bar{r}^{2/3} \end{pmatrix}.\end{aligned} \tag{2.30}$$

(Here, $\tilde{e}_\rho, \tilde{e}_\theta \in \mathbb{S}^1$ are the two dimesional projections of $e_\rho, e_\theta \in \mathbb{S}^2$.) We can satisfy this constraint through a stretch $\tilde{F}_{soft} \equiv \tilde{U}_{soft}$ given by

$$\tilde{U}_{soft} := \begin{pmatrix} \bar{r}^{-1/6} & 0 \\ 0 & \bar{r}^{1/3} \\ 0 & 0 \end{pmatrix}, \tag{2.31}$$

(i.e., an expansion $\bar{r}^{-1/6} < 1$ along e_ρ and a contraction $\bar{r}^{1/3} > 1$ along e_θ since we are considering heating). However, this does not yield a compatible deformation. The intuition is provided in Figure 2.5(b). Alternatively, since we are necessarily stretching the initial radius of the sheet and contracting the circumference, we can accommodate this by *buckling* out-of-plane to form a compatible deformation; in this case, a conical deformation as in Figure 2.5(c). This is done through a rotation $R_{e_\theta}(\phi_{\bar{r}}) \in SO(3)$ (which satisfies $R_{e_\theta}e_\theta = e_\theta$) such that

$$\tilde{F}_{soft} = R_{e_\theta}(\phi_{\bar{r}})\tilde{U}_{soft}, \quad \phi_{\bar{r}} = \pm\arccos(\bar{r}^{1/2}). \tag{2.32}$$

For more details regarding this actuation strategy, we refer to Mode et al. [66, 67].

Now, we have seen that the metric constraint (2.28) admits a non-trivial shape-changing actuation in the conical defect. The reality is, these two dimensional metric constraints admit many such examples since two dimensional deformations are free to escape to the third dimension by buckling out-of-plane, and this freedom enables the existence of many nontrivial compatible deformations under such constraints. Nevertheless, we introduced quite a few assumptions to arrive at the study of this constraint for the heuristics above. In Chapter 4, we show that the study of this constraint can be justified in the setting of elastic energy minimization. Particularly, we study the actuation of a thin sheet $\Omega_h := \omega \times (-h/2, h/2)$ via a deformation $y^h \colon \Omega \to \mathbb{R}^3$ given a heterogeneous program $n_0^h \colon \Omega_h \to \mathbb{S}^2$, with the goal of classifying approximate minimizers under the free energy

$$\mathcal{E}^h_{n_0^h}(y^h, n^h) = \int_{\Omega_h} W^e\Big(\nabla y^h, \frac{\nabla y^h n_0^h}{|\nabla y^h n_0^h|}, n_0^h\Big)dx. \tag{2.33}$$

For heterogeneity in the plane of the sheet via $n_0^h = n_0^h(x_1, x_2)$, the metric constraint (2.28) emerges naturally in this context. (Note, we have introduced a hard kinematic constraint of the deformed director n^h as actuation occurs at low enough energies that the director essentially must satisfy this constraint if there is any non-ideality. Precisely, if we instead consider an energy of the form (2.14) modified appropriately for thin sheets, then we would still arrive at the same results but with simply more details to track (see Remark 4.2.1(iii)). We do consider the more involved model when characterizing the necessity of the metric constraint in Section 4.6.)

Chapter 3

MECHANICAL RESPONSE AND INSTABILITIES OF THIN SHEETS

In this chapter, we systematically develop two dimensional theories for nematic elastomer sheets starting from the three dimensional description of the free energy given in (2.21). These characterize the mechanical response of nematic elastomer sheets due to instabilities such as structural wrinkling and fine-scale material microstructure. Using these theories, we show that taut and appreciably stressed sheets of nematic elastomer are capable of suppressing wrinkling by modifying the expected state of stress through the formation of microstructure.

This chapter is organized as follows: In Section 3.1, we introduce some of the notation and present for clarity a visual summary capturing the hierarchy of theories for nematic elastomers described and developed herein. We introduce the effective membrane theory for nematic elastomer sheets in Section 3.2—with emphasis on its physical implications—and we derive and characterize this theory in Sections 3.3-3.6. We then introduce and develop the Koiter theory for nematic elastomer sheets in Sections 3.7-3.8. Finally, we use these theories to investigate clamped-stretched sheets of nematic elastomer in Sections 3.9-3.10.

The results of this chapter can also be found in Cesana et al. [25] for the membrane theory and Plucinsky et al. [80] for the Koiter theory and simulations.

3.1 Notation and Overview

Some of the notation

We denote with $\mathbb{R}^n$ the n dimensional Euclidian space endowed with the usual scalar product $u \cdot v := u^T v$ and norm $|u| := \sqrt{u \cdot u}$. We denote the unit sphere in $\mathbb{R}^n$ by $\mathbb{S}^{n-1}$ and it is defined as the set of all vectors $u \in \mathbb{R}^n$ with $|u| = 1$. We label with $\mathbb{R}^{m\times n}$ the space of $m \times n$ matrices with real entries. For $n > 1$, we denote with $SO(n)$ the space of rotation matrices (i.e., each $F \in \mathbb{R}^{n\times n}$ such that $F^T F = I_{3\times 3}$ and $\det F = 1$). We take $\mathbb{R}^+$ to be the set of non-negative real numbers.

We often describe the material points of a three dimensional solid with $x := x_1 e_1 + x_2 e_2 + x_3 e_3$ for the fixed right-handed orthonormal basis $\{e_1, e_2, e_3\} \subset \mathbb{R}^3$ depicted in Figure 1.4. Similarly, we often describe the material points of a two dimensional

sheet with $\tilde{x} := x_1\tilde{e}_1 + x_2\tilde{e}_2$ for the analogous two dimensional orthonormal basis $\{\tilde{e}_1, \tilde{e}_2\} \subset \mathbb{R}^2$. As with the basis vectors and material points, we use the tilde as a means to distinguish between two dimensional and three dimensional quantities (if there is no conflict with previous notation). So we use $F \in \mathbb{R}^{3\times3}$ to describe the deformation gradient of a solid and $\tilde{F} \in \mathbb{R}^{3\times2}$ to describe the planar deformation gradient of a sheet; we denote with ∇ the three dimensional gradient (with respect to x) and $\tilde{\nabla}$ the planar gradient (with respect to $\tilde{x}$); . . .; etc. We also introduce the notation

$$\mathrm{adj}\tilde{F} := \tilde{F}\tilde{e}_1 \times \tilde{F}\tilde{e}_2. \tag{3.1}$$

for any $\tilde{F} \in \mathbb{R}^{3\times2}$ as this quantity will be useful in the development of the theories.

Lastly, we find it natural at points to introduce certain mathematical concepts: $W^{1,p}$ Sobolev Spaces and weak convergence (i.e., $\rightharpoonup$) in these spaces, quasiconvexification as a means of relaxation, Γ-convergence as a means of dimension reduction, and the theory of gradient Young measures for characterizing instabilities. We refer to Evans [41], Dacorogna [33], Braides [22] and Müller [74], respectively for introductions into these concepts. We will introduce the relevant mathematical concepts as they are needed.

Overview on the hierarchy of theories for nematic elastomers

In this chapter, we systematically develop two dimensional theories for nematic elastomer sheets by starting from an appropriate three dimensional description of these elastomers [19, 37, 101, 105]. Thus, in the course of this development, we find it natural to introduce several variants of strain energy densities modeling nematic elastomers, for which there is a well-characterized hierarchy. The hierarchy is related to the mathematical treatment of small-length scales (i.e., $\sqrt{\kappa/\mu}$ and h) inherent to nematic elastomer sheets, and how instabilities (both wrinkling and microstructure) are accounted for in this treatment.

Briefly (all of this is expanded upon in the coming sections), a three dimensional nematic elastomer can form fine-scale microstructure on a length scale $\sqrt{\kappa/\mu}$ related to the competition between entropic and Frank elasticity in these solids. In addition to this microstructure, a sheet of nematic elastomer may wrinkle since the thickness h is small compared to the lateral extent of the sheet. In typical sheets, $\sqrt{\kappa/\mu} \ll h$. Thus, to guide the reading of this chapter, we provide a visual summary of the theories which emerge in the competition of these two length scales and their hierarchy (Figure 3.1).

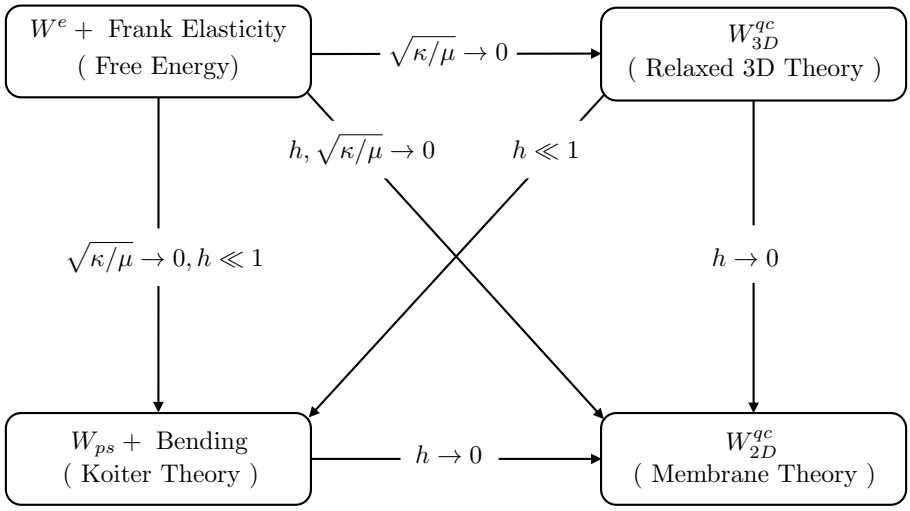

(a) Hierarchy of theories for nematic elastomers.

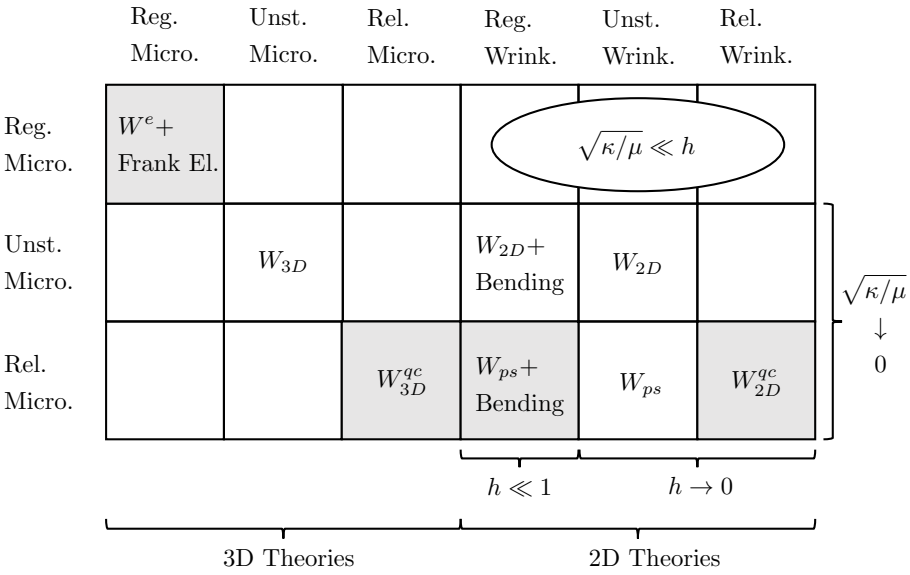

(b) Strain energy densities and their relation to instabilities.

Figure 3.1: (a) Theories which properly account for the formation of microstructure in 3D and both microstructure and wrinkling in 2D. Each theory can be derived in the treatment of the length scale as depicted. (b) The various strain energy densities of nematic elastomers and whether they are stable (i.e., *reg*ularized or *rel*axed) or *unst*able to instabilities: *micro*structure in the case of 3D densities, and both microstructure and *wrink*ling in the case of 2D densities. The stable theories are highlighted. Starting from any strain energy density on this chart, the densities to the right, lower diagonal, and directly below can be derived under the treatment of the length scales as depicted. In principle, the top right of this chart can be populated, though such theories are less physically relevant given the disparity in length scales.

3.2 The effective membrane theory for nematic elastomer sheets

We develop an effective membrane theory for nematic elastomers. Here, we first summarize these results and their physical implications, before turning to the derivation.

We consider a sheet of small thickness h and lateral extent $\omega \subset \mathbb{R}^2$ ($\Omega_h = \omega \times (-h/2, h/2)$), and follow methods in LeDret and Raoult [61] and Conti and Dolzmann [31] to study the asymptotic behavior as $h \to 0$ of the functional $\frac{1}{h}\mathcal{E}^h$ by Γ-convergence (where $\mathcal{E}^h$ denotes the energy (2.14) of a sheet initially occupying a region Ω_h). We show that the behavior of very thin sheets is described by the following energy

$$\mathcal{E}_m(y) := \int_\omega W_{2D}^{qc}(\tilde{\nabla} y) d\tilde{x} \tag{3.2}$$

as the Γ-limit, a result that is independent of the ratio of κ to h (as long as $\kappa \to 0$ as $h \to 0$). Here, quantities with a tilde denote quantities on the midplane ω of the membrane, and $y : \omega \to \mathbb{R}^3$ denotes a deformation of the midplane of the membrane. Thus, $\tilde{\nabla} y$ maps to $\mathbb{R}^{3\times 2}$.

The analytical expression for the membrane energy density W_{2D}^{qc} is obtained from W_{3D} in two steps. In the first step, we obtain a two dimensional or plane-stress reduction of W_{3D} by minimizing over the out-of-plane deformation gradient

$$W_{2D}(\tilde{F}) := \inf_{b\in\mathbb{R}^3} W_{3D}(\tilde{F}|b) \tag{3.3}$$

for any planar deformation gradient $\tilde{F} \in \mathbb{R}^{3\times 2}$. This takes the explicit form

$$W_{2D}(\tilde{F}) = \begin{cases} \varphi_{2D}(\lambda_M(\tilde{F}), \delta(\tilde{F})) & \text{if rank } \tilde{F} = 2 \\ +\infty & \text{otherwise,} \end{cases} \tag{3.4}$$

where

$$\varphi_{2D}(s,t) := \frac{\mu}{2} \begin{cases} r^{1/3}\left(\frac{s^2}{r} + \frac{t^2}{s^2} + \frac{1}{t^2}\right) - 3 & \text{if } (s,t) \in \mathcal{N}_1 \\ r^{1/3}\left(\frac{t^2}{s^2} + \frac{2s}{r^{1/2}t}\right) - 3 & \text{if } (s,t) \in \mathcal{N}_2 \\ r^{1/3}\left(s^2 + \frac{t^2}{s^2} + \frac{1}{rt^2}\right) - 3 & \text{if } (s,t) \in \mathcal{N}_3, \end{cases} \tag{3.5}$$

$$\begin{aligned} \mathcal{N}_1 &:= \{(s,t) \in \mathbb{R}^+ \times \mathbb{R}^+ : t \le s^2,\ t \ge r^{1/2}s^{-1}\}, \\ \mathcal{N}_2 &:= \{(s,t) \in \mathbb{R}^+ \times \mathbb{R}^+ : t \le s^2,\ r^{-1/2}s^{-1} \le t \le r^{1/2}s^{-1}\}, \\ \mathcal{N}_3 &:= \{(s,t) \in \mathbb{R}^+ \times \mathbb{R}^+ : t \le s^2,\ t \le r^{-1/2}s^{-1}\}. \end{aligned} \tag{3.6}$$

Above, $\lambda_M(\tilde{F}) := \sup_{e\in\mathbb{S}^2} |\tilde{F}^T e|$ denotes the maximum principal value of $\tilde{F}$ and $\delta(\tilde{F}) := |\tilde{F}\tilde{e}_1 \times \tilde{F}\tilde{e}_2|$ denotes the product of the two principal values of $\tilde{F}$. Physically,

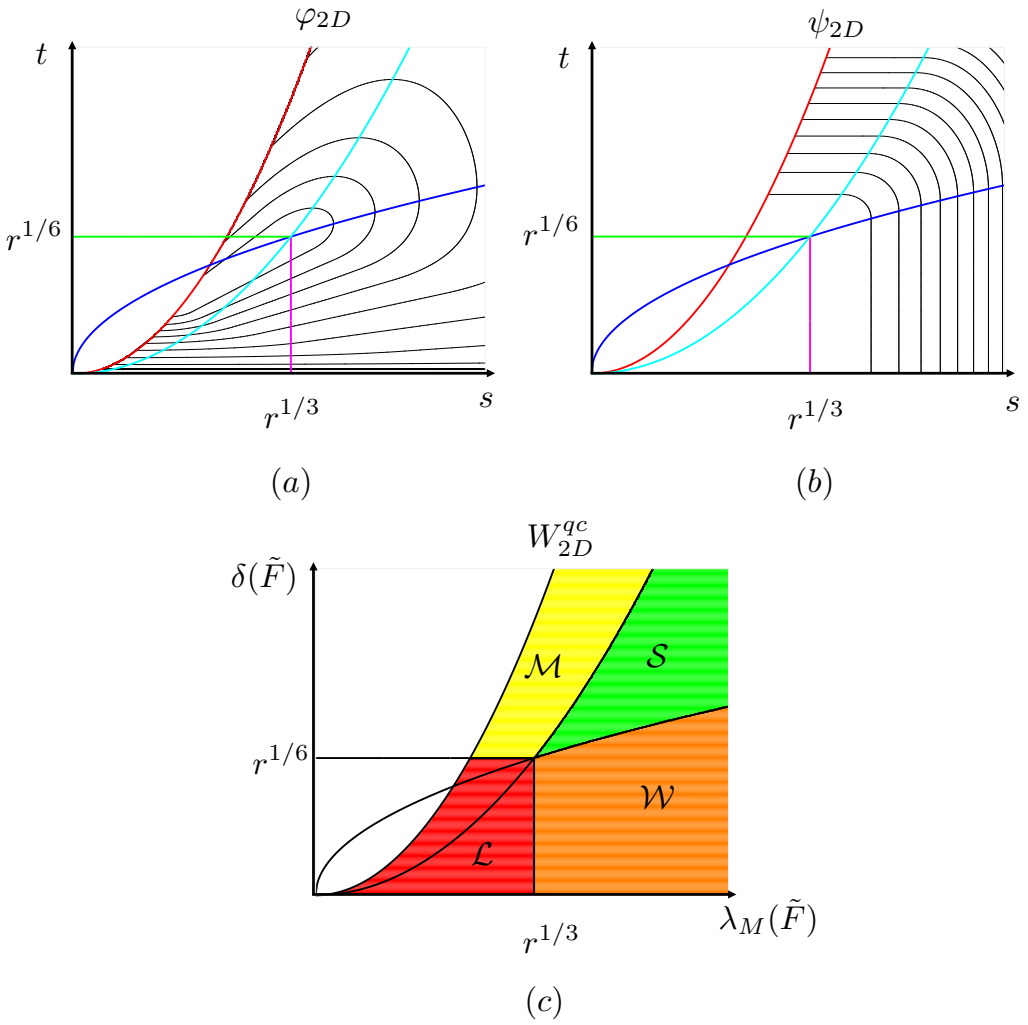

Figure 3.2: Membrane energy density of nematic elastomers. (a) Contour plots of the function φ_{2D} that describes the plane stress energy W_{2D}, (b) contour plots of the function ψ_{3D} that describes the relaxed membrane energy W_{2D}^{qc} (i.e., one that implicitly accounts for microstructure and wrinkling) and (c) identification of the regions $\mathcal{L}, \mathcal{M}, \mathcal{W}$ and $\mathcal{S}$. Microstructure or stripe domains occur in the region $\mathcal{M}$, wrinkling in region $\mathcal{W}$, crumpling and microstructure in region $\mathcal{L}$ and no relaxation in region $\mathcal{S}$.

since we are considering the deformations of the plane, the isotropic invariants of the deformation are given by the principal stretch λ_M and areal stretch δ. The contour plot of φ_{2D} is shown in Figure 3.2(a).

As with W_{3D}, W_{2D} is not quasiconvex. In this case, in addition to microstructure in the form of oscillations in nematic orientation relaxing the energy, boundary conditions which induce compressive stresses associated with W_{2D} can be relaxed through out-of-plane wrinkling and crumpling. We account for this in the second step through the relaxation of W_{2D},

$$\begin{aligned} W_{2D}^{qc}(\tilde{F}) &:= \inf\left\{ \fint_{\omega} W_{2D}(\tilde{F} + \tilde{\nabla}\phi) d\tilde{x} \colon \phi \in W_0^{1,\infty}(\omega, \mathbb{R}^3) \right\} \\ &= \psi_{2D}(\lambda_M(\tilde{F}), \delta(\tilde{F})). \end{aligned} \tag{3.7}$$

Here,

$$\psi_{2D}(s,t) := \frac{\mu}{2} \begin{cases} 0 & \text{if } (s,t) \in \mathcal{L} \\ r^{1/3}\left(\frac{2t}{r^{1/2}} + \frac{1}{t^2}\right) - 3 & \text{if } (s,t) \in \mathcal{M} \\ r^{1/3}\left(\frac{s^2}{r} + \frac{2}{s}\right) - 3 & \text{if } (s,t) \in \mathcal{W} \\ r^{1/3}\left(\frac{s^2}{r} + \frac{t^2}{s^2} + \frac{1}{t^2}\right) - 3 & \text{if } (s,t) \in S, \end{cases} \tag{3.8}$$

$$\begin{aligned} \mathcal{L} &:= \{(s,t) \in \mathbb{R}^+ \times \mathbb{R}^+ \colon t \le s^2, t \le r^{1/6}, s \le r^{1/3}\}, \\ \mathcal{M} &:= \{(s,t) \in \mathbb{R}^+ \times \mathbb{R}^+ \colon t \le s^2, t \ge r^{-1/2}s^2, t \ge r^{1/6}\}, \\ \mathcal{W} &:= \{(s,t) \in \mathbb{R}^+ \times \mathbb{R}^+ \colon t \le s^{1/2}, s \ge r^{1/3}\}, \\ \mathcal{S} &:= \{(s,t) \in \mathbb{R}^+ \times \mathbb{R}^+ \colon t \le r^{-1/2}s^2, t \ge s^{1/2}\}. \end{aligned} \tag{3.9}$$

The contour plot of ψ_{2D} is shown in Figure 3.2(b), and the various regions[1] $\mathcal{L}$ (of zero energy), $\mathcal{M}$ (related to stressed *microstructure*), $\mathcal{W}$ (related to *wrinkling*) and $\mathcal{S}$ (without instability) are shown in Figure 3.2(c).

It is instructive to look at the stress that results from this theory. We can obtain the effective Cauchy stress of a nematic elastomer membrane as

$$\begin{aligned} &\sigma^{mem} := (W_{2D}^{qc})_{,\tilde{F}}\, \tilde{F}^T, \\ &\text{i.e.,} \quad (\sigma^{mem})_{ij} := (W_{2D}^{qc})_{,\tilde{F}_{i\alpha}}\, \tilde{F}_{j\alpha}, \quad \alpha = 1,2, \quad i,j = 1,2,3. \end{aligned} \tag{3.10}$$

[1]The notation $\mathcal{S}$ and $\mathcal{L}$ follows DeSimone and Dolzmann [37] in their derivation of the relaxed three dimensional theory. However, one should avoid the interpretation of *liquid*-like behavior for $\mathcal{L}$ and normal *solid* behavior for $\mathcal{S}$. $\mathcal{L}$ is associated both with crumpling—which is also exhibited by normal thin solids—and liquid-like features due to microstructure. $\mathcal{S}$ is simply a region without instability.

To compute it explicitly, we use the singular value decomposition theorem to write

$$\tilde{F} = \bar{\lambda}_M g_1 \otimes \tilde{f}_1 + \bar{\lambda}_m g_2 \otimes \tilde{f}_2 \tag{3.11}$$

for orthonormal vectors $\{\tilde{f}_1, \tilde{f}_2\} \subset \mathbb{R}^2$ and $\{g_1, g_2\} \subset \mathbb{R}^3$ with $\bar{\lambda}_M \geq \bar{\lambda}_m \geq 0$ the singular values of $\tilde{F}$ (so that $\bar{\delta} = \bar{\lambda}_m \bar{\lambda}_M$). We find (again see [25]),

$$\sigma^{mem} = \mu r^{1/3} \begin{cases} 0 & \text{if } (\bar{\lambda}_M, \bar{\delta}) \in \mathcal{L} \\ \left(\frac{\bar{\delta}}{r^{1/2}} - \frac{1}{\bar{\delta}^2}\right)(g_1 \otimes g_1 + g_2 \otimes g_2) & \text{if } (\bar{\lambda}_M, \bar{\delta}) \in \mathcal{M} \\ \left(\frac{\bar{\lambda}_M^2}{r} - \frac{1}{\bar{\lambda}_M}\right) g_1 \otimes g_1 & \text{if } (\bar{\lambda}_M, \bar{\delta}) \in \mathcal{W} \\ \left(\frac{\bar{\lambda}_M^2}{r} - \frac{1}{\bar{\delta}^2}\right) g_1 \otimes g_1 \left(\frac{\bar{\delta}^2}{\bar{\lambda}_M^2} - \frac{1}{\bar{\delta}^2}\right) g_2 \otimes g_2 & \text{if } (\bar{\lambda}_M, \bar{\delta}) \in \mathcal{S}. \end{cases} \tag{3.12}$$

This formula highlights some striking features the membrane theory for nematic elastomers. For one, the membrane is always in a state of plane stress in the tangent plane. Secondly, the principal stresses (i.e., the eigenvalues of σ^{mem}) are always non-negative. Therefore, these membranes cannot sustain compressive stress. Further, the stress is zero in region $\mathcal{L}$ where crumpling and microstrucutre relax the energy to zero, uniaxial tension in $\mathcal{W}$ where tension wrinkling relaxes the energy, equi-biaxial tension in $\mathcal{M}$ where microstructure relaxes the energy and biaxial tension in $\mathcal{S}$ where no fine-scale features emerge to relax the energy.

For perspective, consider the special case $r = 1$ when this theory reduces to that of the neo-Hookean elastic membrane (recall W^e_{iso} in (2.1) simplifies to the incompressible neo-Hookean energy density in this case). The region $\mathcal{M}$ now disappears and we are left with regions $\mathcal{L}, \mathcal{W}$ and $\mathcal{S}$ with zero, uniaxial tension and biaxial tension respectively. This is the tension field theory originally proposed by Mansfield [64] and later obtained systematically from three dimensional elasticity by Pipkin [78] and expanded upon by Pipkin and Steigmann in [88, 89]. In essence, the theory for nematic elastomer membranes with $r > 1$ generalizes the tension field theory for isotropic membranes to account for nematic anisotropy.

A remarkable feature of nematic elastomers is the additional region $\mathcal{M}$ where the state of stress is equi-biaxial tension. This is true for a large range of unequal principal stretches $(\bar{\lambda}_M, \bar{\lambda}_m)$. In other words, *a nematic elastomer membrane can have shear strain without shear stress* in a certain range.

3.3 Membrane theory by Γ-convergence

We consider a thin nematic elastomer sheet of small thickness h which has a flat stress-free isotropic reference configuration $\Omega_h := \omega \times (-h/2, h.2)$. We assume ω

is a bounded Lipschitz domain in $\mathbb{R}^2$. Let $y^h : \Omega_h \to \mathbb{R}^3$ describe the deformation and $n^h : \Omega_h \to \mathbb{S}^2$ describe the director field so that $\mathcal{E}^h(y^h, n^h)$ is the Helmholtz free energy in (2.14) now parameterized by the thickness of the membrane in its reference configuration. In the energy, we assume $\kappa/2 \equiv \kappa_h$ and $\kappa_h \geq 0$.

To derive the effective membrane theory, we take an asymptotic limit of the energy as $h \to 0$ by Γ-convergence. For this, we follow the theory of Γ-convergence in a topological space endowed with the weak topology. The general theory can be found in Braides [22] or Dal Maso [34].

In order to deal with sequences on a fixed domain, we change variables via

$$\tilde{z}(x) = (z_1(x), z_2(x)) = (x_1, x_2) = \tilde{x}, \quad z_3(x) = \frac{1}{h}x_3, \quad x \in \Omega_h \tag{3.13}$$

and set $\Omega := \omega \times (-1/2, 1/2)$. To each deformation $y^h : \Omega_h \to \mathbb{R}^3$ and director field $n^h : \Omega_h \to \mathbb{S}^2$, we associate, respectively a deformation $w^h : \Omega \to \mathbb{R}^3$ and director field $m^h : \Omega \to \mathbb{S}^2$ such that

$$w^h(z(x)) = y^h(x) \quad \text{and} \quad m^h(z(x)) = n^h(x), \quad x \in \Omega_h. \tag{3.14}$$

We set $\tilde{\mathcal{I}}^h(w^h, m^h) := \mathcal{E}^h(y^h, n^h)/h$, and following the change of variables above, observe that

$$\tilde{\mathcal{I}}^h(w^h, m^h) = \begin{cases} \int_\Omega \left(W^e_{iso}(\nabla_h w^h, m^h) + \frac{\kappa_h}{h^2} |(\nabla m^h)(\mathrm{cof}\nabla w^h)^T|^2 \right) dz & \text{if } (w^h, m^h) \in \mathcal{A} \\ +\infty & \text{else.} \end{cases} \tag{3.15}$$

Here, the *admissible set* $\mathcal{A}$ is defined as

$$\begin{aligned} \mathcal{A} := \Big\{ (w, m) \in & W^{1,2}(\Omega, \mathbb{R}^3) \times W^{1,1}(\Omega, \mathbb{S}^2) \\ & \text{with} \quad (\nabla n)(\mathrm{cof}\nabla y)^T \in L^2(\Omega, \mathbb{R}^{3\times 3}) \Big\} \end{aligned} \tag{3.16}$$

and $\nabla_h w^h := (\tilde{\nabla} w^h | (1/h)\partial_3 w^h)$ with $\tilde{\nabla}$ the in-plane gradient. To obtain the formula (A.35), we used the identity $(\nabla_h m^h)(\mathrm{cof}\nabla_h w^h)^T = (1/h)(\nabla m^h)(\mathrm{cof}\nabla w^h)^T$.

Finally, we take the effective membrane theory to be the Γ-limit as $h \to 0$ of the functional defined on $W^{1,2}(\Omega, \mathbb{R}^3)$,

$$\mathcal{I}^h(w^h) := \inf \left\{ \tilde{\mathcal{I}}^h(w^h, m^h) \colon m^h \in W^{1,1}(\Omega, \mathbb{S}^2) \right\}. \tag{3.17}$$

In this respect:

Theorem 3.3.1 *Let $\mathcal{I}^h$ be as in (4.11) with $\kappa_h \geq 0$ and $\kappa_h \to 0$ as $h \to 0$. Then in the weak topology of $W^{1,2}(\Omega, \mathbb{R}^3)$, $\mathcal{I}^h$ is equicoercive and Γ-converges to*

$$\mathcal{I}^0(y) := \begin{cases} \mathcal{E}_m(y) & \text{if } \partial_3 y = 0 \text{ a.e.} \\ +\infty & \text{otherwise} \end{cases} \tag{3.18}$$

for $\mathcal{E}_m$ defined in (3.2). Equivalently:

(i) for every sequence $\{w^h\} \subset W^{1,2}(\Omega, \mathbb{R}^3)$ such that $\mathcal{I}^h(w^h) \leq C < +\infty$, there exists a $y \in W^{1,2}(\Omega, \mathbb{R}^3)$ independent of z_3 such that up to a subsequence

$$w^h - \fint_\Omega w^h dz \rightharpoonup y \quad \text{in } W^{1,2}(\Omega, \mathbb{R}^3); \tag{3.19}$$

(ii) for every $\{w^h\} \subset W^{1,2}(\Omega, \mathbb{R}^3)$ such that $w^h \rightharpoonup y$ in $W^{1,2}(\Omega, \mathbb{R}^3)$,

$$\liminf_{h \to 0} \mathcal{I}^h(w^h) \geq \mathcal{I}^0(y); \tag{3.20}$$

(iii) for any $y \in W^{1,2}(\Omega, \mathbb{R}^3)$, there exists a sequence $\{w^h\} \subset W^{1,2}(\Omega, \mathbb{R}^3)$ such that $w^h \rightharpoonup y$ in $W^{1,2}(\Omega, \mathbb{R}^3)$ and

$$\limsup_{h \to 0} \mathcal{I}^h(w^h) \leq \mathcal{I}^0(y). \tag{3.21}$$

Remark 3.3.2 *(i) The result for the case $\kappa_h = 0$ was provided by Conti and Dolzmann [31] (Theorem 3.1 there). Indeed, recall W_{3D} in (2.22). They proved that in the weak topology of $W^{1,2}(\Omega, \mathbb{R}^3)$ the functional $\mathcal{I}^h_{\kappa=0}(y) := \int_\Omega W_{3D}(\nabla_h w^h) dz$ is equicoercive and Γ-converges to $\mathcal{I}^0$ given in (3.18).*

(ii) A different dimension reduction theory for hyperelastic incompressible materials was developed by Trabelsi [94, 95] under similar assumptions. Trabelsi showed that the membrane energy density (integrand of $\mathcal{E}_m$) is given by $((W_{2D})^{rc})^{qc}$. We show in sequel (see also Cesana et al. [25]) that $W^{rc}_{2D} = W^{qc}_{2D}$ (and hence $(W^{rc}_{2D})^{qc} = W^{qc}_{2D}$). Thus the two limits agree.

(iii) The fact that the $\Gamma-$limit is independent of κ_h/h is similar to the following result of Shu [87]. He also provides some heuristic insight. Since the membrane limit optimizes the energy density over the third column of the deformation gradient, there is little to be gained by oscillations parallel to the thickness. Consequently, penalizing these oscillations with κ_h does not affect the $\Gamma-$limit.

Shu studied the energy $\int_\Omega (W(\nabla_h w^h) + \kappa_h |\nabla_h \nabla_h w^h|^2) dz$ *with* $W : \mathbb{R}^{3\times 3} \to \mathbb{R}$ *continuous and bounded from above and below by* $|F|^p \pm c$ *respectively for some* c. *He showed that if* $\kappa_h \to 0$ *as* $h \to 0$, *then this energy also* Γ*-converges (in the weak topology of* $W^{1,p}(\Omega, \mathbb{R}^3)$*) to* $\mathcal{I}^0$ *given in (3.18) .*

Proof of Theorem 3.3.1.
We begin with a theorem due to Conti and Dolzmann [31]:

Theorem 3.3.3 *Let* $\mathcal{I}^h_{\kappa=0}(w^h) := \int_\Omega W_{3D}(\nabla_h w^h) dz$ *for* W_{3D} *in (2.22). In the weak topology of* $W^{1,2}(\Omega, \mathbb{R}^3)$, $\mathcal{I}^h_{\kappa=0}$ *is equicoercive and* Γ *converges to* $\mathcal{I}^0$ *in (3.18).*

As a consequence, we have:

Proof of Theorem 3.3.1. Note that trivially,

$$\mathcal{I}^h(w^h) \geq \int_\Omega \inf_{m\in\mathbb{S}^2} W^e_{iso}(\nabla_h w^h, m) dz = \mathcal{I}^h_{\kappa=0}(w^h). \tag{3.22}$$

Therefore, the compactness and lower bound (Properties (i) and (ii) in Theorem 3.3.1) follow from Theorem 3.3.3. It remains to show Property (iii). This is done in Proposition 3.3.4. □

Preliminaries for a recovery sequence
For the construction, we find it useful to remark on some general properties of the purely elastic portion of our nematic elastomer energy density W_{3D} in (2.22). We note that W_{3D} is non-negative, and

$$W_{3D}(F) = \begin{cases} W_0(F) & \text{if } \det F = 1 \\ +\infty, \end{cases} \tag{3.23}$$

where $W_0 : \mathbb{R}^{3\times 3} \to \mathbb{R}$ is Lipschitz continuous, and there exists a constant c such that

$$\frac{1}{c}|F|^2 - c \leq W_0(F) \leq c(|F|^2 + 1). \tag{3.24}$$

The energy W_{2D} in (3.4) is given by

$$W_{2D}(\tilde{F}) = \begin{cases} \min_{b\in\mathbb{R}^3} W_{3D}(\tilde{F}|b) & \text{if } \operatorname{rank} \tilde{F} = 2, \\ +\infty & \text{else}, \end{cases} \tag{3.25}$$

and satisfies on full-rank $\tilde{F} \in \mathbb{R}^{3\times 2}$ the estimate

$$\frac{1}{c}\left(|\tilde{F}|^2 + \frac{1}{\delta(\tilde{F})^2}\right) - c \leq W_{2D}(\tilde{F}) \leq c\left(|\tilde{F}|^2 + \frac{1}{\delta(\tilde{F})^2} + 1\right), \tag{3.26}$$

with $\delta(\tilde{F}) = |\operatorname{adj}(\tilde{F})|$.

Now, it remains to construct a recovery sequence to prove $\mathcal{I}^0$ is the Γ-limit to $\mathcal{I}^h$.

Proposition 3.3.4 *For every $y \in W^{1,2}(\Omega, \mathbb{R}^3)$ independent of z_3, there exists a sequence $\{(w^h, m^h)\} \subset C^\infty(\bar{\Omega}, \mathbb{R}^3) \times C^1(\bar{\Omega}, \mathbb{S}^2)$ such that $w^h \rightharpoonup y$ in $W^{1,2}(\Omega, \mathbb{R}^3)$ and*

$$\limsup_{h\to 0} \tilde{\mathcal{I}}^h(w^h, m^h) \leq \mathcal{I}^0(y). \tag{3.27}$$

Our construction also draws heavily from Conti and Dolzmann [31]. The main difference is that we need additional regularity for our recovery sequence m^h. We summarize the Conti-Dolzmann construction in two lemmas. The first lemma regards the construction of a sequence to go from the energy density W_{2D} to W_{2D}^{qc} on ω. For our analysis, the important observation is that in the limit the deformation gradient is constant on an increasingly large subset of ω. The second lemma regards the extension of smooth maps on ω to incompressible deformations on Ω_h.

Lemma 3.3.5 (S. Conti and G. Dolzmann [31]) *For any $y \in W^{1,2}(\omega, \mathbb{R}^3)$, there exists a sequence $\{y_j\} \subset C^\infty(\bar{\omega}, \mathbb{R}^3)$ such that* $\operatorname{rank} \nabla y_j = 2$ *everywhere, $y_j \rightharpoonup y$ in $W^{1,2}(\omega, \mathbb{R}^3)$ as $j \to \infty$, and*

$$\limsup_{j\to\infty} \int_\omega W_{2D}(\tilde{\nabla} y_j) d\tilde{x} \leq \int_\omega W_{2D}^{qc}(\tilde{\nabla} y) d\tilde{x}. \tag{3.28}$$

Moreover, the sequence has the following properties:

(i) For each $j \in \mathbb{N}$, y_j is defined on a triangulation $\mathcal{T}^j$ of ω which is the set of at most countably many disjoint open triangle ${T_i}^j$ whose union up to a null set is equal to ω, and Γ_j is the jump set given by

$$\Gamma_j := \partial\omega \cup \bigcup_i \partial {T_i}^j. \tag{3.29}$$

(ii) There is a sequence of boundary layers $\{\eta_j\}$ such that $\eta_j > 0$ and $\eta_j \to 0$ as $j \to \infty$, and the set Γ_{η_j} is defined to be

$$\Gamma_{\eta_j} := \{\tilde{x} \in \omega : \operatorname{dist}(\tilde{x}, \Gamma_j) < \eta_j\}. \tag{3.30}$$

(iii) If $T_i^{\,j} \setminus \Gamma_{\eta_j}$ *is nonempty, then* $\tilde{\nabla} y_j$ *is a constant on this set and we set*

$$\tilde{F}_i^{\,j} := \tilde{\nabla} y_j(\tilde{x}), \quad \tilde{x} \in T_i^{\,j} \setminus \Gamma_{\eta_j}. \tag{3.31}$$

(iv) $\operatorname{adj} \tilde{\nabla} y_j$ *is bounded away from zero in the sense that for some* $\epsilon_j > 0$ *sufficiently small, the inequality*

$$|\operatorname{adj} \tilde{\nabla} y_j| \geq \epsilon_j > 0, \tag{3.32}$$

holds everywhere.

Lemma 3.3.6 (Conti and Dolzmann [31]) *Let* $y, v \in C^\infty(\bar{\omega}, \mathbb{R}^3)$ *satisfy*

$$\det(\tilde{\nabla} y | v) = 1 \quad \text{in } \omega. \tag{3.33}$$

Then there exists an $h_0 > 0$ *and an extension* $y^{h_0} \in C^\infty(\bar{\omega} \times (-h_0, h_0), \mathbb{R}^3)$ *such that* $y^{h_0}(\tilde{x}, 0) = y(\tilde{x})$ *and* $\det \nabla y^{h_0} = 1$ *everywhere. Moreover, for all* $x_3 \in (-h_0, h_0)$ *the pointwise bound*

$$|\nabla y^{h_0}(x) - (\tilde{\nabla} y | v)(x')| \leq C|x_3| \tag{3.34}$$

holds, where C can depend on y and v.

We construct a recovery sequence and thereby prove Proposition 3.3.4 in four parts. In Part 1, we take a sequence of smooth maps y_j as in Lemma 3.3.5 and show that we can construct a sequence of smooth vector fields b_j such that $\det(\tilde{\nabla} y_j | b_j) = 1$ in ω. In Part 2, we use Lemma 3.3.6 to extend y_j appropriately to a deformation on Ω, i.e $w_j^{\,h}$. In Part 3, we construct a sequence of C^1 director fields $m_j^{\,h}$ on Ω which enables passage from W_{iso}^e to W_{2D}. Finally, in Part 4 we show that we can take an appropriate diagonal sequence $h_j \to 0$ as $j \to \infty$ which proves Proposition 3.3.4.

Proof of Propsition 3.3.4

Proof of Proposition 3.3.4. Let $y \in W^{1,2}(\Omega, \mathbb{R}^3)$ independent of z_3. Then y is bounded in $W^{1,2}(\omega, \mathbb{R}^3)$ (with abuse of notation). By Lemma 3.3.5, we find a sequence $\{y_j\} \subset C^\infty(\bar{\omega}, \mathbb{R}^3)$ such that $\operatorname{rank} \tilde{\nabla} y_j = 2$ everywhere, $y_j \rightharpoonup y$ in $W^{1,2}(\omega, \mathbb{R}^3)$, the energy is bounded in the sense of (3.28), and the sequence satisfies properties (i)-(iv) from the lemma.

Part 1. We define the smooth vector field b_j on the triangulation $\mathcal{T}^{\,j}$ for y_j in Lemma 3.3.5 (i). On each nonempty $T_i^{\,j} \setminus \Gamma_{\eta_j}$ there exists a constant $\tilde{F}_i^{\,j}$ defined in

Lemma 3.3.5 (iii), and it is full rank. Then by (3.25), $W_{3D}(\tilde{F_i}^j|b)$ has a minimizer for $b \in \mathbb{R}^3$. Motivated by this observation, we let

$$b_i^j := \arg\min_{b\in\mathbb{R}^3} W_{3D}(\tilde{F_i}^j|b), \tag{3.35}$$

which via (2.22) implies

$$\det(\tilde{F_i}^j|b_i^j) = 1. \tag{3.36}$$

Consider the vector field,

$$b_0^j := \frac{\operatorname{adj}\tilde{\nabla}y_j}{|\operatorname{adj}\tilde{\nabla}y_j|^2}. \tag{3.37}$$

This is well-defined given Lemma 3.3.5 (iv). Moreover, since y_j is smooth, $b_0^j \in C^\infty(\bar{\omega}, \mathbb{R}^3)$. Further, since $\det(\tilde{F}|b) = (\operatorname{adj}\tilde{F})^T b$, we have

$$\det(\tilde{\nabla}y_j|b_0^j) = 1 \quad \text{ in } \omega. \tag{3.38}$$

Let $b_j \in C^\infty(\bar{\omega}, \mathbb{R}^3)$ be given by

$$b_j := \begin{cases} b_0^j + \psi_i\left(b_i^j - b_0^j\right) & \text{on each } T_i^j \setminus \Gamma_{\eta_j} \text{ with nonempty open subsets,} \\ b_0^j & \text{otherwise on } \omega. \end{cases} \tag{3.39}$$

Here $\psi_i \in C_0^\infty(T_i^j \setminus \Gamma_{\eta_j}, [0,1])$ is a cutoff function which equals 1 at least on the entirety of the subset $T_i^j \setminus \Gamma_{2\eta_j}$. Notice when $b_j = b_0^j$, the determinant constraint is satisfied trivially by (3.38). Conversely, combining (3.36) and (3.38),

$$\begin{aligned} \det(\tilde{\nabla}y_j|b_j) &= (\operatorname{adj}\tilde{\nabla}y_j)^T\left(b_0^j + \psi_i\left(b_i^j - b_0^j\right)\right) \\ &= \det(\tilde{\nabla}y_j|b_0^j) + \psi_i\left(\det(\tilde{F_i}^j|b_i^j) - \det(\tilde{\nabla}y_j|b_0^j)\right) \\ &= 1 \quad \text{ on each } T_i^j \setminus \Gamma_{\eta_j} \text{ with nonempty open subsets}, \end{aligned} \tag{3.40}$$

since $\tilde{\nabla}y_j = \tilde{F_i}^j$ on this set. We then conclude $\det(\tilde{\nabla}y_j|b_j) = 1$ in ω, and this completes Part 1.

Part 2. Fix $j \in \mathbb{N}$. From Part 1 we have $y_j, b_j \in C^\infty(\bar{\omega}, \mathbb{R}^3)$ satisfying $\det(\tilde{\nabla}y_j|c_j) = 1$ in ω. Hence, there exists an $h_0^j > 0$ and a $y^{h_0^j} \in C^\infty(\bar{\omega} \times (-h_0^j, h_0^j))$ such that the properties of Lemma 3.3.6 hold, replacing y with y_j and b with b_j. Let $h \in (0, h_0^j)$ and $y_j^h \in C^\infty(\overline{\Omega}_h, \mathbb{R}^3)$ be the restriction of $y^{h_0^j}$ to Ω_h. Further, let $w_j^h \in C^\infty(\overline{\Omega}, \mathbb{R}^3)$

be associated to y_j^h using (3.14). From Lemma 3.3.6, we conclude $w_j^h(\tilde{z}, 0) = y_j(\tilde{z})$, $\det \nabla_h w_j^h(z) = 1$ and

$$|\nabla_h w_j^h(z) - (\tilde{\nabla} w_j | c_j)(\tilde{z})| \leq C_j h |z_3| \leq C_j h, \quad z \in \Omega. \tag{3.41}$$

Here C_j is a constant depending on y_j and c_j, and the second inequality above follows since $z_3 \in (-1/2, 1/2)$. From these properties we conclude as $h \to 0$,

$$w_j^h \to y_j \text{ in } W^{1,2}(\Omega, \mathbb{R}^3) \quad \text{and} \quad \frac{1}{h}\partial_3 w_j^h \to b_j \text{ in } L^2(\Omega, \mathbb{R}^3). \tag{3.42}$$

This concludes Part 2.

Part 3. As in Part 2, we keep $j \in \mathbb{N}$ fixed. From Lemma 3.3.5 (i) we have that $\bigcup_i T_i^j = \omega$ (up to a set of zero measure), though this union can be countably infinite. From herein, we choose a finite collection of $N(j)$ triangles so that

$$\int_{\omega \setminus \cup_{i=1}^{N(j)} T_i^j} \left\{ W_{2D}(\tilde{\nabla} y_j) + 1 \right\} d\tilde{z} \leq \frac{1}{j}. \tag{3.43}$$

Then for each of the $N(j)$ triangles for which the set $T_i^j \setminus \Gamma_{\eta_j}$ is nonempty, let

$$n_i^j := \arg\min_{n \in \mathbb{S}^2} W_{iso}^e(\tilde{F}_i^j | b_i^j, n). \tag{3.44}$$

Further, let q_j be the piecewise constant function on $\mathbb{R}^2$ given by

$$q_j(\tilde{z}) := \begin{cases} n_i^j & \text{if } i \in \{1, \ldots, N(j)\},\ T_i^j \setminus \Gamma_{\eta_j} \text{ is nonempty, and } \tilde{z} \in T_i^j, \\ q & \text{otherwise in } \mathbb{R}^2. \end{cases} \tag{3.45}$$

Here q is a fixed vector in $\mathbb{S}^2$. Then q_j maps to $\mathbb{S}^2$, but it is not in C^1. To correct this, we employ the approach used by DeSimone in [36] (see Assertion 1).

Observe by construction the range of q_j is finite. Hence, there exists an $s_j \in \mathbb{S}^2$ and a closed ball $B_\epsilon(s_j)$ of radius $\epsilon > 0$ centered at s_j such that $(\text{range } q_j) \cap B_\epsilon(s_j) = \emptyset$. Then the stereographic projection π_{s_j} with the projection point as s_j maps the range of q_j to a bounded subset of $\mathbb{R}^2$. Let ψ_{η_j} be a standard mollifier with η_j as in Lemma 3.3.5 (ii), and consider the composition

$$n_j := \pi_{s_j}^{-1} \circ \left(\psi_{\eta_j} * \left(\pi_{s_j} \circ q_j \right) \right). \tag{3.46}$$

This composition is well-defined since the range of q_j is outside a neighborhood of the projection point s_j. Further, n_j maps to $\mathbb{S}^2$ using the definition of the inverse

of the stereographic projection. Moreover, $\pi_{s_j}^{-1}$ is differentiable and its argument $\psi_{\eta_j} * (\pi_{s_j} \circ q_j)$ is smooth. Hence, $n_j \in C^1(\mathbb{R}^2, \mathbb{S}^2)$.

Let $m_j \in C^1(\bar{\omega}, \mathbb{S}^2)$ be the restriction of n_j to the closure of ω. Further, let $m_j^h \in C^1(\bar{\Omega}, \mathbb{S}^2)$ be the extension of m_j to Ω via $m_j^h(z) := m_j(\tilde{z})$ for each $z \in \Omega$. As a final remark for this part, observe for $i \in \{1, \dots, N(j)\}$ and $\tilde{z} \in T_i^{\,j} \setminus \Gamma_{2\eta_j}$,

$$\begin{aligned} m_j^h(z) = m_j(\tilde{z}) &= \pi_{s_j}^{-1} \circ \left(\psi_{\eta_j} * \left(\pi_{s_j} \circ q_j\right)\right)(\tilde{z}) \\ &= \pi_{s_j}^{-1} \circ \left(\int_{\mathbb{R}^2} \psi_{\eta_j}(\tilde{z} - \tilde{\xi})(\pi_{s_j} \circ q_j)(\xi) d\tilde{\xi}\right) \\ &= \pi_{s_j}^{-1} \circ \left((\pi_{s_j} \circ q_j) \int_{B_{\eta_j}(z)} \psi_{\eta_j}(\tilde{z} - \tilde{\xi}) d\tilde{\xi}\right) \\ &= \pi_{s_j}^{-1} \circ (\pi_{s_j} \circ q_j) = n_i^{\,j}, \end{aligned} \tag{3.47}$$

since $B_{\eta_j}(\tilde{z}) \cap \partial T_i^{\,j} = \emptyset$ and so q_j is constant on $B_{\eta_j}(\tilde{z})$, see (3.45). This completes Part 3.

Part 4. From Parts 1-3, we have for each $j \in \mathbb{N}$ the functions $w_j^h \in C^\infty(\bar{\Omega}, \mathbb{R}^3)$ and $m_j^h \in C^1(\bar{\Omega}, \mathbb{S}^2)$ parameterized by $h \in (0, h_0^{\,j})$. It remains to bound the functional $\mathcal{I}^h$ appropriately and take the lim sup. For the bounding arguments, C shall refer to a positive constant independent of h and j which may change from line to line. From (2.1), when W_{iso}^e is finite, it satisfies a Lipschitz condition

$$\begin{aligned} |W_{iso}^e(F, n) - W_{iso}^e(G, n)| &\le |(\ell_n^*)^{-1/2}|^2 \left(|F| + |G|\right) |F - G| \\ &\le C \left(|F| + |G|\right) |F - G|. \end{aligned} \tag{3.48}$$

As asserted above, $|(\ell_n^*)^{-1/2}|$ is uniformly bounded for $n \in \mathbb{S}^2$. Then since for every $z \in \Omega$, $\det(\nabla_h w_j^h)(z) = 1$, $\det(\tilde{\nabla} y_j | b_j)(z') = 1$ and $m_j^h(z) = m_j(z) \in \mathbb{S}^2$,

$$\begin{aligned} \int_\Omega W_{iso}^e(\nabla_h w_j^h, m_j^h) dz &\le \int_\omega W_{iso}^e(\tilde{\nabla} y_j | b_j, m_j) d\tilde{z} \\ &\quad + \int_\Omega |W_{iso}^e(\nabla_h w_j^h, m_j^h) - W_{iso}^e((\tilde{\nabla} y_j | b_j), m_j^h)| dz \\ &\le \int_\omega W_{iso}^e(\tilde{\nabla} y_j | b_j, m_j) d\tilde{z} + E_{h,j}^1. \end{aligned} \tag{3.49}$$

Here $E_{h,j}^1$ is the estimate obtained from the Lipschitz condition and an application of Hölder's inequality,

$$E_{h,j}^1 := C \left(\|\nabla_h w_j^h\|_{L^2(\Omega, \mathbb{R}^3)} + \|(\tilde{\nabla} y_j | b_j)\|_{L^2(\Omega, \mathbb{R}^3)}\right) \|\nabla_h w_j^h - (\tilde{\nabla} y_j | b_j)\|_{L^2(\Omega, \mathbb{R}^3)}. \tag{3.50}$$

We now focus on the first term in the upper bound (3.49). For $i \in \{1, ..., N(j)\}$ and $\tilde{z} \in {T_i}^j \setminus \Gamma_{2\eta_j}$, observe

$$\begin{aligned} W^e_{iso}(\tilde{\nabla} y_j(\tilde{z})|b_j(\tilde{z}), m_j(\tilde{z})) &= W^e_{iso}(\tilde{F_i}^j|{b_i}^j, {n_i}^j) \\ &= \min_{n\in\mathbb{S}^2} W^e_{iso}(\tilde{F_i}^j|{b_i}^j, n) \\ &= \min_{c\in\mathbb{R}^3} W_{3D}(\tilde{F_i}^j|b) \\ &= W_{2D}(\tilde{F_i}^j) = W_{2D}(\tilde{\nabla} y_j(\tilde{z})) \end{aligned} \tag{3.51}$$

by the definitions of the arguments. Then,

$$\begin{aligned} \int_\omega W^e_{iso}(\tilde{\nabla} y_j|b_j, m_j)d\tilde{z} \leq &\int_{(\cup_{i=1}^{N(j)} {T_i}^j)\setminus\Gamma_{2\eta_j}} W_{2D}(\tilde{\nabla} y_j)d\tilde{z} \\ &+ \int_{\omega\setminus\cup_{i=1}^{N(j)} {T_i}^j} W^e_{iso}(\tilde{\nabla} y_j|b_j, m_j)d\tilde{z} + \int_{\Gamma_{2\eta_j}} W^e_{iso}(\tilde{\nabla} y_j|b_j, m_j)d\tilde{z}, \end{aligned} \tag{3.52}$$

using our result for W^e_{iso} and since each integrand is nonnegative.

We bound $W^e_{iso}(\tilde{\nabla} y_j|b_j, m_j)$ in (3.52). To obtain this bound notice $|{b_0}^j|^2 = 1/|\operatorname{adj} \tilde{\nabla} y_j|^2$ from (3.37). Further, using the coercivity condition of W_0 in (3.24), the definition of ${b_i}^j$ in (3.35), and the growth in (3.26),

$$|{b_i}^j|^2 \leq W_0(\tilde{F_i}^j|{b_i}^j) = W_{2D}(\tilde{F_i}^j) \leq c\left(|\tilde{F_i}^j|^2 + \frac{1}{|\operatorname{adj} \tilde{F_i}^j|^2} + 1\right). \tag{3.53}$$

Following these observations, we notice on the sets $T_i^j \setminus \Gamma_{\eta_j}$, $\tilde{\nabla} y_j = \tilde{F_i}^j$ by definition (see Lemma 3.3.5 (iii)) and therefore,

$$|b_j|^2 \leq 2(|{b_0}^j|^2 + |{b_i}^j|^2) \leq C\left(|\tilde{\nabla} y_j|^2 + \frac{1}{|\operatorname{adj} \tilde{\nabla} y_j|^2} + 1\right) \tag{3.54}$$

since b_j is as in (3.39). On the exceptional sets, by definition $b_j = {b_0}^j$, and the right side above is still an upper bound to $|b_j|^2$. Hence, everywhere in ω,

$$\begin{aligned} W^e_{iso}(\tilde{\nabla} y_j|b_j, m_j) &\leq c\left(|\tilde{\nabla} y_j|^2 + |b_j|^2 + 1\right) \\ &\leq C\left(|\nabla' y_j|^2 + \frac{1}{|\operatorname{adj} \tilde{\nabla} y_j|^2} + 1\right) \\ &\leq C\left(W_{2D}(\tilde{\nabla} y_j) + 1\right), \end{aligned} \tag{3.55}$$

using the growth in Proposition A.1.2, the bound above and the coercivity in (3.26). This implies the bound

$$\int_\omega W^e_{iso}(\tilde{\nabla} y_j|b_j, m_j)d\tilde{z} \leq \int_\omega W_{2D}(\tilde{\nabla} y_j)d\tilde{z} + E_j^2, \tag{3.56}$$

where recalling (3.52) and (3.43), the remainder E_j^2 is given by

$$E_j^2 := C\left(\int_{\Gamma_{2\eta_j}} \Big(W_{2D}(\tilde{\nabla} y_j) + 1\Big) d\tilde{z} + \frac{1}{j}\right). \tag{3.57}$$

To recap, from (3.49) and (3.56), the entropic part of the energy is bounded above by the estimate

$$\int_\Omega W_{iso}^e(\nabla_h w_j^h, m_j^h) \le \int_\omega W_{2D}(\tilde{\nabla} y_j) d\tilde{z} + E_{h,j}^1 + E_j^2. \tag{3.58}$$

It remains to bound the Frank elasticity.

Consider the second term of $\tilde{I}^h$ in (A.35). Our deformations and director fields have sufficient regularity, so

$$\frac{\kappa_h}{h^2}\int_\Omega |(\nabla m_j^h)(\operatorname{adj} \nabla w_j^h)|^2 dz = \kappa_h \int_\Omega |(\tilde{\nabla} m_j|0)(\operatorname{adj} \nabla_h w_j^h)|^2 dz. \tag{3.59}$$

Here, we used the identity $(1/h)(\nabla m_j)(\operatorname{adj} \nabla w_j^h) = (\nabla_h m)(\nabla_h w_j^h)$ and the definition $m_j^h(z) := m_j(\tilde{z})$. We bound the integrand by a constant independent of h. To do this, we first consider the pointwise estimate in (3.41). An application of the reverse triangle inequality on this bound yields for small h the pointwise estimate

$$\begin{aligned} |\partial_1 w_j^h(z)|^2 + |\partial_2 w_j^h(z)|^2 + \frac{1}{h^2}|\partial_3 w_j^h(z)|^2 &= |\nabla_h w_j^h(z)|^2 \\ &\le \Big(C_j h + |(\tilde{\nabla} y_j|b_j)(\tilde{z})|\Big)^2 \le (\tilde{M}_j/3)^{1/2}, \quad z \in \Omega. \end{aligned} \tag{3.60}$$

Here, $\tilde{M}_j$ is a constant which depends only on y_j and b_j. Then $F = (f_1|f_2|f_3) \in \mathbb{R}^{3\times 3}$ satisfies

$$\begin{aligned} |\operatorname{adj} F|^2 = |\operatorname{cof} F|^2 &= |(f_2 \times f_3|f_3 \times f_1|f_1 \times f_2)|^2 \\ &= |f_2 \times f_3|^2 + |f_3 \times f_1|^2 + |f_1 \times f_2|^2 \\ &\le |f_2|^2|f_3|^2 + |f_3|^2|f_1|^2 + |f_1|^2|f_2|^2, \end{aligned} \tag{3.61}$$

and so we can bound from above (3.59),

$$\begin{aligned} &\kappa_h \int_\Omega |(\tilde{\nabla} m_j|0)(\operatorname{adj} \nabla_h w)|^2 dz \le \kappa_h \int_\Omega |\tilde{\nabla} m_j|^2 |\operatorname{adj} \nabla_h w_j^h|^2 dz \\ &\le \kappa_h \int_\Omega |\tilde{\nabla} m_j|^2 \left(\frac{1}{h^2}|\partial_2 w_j^h|^2|\partial_3 w_j^h|^2 + \frac{1}{h^2}|\partial_3 w_j^h|^2|\partial_1 w_j^h|^2 + |\partial_1 w_j|^2|\partial_2 w_j|^2\right) dz. \end{aligned} \tag{3.62}$$

Applying the bound in (3.60) to this estimate, we conclude as desired

$$\frac{\kappa_h}{h^2}\int_\Omega |(\operatorname{adj} \nabla m_j^h)(\nabla w_j^h)|^2 dz \le \kappa_h \tilde{M}_j \int_\Omega |\tilde{\nabla} m_j|^2 dz =: \kappa_h M_j. \tag{3.63}$$

Here, M_j is a constant depending only on y_j, b_j and m_j.

To complete the proof of Proposition 3.3.4, it remains to show that in the limit as $h \to 0$, the energy is bounded as in (3.27). From (3.58) and (3.63),

$$\tilde{\mathcal{I}}^h(w_j^h, m_j^h) \leq \int_\omega W_{2D}(\tilde{\nabla} y_j) d\tilde{z} + E^1_{h,j} + E^2_j + \kappa_h M_j. \tag{3.64}$$

We now fix $j \in \mathbb{N}$ and take the limit as $h \to 0$. Notice from (3.42), $\|\nabla_h w_j^h - (\tilde{\nabla} y_j | b_j)\|_{L^2} \to 0$ as $h \to 0$. This implies $\|\nabla_h w_j^h\|_{L^2} \leq C_j$ for some constant C_j independent of h. With these two observations, we conclude $E^1_{h,j} \to 0$ as $h \to 0$, see (3.50). Further, since $\kappa_h \to 0$ as $h \to 0$, $\kappa_h M_j \to 0$ since M_j is independent of h. Collecting these results and combining with (3.64),

$$\begin{aligned} \limsup_{h\to 0} \tilde{\mathcal{I}}^h(w_j^h, m_j^h) &\leq \limsup_{h\to 0} \left(\int_\omega W_{2D}(\tilde{\nabla} y_j) d\tilde{z} + E^1_{h,j} + E^2_j + \kappa_h M_j \right) \\ &= \int_\omega W_{2D}(\tilde{\nabla} y_j) d\tilde{z} + E^2_j. \end{aligned} \tag{3.65}$$

Finally, using (3.28), the fact that $|\Gamma_{2\eta_j}| \to 0$ as $j \to \infty$ ($\eta_j \to 0$, see Lemma 3.3.5 (ii)), and (3.57) we conclude

$$\begin{aligned} \limsup_{j\to\infty} \limsup_{h\to 0} \tilde{\mathcal{I}}^h(w_j^h, m_j^h) &\leq \limsup_{j\to\infty} \left(\int_\omega W_{2D}(\tilde{\nabla} y_j) d\tilde{z} + E^2_j \right) \\ &\leq \int_\omega W^{qc}_{2D}(\tilde{\nabla} y) d\tilde{z}. \end{aligned} \tag{3.66}$$

We now choose a diagonal sequence $h_j \to 0$ as $j \to \infty$ so that this estimate is satisfied and $w^{h_j} \rightharpoonup y$ in $W^{1,2}(\Omega, \mathbb{R}^3)$. This completes the proof. □

3.4 Explicit formula for membrane energy density

Simply put, we have the following theorem:

Theorem 3.4.1 *The effective energy density $W^{qc}_{2D} \colon \mathbb{R}^{3\times 2} \to \mathbb{R}$ defined by*

$$W^{qc}_{2D}(\tilde{F}) := \inf \left\{ \fint_\omega W_{2D}(\tilde{F} + \tilde{\nabla}\phi) d\tilde{x} \colon \phi \in W^{1,\infty}_0(\omega, \mathbb{R}^3) \right\} \tag{3.67}$$

is, in fact, given explicitly by

$$W^{qc}_{2D}(\tilde{F}) = \psi_{2D}(\lambda_M(\tilde{F}), \delta(\tilde{F})) \tag{3.68}$$

for all $\tilde{F} \in \mathbb{R}^{3\times 2}$. Here, ψ_{2D} is defined explicitly in (3.8), $\lambda_M(\tilde{F}) := \sup_{e\in\mathbb{S}^1} |\tilde{F}e|$ and $\delta(\tilde{F}) := \operatorname{adj} \tilde{F}$.

For this theorem, we let

$$W^{mem}(\tilde{F}) := \psi_{2D}(\lambda_M(\tilde{F}), \delta(\tilde{F})), \tag{3.69}$$

for ψ_{2D} given explicitly in (3.8). We need to show that this characterizes the effective energy density of a membrane of nematic elastomer, i.e., that $W_{2D}^{qc} = W^{mem}$.

Preliminaries

For the proof, we first recall some concepts from the calculus of variations (cf. Dacorogna [33]).

We say that $f : \mathbb{R}^{3\times 2} \to \mathbb{R} \cup \{+\infty\}$ is polyconvex if there exists a convex function g which depends on $(\tilde{F}, \operatorname{adj} \tilde{F})$ (i.e., all of the minors of $\tilde{F} \in \mathbb{R}^{3\times 2}$) such that $f(\tilde{F}) = g(\tilde{F}, \operatorname{adj} \tilde{F})$. We say that $f : \mathbb{R}^{3\times 2} \to \mathbb{R} \cup \{+\infty\}$ is quasiconvex if, at every $\tilde{F} \in \mathbb{R}^{3\times 2}$, we have

$$\int_{(0,1)^2} f(\tilde{F}) d\tilde{x} \leq \int_{(0,1)^2} f(\tilde{F} + \tilde{\nabla}\phi) d\tilde{x} \tag{3.70}$$

for every $\phi \in W_0^{1,\infty}((0,1)^2, \mathbb{R}^3)$. Note that the foregoing inequality holds for every D open and bounded subset of $\mathbb{R}^2$ with $|\partial D| = 0$ (see, for instance, Ball and Murat [7]). Finally, $f : \mathbb{R}^{3\times 2} \to \mathbb{R} \cup \{+\infty\}$ is rank-one convex if $t \to f(\tilde{F} + t\tilde{A})$ is a convex function for all $\tilde{F}, \tilde{A} \in \mathbb{R}^{3\times 2}$ with rank $\tilde{A} = 1$.

If a function $f : \mathbb{R}^{3\times 2} \to \mathbb{R} \cup \{+\infty\}$ is not quasiconvex, we define f^{qc}, the quasiconvex envelope of f, as

$$f^{qc} := \sup\{h \leq f, h \text{ quasiconvex}\}. \tag{3.71}$$

Analogously, we define f^c, f^{pc}, f^{rc} as the convex, polyconvex and rank-one convex envelopes respectively of f. In the general case of extended-value functions, convexity implies polyconvexity and polyconvexity implies both rank-one convexity and quasiconvexity, but quasiconvexity alone does not imply rank-one convexity. Therefore, if $f : \mathbb{R}^{m\times n} \to \mathbb{R} \cup \{+\infty\}$, we have

$$f^{pc} \leq f^{qc}, \quad f^{pc} \leq f^{rc}. \tag{3.72}$$

On the other hand, in the case of a real-valued functions, quasiconvexity implies rank-one convexity and hence, if $f : \mathbb{R}^{m\times n} \to \mathbb{R}$, we have

$$f^c \leq f^{pc} \leq f^{qc} \leq f^{rc}. \tag{3.73}$$

We give an alternative representation formula for the rank-one convex envelope of a function $f : \mathbb{R}^{m\times n} \to \mathbb{R} \cup \{+\infty\}$:

$$f^{rc}(F) := \inf\Big\{\sum_i^K \lambda_i f(\tilde{F}_i) : \sum_i^K \lambda_i \tilde{F}_i = \tilde{F}, (\lambda_i, \tilde{F}_i) \text{ satisfy } H_K\Big\}, \tag{3.74}$$

with $\lambda_i \geq 0$ and $\sum_i^K \lambda_i = 1$. Family $(\lambda_i, \tilde{F}_i)$ satisfies a compatibility condition here labelled with H_K and defined in [33, Sec. 5.2.5]. In the same spirit we define semiconvex hulls of a compact set $\mathcal{K} \subset \mathbb{R}^{m\times n}$. The set

$$\begin{aligned}\mathcal{K}^{pc} =&\Big\{\tilde{F} \in \mathbb{R}^{m\times n} : \\ &f(\tilde{F}) \leq \sup_{\tilde{A}\in\mathcal{K}} f(\tilde{A}) \text{ for all } f : \mathbb{R}^{m\times n} \to \mathbb{R} \text{ polyconvex}\Big\}\end{aligned} \tag{3.75}$$

is the polyconvex hull of $\mathcal{K}$. The quasiconvex hull $\mathcal{K}^{qc}$ and the rank-one convex hull $\mathcal{K}^{rc}$ are defined analogously. The lamination convex hull $\mathcal{K}^{lc}$ of $\mathcal{K}$ is defined

$$\begin{aligned}\mathcal{K}^{lc} = &\Big\{\tilde{F} \in \mathbb{R}^{3\times 2} : \\ &f(\tilde{F}) \leq \sup_{\tilde{A}\in\mathcal{K}} f(\tilde{A}) \text{ for all } f : \mathbb{R}^{3\times 2} \to \mathbb{R} \cup \{+\infty\} \text{ rank-one convex}\Big\}.\end{aligned} \tag{3.76}$$

Equivalently, $\mathcal{K}^{lc}$ can be defined by successively adding rank-one segments (see DeSimone and Dolzmann [37]), i.e.,

$$\mathcal{K}^{lc} = \bigcup_{i=0}^{\infty} \mathcal{K}^{(i)}, \tag{3.77}$$

where $\mathcal{K}^0 = \mathcal{K}$ and

$$\begin{aligned}\mathcal{K}^{(i+1)} = \mathcal{K}^{(i)} \cup \Big\{\tilde{F} = \lambda\tilde{F}_1 + (1-\lambda)\tilde{F}_2 : \tilde{F}_1, \tilde{F}_2 \in \mathcal{K}^{(i)}, \\ \operatorname{rank}(\tilde{F}_1 - \tilde{F}_2) \leq 1, \lambda \in [0,1]\Big\}.\end{aligned} \tag{3.78}$$

The relations between the different notions of convexity imply the inclusions (see DeSimone and Dolzmann [37])

$$\mathcal{K}^{lc} \subseteq \mathcal{K}^{rc} \subseteq \mathcal{K}^{qc} \subseteq \mathcal{K}^{pc}. \tag{3.79}$$

We refer the interested reader to Dacarogna [33] for a discussion of all the different notions of convexity and their relations.

Proof of Theorem 3.4.1

Before we proceed with the proof of the theorem, we begin with two remarks regarding notions of quasiconvexity for extended value functions (i.e., functions taking the value $+\infty$):

Remark 3.4.2 *(i) Building off techniques due to Fonseca [42], it is well established (see [3, 31]) that since the extended value $W_{2D}\colon \mathbb{R}^{3\times 2} \to \mathbb{R}\cup\{+\infty\}$ satisfies (3.26) on full-rank matrices, the effective energy density W_{2D}^{qc} is quasiconvex, Lipschitz continuous on bounded sets, and its definition does not depend on the choice of the domain ω, as long as it is open, bounded and $|\partial\omega| = 0$. Furthermore, there exists (cf. Lemma 3.1, [31]) a constant c' such that*

$$\frac{1}{c'}|\tilde{F}|^2 - c' \leq W_{2D}^{qc}(\tilde{F}) \leq c'|\tilde{F}|^2 + c'. \tag{3.80}$$

(ii) Some care needs to be taken when dealing with extended real-valued quasiconvex functions. Indeed, the fact that a function $f : \mathbb{R}^{3\times 2} \to \mathbb{R}\cup\{+\infty\}$ is quasiconvex (according to the definition above) does not imply that the associated functional $\int_\omega f(\tilde{\nabla} y)d\tilde{x}$ is sequentially weak* lower semicontinuous on $W^{1,\infty}(\omega,\mathbb{R}^3)$ [7]. In the current situation, thanks to (i), the relaxed energy density has polynomial growth and therefore weak lower semincontinuity is true for the relaxed functional. Alternatively, we refer the interested reader to Ball and James [5] where a more restrictive definition of quasiconvexity for extended real value functions is presented. This definition guarantees weak lower semicontinuity of functionals associated to extended real value integrand functions. It is an easy computation to show that both the approach pursued in what follows and the relaxation technique based on the alternative definition of the quasiconvex envelope give the same results for the functional considered in this thesis.

Proof of Theorem 3.4.1. Recall that the quasiconvex envelope of an extended value function is not in general bounded from above by the rank-one convex envelope. However, we show that this bound is true for W_{2D}. By Remark 3.4.2(i), W_{2D}^{qc} is a finite-valued, a quasiconvex function and $W_{2D}^{qc} = (W_{2D}^{qc})^{qc}$. Therefore, if we substitute $f = W_{2D}^{qc}$ in (3.73) we obtain

$$(W_{2D}^{qc})^{pc} \leq (W_{2D}^{qc})^{qc} \leq (W_{2D}^{qc})^{rc}. \tag{3.81}$$

Then, by (3.72) we conclude

$$W_{2D}^{pc} \equiv (W_{2D}^{pc})^{pc} \leq (W_{2D}^{qc})^{pc} \leq (W_{2D}^{qc})^{qc} \leq (W_{2D}^{qc})^{rc} \leq W_{2D}^{rc} \tag{3.82}$$

and recover the classical inequality

$$(W_{2D})^{pc} \leq (W_{2D})^{qc} \leq (W_{2D})^{rc}. \tag{3.83}$$

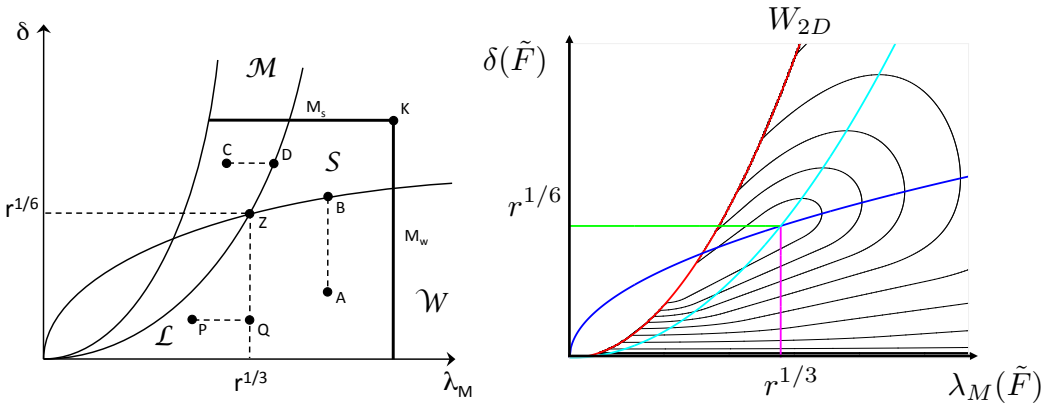

Figure 3.3: (a) Idea of the proof of Lemma 3.4.5. (b) Level curves of W_{2D} in the space (λ_M, δ).

We show in Lemma 3.4.3 and Lemma 3.4.4 that $W^{mem} \leq W^{pc}_{2D}$. We show in Lemma 3.4.5 that $W^{rc}_{2D} \leq W^{mem}$. Combining these with (3.231),

$$W^{mem} \leq W^{pc}_{2D} \leq W^{qc}_{2D} \leq W^{rc}_{2D} \leq W^{mem}, \tag{3.84}$$

and the result follows. □

Step 1: A formula for W_{2D}

Lemma 3.4.3 *W_{2D} defined in (3.3) has the explicit form as provided in (3.4), (3.5) and (3.6). Equivalently,*

$$W_{2D}(\tilde{F}) = \begin{cases} \min_{i=1,2,3} \varphi_i(\lambda_M(\tilde{F}), \delta(\tilde{F})) & \text{if } \operatorname{rank} \tilde{F} = 2 \\ +\infty & \text{otherwise,} \end{cases} \tag{3.85}$$

where

$$\begin{aligned} \varphi_1(\lambda_M, \delta) &:= \frac{\mu}{2}\left(r^{1/3}\left(\frac{\lambda_M}{r} + \frac{\delta^2}{\lambda_M^2} + \frac{1}{\delta^2} \right) - 3 \right), \\ \varphi_2(\lambda_M, \delta) &:= \frac{\mu}{2}\left(r^{1/3}\left(\lambda_M^2 + \frac{\delta^2}{\lambda_M^2} + \frac{1}{r\delta^2} \right) - 3 \right), \\ \varphi_3(\lambda_M, \delta) &:= \begin{cases} \frac{\mu}{2}\left(r^{1/3}\left(\frac{\delta^2}{\lambda_M^2} + 2\frac{\lambda_M}{r^{1/2}\delta} \right) - 3 \right), & \text{if } \lambda_M \delta \in (r^{-1/2}, r^{1/2}) \\ +\infty & \text{otherwise.} \end{cases} \end{aligned} \tag{3.86}$$

Proof. The proof is an explicit calculation. To begin, if $\operatorname{rank} \tilde{F} \neq 2$, then $\det(\tilde{F}|b) = 0$ for every $b \in \mathbb{R}^3$. This implies $W^e_{iso}(\tilde{F}|b, n) = +\infty$ for every $b \in \mathbb{R}^3$. Then

$W_{2D}(\tilde{F}) = +\infty$. Thus for the remainder of this section, we restrict our attention to the case that rank $\tilde{F} = 2$.

Let $f_{\tilde{F},n}(b) := W_0(\tilde{F}|b,n)$ and $g_{\tilde{F}}(b) := b^T \operatorname{adj} \tilde{F} - 1$. Then, $\inf_{b\in\mathbb{R}^3} W^e_{iso}(\tilde{F}|b,n)$ is equivalent to the optimization

$$\inf_{b\in\mathbb{R}^3} \left\{ f_{\tilde{F},n}(b) : g_{\tilde{F}}(b) = 0 \right\}. \tag{3.87}$$

Here $f_{\tilde{F},n}$ is a convex, differentiable function and $g_{\tilde{F}}$ is an affine equality constraint. It follows that b_0 is a global minimizer of this optimization if and only if there exists a $\lambda \in \mathbb{R}$ such that $\nabla f_{\tilde{F},n}(b_0) + \lambda \nabla g_{\tilde{F}}(b_0) = 0$ (see, for instance, Boyd and Vandenberghe [21], Section 5.5.3). Solving this equation, we obtain

$$b_0 = \frac{(\ell^*_n) \operatorname{adj} \tilde{F}}{|(\ell^*_n)^{1/2} \operatorname{adj} \tilde{F}|^2} \tag{3.88}$$

for (ℓ^*_n) defined in (2.20).

Let $\widetilde{W}(\tilde{F},n) := W_0(\tilde{F}|b_0,n)$. Since b_0 is a global minimizer for the constrained optimization above, $\widetilde{W}(\tilde{F},n) = \inf_{b\in\mathbb{R}^3} W^e_{iso}(\tilde{F}|c,n)$. Then from (3.4), it follows that $\inf_{n\in\mathbb{S}^2} \widetilde{W}(\tilde{F},n) = W_{2D}(\tilde{F})$. For this optimization, we simplify the analysis through a change of variables. We write $\tilde{F} = Q\tilde{D}\tilde{R}$ for $Q \in SO(3)$, $\tilde{R} \in O(2)$ and $\tilde{D} = \operatorname{diag}(\lambda_M, \lambda_m)$ with $\lambda_M \geq \lambda_m > 0$ as the singular values. We can say $\lambda_m > 0$ since rank $\tilde{F} = 2$. Additionally, we set $n = Qm$, and impose the $\mathbb{S}^2$ constraint via $m_3^2 = 1 - m_1^2 - m_2^2$. Then by direct substitution,

$$\begin{aligned} \widetilde{W}(Q\tilde{D}\tilde{R}, Qm) &= \frac{\mu}{2}\left(r^{1/3}\Big(\gamma\lambda_M^2 - \xi_2(\lambda_M^2 - \lambda_m^2) + \frac{1}{r(\gamma-1)\lambda_M^2\lambda_m^2}\Big) - 3\right) \\ &=: \widetilde{\varphi}(\lambda_M, \lambda_m, \gamma, \xi_2), \end{aligned} \tag{3.89}$$

where

$$\gamma = \xi_1 + \xi_2, \quad \xi_i(m_i) = 1 - \alpha m_i^2, \quad i = 1,2, \quad \alpha = \frac{r-1}{r}. \tag{3.90}$$

Here $\alpha \in [0,1)$ since $r \geq 1$. Further, we let $\delta = \lambda_M\lambda_m$, and set

$$\begin{aligned} \varphi(\lambda_M, \delta, \xi_1, \xi_2) &:= \widetilde{\varphi}(\lambda_M, \delta/\lambda_M, \xi_1, \xi_2) \\ &= \frac{\mu}{2}\left(r^{1/3}\Big(\gamma\lambda_M^2 - \xi_2\Big(\lambda_M^2 - \frac{\delta^2}{\lambda_M^2}\Big) + \frac{1}{r(\gamma-1)\delta^2}\Big) - 3\right). \end{aligned} \tag{3.91}$$

Note that the constraint $\lambda_M \geq \lambda_m > 0$ implies $\lambda_M^2 \geq \delta > 0$.

$\widetilde{W}$ is dependent on only four constrained variables. Consider the closed set

$$\mathcal{B} := \{(\gamma, \xi_2) : \ \gamma - \xi_2 \leq 1, \ \xi_2 \in [1-\alpha, 1] \text{ and } \gamma \in [2-\alpha, 2]\}. \tag{3.92}$$

$\mathcal{B}$ combined with the constraint $\lambda_M^2 \geq \delta > 0$ gives the admissible set for φ. Hence, we have

$$\begin{aligned} W_{2D}(\tilde{F}) &= \inf_{n\in\mathbb{S}^2} \widetilde{W}(\tilde{F}, n) \\ &= \inf_{\gamma,\xi_2} \left\{\varphi(\lambda_M(\tilde{F}), \delta(\tilde{F}), \gamma, \xi_2) : \lambda_M^2 \geq \delta > 0, (\gamma, \xi_2) \in \mathcal{B}\right\}. \end{aligned} \tag{3.93}$$

Observe that

$$\begin{aligned} \inf_{\xi_2} \left\{\varphi(\lambda_M, \delta, \gamma, \xi_2) : \lambda_M^2 \geq \delta > 0, (\gamma, \xi_2) \in \mathcal{B}\right\} &= \varphi(\lambda_M, \delta, \gamma, 1) \\ &=: \varphi_0(\lambda_M, \delta, \gamma) \end{aligned} \tag{3.94}$$

by (3.91) since $\lambda_M^2 - (\delta/\lambda_M)^2 \geq 0$. Then,

$$W_{2D}(\tilde{F}) = \inf_{\gamma} \left\{\varphi_0(\lambda_M(\tilde{F}), \delta(\tilde{F}), \gamma) : \lambda_M^2 \geq \delta > 0, \gamma \in [2-\alpha, 2]\right\}, \tag{3.95}$$

where

$$\varphi_0(\lambda_M, \delta, \gamma) = \frac{\mu}{2}\left(r^{1/3}\left((\gamma-1)\lambda_M^2 + \left(\frac{\delta}{\lambda_M}\right)^2 + \frac{1}{r(\gamma-1)\delta^2}\right) - 3\right). \tag{3.96}$$

φ_0 is a continuous function on this constrained set (which is moreover bounded in γ). It is also differentiable for γ in the open domain $(2-\alpha, 2)$. It follows that the infimum is attained. Further, $\bar{\gamma}$ minimizes φ_0 only if it is on the boundary, i.e $\bar{\gamma} = 2-\alpha$ or $\bar{\gamma} = 2$, or it is a critical point, i.e. $\partial_\gamma \varphi_0(\lambda_M, \delta, \bar{\gamma}) = 0$ and $\bar{\gamma} \in (2-\alpha, 2)$.

We proceed case by case. For this, we observe that in letting $\bar{\gamma} = 2-\alpha$, $\varphi_0(\lambda_M, \delta, 2-\alpha) = \varphi_1(\lambda_M, \delta)$. For the other boundary, $\bar{\gamma} = 2$, we obtain $\varphi_0(\lambda_M, \delta, 2) = \varphi_2(\lambda_M, \delta)$. Finally, in computing the critical point $\partial_\gamma \varphi_0(\lambda_M, \delta, \bar{\gamma}) = 0$, we obtain

$$\bar{\gamma} = \frac{r^{-1/2}}{\lambda_M \delta} + 1 \in (2-\alpha, 2). \tag{3.97}$$

Direct substitution $\varphi_0(\lambda_M, \delta, \bar{\gamma})$ yields the finite portion of φ_3 over its entire domain of validity $\lambda_M\delta \in (r^{-1/2}, r^{1/2})$ (i.e., since the admissible set for $\bar{\gamma}$ is provided by the inclusion in (3.97)).

To complete the proof, first observe that on $\lambda_M\delta \in (r^{-1/2}, r^{1/2})$,

$$\begin{aligned} \varphi_1 - \varphi_3 &= \frac{\mu}{2} r^{1/3}\left(r^{-1/2}\lambda_M - \frac{1}{\delta}\right)^2 \geq 0 \quad \Rightarrow \quad \varphi_3 \leq \varphi_1, \\ \varphi_2 - \varphi_3 &= \frac{\mu}{2} r^{1/3}\left(\lambda_M - \frac{r^{-1/2}}{\delta}\right)^2 \geq 0 \quad \Rightarrow \quad \varphi_3 \leq \varphi_2. \end{aligned} \tag{3.98}$$

This proves that $W_{2D} = \varphi_3 \circ (\lambda_M, \delta)$ in the region $\lambda_M \delta \in (r^{-1/2}, r^{1/2})$. To complete the computation in the remaining regions observe that

$$\varphi_1 - \varphi_2 = \frac{\mu}{2} r^{1/3} \Big(1 - \frac{1}{r}\Big)\Big(\frac{1}{\delta} + \lambda_M\Big)\Big(\frac{1}{\delta} - \lambda_M\Big), \tag{3.99}$$

yielding $\varphi_1 \leq \varphi_2$ if $\delta \geq \lambda_M^{-1}$ and $\varphi_2 \leq \varphi_1$ if $\delta \leq \lambda_M^{-1}$. Therefore we have

$$W_{2D} = \varphi_1 \circ (\lambda_M, \delta) \quad \text{ if } \lambda_M \delta \geq r^{1/2}, \delta \leq \lambda_M^2 \tag{3.100}$$

and

$$W_{2D} = \varphi_2 \circ (\lambda_M, \delta) \quad \text{ if } \lambda_M \delta \leq r^{-1/2}, \delta \leq \lambda_M^2 \tag{3.101}$$

as required. □

Step 2: Upper bound or $W^{mem} \leq W_{2D}^{pc}$

Lemma 3.4.4 *Let W^{mem} be as in (3.69) and W_{2D} as in (3.3). Then for each $\tilde{F} \in \mathbb{R}^{3\times 2}$,*

$$W^{mem}(\tilde{F}) \leq W_{2D}^{pc}(\tilde{F}). \tag{3.102}$$

Proof. We prove this in two parts. In Part 1, we prove that W^{mem} is polyconvex and in Part 2 we prove that $W^{mem} \leq W_{2D}$. The result follows.

Part 1. We now show that W^{mem} is polyconvex. First, observe from (3.69) that there exists a function $\psi : \mathbb{R}^2_+ \to \mathbb{R}$ (here by $\mathbb{R}_+$ we denote the set of all non-negative real numbers) such that

$$W^{mem}(\tilde{F}) = \psi(\lambda_M(\tilde{F}), \delta(\tilde{F})). \tag{3.103}$$

It also follows by verification (also see Proposition 2 of DeSimone and Dolzmann [37]) that ψ is convex and ψ is non-decreasing in each argument (i.e., $\psi(s,t)$ in nondecreasing in s for fixed t and nondecreasing in t for fixed s. We then notice that $\lambda_M(\tilde{F}) = \sup_{m\in\mathbb{S}^1} |\tilde{F}m|$ is convex in $\tilde{F}$. Further, $\delta(\tilde{F}) = |\operatorname{adj} \tilde{F}|$ is convex in $\operatorname{adj} \tilde{F}$. Since the composition of a convex function with a non-decreasing and convex function results in a convex function, we conclude that there exists a convex function $g : \mathbb{R}^{3\times 2} \times \mathbb{R}^3 \to \mathbb{R}$ such that

$$\psi(\lambda_M(\tilde{F}), \delta(\tilde{F})) = g(\tilde{F}, \operatorname{adj} \tilde{F}). \tag{3.104}$$

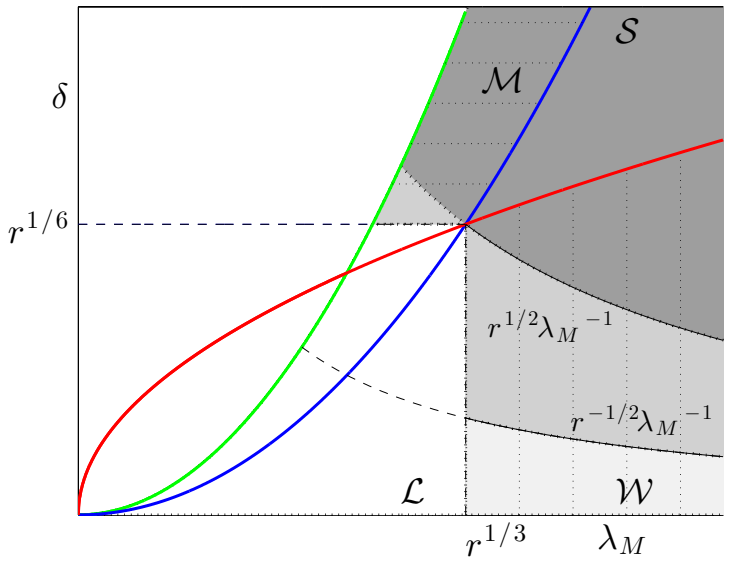

Figure 3.4: Regions where the comparison for W^{mem} and the functions φ_1 (dark gray), φ_2 (light gray) and φ_3 (silver/intermediate gray) occurs.

Combining with (3.103), we conclude that

$$W^{mem}(\tilde{F}) = g(\tilde{F}, \operatorname{adj}\tilde{F}) \tag{3.105}$$

for convex g. By definition of polyconvexity, W^{mem} is polyconvex.

Part 2. We now show that $W^{mem} \leq W_{2D}$. We show by explicit calculation that

$$W^{mem}(\tilde{F}) \leq \varphi_i(\lambda_m(\tilde{F}), \delta(\tilde{F})), \quad i = 1, \dots 3. \tag{3.106}$$

It follows that

$$\begin{aligned} W^{mem}(\tilde{F}) &= \psi_{2D}(\lambda_M(\tilde{F}), \delta(\tilde{F})) \\ &\leq \min_{i\in\{1,\dots,3\}} \varphi_i(\lambda_m(\tilde{F}), \delta(\tilde{F})) = W_{2D}(\tilde{F}) \end{aligned} \tag{3.107}$$

from (3.85).

$\psi_{2D} \leq \varphi_2$: First, in the region $\mathcal{L}$ of liquid behavior there is nothing to prove. Therefore, referring to Figure 3.4, we are left with showing that $\psi_{2D} \leq \varphi_2$ in the light gray region of equations for $r^{1/3} < \lambda_M \leq r^{-1/2}\delta^{-1}$. Recalling that in this region $\psi_{2D} = \frac{\mu}{2}(r^{1/3}(\lambda_M^2 r^{-1} + 2\lambda_M^{-1} - 3)$, it is enough to prove that

$$\frac{\lambda_M^2}{r} + \frac{2}{\lambda_M} \leq \inf_{\delta}\left\{\left(\lambda_M^2 + \frac{\delta^2}{\lambda_M^2} + \frac{1}{r\delta^2}\right) \quad \text{for: } \delta \leq r^{-1/2}\lambda_M^{-1},\ \lambda_M > r^{1/3}\right\}. \tag{3.108}$$

The critical point of $\lambda_M^2 + \delta^2\lambda_M^{-2} + r^{-1}\delta^{-2}$ is attained at $\delta^2 = \lambda_M r^{-1/2}$. This corresponds to a minimum, yielding the following inequality

$$\frac{\lambda_M^2}{r} + \frac{2}{\lambda_M} \leq \lambda_M^2 + \frac{2}{\lambda_M r^{1/2}} \tag{3.109}$$

which is indeed true for $\lambda_M > r^{1/3}$. Then, evaluation of $\lambda_M^2 + \delta^2\lambda_M^{-2} + r^{-1}\delta^{-2}$ along the curve $\delta = r^{-1/2}\lambda_M^{-1}$ does not improve the inequality above.

$\psi_{2D} \leq \varphi_1$: We focus on the interval $\delta \geq r^{1/2}\lambda_M^{-1}$ corresponding (if again we ignore the region $\mathcal{L}$) to the dark gray area in Figure 3.4. This set has a non-empty intersection with both the simple-laminate regions $\mathcal{M}$, $\mathcal{W}$ and the regime of solid behavior $\mathcal{S}$. First of all, notice that if $(\lambda_M, \delta) \in \mathcal{S}$ then $W^{mem} \equiv W_{2D}$ and there is nothing to prove.

Let us assume $r^{-1/2}\lambda_M^2 < \delta \leq \lambda_M^2$, $\delta \geq r^{1/2}\lambda_M^{-1}$. This corresponds to a subset of $\mathcal{M}$ for which we have $\psi_{2D} = \frac{\mu}{2}(r^{1/3}(2\delta r^{-1/2} + \delta^{-2}) - 3)$. We are left with the inequality

$$\frac{2\delta}{r^{1/2}} + \frac{1}{\delta^2} \leq \frac{\lambda_M^2}{r} + \frac{\delta^2}{\lambda_M^2} + \frac{1}{\delta^2} \quad \text{for } r^{-1/2}\lambda_M^2 < \delta \leq \lambda_M^2, \delta \geq r^{1/2}\lambda_M^{-1}, \tag{3.110}$$

which is trivially true.

Then, let us assume $r^{1/2}\lambda_M^{-1} \leq \delta < \lambda_M^{1/2}$. This is a subset of the region $\mathcal{W}$ for which we have $\psi_{2D} = \frac{\mu}{2}(r^{1/3}((\lambda_M^2 r^{-1} + 2\lambda_M^{-1}) - 3)$. The inequality

$$\frac{\lambda_M^2}{r} + \frac{2}{\lambda_M} \leq \frac{\lambda_M^2}{r} + \frac{\delta^2}{\lambda_M^2} + \frac{1}{\delta^2} \quad \text{for } r^{1/2}\lambda_M^{-1} \leq \delta < \lambda_M^{1/2}, \tag{3.111}$$

follows trivially.

$\psi_{2D} \leq \varphi_3$: We now focus on the interval $\delta^{-1}r^{-1/2} < \lambda_M < \delta^{-1}r^{1/2}$ corresponding to the silver/intermediate gray area in Fig. 3.4. Notice that if we remove the region $\mathcal{L}$ (for which there is nothing to prove), we are left with two disjoint subsets.

We begin with considering $\lambda_M > r^{1/3}$. Since in this region $\psi_{2D} = \frac{\mu}{2}(r^{1/3}(\lambda_M^2 r^{-1} + 2\lambda_M^{-1} - 3)$, it is enough to show that

$$\begin{aligned} \frac{\lambda_M^2}{r} + \frac{2}{\lambda_M} \leq \inf\Big\{\Big(&\frac{\delta^2}{\lambda_M^2} + \frac{2\lambda_M}{r^{1/2}\delta}\Big) \\ &\text{for } \frac{1}{\lambda_M}r^{-1/2} < \delta < \frac{1}{\lambda_M}r^{1/2}, \lambda_M > r^{1/3}\Big\}, \end{aligned} \tag{3.112}$$

which is equivalent to

$$\frac{\lambda_M^2}{r} + \frac{2}{\lambda_M} \leq \inf\Big\{\Big(\lambda_m^2 + 2\frac{1}{r^{1/2}\lambda_m}\Big) \quad \text{for } \frac{1}{\lambda_M^2} r^{-1/2} < \lambda_m < \frac{1}{\lambda_M^2} r^{1/2}, \lambda_M > r^{1/3}\Big\}. \tag{3.113}$$

The critical point of $\lambda_m^2 + 2r^{-1/2}\lambda_m^{-1}$ is attained at $(\lambda_m, \lambda_M) = (r^{-1/6}, r^{1/3}) \in \mathcal{L}$. Then, we have to evaluate $\lambda_m^2 + 2r^{-1/2}\lambda_m^{-1}$ on the curves of equations $\lambda_m = \lambda_M^{-2} r^{-1/2}$ and $\lambda_m = \lambda_M^{-2} r^{1/2}$. Notice that, for $\lambda_m = r^{1/2}\lambda_M^{-2}$ we have that $\varphi_3 = \varphi_1$ while for $\lambda_m = r^{-1/2}\lambda_M^{-2}$ we have $\varphi_3 = \varphi_2$ and from discussion of these cases previously, it therefore follows that (3.113) is true.

To conclude, we have to prove that the inequality $\psi_{2D} \leq \varphi_3$ holds in the remaining subregion defined by $\lambda_M^2 \geq \delta$, $\delta > r^{1/6}$ and $\delta < r^{1/2}\lambda_M^{-1}$. This subset is contained in the region $\mathcal{M}$ in which case we have $\psi_{2D} = \frac{\mu}{2}(r^{1/3}(2\delta r^{-1/2} + \delta^{-2}) - 3)$. Therefore, we are left with proving the inequality

$$\frac{2\delta}{r^{1/2}} + \frac{1}{\delta^2} \leq \inf\Big\{\Big(\frac{\delta^2}{\lambda_M^2} + \frac{2\lambda_M}{r^{1/2}\delta}\Big) \quad \text{for } \delta^{1/2} \leq \lambda_M, \delta > r^{1/6}, \delta < \frac{r^{1/2}}{\lambda_M}\Big\}, \tag{3.114}$$

i.e., equivalently

$$\frac{2\delta}{r^{1/2}} + \frac{1}{\delta^2} \leq \inf\Big\{\Big(\lambda_m^2 + \frac{2}{r^{1/2}\lambda_m}\Big) \quad \text{for } \lambda_m \leq \delta^{1/2}, \delta > r^{1/6}, \lambda_m > r^{-1/2}\delta^2\Big\}. \tag{3.115}$$

In order to prove the inequality above, it is enough to evaluate the function $\lambda_m^2 + 2r^{-1/2}\lambda_m^{-1}$ on the boundary of the region defined on the right hand side of (3.115). This yields the following two relations

$$\begin{aligned} &\frac{2\delta}{r^{1/2}} + \frac{1}{\delta^2} \leq \delta + \frac{2}{r^{1/2}\delta^{1/2}} \quad \text{for } \delta \in (r^{1/6}, r^{1/3}), \\ &\frac{2\delta}{r^{1/2}} + \frac{1}{\delta^2} \leq r^{-1}\delta^4 + \frac{2}{\delta^2} \quad \text{for } \delta \in (r^{1/6}, r^{1/3}), \end{aligned} \tag{3.116}$$

obtained by evaluating $\lambda_m^2 + 2r^{-1/2}\lambda_m^{-1}$ for $\lambda_m = \delta^{1/2}$ and $\lambda_m = r^{-1/2}\delta^2$, respectively. To show that the former holds it is convenient to operate the change of variable $(r^{1/4}, r^{1/2}) \ni \xi := \delta^{3/2}$ and thus, writing the former equation in (3.116) as follows,

$$\xi^2(r^{1/2} - 2) + 2\xi - r^{1/2} \geq 0 \quad \text{for } \xi \in (r^{1/4}, r^{1/2}), \tag{3.117}$$

which can be easily shown to be true for all $r \geq 1$. Then, it is immediate to prove the latter inequality in (3.116).

This exhausts all cases, and so the proof is complete. □

Step 3: Lower bound or $W_{2D}^{rc} \leq W^{mem}$

Lemma 3.4.5 *Let W^{mem} be as in (3.69) and W_{2D} as in (3.4). Then, for each $\tilde{F} \in \mathbb{R}^{3\times 2}$,*

$$W_{2D}^{rc}(\tilde{F}) \leq W^{mem}(\tilde{F}). \tag{3.118}$$

The proof makes repeated use of lamination. We collect the calculations in the following proposition.

Proposition 3.4.6 *Let $q, d \in \mathbb{R}$ with $q > 0$, $q^2 \geq d$ and define*

$$\begin{aligned} \mathcal{K} &:= \{\tilde{F} \in \mathbb{R}^{3\times 2} : \lambda_M(\tilde{F}) = q,\ \delta(\tilde{F}) = d\}, \\ \mathcal{K}_w &:= \{\tilde{F} \in \mathbb{R}^{3\times 2} : \lambda_M(\tilde{F}) = q,\ \delta(\tilde{F}) \in [0, d]\}, \\ \mathcal{K}_s &:= \{\tilde{F} \in \mathbb{R}^{3\times 2} : \lambda_M(\tilde{F}) \in [d^{1/2}, q],\ \delta(\tilde{F}) = d\}. \end{aligned} \tag{3.119}$$

Then, for $d > 0$, $\mathcal{K}_w \subset \mathcal{K}^{(1)}$ and for $d \geq 0$, $\mathcal{K}_s \subset \mathcal{K}^{(1)}$.

Proof. We begin with $\mathcal{K}_w$. Let $\tilde{F} \in \mathcal{K}_w$ with $\lambda_M(\tilde{F}) = q$, $\delta(\tilde{F}) = \bar{\delta} \in [0, d]$. Using the polar decomposition theorem we can take

$$\tilde{F} = \begin{pmatrix} q & 0 \\ 0 & \frac{\bar{\delta}}{q} \\ 0 & 0 \end{pmatrix}. \tag{3.120}$$

Define

$$\tilde{F}^{\pm} = \begin{pmatrix} q & 0 \\ 0 & \pm\frac{d}{q} \\ 0 & 0 \end{pmatrix}; \quad \theta = \frac{1}{2}\left(1 + \frac{\bar{\delta}}{d}\right). \tag{3.121}$$

Note that $\tilde{F}^{\pm} \in \mathcal{K}$, $\theta \in [0, 1]$ since $\bar{\delta} \leq d$, rank $(\tilde{F}^{+} - \tilde{F}^{-}) = 1$ and $\tilde{F} = \theta\tilde{F}^{+} + (1 - \theta)\tilde{F}^{-}$. Therefore, $\mathcal{K}_w \subset \mathcal{K}^{(1)}$.

The proof of $\mathcal{K}_s \subset \mathcal{K}^{(1)}$ is similar (also see [37, Theorem 3.1]). Again, using the polar decomposition theorem, we can take $\tilde{F} \in \mathcal{K}_s$ as a diagonal matrix. First, let

us assume $c \neq 0$ and $\sqrt{d} \leq c \leq q$ which corresponds to $c \geq d/c$ and define

$$\tilde{F}^{\pm} := \begin{pmatrix} c & \pm\xi \\ 0 & \frac{d}{c} \\ 0 & 0 \end{pmatrix}. \tag{3.122}$$

Note $\delta(\tilde{F}^{\pm}) = d$. Further, the eigenvalues of $(\tilde{F}^{\pm})^T \tilde{F}^{\pm}$ are

$$\frac{1}{2}\left(\xi^2 + \frac{d^2}{c^2} + c^2\right) \pm \sqrt{\frac{1}{4}\left(\xi^2 + \frac{d^2}{c^2} + c^2\right)^2 - d^2}. \tag{3.123}$$

So the choice

$$\xi^2 = \frac{d^2}{q^2} + q^2 - \frac{d^2}{c^2} - c^2 = \frac{1}{q^2}\Big[q^2 - \frac{d^2}{c^2}\Big]\Big[q^2 - c^2\Big] \geq 0 \tag{3.124}$$

makes $\lambda_M(\tilde{F}^{\pm}) = q$. Therefore, $\tilde{F}^{\pm} \in \mathcal{K}$. Further, $\tilde{F} = \frac{1}{2}\tilde{F}^{+} + \frac{1}{2}\tilde{F}^{-}$ and rank $(\tilde{F}^{+} - \tilde{F}^{-}) \leq 1$. For the case $\tilde{F} \in \mathcal{K}_s$ such that $\tilde{F} = 0$, replace the diagonal entries in (3.122) with 0 and repeat the argument. Therefore, $\mathcal{K}_s \subset \mathcal{K}^{(1)}$. □

Proof of Lemma 3.4.5. We show that

$$W_{2D}^{rc}(\tilde{F}) \leq W^{mem}(\tilde{F}) \tag{3.125}$$

region by region. In the region $\mathcal{S}$, note $W_{2D} = W^{mem}$ and the result follows.

Now, let $\tilde{F} \in \mathcal{W}$ with $q = \lambda_M(\tilde{F}) \geq r^{1/3}$ and $d = \delta(\tilde{F}) \leq q^{1/2}$. This corresponds to the point A in Figure 3.3(a). Let

$$\tilde{\mathcal{K}} := \{\tilde{G} \in \mathbb{R}^{3\times 2} : \lambda_M(\tilde{G}) = q,\ \delta(\tilde{G}) = q^{1/2}\} \tag{3.126}$$

that corresponds to the point B in Figure 3.3(a). By Proposition 3.4.6, we have $\tilde{F} \in \tilde{\mathcal{K}}^{(1)}$. Therefore, there exists $\lambda \in [0,1]$ and $\tilde{G}_1, \tilde{G}_2 \in \tilde{\mathcal{K}}$ with $\operatorname{rank}(\tilde{G}_1 - \tilde{G}_2) \leq 1$ such that

$$\begin{aligned} W_{2D}^{rc}(\tilde{F}) &\leq \lambda W_{2D}^{rc}(\tilde{G}_1) + (1-\lambda) W_{2D}^{rc}(\tilde{G}_2) \\ &\leq \lambda W_{2D}(\tilde{G}_1) + (1-\lambda) W_{2D}(\tilde{G}_2) \\ &= \frac{\mu}{2}\Big[r^{1/3}\Big(\frac{q^2}{r} + \frac{2}{q}\Big) - 3\Big] \\ &= W^{mem}(\tilde{F}). \end{aligned} \tag{3.127}$$

Above, the two inequalities follow from the fact W_{2D}^{rc} is rank-one convex and $W_{2D}^{rc} \leq W_{2D}$. The two equalities follow by explicit verification of the formula.

Now, let $\tilde{F} \in \mathcal{M}$ with $d = \delta(\tilde{F}) \geq r^{1/6}$ and $q = \lambda_M(\tilde{F}) \in [d^{1/2}, r^{1/4}d^{1/2}]$. This corresponds to the point C in Figure 3.3a. Let

$$\tilde{\mathcal{K}} = \{\tilde{G} \in \mathbb{R}^{3\times 2} : \lambda_M(\tilde{G}) = r^{1/4}d^{1/2},\ \delta(\tilde{G}) = d\} \tag{3.128}$$

that corresponds to the point D in Figure 3.3(a). Therefore, by Proposition 3.4.6, we have $\tilde{F} \in \tilde{\mathcal{K}}^{(1)}$. Therefore, arguing as before, $W_{2D}^{rc}(\tilde{F}) \leq W^{mem}(\tilde{F})$.

Finally, let $\tilde{F} \in L$ with $q = \lambda_M(\tilde{F}) \leq r^{1/3}$ and $d = \delta(\tilde{F}) \leq \min\{q^2, r^{1/6}\}$. This corresponds to the point P in Figure 3.3a. Let

$$\tilde{\mathcal{K}} = \{\tilde{G} \in \mathbb{R}^{3\times 2} : \lambda_M(\tilde{G}) = r^{1/3},\ \delta(\tilde{G}) = d\} \tag{3.129}$$

and

$$\mathcal{K} = \{\tilde{G} \in \mathbb{R}^{3\times 2} : \lambda_M(\tilde{G}) = r^{1/3},\ \delta(\tilde{G}) = r^{1/6}\} \tag{3.130}$$

that correspond to the points Q and Z in Figure 3.3(a), respectively. From Proposition 3.4.6, $\tilde{F} \in \tilde{\mathcal{K}}^{(1)}$. Further, again by Proposition 3.4.6, $\tilde{\mathcal{K}} \subset \mathcal{K}^{(1)}$. In other words, $\tilde{F} \in \mathcal{K}^{(2)}$. We can again argue as above to show that $W_{2D}^{rc}(\tilde{F}) \leq 0 = W^{mem}(\tilde{F})$ as required. □

3.5 Characterization of fine-scale features

The energy density W_{2D} in (3.3) is not quasiconvex. Thus a membrane with this energy density is able to relax its energy to that of W_{2D}^{qc} through the introduction of fine-scale features. In this section, we characterize these features. Briefly, we show that the features in region $\mathcal{M}$ are essentially planar involving oscillations of the director (i.e., no wrinkling) while those in $\mathcal{W}$ are necessarily wrinkles (i.e., uniform director and out-of-plane oscillations). Further, we show that there are no fine-scale features in region $\mathcal{S}$.

To characterize the fine-scale features, we consider the two-dimensional energy

$$\mathcal{E}_{2D}(y) = \int_\omega W_{2D}(\tilde{\nabla} y)d\tilde{x} \tag{3.131}$$

subject to affine boundary conditions, i.e., the space of deformations $\mathcal{A}_{\tilde{F}_0} := \{y \in W^{1,2}(\omega, \mathbb{R}^3) :\ y - \tilde{F}_0\tilde{x} \in W_0^{1,2}(\omega, \mathbb{R}^3)\}$ with $\tilde{F}_0 \in \mathbb{R}^{3\times 2}$. It is known (cf. Lemma 3.1(ii) and Lemma 6.2, [31]) that there exist weakly converging minimizing sequences that satisfy

$$\begin{aligned} &y_j \rightharpoonup \tilde{F}_0\tilde{x} \ \text{ in } \ W^{1,2}(\omega, \mathbb{R}^3) \\ &\quad \text{with } \ \mathcal{E}_{2D}(y_j) \to \inf_{\mathcal{A}_{\tilde{F}_0}} \mathcal{E}_{2D} = |\omega| W_{2D}^{qc}(\tilde{F}_0) \ \text{ as } \ j \to \infty. \end{aligned} \tag{3.132}$$

Let $\nu_{\tilde{x}}$ be any $W^{1,2}$ gradient Young measure generated by such a sequence. Since $\{y_j\}$ is a minimizing sequence for I_{2D}, it is also a minimizing sequence for the relaxation $\int_\omega W_{2D}^{qc}(\tilde{\nabla} y)d\tilde{x}$. Further, since W_{2D}^{qc} is non-negative and bounded as in (3.80), it follows from Theorem 1.3 of Kinderlehrer and Pedregal [55] that

$$\begin{aligned} &f(\nabla y_j) \rightharpoonup \langle \nu_{\tilde{x}}, f\rangle \quad \text{in } L^1(A) \\ &\qquad \text{for any } f \in \left\{ g \in C(\mathbb{R}^{3\times 2}) \colon \sup_{\tilde{F}\in\mathbb{R}^{3\times 2}} \frac{|g(\tilde{F})|}{|\tilde{F}|^2+1} < +\infty \right\}, \end{aligned} \tag{3.133}$$

and for every measurable $A \subset \omega$ whenever the sequence $\{f(\nabla y_j)\}$ converges. As an immediate consequence, we obtain the identities

$$\langle \nu_{\tilde{x}}, \mathrm{id}\,\rangle = \tilde{F}_0, \quad \langle \nu_{\tilde{x}}, W_{2D}^{qc}\rangle = W_{2D}^{qc}(\tilde{F}_0) \quad \text{a.e. } x \in \omega. \tag{3.134}$$

Now, since W_{2D} is a normal integrand, the fundamental theorem of Young measures gives an inequality, $\liminf_{j\to\infty} I_{2D}(y_j) \geq \int_\omega \langle \nu_{\tilde{x}}, W_{2D}\rangle d\tilde{x}$ (cf. Definition 6.27 and Theorem 8.6 in Fonseca and Leoni [43]). Thus,

$$\begin{aligned} |\omega| W_{2D}^{qc}(\tilde{F}_0) = \lim_{j\to\infty} I_{2D}(y_j) &\geq \int_\omega \langle \nu_{\tilde{x}}, W_{2D}\rangle d\tilde{x} \\ &\geq \int_\omega \langle \nu_{\tilde{x}}, W_{2D}^{qc}\rangle d\tilde{x} = |\omega| W_{2D}^{qc}(\tilde{F}_0), \end{aligned} \tag{3.135}$$

where we use the fact that $W_{2D} \geq W_{2D}^{qc}$. It follows $|\omega| W_{2D}^{qc}(\tilde{F}_0) = \int_\omega \langle \nu_{\tilde{x}}, W_{2D}\rangle d\tilde{x}$. Again using the fact that $W_{2D} \geq W_{2D}^{qc}$ and (3.134), we conclude

$$\langle \nu_{\tilde{x}}, W_{2D}\rangle = W_{2D}^{qc}(\tilde{F}_0) \quad \text{a.e. } \tilde{x} \in \omega. \tag{3.136}$$

By the localizing properties of $W^{1,2}$ gradient Young measures (cf. Theorem 2.3 of Kinderlehrer and Pedregal [54]), we conclude that the fine-scale features which arise from minimizing sequences of W_{2D} are described by the homogenous $W^{1,2}$ gradient Young measures admitting the identities

$$\langle \nu, \mathrm{id}\,\rangle = \tilde{F}_0, \quad \langle \nu, W_{2D}\rangle = W_{2D}^{qc}(\tilde{F}_0). \tag{3.137}$$

The support of such Young measures is highly restricted:

Theorem 3.5.1 *Let $r > 1$, $\tilde{F}_0 \in \mathbb{R}^{3\times 2}$ and let*

$$M_{\tilde{F}_0} := \left\{ \nu \in M^{qc},\ \langle \nu, id\,\rangle = \tilde{F}_0,\ \langle \nu, W_{2D}\rangle = W_{2D}^{qc}(\tilde{F}_0) \right\} \tag{3.138}$$

be the set of homogenous $W^{1,2}$ gradient Young measures that satisfy (3.137). This set is non-empty and the following is true:

(i) (The region $\mathcal{M}$.) Suppose $(\lambda_M(\tilde{F}_0), \delta(\tilde{F}_0)) \in \mathcal{M}$. Set $\bar{\delta} := \delta(\tilde{F}_0)$ and $\bar{\lambda}_M := \lambda_M(\tilde{F}_0)$. Let the singular value decomposition of $\tilde{F}_0$ be given by $\tilde{F}_0 := Q_0\tilde{D}_0\tilde{R}_0$ for $Q_0 \in SO(3), \tilde{R}_0 \in O(2)$ and $\tilde{D}_0 := diag\,(\bar{\lambda}_M, \bar{\delta}/\bar{\lambda}_M) \in \mathbb{R}^{3\times 2}$.

Then any $\nu_{\tilde{F}_0} \in M_{\tilde{F}_0}$ satisfies

$$\begin{aligned} supp\ \nu_{\tilde{F}_0} \subset \mathcal{K}_{\mathcal{M}} := \Big\{ \tilde{F} \in \mathbb{R}^{3\times 2} \colon\ & \tilde{F} = Q_0 Q \tilde{D}_{\bar{\delta}} \tilde{R}, \\ & s.t.\ \ Q \in SO(3),\ \tilde{R} \in O(2),\ \det(\tilde{R})Qe_3 = \det(\tilde{R}_0)e_3 \Big\}, \end{aligned} \tag{3.139}$$

where $e_3 \in \mathbb{S}^2$ is orthogonal to the plane of the reference configuration of the membrane and $\tilde{D}_{\bar{\delta}} := \bar{\delta}^{1/2} diag\,(r^{1/4}, r^{-1/4}) \in \mathbb{R}^{3\times 2}$.

(ii) (The region $\mathcal{W}$.) Suppose $(\lambda_M(\tilde{F}_0), \delta(\tilde{F}_0)) \in \mathcal{W}$. Set $\bar{\lambda}_M = \lambda_M(\tilde{F}_0)$. Further, let $e_M \in \mathbb{S}^2$ and $\tilde{e}_M \in \mathbb{S}^1$ be the unique pair (up to a change in sign) of vectors which satisfy $\tilde{F}_0\tilde{e}_M = \bar{\lambda}_M e_M$.

Then any $\nu_{\tilde{F}_0} \in M_{\tilde{F}_0}$ satisfies

$$\begin{aligned} supp\ \nu_{\tilde{F}_0} \subset \mathcal{K}_{\mathcal{W}} := \Big\{ \tilde{F} \in \mathbb{R}^{3\times 2} : & (\lambda_M, \delta)(\tilde{F}) = (\bar{\lambda}_M, \bar{\lambda}_M^{1/2}), \\ & s.t.\ \ \tilde{F}\tilde{e}_M = \bar{\lambda}_M e_M \Big\}. \end{aligned} \tag{3.140}$$

(iii) (The region $\mathcal{L}$.) Suppose $(\lambda_M(\tilde{F}_0), \delta(\tilde{F}_0)) \in \mathcal{L}$.

Then any $\nu_{\tilde{F}_0} \in M_{\tilde{F}_0}$ satisfies

$$\begin{aligned} supp\ \nu_{\tilde{F}_0} \subset \mathcal{K}_{\mathcal{L}} := \Big\{ \tilde{F} \in \mathbb{R}^{3\times 2} : & (\lambda_M, \delta)(\tilde{F}) \in \mathcal{L} \\ & s.t.\ \ \lambda_M(\tilde{F})/\delta(\tilde{F}) = r^{-1/6} \Big\}. \end{aligned} \tag{3.141}$$

(iv) (The region $\mathcal{S}$.) Suppose $(\lambda_M(\tilde{F}_0), \delta(\tilde{F}_0)) \in \mathcal{S}$. Then any $\nu_{\tilde{F}_0} \in M_{\tilde{F}_0}$ is a Dirac mass, i.e., supp $\nu_{\tilde{F}_0} = \{\tilde{F}_0\}$.

This result has striking physical implications related to the instabilities of *microstructure* and *wrinkling*:

Remark 3.5.2 *(i) (The region $\mathcal{M}$.) First consider the particular case when $Q_0 = I$. Consider any $\tilde{F} \in supp\ \nu_{\tilde{F}_0}$ and its characterization in (3.139). Since $\det(\tilde{R})Qe_3 = \det(\tilde{R}_0)e_3$, it follows $Q\tilde{D}_{\bar{\delta}}\tilde{R}\tilde{v} \cdot e_3 = 0$ for each $\tilde{v} \in \mathbb{R}^2$. In other words, $Q\tilde{D}_{\bar{\delta}}\tilde{R}$ maps $\mathbb{R}^2$ to $\mathbb{R}^2$. Thus, all the oscillations are in the plane. Further, for such matrices $\tilde{F}$, $W_{2D}(\tilde{F}) = W_{3D}(\tilde{F}|c) = W^e_{iso}(\tilde{F}|b, n)$ for $b = (0, 0, \bar{\delta}^{-1})^T$ and $n \cdot e_3 = 0$. The first of these identities follows from*

the fact that $(\lambda_M(\tilde{F}), \delta(\tilde{F})) \in \mathcal{S}$ *(see Lemma 5.3 and 6.2 in Cesana et al. [25]), while the second follows from the fact that the largest principal value of* $(\tilde{F}|c)$ *is* $\lambda_M(\tilde{F})$*. Importantly, the director is always in the plane. In summary, the director oscillates in the plane and oscillations create no out-of-plane deformation. The case* $Q_0 \neq I_{3\times 3}$ *is similar except the plane is oriented by the rotation* Q_0*. Thus, the fine-scale features in* $\mathcal{M}$ *are limited to in-plane oscillations of the director. In other words, they are related to the formation of material microstructure and not structural wrinkling.*

(ii) (The region $\mathcal{W}$*.) First consider the case when* $e_M = (\tilde{e}_M, 0)^T$*. Using an argument as before, for any* $\tilde{F} \in \text{supp } \nu_{\tilde{F}_0}$*,* $W_{2D}(\tilde{F}) = W_{3D}(\tilde{F}|c) = W^e(\tilde{F}|b, n)$ *for* $b \cdot e_M = 0$*,* $|b| = \bar{\lambda}_M^{-1/2}$ *and* $n = e_M$*. In other words, the director* n *is fixed with an in-plane direction* e_M*. Further, notice* $\tilde{F}$ *in the* $\{e_M, (\tilde{e}_M^{\perp}, 0)^T, e_3\}$ *frame is necessarily of the form* $\tilde{F} = Q\tilde{D}_M$ *for* $\tilde{D}_M := diag\,(\bar{\lambda}_M, \bar{\lambda}_M^{-1/2}) \in \mathbb{R}^{3\times 2}$ *and for some* $Q \in SO(3)$ *that satisfies* $Qe_M = e_M$*. In other words, the membrane is uniformly stretched by a factor* $\bar{\lambda}_M$ *in the* e_M *direction, uniformly contracted transverse to the stretch by a factor* $\bar{\lambda}_M^{-1/2}$*, and with the fine features related to rotations about the fixed axis of stretch* e_M*. That is, these oscillations represent wrinkling or undulations perpendicular to* e_M *(i.e., the direction of maximum stretch). The general case* $e_M \neq (\tilde{e}_M, 0)^T$ *is similar except a uniform rotation orients* $(\tilde{e}_M, 0)^T$ *to* e_M*. In summary, the maximum stretch and director are fixed for this region, and undulations occur transverse to this direction. Thus, the fine-scale features in* $\mathcal{W}$ *are related to the structural wrinkling and not material microstructure.*

(iii) (The region $\mathcal{L}$*.) The region* $\mathcal{L}$ *involves only the spontaneously deformed states. However, these can be arranged in a manner such that the effective deformation is due to soft elasticity and/or crumpling.*

(iv) (The region $\mathcal{S}$*.) There are no fine-scale features associated to* $\mathcal{S}$ *since the support of* $\nu_{\tilde{F}_0}$ *is a Dirac mass.*

In summary, this theorem guarantees that effective deformation in region $\mathcal{M}$ necessarily corresponds to material microstructure only, effective deformation in region $\mathcal{W}$ necessarily corresponds to structural wrinkling only, and effective deformation in region $\mathcal{S}$ is without instability.

Proof of Theorem 3.5.1.

We now turn to the proof of the Theorem 3.5.1, which provides a characterization of the fine-scale features in the membrane. It relies on the following lemmas.

For definiteness and completeness, we introduce the notion of a gradient Young measure, which characterizes the statistics of the fine-scale oscillations in the gradients weakly converging sequences (cf. Müller [74]). We define a homogenous $W^{1,2}$ gradient Young measure to be a probability measure that satisfies Jensen's inequality for every quasiconvex function $f : \mathbb{R}^{3\times 2} \to \mathbb{R}$ whose norm can be bounded by a quadratic function. Let M denote the space of signed Radon measures on $\mathbb{R}^{3\times 2}$ with the finite mass paring

$$\langle \mu, f\rangle = \int_{\mathbb{R}^{3\times 2}} f(\tilde{F}) d\mu(\tilde{F}). \tag{3.142}$$

Then the space of homogenous $W^{1,2}$ gradient Young measures is given by

$$\begin{aligned} M^{qc} :=& \{\nu \in M : ||\nu|| = 1, \langle \nu, f\rangle \geq f(\langle \nu, \mathrm{id}\rangle) \\ & \forall \ \ f : \mathbb{R}^{3\times 2} \to \mathbb{R} \text{ quasiconvex with } |f(\tilde{F})| \leq C(|\tilde{F}|^2 + 1)\}. \end{aligned} \tag{3.143}$$

The proof of the theorem relies on the following lemmas:

Lemma 3.5.3 *Let $\tilde{F}_0 \in \mathbb{R}^{3\times 2}$ and $\bar{\delta}$ satisfy the hypotheses in Theorem 3.5.1 Part (i). Then any $\nu_{\tilde{F}_0} \in M_{\tilde{F}_0}$ satisfies*

$$\operatorname{supp} \nu_{\tilde{F}_0} \subset \{\tilde{F} \in \mathbb{R}^{3\times 2} : (\lambda_M, \delta)(\tilde{F}) = (r^{1/4}\bar{\delta}^{1/2}, \bar{\delta})\}. \tag{3.144}$$

Lemma 3.5.4 *Let $\tilde{F}_0 \in \mathbb{R}^{3\times 2}$ and $\bar{\lambda}_M$ satisfy the hypotheses of Theorem 3.5.1 Part (ii). Then any $\nu_{\tilde{F}_0} \in M_{\tilde{F}_0}$ satisfies*

$$\operatorname{supp} \nu_{\tilde{F}_0} \subset \{\tilde{F} \in \mathbb{R}^{3\times 2} : (\lambda_M, \delta)(\tilde{F}) = (\bar{\lambda}_M, \bar{\lambda}_M^{1/2})\}. \tag{3.145}$$

Proof of Lemma 3.5.3. Recall from the previous section that we may write $W_{2D}^{qc} = \psi \circ (\lambda_M, \delta)$ and $W_{2D} = \varphi \circ (\lambda_M, \delta)$ where ψ $(\varphi) : \mathcal{R} \to \mathbb{R}$ $(\mathbb{R} \cup \{+\infty\})$, respectively for $\mathcal{R} = \{(s,t) \in \mathbb{R}^2 : s^2 \geq t, t \geq 0\}$. Recall also that ψ is a convex, and it is non-decreasing in each argument. Also, $\psi \leq \varphi$. Finally, $(\lambda_M, \delta) : \mathbb{R}^{3\times 2} \to \mathcal{R}$ are quasiconvex functions bounded quadratically. Therefore, for every homogenous $W^{1,2}$ gradient Young measure with $\langle \nu, \mathrm{id}\rangle = \tilde{F}_0$,

$$\begin{aligned} W_{2D}^{qc}(\tilde{F}_0) &= \psi \circ (\lambda_M, \delta)(\langle \nu, \mathrm{id}\rangle) \\ &\leq \psi(\langle \nu, \lambda_M\rangle, \langle \nu, \delta\rangle) \\ &\leq \langle \nu, \psi \circ (\lambda_M, \delta)\rangle \\ &\leq \langle \nu, \varphi \circ (\lambda_M, \delta)\rangle = \langle \nu, W_{2D}\rangle. \end{aligned} \tag{3.146}$$

Here, the first inequality follows from the Jensen's inequality satisfied by homogenous $W^{1,2}$ gradient Young measures since (λ_M, δ) are quasiconvex with the appropriate growth and ψ is non-decreasing in each argument. The second inequality follows from the convexity of ψ, and the third follows since $\psi \leq \varphi$.

Now, for any $\nu_{\tilde{F}_0} \in M_{\tilde{F}_0}$, each inequality in (3.146) is an equality. This restricts the support of $\nu_{\tilde{F}_0}$. To deduce this restriction, suppose that the point $(\lambda_M(\tilde{F}_0), \delta(\tilde{F}_0)) \in \mathcal{M}$ corresponds to point C in Figure 3.3(a).

Consider the first inequality. By quasiconvexity and growth conditions, $\langle \nu_{\tilde{F}_0}, \lambda_M \rangle \geq \lambda_M(\tilde{F}_0)$ and $\langle \nu_{\tilde{F}_0}, \delta \rangle \geq \delta(\tilde{F}_0)$. In the (λ_M, δ) space in Figure 3.3(a), these inequalities imply the point $(\langle \nu_{\tilde{F}_0}, \lambda_M \rangle, \langle \nu_{\tilde{F}_0}, \delta \rangle)$ cannot be to the left or below point C. Further, every point to the right and above the point C has higher ψ (cf. Figure 3.2) except the line between and including the points C and D. Hence,

$$(\langle \nu_{\tilde{F}_0}, \lambda_M \rangle, \langle \nu_{\tilde{F}_0}, \delta \rangle) \in CD. \tag{3.147}$$

Next, consider the last inequality. Since $\varphi = \psi$ only on $\mathcal{S} \cup \{(s,t) \in \mathcal{L} : t/s = r^{-1/6}\} =: \mathcal{S}'$ (see Figure 3.3(b)), we conclude

$$\operatorname{supp} \nu_{\tilde{F}_0} \subset \left\{ \tilde{F} \in \mathbb{R}^{3\times 2} : (\lambda_M, \delta)(\tilde{F}) \in \mathcal{S}' \right\}. \tag{3.148}$$

It remains to consider the middle inequality in (3.146). We do this in Proposition 3.5.5 below. If the middle inequality is an equality, we show in the proposition the support of $\nu_{\tilde{F}_0}$ satisfies (3.144). This completes the proof. □

Proposition 3.5.5 *Let $\tilde{F}_0$ and $\bar{\delta}$ be as in the Theorem 3.5.1 Part (i). If $\nu_{\tilde{F}_0}$ satisfies (3.147),(3.148) and*

$$\psi(\langle \nu_{\tilde{F}_0}, \lambda_M \rangle, \langle \nu_{\tilde{F}_0}, \delta \rangle) = \langle \nu_{\tilde{F}_0}, \psi \circ (\lambda_M, \delta) \rangle, \tag{3.149}$$

then the support of $\nu_{\tilde{F}_0}$ satisfies (3.144) in Lemma 3.5.3.

Proof. Set $\mathcal{A}^+ = \{\tilde{F} : (\lambda_M, \delta)(\tilde{F}) \in \mathcal{S} \cap \{\delta > \bar{\delta}\}\}$ and

$$\theta^+ = \int_{\mathcal{A}^+} d\nu_{\tilde{F}_0}(\tilde{F}). \tag{3.150}$$

If $\theta^+ = 1$, then by the polyconvexity of δ, $\langle \nu_{\tilde{F}_0}, \delta \rangle > \bar{\delta}$ contradicting (3.147). Now consider the case $1 > \theta^+ > 0$. Set

$$\begin{aligned} \lambda_M^+ &:= \frac{1}{\theta^+} \int_{\mathcal{A}^+} \lambda_M(\tilde{F}) d\nu_{\tilde{F}_0}(\tilde{F}), \quad \lambda_M^- := \frac{1}{1-\theta^+} \int_{\mathbb{R}^{3\times 2}\setminus\mathcal{A}^+} \lambda_M(\tilde{F}) d\nu_{\tilde{F}_0}(\tilde{F}), \\ \delta^+ &:= \frac{1}{\theta^+} \int_{\mathcal{A}^+} \delta(\tilde{F}) d\nu_{\tilde{F}_0}(\tilde{F}), \qquad \delta^- := \frac{1}{1-\theta^+} \int_{\mathbb{R}^{3\times 2}\setminus\mathcal{A}^+} \delta(\tilde{F}) d\nu_{\tilde{F}_0}(\tilde{F}). \end{aligned} \tag{3.151}$$

Clearly, $\delta^+ > \bar{\delta}$ and

$$\begin{aligned} \theta^+ \lambda_M^+ + (1-\theta^+)\lambda_M^- &= \langle \nu_{\tilde{F}_0}, \lambda_M \rangle, \\ \theta^+ \delta^+ + (1-\theta^+)\delta^- &= \langle \nu_{\tilde{F}_0}, \delta \rangle. \end{aligned} \tag{3.152}$$

From the equality in (3.152), $\delta^- < \bar{\delta}$. Further, notice from the convexity of ψ that

$$\begin{aligned} \psi(\lambda_M^+, \delta^+) &\leq \frac{1}{\theta^+} \int_{\mathcal{A}^+} \psi\left(\lambda_M(\tilde{F}), \delta(\tilde{F})\right) d\nu_{\tilde{F}_0}(\tilde{F}), \\ \psi(\lambda_M^-, \delta^-) &\leq \frac{1}{1-\theta^+} \int_{\mathbb{R}^{3\times 2}\setminus\mathcal{A}^+} \psi\left(\lambda_M(\tilde{F}), \delta(\tilde{F})\right) d\nu_{\tilde{F}_0}(\tilde{F}) \ . \end{aligned} \tag{3.153}$$

Now, in the (λ_M, δ) space shown in Figure 3.3(a), the definitions above imply that the point (λ_M^+, δ^+) is a point above the line CD while (λ_M^-, δ^-) is below the line CD such that the line joining these points intersects CD. It is easy to verify by explicitly computing the derivative along such lines (or by inspecting Figure 3.2), that ψ is strictly convex in such segments. Therefore,

$$\begin{aligned} \psi(\langle \nu_{\tilde{F}_0}, \lambda_M \rangle, \langle \nu_{\tilde{F}_0}, \delta \rangle) &= \psi\left(\theta^+ \lambda_M^+ + (1-\theta^+)\lambda_M^-, \theta^+ \delta^+ + (1-\theta^+)\delta^-\right) \\ &< \theta^+ \psi(\lambda_M^+, \delta^+) + (1-\theta^+)\psi(\lambda_M^-, \delta^-) \\ &\leq \langle \nu_{\tilde{F}_0}, \psi \circ (\lambda_M, \delta) \rangle. \end{aligned} \tag{3.154}$$

The last inequality follows from (3.153). However, this contradicts the assumption (3.149).

Therefore, $\theta^+ = 0$, and

$$\operatorname{supp} \nu_{\tilde{F}_0} \subset \{(\lambda_M, \delta)(\tilde{F}) \in \mathcal{S}' : \delta(\tilde{F}) \leq \bar{\delta}\}, \tag{3.155}$$

which is the compliment of $\mathcal{A}^+$ in the set given in (3.148).

Finally, given (3.155) and since $\bar{\delta} = \langle \nu_{\tilde{F}_0}, \delta \rangle$ (see 3.147), it follows that $\operatorname{supp} \nu_{\tilde{F}_0} \subset \{(\lambda_M, \delta)(\tilde{F}) \in \mathcal{S}' : \delta(\tilde{F}) = \bar{\delta}\}$. But this is just a single point in the (λ_M, δ) space, and it's given by (3.144). Thus, we conclude the proposition. □

The proof of Lemma 3.5.4 is very similar and omitted.

Proof of Theorem 3.5.1. Existence of a $\nu_{\tilde{F}_0} \in M_{\tilde{F}_0}$ follows from the construction in the previous section.

Part (i). For any $\tilde{F}_0$ with $(\lambda_M(\tilde{F}_0), \delta(\tilde{F}_0)) \in \mathcal{M}$ and for any $\nu_{\tilde{F}_0} \in M_{\tilde{F}_0}$, the support of $\nu_{\tilde{F}_0}$ satisfies (3.144) by Lemma 3.5.3. Note that $(\lambda_M, \delta)(\tilde{F}) = (r^{1/4}\bar{\delta}^{1/2}, \bar{\delta})$ is equivalent to stating that the principal values of $\tilde{F}$ are $r^{1/4}\bar{\delta}^{1/2}$ and $r^{-1/4}\bar{\delta}^{1/2}$. Therefore, by the singular value decomposition theorem, it follows that

$$\operatorname{supp} \nu_{\tilde{F}_0} \subset \{\tilde{F} \in \mathbb{R}^{3\times 2} : \tilde{F} = Q\tilde{D}_{\bar{\delta}}\tilde{R}, Q \in SO(3), \tilde{R} \in O(2)\} =: \mathcal{K}_{supp} \tag{3.156}$$

for $\tilde{D}_{\bar{\delta}}$ given in the statement of the theorem for Part (i).

Now, for any $\tilde{D} \in \mathbb{R}^{3\times 2}, Q \in SO(3), \tilde{R} \in O(2)$, it is an easy calculation to find that $\operatorname{adj}(Q\tilde{D}\tilde{R}) = \det(\tilde{R})Q \operatorname{adj} \tilde{D}$. Further for $\tilde{D} = \operatorname{diag}(\lambda_1, \lambda_2)$, $\operatorname{adj} \tilde{D} = \lambda_1\lambda_2 e_3$. Further, the adjugate is a minor and therefore $\langle \nu_{\tilde{F}_0}, \operatorname{adj}\rangle = \operatorname{adj}(\langle \nu_{\tilde{F}_0}, \mathrm{id}\rangle) = \operatorname{adj} \tilde{F}_0$. Recalling the support (3.156) of $\nu_{\tilde{F}_0}$, we conclude

$$\begin{aligned} \det(\tilde{R}_0)Q_0e_3 &= \frac{1}{\bar{\delta}}\langle \nu_{\tilde{F}_0}, \operatorname{adj}\rangle = \frac{1}{\bar{\delta}}\int_{\mathbb{R}^{3\times 2}} \operatorname{adj} \tilde{F} d\nu_{\tilde{F}_0}(\tilde{F}) \\ &= \int_{\mathcal{K}_{supp}} \Big(\det(\tilde{R}(\tilde{F}))Q(\tilde{F})e_3\Big) d\nu_{\tilde{F}_0}(\tilde{F}). \end{aligned} \tag{3.157}$$

Note that $\det(\tilde{R}_0)Q_0e_3 \in \mathbb{S}^2$, and $\det(\tilde{R}(\tilde{F}))Q(\tilde{F})e_3 \in \mathbb{S}^2$ for each $\tilde{F} \in \mathcal{K}_{supp}$. In other words, the equation above states that an average of a distribution on $\mathbb{S}^2$ yields an element of $\mathbb{S}^2$. However, since each element of $\mathbb{S}^2$ is an extreme point, it means that the distribution is concentrated at a single point on $\mathbb{S}^2$. That is, if we let $Q^*(\tilde{F}) = Q_0^T Q(\tilde{F})$, then $\det(\tilde{R}_0)e_3 = \det(\tilde{R}(\tilde{F}))Q^*(\tilde{F})e_3$. The result follows.

Part (ii). For any $\tilde{F}_0$ with $(\lambda_M(\tilde{F}_0), \delta(\tilde{F}_0)) \in \mathcal{W}$ and for any $\nu_{\tilde{F}_0} \in M_{\tilde{F}_0}$, it follows from the definition of $e_M, \tilde{e}_M$ that

$$\int_{\mathbb{R}^{3\times 2}} \tilde{F}\tilde{e}_M d\nu_{\tilde{F}_0}(\tilde{F}) = \bar{\lambda}_M e_M. \tag{3.158}$$

So,

$$\int_{\mathbb{R}^{3\times 2}} |\tilde{F}\tilde{e}_M| d\nu_{\tilde{F}_0}(\tilde{F}) \geq \left|\int_{\mathbb{R}^{3\times 2}} \tilde{F}\tilde{e}_M d\nu_{\tilde{F}_0}(\tilde{F})\right| = |\tilde{F}_0\tilde{e}_M| = \bar{\lambda}_M. \tag{3.159}$$

However, from Lemma 3.5.4, we see that $\max_{e\in\mathbb{S}^1} |\tilde{F}e| = \lambda_M(\tilde{F}) = \bar{\lambda}_M$ for each $\tilde{F} \in \operatorname{supp} \nu_{\tilde{F}_0}$. Therefore, $|\tilde{F}\tilde{e}_M| \leq \bar{\lambda}_M$ for each $\tilde{F} \in \operatorname{supp} \nu_{\tilde{F}_0}$. We conclude that $|\tilde{F}\tilde{e}_M| = \bar{\lambda}_M$ for each $\tilde{F} \in \operatorname{supp} \nu_{\tilde{F}_0}$. Setting $\tilde{F}\tilde{e}_M = \bar{\lambda}_M e(\tilde{F})$ for $e(\tilde{F}) \in \mathbb{S}^2$ and

substituting in (3.158), we conclude that $e(\tilde{F}) = e_M$ for each $\tilde{F} \in \operatorname{supp} \nu_{\tilde{F}_0}$. The result follows.

Part (iii). For any $\tilde{F}_0$ with $(\lambda_M(\tilde{F}_0), \delta(\tilde{F}_0)) \in \mathcal{L}$, the result follows from the fact that W_{2D} is non-negative and $W_{2D}(\tilde{F}) = 0$ if and only if $\tilde{F} \in \mathcal{K}_{\mathcal{L}}$.

Part (iv). Finally, let $\tilde{F}_0 \in \mathbb{R}^{3\times 2}$ such that $(\lambda_M(\tilde{F}_0), \delta(\tilde{F}_0)) \in \mathcal{S}$, $\nu_{\tilde{F}_0} \in M_{\tilde{F}_0}$. Recall $W_{2D} = \varphi \circ (\lambda_M, \delta)$ and φ is strictly convex in $\mathcal{S}$. Thus,

$$\operatorname{supp} \nu_{\tilde{F}_0} \subset \{\tilde{F} \in \mathbb{R}^{3\times 2} \colon (\lambda_M, \delta)(\tilde{F}) = (\lambda_M, \delta)(\tilde{F}_0)\}. \tag{3.160}$$

This is actually equivalent to the set (3.162) given in Proposition 3.5.6 below since $\lambda_m = \delta/\lambda_M$. The result follows from the proposition. □

Proposition 3.5.6 *Let $\tilde{F}_0 \in \mathbb{R}^{3\times 2}$ such that the singular values satisfy the strict inequality*

$$\lambda_M(\tilde{F}_0) > \lambda_m(\tilde{F}_0) \geq 0. \tag{3.161}$$

Suppose ν is a probability measure on the space of $\mathbb{R}^{3\times 2}$ matrices such that $\langle \nu, \mathrm{id}\rangle = \tilde{F}_0$ and

$$\operatorname{supp} \nu \subset \{\tilde{F} \in \mathbb{R}^{3\times 2} \colon (\lambda_M, \lambda_m)(\tilde{F}) = (\lambda_M, \lambda_m)(\tilde{F}_0)\}. \tag{3.162}$$

Then ν (up to a set of measure zero) is a Dirac mass at $\tilde{F}_0$.

Proof. To begin, set $(\bar{\lambda}_M, \bar{\lambda}_m) = (\lambda_M(\tilde{F}_0), \lambda_m(\tilde{F}_0))$. We let $\{g_{01}, g_{02}\} \subset \mathbb{R}^3$ and $\{\tilde{f}_{01}, \tilde{f}_{02}\} \subset \mathbb{R}^2$ be sets of orthonormal vectors such that

$$\tilde{F}_0 = \bar{\lambda}_M g_{01} \otimes \tilde{f}_{01} + \bar{\lambda}_m g_{02} \otimes \tilde{f}_{02}. \tag{3.163}$$

Let $\varphi_{\tilde{f}_{01}}(\tilde{F}) := |\tilde{F}\tilde{f}_{01}|^2$. This is a convex function. Therefore, by Jensen's inequality and given $\langle \nu, \mathrm{id}\rangle = \tilde{F}_0$ with $\tilde{F}_0$ satisfying (3.163),

$$\langle \nu, \varphi_{\tilde{f}_{01}}\rangle \geq \varphi_{\tilde{f}_{01}}(\tilde{F}_0) = \bar{\lambda}_M^2. \tag{3.164}$$

Conversely, applying a similar change of variables (3.163) to the $\tilde{F} \in \operatorname{supp} \nu$, we see

$$\begin{aligned} \langle \nu, \varphi_{\tilde{f}_{01}}\rangle &= \int \left(|(\bar{\lambda}_M g_1 \otimes \tilde{f}_1 + \bar{\lambda}_m g_2 \otimes \tilde{f}_2)\tilde{f}_{01}|^2\right)(\tilde{F}) d\nu(\tilde{F}) \\ &= \int \left(\bar{\lambda}_M^2 \cos(\theta(\tilde{F}))^2 + \bar{\lambda}_m^2 \sin(\theta(\tilde{F}))^2\right) d\nu(\tilde{F}) \\ &\begin{cases} = \bar{\lambda}_M^2 & \text{if} \quad \nu(\{\tilde{F} \in \mathbb{R}^{3\times 2} \colon \sin(\theta(\tilde{F})) \neq 0\}) = 0 \\ < \bar{\lambda}_M^2 & \text{otherwise,} \end{cases} \end{aligned} \tag{3.165}$$

since by assumption $\bar{\lambda}_M > \bar{\lambda}_m$. Here, $\cos\theta$ denotes the direction cosine between $\tilde{f}_1$ and $\tilde{f}_{01}$. Combining this observation with (3.164), we deduce (up to a set of measure zero), $\sin(\theta(\tilde{F})) = 0$. This implies (up to a change in sign) $\tilde{f}_1 = \tilde{f}_{01}$ in measure. Since $\tilde{f}_1$ and $\tilde{f}_2$ are orthogonal, it follows that (up to a change in sign) $\tilde{f}_2 = \tilde{f}_{02}$ in measure.

We repeat this argument substituting $\varphi_{\tilde{f}_{01}}$ with the convex function $\varphi_{g_{01}}(\tilde{F}) = |\tilde{F}^T g_{01}|^2$. It follows that (up to a change in sign) $g_1 = g_{01}$ and $g_2 = g_{02}$ in measure. The fact that $\langle \nu, \mathrm{id}\rangle = \tilde{F}_0$ ensures the eigenvectors are fixed and not oscillating in sign with some non-zero measure. The conclusion follows. □

3.6 State of stress and connection to tension field theory

In this section, we seek to understand the state of stress in the membrane.

Consider an incompressible energy density W_{3D} of the form in (2.22) and assume W_0 is C^1 differentiable. The Piola-Kirchhoff and the Cauchy stress are defined as

$$P(F) = \nabla_F W_0(F) - p(\mathrm{cof}F) \quad \sigma(F) = (\nabla_F W_0(F))F^T - pI_{3\times 3}, \tag{3.166}$$

where p is the indeterminate pressure (Lagrange multiplier to enforce incompressibility) and $I_{3\times 3}$ is identity. We find p by requiring the tractions to be zero on faces of the membrane. Alternately, recall that we obtain the membrane energy density W_{2D} by writing $F = (\tilde{F}|c)$ and minimizing with c (when $\tilde{F}$ is full rank). The minimizer $c_{\tilde{F}}$ satisfies

$$\begin{aligned} &\nabla_c W_0(\tilde{F}|c_{\tilde{F}}) - p(\mathrm{adj}\tilde{F}) = 0 \quad \text{and} \quad c_{\tilde{F}} \cdot \mathrm{adj}\tilde{F} = \det(\tilde{F}|c_{\tilde{F}}) = 1 \\ &\quad \implies p = \nabla_c W_0(\tilde{F}|c_{\tilde{F}}) \cdot c_{\tilde{F}}. \end{aligned} \tag{3.167}$$

Above, ∇_c denotes derivative with respect to the third column of the deformation gradient. Substituting this back in (3.166) and writing $\nabla_F W_0 = (\nabla_{\tilde{F}} W_0 | \nabla_c W_0)$ we obtain a characterization of the state of stress in the membrane.

$$\begin{aligned} P_{2D}(\tilde{F}) &:= P(\tilde{F}|c_{\tilde{F}}) = (\nabla_{\tilde{F}} W_0|0) = (\nabla_{\tilde{F}} W_{2D}|0), \\ \sigma_{2D}(\tilde{F}) &:= \sigma(\tilde{F}|c_{\tilde{F}}) = (\nabla_{\tilde{F}} W_{2D})\tilde{F}^T. \end{aligned} \tag{3.168}$$

Notice that these depend only on W_{2D}.

However, the effective energy of the membrane is not W_{2D} but its relaxation W_{2D}^{qc}. In other words, energy minimization with the integral of W_{2D} can lead to fine-scale oscillations, and thus the stress may also oscillate on a fine scale. Therefore, we need to understand the overall of effective stress. Ball et al. [6] have shown that if

$f : \mathbb{R}^{n\times m} \to \mathbb{R}$ is differentiable and satisfies certain growth conditions, then f^{qc} is a C^1 function. Moreover, ∇f^{qc} can be written in terms of ∇f and a homogeneous $W^{1,p}$ gradient Young measure ν generated by minimizing sequences of $\int_\Omega f(\nabla y)dx$, i.e.,

$$\nabla f^{qc} = \int \nabla f d\nu. \tag{3.169}$$

Unfortunately, W_{2D} is an extended function (equal to $+\infty$ when rank $\tilde{F} < 2$), and the analogous result is unknown. However, our resulting effective energy W_{2D}^{qc} is finite everywhere and is differentiable (except perhaps on a boundary). Consequently, we have the following characterization of the stress:

Theorem 3.6.1 *Let $r > 1$, let $\mathcal{D} \subset \mathbb{R}^2$ be the open set $\mathcal{D} := \{(s,t) \in \mathbb{R}^2_+ : 0 < t < s^2\}$, and let $\tilde{F}_0 \in \mathbb{R}^{3\times 2}$ such that $(\lambda_M(\tilde{F}_0), \delta(\tilde{F}_0)) \in \mathcal{D}$. If $\nu_{\tilde{F}_0}$ is a homogenous $W^{1,2}$ gradient Young measure generated by minimizing sequences for the energy I_{2D} in the space $\mathcal{A}_{\tilde{F}_0}$ (see (3.131)) with support in $\mathcal{D}$, then*

$$\begin{aligned} \nabla_{\tilde{F}_0} W_{2D}^{qc} &= \int \nabla_{\tilde{F}} W_{2D} d\nu_{\tilde{F}_0}(\tilde{F}), \\ (\nabla_{\tilde{F}_0} W_{2D}^{qc})\tilde{F}_0^T &= \int (\nabla_{\tilde{F}} W_{2D})\tilde{F}^T d\nu_{\tilde{F}_0}(\tilde{F}). \end{aligned} \tag{3.170}$$

Further, the Cauchy stress $\sigma^{mem}(\tilde{F}) := (\nabla_{\tilde{F}} W_{2D}^{qc})\tilde{F}^T$ has the explicit characterization in (3.12) for any $\tilde{F} \in \mathcal{D}$.

The formula for the Cauchy stress σ^{mem} defined above is quite revealing, and we refer back to the end of Section 3.2 for the discussion on this matter.

Proof of Theorem 3.6.1.

We turn now to the proof of Theorem 3.6.1.

Proof of Theorem 3.6.1. Recall from the previous two sections that we may write $W_{2D} = \varphi \circ (\lambda_M, \delta)$ and $W_{2D}^{qc} = \psi \circ (\lambda_M, \delta)$. Now, any $\tilde{F} \in \mathbb{R}^{3\times 2}$ has the representation

$$\tilde{F} = \lambda_M g_1 \otimes \tilde{f}_1 + \lambda_m g_2 \otimes \tilde{f}_2, \tag{3.171}$$

where $\{g_1, g_2\} \subset \mathbb{R}^3$ and $\{\tilde{f}_1, \tilde{f}_2\} \subset \mathbb{R}^2$ are orthonormal and $\lambda_M \geq \lambda_m \geq 0$ are the singular values of $\tilde{F}$. These singular values (and therefore $\delta = \lambda_m \lambda_M$) are continuously differentiable with respect to $\tilde{F}$ as long as they are distinct, i.e. $\lambda_M > \lambda_m$ with

$$\nabla_{\tilde{F}} \lambda_M = g_1 \otimes \tilde{f}_1, \quad \nabla_{\tilde{F}} \lambda_m = g_2 \otimes \tilde{f}_2, \tag{3.172}$$

(cf. Corollary 3.5 and Theorem 5.1, [83]). We can use this fact and the representation for φ, ψ in Theorem 3.4.1 and Lemma 3.4.3 to conclude that W_{2D} and W_{2D}^{qc} are continuously differentiable on $\{\tilde{F} : (\lambda_M(\tilde{F}), \delta(\tilde{F})) \in \mathcal{D}\}$.

The rest of the proof is by computation and verification:

Case 1: $(\lambda_M(\tilde{F}_0), \delta(\tilde{F}_0)) \in \mathcal{M} \cap \mathcal{D}$. Set $\bar{\delta} = \delta(\tilde{F}_0)$. According to Theorem 3.5.1 Part (i), $\operatorname{supp} \nu_{\tilde{F}_0} \subset \mathcal{K}_{\mathcal{M}}$. We can now apply the representation (3.171) to $\tilde{F}_0$ and $\tilde{F} \in \operatorname{supp} \nu_{\tilde{F}_0}$ to write the identity $\tilde{F}_0 = \langle \nu_{\tilde{F}_0}, \mathrm{id} \rangle$ as

$$\begin{aligned} &\bar{\lambda}_M g_{01} \otimes \tilde{f}_{01} + \left(\frac{\bar{\delta}}{\bar{\lambda}_M}\right) g_{02} \otimes \tilde{f}_{02} \\ &\qquad = \bar{\delta}^{1/2} \int_{\mathcal{K}_{\mathcal{M}}} \left(r^{1/4} g_1 \otimes \tilde{f}_1 + r^{-1/4} g_2 \otimes \tilde{f}_2 \right)(\tilde{F}) d\nu_{\tilde{F}_0}(\tilde{F}). \end{aligned} \tag{3.173}$$

Another implication of Theorem 3.5.1 is any $\tilde{F} \in \operatorname{supp} \nu_{\tilde{F}_0}$ can be written as $Q_0 Q D_{\bar{\delta}} \tilde{R}$ where $Q_0 \in SO(3)$ arises from the identity $\tilde{F}_0 = Q_0 \tilde{D}_0 \tilde{R}_0$, for some $Q \in SO(3)$ and $\tilde{R} \in O(2)$ such that $\det(\tilde{R}) Q e_3 = \det(R_0) e_3$. Here, $e_3 \in \mathbb{S}^2$ is orthogonal to the reference configuration of the membrane. Without loss of generality, we assume $e_3 = (0, 0, 1)^T$. Now for each $\alpha = 1, 2$ there is a corresponding $c_\alpha > 0$ such that $g_\alpha \cdot (Q_0 e_3) = c_\alpha (Q_0 Q \tilde{D}_{\bar{\delta}} \tilde{R} \tilde{f}_\alpha) \cdot (Q_0 e_3) = c_\alpha (\tilde{D}_{\bar{\delta}} \tilde{R} \tilde{f}_\alpha) \cdot (Q^T e_3) = c_\alpha (\det \tilde{R} / \det \tilde{R}_0)(\tilde{D}_{\bar{\delta}} \tilde{R} \tilde{f}_\alpha) \cdot e_3 = 0$. In other words, the vectors g_1 and g_2 span the plane perpendicular to $Q_0 e_3$ for each $\tilde{F} \in \operatorname{supp} \nu_{\tilde{F}_0}$. Moreover $Q_0 e_3 = g_{01} \times g_{02}$, and therefore g_{01} and g_{02} also span this plane. Now, let $\tilde{R}_0^*$ be a 90 degree rotation about e_3 and Q_0^* be a 90 degree rotation about $Q_0 f_3$ so that $(\tilde{R}_0^*)^T \tilde{f}_{01} = \tilde{f}_{02}$, $(\tilde{R}_0^*)^T \tilde{f}_{02} = -\tilde{f}_{01}$ and $Q_0^* g_{01} = g_{02}$, $Q_0^* g_{02} = -g_{01}$. Since $\{g_1, g_2\}$ span the same plane as $\{g_{01}, g_{02}\}$, and $\{\tilde{f}_1, \tilde{f}_2\}$ the same plane as $\{\tilde{f}_{01}, \tilde{f}_{02}\}$, we have the following relation: If $\det(\tilde{R}_0) = 1$, then

$$\begin{aligned} &(\tilde{R}_0^*)^T \tilde{f}_1 = \tilde{f}_2, \quad Q_0^* g_1 = g_2 \quad \text{if} \quad \det(\tilde{R}) = 1, \\ &(\tilde{R}_0^*)^T \tilde{f}_1 = -\tilde{f}_2, \quad Q_0^* g_1 = -g_2 \quad \text{if} \quad \det(\tilde{R}) = -1. \end{aligned} \tag{3.174}$$

If $\det(\tilde{R}_0) = -1$, then

$$\begin{aligned} &(\tilde{R}_0^*)^T \tilde{f}_1 = -\tilde{f}_2, \quad Q_0^* g_1 = -g_2, \quad \text{if} \quad \det(\tilde{R}) = 1, \\ &(\tilde{R}_0^*)^T \tilde{f}_1 = \tilde{f}_2, \quad Q_0^* g_1 = g_2, \quad \text{if} \quad \det(\tilde{R}) = -1. \end{aligned} \tag{3.175}$$

Thus, pre-multiplying and post-multiplying the identity in (3.173) by $\bar{\delta}^{-1/2} Q_0^*$ and

$\tilde{R}_0^*$ respectively yields the identity

$$\begin{aligned}
&\left(\frac{\bar{\lambda}_M}{\bar{\delta}^{1/2}}\right) g_{02} \otimes \tilde{f}_{02} + \left(\frac{\bar{\delta}^{1/2}}{\bar{\lambda}_M}\right) g_{01} \otimes \tilde{f}_{01} \\
&\quad = \int_{\mathcal{K}_\mathcal{M}} \left(r^{1/4} Q_0^* g_1 \otimes (\tilde{R}_0^*)^T \tilde{f}_1 + r^{-1/4} Q_0^* g_2 \otimes (\tilde{R}_0^*)^T \tilde{f}_2 \right) (\tilde{F}) d\nu_{\tilde{F}_0}(\tilde{F}) \\
&\quad = \int_{\mathcal{K}_\mathcal{M}} \left(r^{1/4} g_2 \otimes \tilde{f}_2 + r^{-1/4} g_1 \otimes \tilde{f}_1 \right) (\tilde{F}) d\nu_{\tilde{F}_0}(\tilde{F})
\end{aligned} \tag{3.176}$$

by (3.174) and (3.175).

It is easy to verify $\frac{\partial \varphi}{\partial \lambda_M}(r^{1/4}\bar{\delta}^{1/2}, \bar{\delta}) = 0$. Thus, combining explicit differentiation evaluated in $\mathcal{K}_\mathcal{M}$ with the identity (3.176), we observe

$$\begin{aligned}
\int \nabla_{\tilde{F}} W_{2D} d\nu_{\tilde{F}_0}(\tilde{F}) &= \int \left(\frac{\partial \varphi}{\partial \lambda_M} \nabla_{\tilde{F}} \lambda_M + \frac{\partial \varphi}{\partial \delta} \nabla_{\tilde{F}} \delta \right) d\nu_{\tilde{F}_0}(\tilde{F}) \\
&= \int_{\mathcal{K}_\mathcal{M}} \left(\frac{\partial \varphi}{\partial \delta} \left[\frac{\delta}{\lambda_M} g_1 \otimes \tilde{f}_1 + \lambda_M g_2 \otimes \tilde{f}_2 \right] \right) (\tilde{F}) d\nu_{\tilde{F}_0}(\tilde{F}) \\
&= \mu r^{1/3} \int_{\mathcal{K}_\mathcal{M}} \left(\left[\frac{\delta}{\lambda_M^2} - \frac{1}{\delta^3} \right] \left[\frac{\delta}{\lambda_M} g_1 \otimes \tilde{f}_1 + \lambda_M g_2 \otimes \tilde{f}_2 \right] \right) (\tilde{F}) d\nu_{\tilde{F}_0}(\tilde{F}) \\
&= \mu r^{1/3} \left(\frac{\bar{\delta}^{1/2}}{r^{1/2}} - \frac{1}{\bar{\delta}^{3/2}} \right) \int_{\mathcal{K}_\mathcal{M}} \left(r^{-1/4} g_1 \otimes \tilde{f}_1 + r^{1/4} g_2 \otimes \tilde{f}_2 \right) (\tilde{F}) d\nu_{\tilde{F}_0}(\tilde{F}) \\
&= \mu r^{1/3} \left(\frac{\bar{\delta}^{1/2}}{r^{1/2}} - \frac{1}{\bar{\delta}^{3/2}} \right) \left(\left(\frac{\bar{\delta}^{1/2}}{\bar{\lambda}_M} \right) g_{01} \otimes \tilde{f}_{01} + \left(\frac{\bar{\lambda}_M}{\bar{\delta}^{1/2}} \right) g_{02} \otimes \tilde{f}_{02} \right) \\
&= \mu r^{1/3} \left\{ \left(\frac{\bar{\delta}}{\bar{\lambda}_M r^{1/2}} - \frac{1}{\bar{\lambda}_M \bar{\delta}} \right) g_{01} \otimes \tilde{f}_{01} + \left(\frac{\bar{\lambda}_M}{r^{1/2}} - \frac{\bar{\lambda}_M}{\bar{\delta}^2} \right) g_{02} \otimes \tilde{f}_{02} \right\}.
\end{aligned} \tag{3.177}$$

Finally, it can be verified explicitly that $\nabla_{\tilde{F}_0} W_{2D}^{qc}$ coincides with (3.177). This gives the former identity (3.170) for region $\mathcal{M} \cap \mathcal{D}$.

Similarly,

$$\begin{aligned}
\int \nabla_{\tilde{F}} W_{2D} \tilde{F}^T d\nu_{\tilde{F}_0}(\tilde{F}) &= \int_{\mathcal{K}_\mathcal{M}} \left(\frac{\partial \varphi}{\partial \delta} \nabla_{\tilde{F}} \delta \right) \tilde{F}^T d\nu_{\tilde{F}_0}(\tilde{F}) \\
&= \mu r^{1/3} \int_{\mathcal{K}_\mathcal{M}} \left(\frac{\delta^2}{\lambda_M^2} - \frac{1}{\delta^2} \right) (g_1 \otimes g_1 + g_2 \otimes g_2) (\tilde{F}) d\nu_{\tilde{F}_0}(\tilde{F}) \\
&= \mu r^{1/3} \left(\frac{\bar{\delta}}{r^{1/2}} - \frac{1}{\bar{\delta}^2} \right) \int_{\mathcal{K}_\mathcal{M}} (g_1 \otimes g_1 + g_2 \otimes g_2)(\tilde{F}) d\nu_{\tilde{F}_0}(\tilde{F}) \\
&= \mu r^{1/3} \left(\frac{\bar{\delta}}{r^{1/2}} - \frac{1}{\bar{\delta}^2} \right) \left(g_{01} \otimes g_{01} + g_{02} \otimes g_{02} \right).
\end{aligned} \tag{3.178}$$

The fourth equality uses the fact that the basis $\{g_1(\tilde{F}), g_2(\tilde{F})\}$ always spans the same plane, and the plane spanned by $\{g_{01}, g_{02}\}$. Finally, it can be verified explicitly

that $\nabla_{\tilde{F}_0} W_{2D}^{qc} \tilde{F}_0^T$ coincides with (3.178) in this region. This gives the latter identity (3.170) for region $\mathcal{M} \cap \mathcal{D}$.

Case 2: $(\lambda_M(\tilde{F}_0), \delta(\tilde{F}_0)) \in \mathcal{W} \cap \mathcal{D}$. Set $\bar{\lambda}_M = \lambda_M(\tilde{F}_0)$. Following Theorem 3.5.1 Part (ii), $\operatorname{supp} \nu_{\tilde{F}_0} \subset \mathcal{K}_{\mathcal{W}}$ and so any $\tilde{F} \in \operatorname{supp} \nu_{\tilde{F}_0}$ satisfies $(\lambda_M(\tilde{F}), \delta(\tilde{F})) = (\bar{\lambda}_M, \bar{\lambda}_M^{1/2})$. In addition, for the vectors $\tilde{f}_{01} \in \mathbb{S}^1$ and $g_{01} \in \mathbb{S}^2$ such that $\tilde{F}_0 \tilde{f}_{01} = g_{01}$, $\tilde{F} \in \operatorname{supp} \nu_{\tilde{F}_0}$ also satisfies $\tilde{F} \tilde{f}_{01} = g_{01}$. Writing $\tilde{F} \in \operatorname{supp} \nu_{\tilde{F}_0}$ as in (3.171), we observe using the properties of the set $\mathcal{K}_{\mathcal{W}}$,

$$\begin{aligned} \tilde{F} \tilde{f}_{01} &= (\lambda_M g_1 \otimes \tilde{f}_1 + (\delta/\lambda_M) g_2 \otimes f_2) \tilde{f}_{01} \\ &= (\bar{\lambda}_M g_1 \otimes \tilde{f}_1 + \bar{\lambda}_M^{-1/2} g_2 \otimes f_2) \tilde{f}_{01} \\ &= \bar{\lambda}_M \cos(\theta) g_1 + \bar{\lambda}_M^{-1/2} \sin(\theta) g_2 = \bar{\lambda}_M g_{01}. \end{aligned} \tag{3.179}$$

Here, $\cos(\theta)$ denotes the direction cosine from $\tilde{f}_{01}$ to $\tilde{f}_1$. Applying the squared norm to the identities in (3.179) yields $|\tilde{F} \tilde{f}_{01}|^2 = (\bar{\lambda}_M)^2 \cos(\theta)^2 + \bar{\lambda}_M^{-1} \sin(\theta)^2 = \bar{\lambda}_M^2$. Since $\bar{\lambda}_M^2 > \bar{\lambda}_M^{-1}$ in $\mathcal{W}$, we deduce from this equation that $\cos(\theta) = \pm 1$. That is, $\tilde{f}_1$ is up to a change in sign equal to $\tilde{f}_{01}$. Substituting for $\tilde{f}_1$ back into (3.179), we find $g_1 = \pm g_{01}$ when $\tilde{f}_1 = \pm \tilde{f}_{01}$, or alternatively

$$g_1 \otimes \tilde{f}_1 = g_{01} \otimes \tilde{f}_{01} \quad \forall \ \tilde{F} \in \operatorname{supp} \nu_{\tilde{F}_0}. \tag{3.180}$$

Now, it is easy to verify explicitly $\frac{\partial \varphi}{\partial \delta}(\bar{\lambda}_M, \bar{\lambda}_M^{1/2}) = 0$. Thus, combining explicit differentiation evaluated in $\mathcal{K}_{\mathcal{W}}$ with (3.180),

$$\begin{aligned} \int \nabla_{\tilde{F}} W_{2D} d\nu_{\tilde{F}_0}(\tilde{F}) &= \int_{\mathcal{K}_{\mathcal{W}}} \left(\frac{\partial \varphi}{\partial \lambda_M} \nabla_{\tilde{F}} \lambda_M \right) d\nu_{\tilde{F}_0}(\tilde{F}) \\ &= \mu r^{1/3} \int_{\mathcal{K}_{\mathcal{W}}} \left(\left[\frac{\lambda_M}{r} - \frac{\delta^2}{\lambda_M^3} \right] g_1 \otimes f_1 \right) (\tilde{F}) d\nu_{\tilde{F}_0}(\tilde{F}) \\ &= \mu r^{1/3} \left(\frac{\bar{\lambda}_M}{r} - \frac{1}{\bar{\lambda}_M^2} \right) \int_{\mathcal{K}_{\bar{\lambda}_M}} g_1 \otimes f_1(\tilde{F}) d\nu_{\tilde{F}_0}(\tilde{F}) \\ &= \mu r^{1/3} \left(\frac{\bar{\lambda}_M}{r} - \frac{1}{\bar{\lambda}_M^2} \right) g_{01} \otimes \bar{f}_1. \end{aligned} \tag{3.181}$$

Finally, it can be verified explicitly that $\nabla_{\tilde{F}_0} W_{2D}^{qc}$ coincides with (3.181). Therefore, the former identity (3.170) is satisfied for $\mathcal{W}$.

Similarly,

$$\begin{aligned}\int \nabla_{\tilde{F}} W_{2D} \tilde{F}^T d\nu_{\tilde{F}_0}(\tilde{F}) &= \int_{\mathcal{K}_{\mathcal{W}}} \left(\frac{\partial \varphi}{\partial \lambda_M} \nabla_{\tilde{F}} \lambda_M \right) \tilde{F}^T d\nu_{\tilde{F}_0}(\tilde{F}) \\ &= \mu r^{1/3} \int_{\mathcal{K}_{\mathcal{W}}} \left(\frac{\lambda_M^2}{r^2} - \frac{\delta^2}{\lambda_M^2} \right) g_1 \otimes g_1(\tilde{F}) d\nu_{\tilde{F}_0}(\tilde{F}) \\ &= \mu r^{1/3} \left(\frac{\bar{\lambda}_M^2}{r} - \frac{1}{\bar{\lambda}_M} \right) \int_{\mathcal{K}_{\bar{\lambda}_M}} g_1 \otimes g_1(\tilde{F}) d\nu_{\tilde{F}_0}(\tilde{F}) \\ &= \mu r^{1/3} \left(\frac{\bar{\lambda}_M^2}{r} - \frac{1}{\bar{\lambda}_M} \right) g_{01} \otimes g_{01}.\end{aligned} \tag{3.182}$$

For the last equality, recall $g_1 = \pm g_{01}$ for $\tilde{F} \in \operatorname{supp} \nu_{\tilde{F}_0}$. Finally, it is easy to verify explicitly that $\nabla_{\tilde{F}_0} W_{2D}^{qc} \tilde{F}_0^T$ coincides with (3.182) in this region. Thus, we have the latter identity (3.170) for region $\mathcal{W} \cap \mathcal{D}$.

Case 3: $(\lambda_M(\bar{F}), \delta(\bar{F})) \in \mathcal{L} \cap \mathcal{D}$. According to Theorem 3.5.1 Part (iii), $\operatorname{supp} \nu_{\tilde{F}_0} \subset \mathcal{K}_{\mathcal{L}}$. We see that $\nabla W_{2D} = 0$ on $\mathcal{K}_{\mathcal{L}}$ and similarly $\nabla W_{2D}^{qc} = 0$ on $\mathcal{L} \cap \mathcal{D}$. The identities (3.170) follow for region $\mathcal{L} \cap \mathcal{D}$.

Case 4: $(\lambda_M(\bar{F}), \delta(\bar{F})) \in \mathcal{S} \cap \mathcal{D}$. According to Theorem 3.5.1 Part (iv), $\operatorname{supp} \nu_{\tilde{F}_0}$ is a Dirac mass. According to Theorem 3.4.1, W_{2D} and W_{2D}^{qc} coincide on $\mathcal{S} \cap \mathcal{D}$. The identities (3.170) follow for region $\mathcal{S} \cap \mathcal{D}$. □

3.7 The Koiter theory for nematic elastomer sheets

The effective membrane energy described in the previous section relaxes over both microstructure and wrinkling. While this can provide insights, it is not sufficient for the purpose of understanding the formation of wrinkles or their geometry (i.e., an explicit description of the out-of-plane undulations including their amplitude and frequency). Thus, we seek also a theory that can explicitly describe the wrinkles. However, nematic elastomers can also form microstructure, and for the sheets relevant to the clamped stretch experiments, this microstructure is very fine compared to the wrinkles since $\sqrt{\kappa/\mu} \ll h$. Therefore, we seek a theory that simultaneously relaxes over microstructure and resolves wrinkles. This motivated our development of a Koiter-type theory for nematic elastomer sheets in Plucinsky and Bhattacharya [80]. Here, we first introduce the theory and comment on some of its more illuminating features. In the next section, we show that it can be obtained systematically as a dimension reduction of three dimensional elasticity.

We consider a nematic sheet with midplane $\omega \subset \mathbb{R}^2$ in the isotropic reference state. For a midplane deformation $y \colon \omega \to \mathbb{R}^3$ of the sheet, we take the Koiter elastic strain

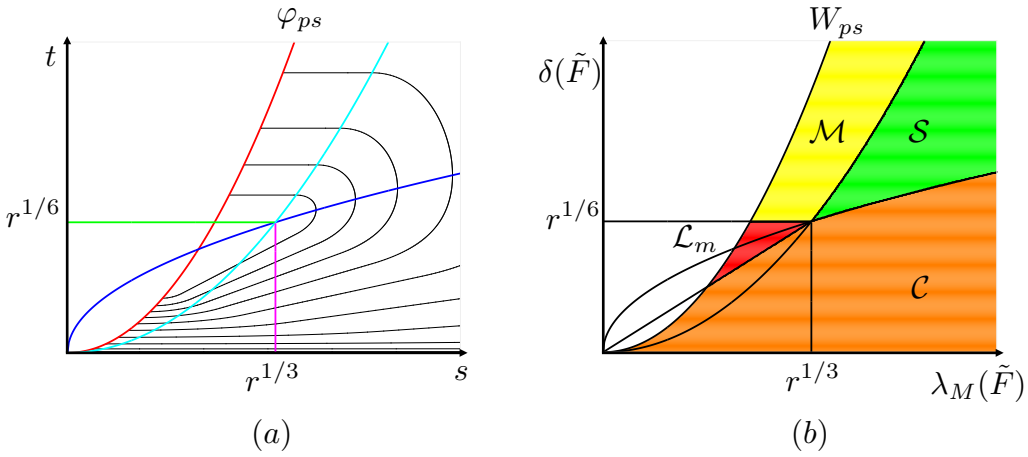

Figure 3.5: The plane-stress energy density W_{ps} for nematics. (a) Contour plots of the function φ_{ps} that describes the plane stress energy W_{ps}, (b) identification of the regions $\mathcal{L}_m, \mathcal{M}, \mathcal{C}$ and $\mathcal{S}$.

energy to be

$$\mathcal{E}_K^h(y) := h \int_\omega \left(W_{ps}(\tilde{\nabla} y) + \frac{\mu r^{1/3} h^2}{6} |\mathrm{II}_y|^2 \right) d\tilde{x}. \tag{3.183}$$

Here, the first term is term proportional to the thickness and describes the in-plane deformation accounting for the microstructure. It is given by the nematic plane-stress energy density

$$W_{ps}(\tilde{F}) := \varphi_{ps}(\lambda_M(\tilde{F}), \delta(\tilde{F})), \tag{3.184}$$

$$\varphi_{ps}(s,t) := \begin{cases} \varphi_{2D}(s,t) & \text{if } (s,t) \in \mathcal{C} \\ \psi_{2D}(s,t) & \text{if } (s,t) \in \mathcal{L}_m \cup \mathcal{M} \cup \mathcal{S}, \end{cases} \tag{3.185}$$

$$\begin{aligned} \mathcal{L}_m &:= \{(s,t) \in \mathbb{R}^+ \times \mathbb{R}^+ : t \le s^2, r^{1/6} \ge t \ge r^{-1/6} s\}, \\ \mathcal{M} &:= \{(s,t) \in \mathbb{R}^+ \times \mathbb{R}^+ : t \le s^2, t \ge r^{-1/2} s^2, t \ge r^{1/6}\}, \\ \mathcal{S} &:= \{(s,t) \in \mathbb{R}^+ \times \mathbb{R}^+ : t \le r^{-1/2} s^2, t \ge s^{1/2}\}, \\ \mathcal{C} &:= \{(s,t) \in \mathbb{R}^+ \times \mathbb{R}^+ : t \le s^{1/2}, t \le r^{-1/6} s, t \le s^{1/2}\}. \end{aligned} \tag{3.186}$$

Further, the second term is proportional to the cube of the thickness and describes the bending. It penalizes the second fundamental form of the deformed membrane,

$$\mathrm{II}_y := (\tilde{\nabla} y)^T \tilde{\nabla} N_y, \quad N_y := \frac{\partial_1 y \times \partial_2 y}{|\partial_1 y \times \partial_2 y|}. \tag{3.187}$$

Note that N_y is the surface normal to the deformed midplane of the sheet (it is *not* to be confused with the director fields n, n_0, etc.).

Before proceeding with the derivation of this theory (Section 3.8), we comment on some of its more striking features:

First, the plane-stress energy density W_{ps} has a revealing interpretation. We note that it is actually derived from W_{3D}^{qc}, an energy density for which microstructure is already completely relaxed. (This is made precise in the coming sections: see, for instance, (3.193)). Therefore, *microstructure is completely relaxed in this plane stress energy density*. Particularly, the region $\mathcal{L}_m$ (of *liquid*-like behavior) corresponds to the relaxation of microstructure and a state of zero energy and stress, and regions $\mathcal{M}$ and $\mathcal{S}$ are exactly as in the effective membrane theory.

Next, note that wrinkling and crumpling are not relaxed in this theory as region C (which coincides with unstable regions of W_{2D}, see (3.198)) is a region of *compressive* stresses in this plane-stress energy density. These instabilities are instead regularized by bending (i.e., the second term in (3.183)).

Next, turning to bending, note that the modulus of bending here is $\mu r^{1/3} h^3/3$ (two times the constant in front of the bending term in (3.183) as the modulus is by convention proportional to the stress, not the energy). This can be rewritten in terms of the Young's Modulus E as $Eh^3 r^{1/3}/9$ since nematic elastomers are incompressible with a Poisson's ratio of $1/2$. In setting $r = 1$, corresponding to an incompressible neo-Hookean sheet, this reduces to $Eh^3/9 = D$ for D the bending modulus of an incompressible and isotropic plate of initial thickness h in classical plate theory. Thus, this bending modulus is consistent with classical plate theory.

As a final comment related to bending, note that changes in thickness associated with finite-deformation are properly accounted for even though it appears that the modulus only depends on the initial thickness h. This is a consequence of the fact that the second fundamental form (3.187) is computed with respect to the reference configuration. For instance, imagine first deforming the specimen from the stress-free isotropic configuration ω to a stretched configuration $\omega_\lambda := (\lambda \tilde{e}_1 \otimes \tilde{e}_1 + \lambda^{-1/2} \tilde{e}_2 \otimes \tilde{e}_2)\omega$ (i.e., accounting for the natural lateral contraction due to incompressibility). Then imagine measuring bending transverse to this stretch while taking ω_λ as the reference configuration. In this scenario, the modulus of bending is $\mu r^{1/3} h_\lambda^3/3$ for $h_\lambda = h\lambda^{-1/2}$. Thus as expected, the modulus depends on the deformed thickness associated with the natural transverse contraction of an incompressible sheet under stretch.

3.8 Derivation of the Koiter theory by dimension reduction

Outline of the derivation

We first sketch the derivation of the Koiter theory: We show how the plane stress energy generically emerges from the relaxed three dimensional free energy for any given midplane deformation. Then, we outline the argument for the bending term, which accounts for the energy due to tension wrinkling. All this is developed in more detail in the coming sections.

Let us first consider a nematic elastomer sheet with finite but small thickness $h \ll 1$ occupying the region $\Omega_h := \omega \times (-h/2, h/2)$ where $\omega \subset \mathbb{R}^2$ is the midplane in its isotropic reference state. We assume that the microstructure is fully-relaxed so that a deformation of this region $y^h \colon \Omega_h \to \mathbb{R}^3$ is subject to a strain energy

$$\mathcal{E}^h_{3D}(y^h) := \int_{\Omega_h} W^{qc}_{3D}(\nabla y^h) dx. \tag{3.188}$$

Since we are dealing with a thin sheet, we make the ansatz that any low energy deformation y^h with corresponding midplane deformation $y(\tilde{x}) := y^h(\tilde{x}, 0)$ behaves to leading order in x_3 as

$$y^h(\tilde{x}, x_3) \approx y(\tilde{x}) + x_3 b(\tilde{x}) \tag{3.189}$$

for some vector $b \colon \omega \to \mathbb{R}^3$. (Note, this approximation can be obtained by Taylor expanding y^h in x_3 about $x_3 = 0$, observing that $x_3 \in (-h/2, h/2)$ is small, and neglecting terms of $O(x_3^2)$ and above). Thus, assuming the y^h is incompressible (i.e., $\det \nabla y^h = 1$ on Ω_h), we find, in substituting (3.189) into (3.188), that the energy for these generic deformations scales with the thickness as

$$\mathcal{E}^h_{3D}(y^h) = h \int_\omega W^{qc}_{3D}(\tilde{\nabla} y | b) d\tilde{x} + O(h^2) \tag{3.190}$$

due to the Lipschitz continuity of W^{qc}_{3D} (on matrices with $\det F = 1$). Now, in fixing the midplane deformation $y \colon \omega \to \mathbb{R}^3$, we observe that, for sufficiently thin sheets, setting

$$b(\tilde{x}) = \arg\min_{\mathbb{R}^3} W^{qc}_{3D}(\tilde{\nabla} y(\tilde{x}) | \cdot), \quad \tilde{x} \in \omega \tag{3.191}$$

approximately minimizes the relaxed three dimensional strain energy. Therefore, we expect the energy for a generic midplane deformation of a sufficiently thin nematic elastomer sheet to behave as

$$\mathcal{E}^h_{3D}(y^h) = h \int_\omega W_{ps}(\tilde{\nabla} y) d\tilde{x} + O(h^2) \tag{3.192}$$

since actually

$$W_{ps}(\tilde{F}) = (W_{3D}^{qc})_{2D}(\tilde{F}) := \inf_{\mathbb{R}^3} W_{3D}^{qc}(\tilde{F}|\cdot) \tag{3.193}$$

(for this equality, see Theorem 3.8.1 below). Thus, the first term in the energy (3.192) coincides with the first term in the Koiter theory (3.183).

We will show that W_{ps} is not quasiconvex[2]. This means that there are certain midplane deformations y which can be approximated by deformations $y_k \approx y$ which lower the energy through fine scale instabilities. Mathematically, these midplane deformations have the property

$$\begin{gathered}\lim_{k\to\infty}\int_\omega W_{ps}(\tilde{\nabla} y_k)d\tilde{x} = \int_\omega W_{2D}^{qc}(\tilde{\nabla} y)d\tilde{x} < \int_\omega W_{ps}(\tilde{\nabla} y)d\tilde{x} \\ \text{for some} \quad y_k \rightharpoonup y \text{ in } W^{1,2}(\omega,\mathbb{R}^3) \quad \text{as } k\to\infty.\end{gathered} \tag{3.194}$$

In particular, this can happen for taut membranes when the deformation gradient $\tilde{F}_0 \in \mathbb{R}^{3\times 2}$ corresponds to a point in the region $\mathcal{W}$. We will show that the instabilities (in the sense of (3.194) with $y = \tilde{F}_0\tilde{x}$) necessarily correspond to deformations of the form

$$y_k(\tilde{x}) = \bar{\lambda}_M x_1 e_1 + \bar{\lambda}_M^{-1/2}\gamma_k(x_2), \quad \tilde{x}\in\omega \tag{3.195}$$

for $\bar{\lambda}_M := \lambda_M(\tilde{F}_0)$ and some one-dimensional *wrinkled* curve γ_k satisfying pointwise the constraints

$$\gamma_k \cdot e_1 = 0, \quad |\gamma_k'| = 1 \tag{3.196}$$

up to a rigid body rotation and/or a change in coordinates frame (dictated by $\tilde{F}_0$). Further, the wrinkled curves γ_k become finer and finer as k increases so that in the limit the wrinkles are infinitely fine.

However on this last point, we recognize this fineness as an artifact of the fact that we have not taken into account terms in (3.192) which are higher order in the thickness h, and that bending (at a scale h^3) should emerge to resist or *regularize* such infinitely fine wrinkles. Therefore, we extend the midplane deformations (3.195) to the entire sheet Ω_h while respecting incompressiblity (i.e., through an incompressible deformation $y_k^h\colon \Omega_h \to \mathbb{R}^3$ with $y_k^h(\tilde{x},0) = y_k(\tilde{x})$), and we find that bending emerges as the energy is characterized by

$$\mathcal{E}_{3D}^h(y_k^h) \approx \mathcal{E}_K^h(y_k). \tag{3.197}$$

[2]Specifically, we show that $W_{ps} = W_{2D}^{qc}$ everywhere except the region C which crucially includes $\mathcal{W}$.

Consequently, the Koiter theory (3.183) appropriately captures the wrinkling behavior of taut nematic elastomer sheets.

Characterization of midplane deformations during tension wrinkling

To develop the Koiter theory, and in particular the bending term which emerges to regularize wrinkling, we first characterize tension wrinkling deformations in the asymptotic context of (3.194). We sketch a few ideas related to this development in Figure 3.6.

We begin with a theorem regarding the plane-stress energy density in the Koiter theory:

Theorem 3.8.1 *Let $(W_{3D}^{qc})_{2D}$ be the energy after taking the infimum as defined in (3.193). We actually have that*

$$W_{ps}(\tilde{F}) = (W_{3D}^{qc})_{2D}(\tilde{F}) = \begin{cases} W_{2D}(\tilde{F}) & \text{if } (\lambda_M(\tilde{F}), \delta(\tilde{F})) \in \mathcal{C} \\ W_{2D}^{qc}(\tilde{F}) & \text{if } (\lambda_M(\tilde{F}), \delta(\tilde{F})) \in \mathcal{L}_m \cup \mathcal{M} \cup \mathcal{S}. \end{cases} \tag{3.198}$$

Moreover, the infimum in (3.193) is attained for each full-rank $\tilde{F} \in \mathbb{R}^{3\times 2}$ by setting

$$b^* := \arg\min_{b\in\mathbb{R}^3} W_{3D}^{qc}(\tilde{F}|b) = \frac{\tilde{F}\tilde{e}_1 \times \tilde{F}\tilde{e}_2}{|\tilde{F}\tilde{e}_1 \times \tilde{F}\tilde{e}_2|^2}. \tag{3.199}$$

The equalities asserted in this theorem for W_{ps} (i.e., (3.198)) are an equivalent representation to (3.184). We prove this result at the end of this section.

From this result, we see that W_{ps} differs from the relaxed membrane energy W_{2D}^{qc} only in the region $\mathcal{C}$—consisting of the region $\mathcal{W}$ where wrinkling instability occurs and (a large portion of) the region $\mathcal{L}$ where one has crumpling or compression in both directions. Therefore, all instabilities of W_{ps} (i.e., (3.194)) are related to mesoscale deformation gradients in the region $\mathcal{C}$.

We are interested in characterizing tension wrinkling, i.e., the instabilities due to mesoscale deformation gradients in $\mathcal{W}$. Hence, these are our focus. Specifically, we take a (region of a) membrane whose midplane is a unit square (i.e., $\omega = (0,1)^2$ the unit square) and subject it to a mesoscale deformation gradient $\tilde{F}_0 \in \mathbb{R}^{3\times 3}$ in the wrinkling region, i.e., having $(\lambda_M(\tilde{F}_0), \delta(\tilde{F}_0)) \in \mathcal{W}$. Since it develops instability,

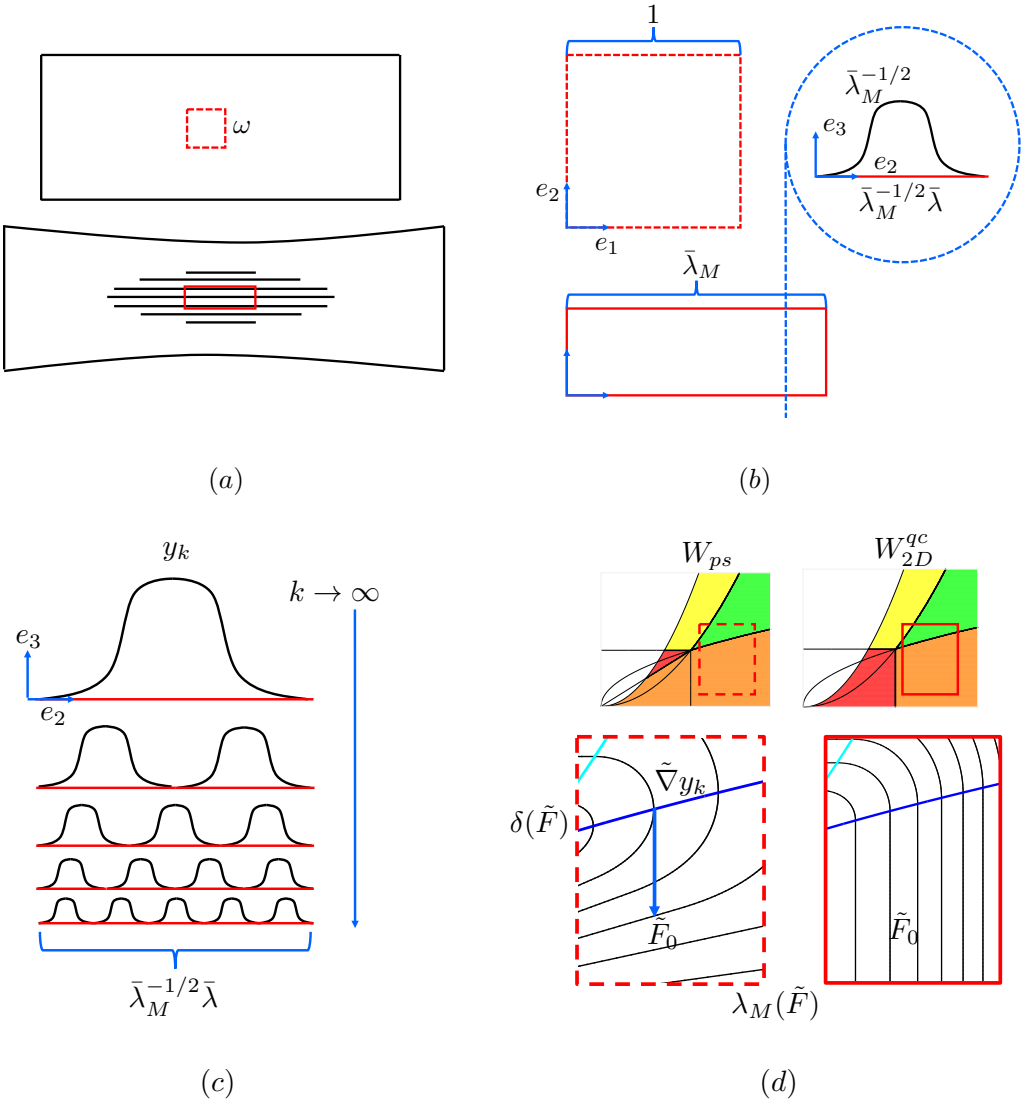

Figure 3.6: A few ideas related to the development of the Koiter theory for nematic elastomer sheets. (a) A schematic representation of the clamped-stretch experiment. (b) The mesoscale deformation of a square shown outlined in red from part (a), and the construction of one wrinkle. (c) A cross-section through the line marked in part (b) showing the canonical construction of a sequence of finer and finer wrinkles converging weakly to a flat deformation. (d) The overall deformation gradient $\tilde{F}_0$ corresponding to the point marked is obtained by deformations whose gradient takes the pointwise values corresponding to the point marked $\tilde{\nabla} y_k$. This relaxes the energy W_{ps} to the membrane energy W_{2D}^{qc}.

we can find a sequences of midplane deformations y_k that satisfy

$$y_k \rightharpoonup \tilde{F}_0\tilde{x} \quad \text{in } W^{1,2}(\omega,\mathbb{R}^3), \qquad \int_\omega W_{ps}(\tilde{\nabla} y_k)d\tilde{x} \to W_{2D}^{qc}(\tilde{F}_0) \quad \text{as } k\to\infty. \tag{3.200}$$

We show that such sequences are necessarily of the form (3.195) up to a rigid body rotation and/or a change in coordinates frame.

For this characterization, we note that due to the frame invariance and isotropy of W_{2D}^{qc} and W_{ps} – the fact that $W_{2D}^{qc}(Q\tilde{F}\tilde{R}) = W_{2D}^{qc}(\tilde{F})$ for all $\tilde{F}\in\mathbb{R}^{3\times 2}$, $Q\in SO(3)$ and $\tilde{R}\in SO(2)$ (and similarly for W_{ps}) – we only need to consider the case that $\tilde{F}_0$ is diagonal, i.e.,

$$\tilde{F}_0 = \begin{pmatrix} \bar{\lambda}_M & 0 \\ 0 & \bar{\delta}/\bar{\lambda}_M \\ 0 & 0 \end{pmatrix}, \quad (\bar{\lambda}_M,\bar{\delta})\in\mathcal{W}. \tag{3.201}$$

In this setting, $\bar{\lambda}_M > r^{1/3}$ and $\bar{\delta} < \bar{\lambda}_M^{1/2}$ (recall the definition of $\mathcal{W}$ in (3.9)). For future use we set

$$\bar{\delta} = \bar{\lambda}_M^{1/2}\bar{\lambda}, \quad \bar{\lambda}\in(0,1). \tag{3.202}$$

Now, it follows from Theorem 3.5.1(i) (see also Cesana et al. [25]) that sequences that satisfy (3.200) have the property that

$$\tilde{\nabla} y_k(\tilde{x}) \in K_{\mathcal{W}} \tag{3.203}$$

on ω except perhaps in boundary layers[3]. Here,

$$K_{\mathcal{W}} := \left\{\tilde{F}\in\mathbb{R}^{3\times 2}\colon (\lambda_M(\tilde{F}),\delta(\tilde{F})) = (\bar{\lambda}_M,\bar{\lambda}_M^{1/2}), \quad \tilde{F}\tilde{e}_1 = \bar{\lambda}_M e_1\right\}. \tag{3.204}$$

We note that the condition (3.203) is exactly equivalent to the characterization in (3.195) and (3.196). First, it follows from the definition of $K_{\mathcal{W}}$ that $\partial_1 y_k = \bar{\lambda}_M e_1$. Integrating this yields $y_k(\tilde{x}) = \bar{\lambda}_M x_1 e_1 + \bar{\lambda}_M^{-1/2}\gamma_k(x_2)$ for some $\gamma_k\colon(0,1)\to\mathbb{R}^3$. Second, it follows from definition of $K_{\mathcal{W}}$ that $\lambda_M(\tilde{\nabla} y_k) = \bar{\lambda}_M$, and this leads necessarily to the conclusion $\gamma_k'\cdot e_1 = 0$. Hence, $\delta(\tilde{\nabla} y_k) = \bar{\lambda}_M^{1/2}|\gamma_k'|$. Finally, the requirement from $K_{\mathcal{W}}$ that $\delta(\tilde{\nabla} y_k) = \bar{\lambda}_M^{1/2}$ implies that $|\gamma_k'| = 1$. Thus, we obtain (3.195) and (3.196) as asserted.

[3]Specifically, this result shows that the Young measure is supported on $K_{\mathcal{W}}$, which implies (3.203) in an appropriate sense.

Rather strikingly, these deformations correspond to pure uniaxial tension where the membrane stretches along its length by a factor $\bar{\lambda}_M$ and deforms transversely out-of-plane to preserve its natural width and avoid compression. Moreover, the convergence (3.200) which leads to the relaxation is assured if and only if

$$\gamma_k \rightharpoonup \bar{\lambda} x_2 e_2 \quad \text{ in } W^{1,2}((0,1),\mathbb{R}^3) \quad \text{ as } k \to \infty. \tag{3.205}$$

This combined with the constraint (3.196) implies that the curves γ_k must oscillate out-of-plane on a fine-scale as $k \to \infty$ to relax the energy.

It is useful to illustrate these concepts through a canonical construction of tension-wrinkling curves which have the properties (3.196) and (3.205): Consider any smooth curve $\gamma\colon (0,1) \to \mathbb{R}^3$ in the $\{e_2, e_3\}$ plane describing a single wrinkle which has a total length of 1, is given by a regular parameterization (i.e., $\gamma' \neq 0$ on $(0,1)$), and satisfies $\gamma(0) = 0$, $\gamma(1) = \bar{\lambda} e_2$, $\gamma \cdot e_3 = 0$ in a neighborhood of 0 and 1. The example curve $\bar{\lambda}_M^{-1/2}\gamma$ in Figure 3.6(b) has each of these properties for γ. Importantly, any curve γ with these properties can be reparameterized by its arc-length yielding a new parametrization $\gamma_0\colon (0,1) \to \mathbb{R}^3$ corresponding to the same curve which satisfies (3.196). For a curve γ_k of k wrinkles which satisfies (3.196), we simply extend γ_0 periodically to all of $\mathbb{R}$ so that $\gamma_0(x_2 + 1) = \gamma_0(x_2)$ for $x_2 \in \mathbb{R}$ and set

$$\gamma_k(x_2) = k^{-1}\gamma_0(k x_2), \quad x_2 \in (0,1). \tag{3.206}$$

This rescaling is akin to the depiction in Figure 3.6(c) where the curve in (b) is rescaled in precisely the same manner to obtain a curve of k wrinkles of wavelength $1/k$. Moreover, any curve γ_k constructed in this manner satisfies (3.205) and obeys the estimates

$$\begin{gathered} \|\gamma_k - \bar{\lambda} x_2 e_2\|_{L^\infty} = k^{-1}\|\gamma_0 - \bar{\lambda} x_2 e_2\|_{L^\infty} \\ \|\gamma_k''\|_{L^\infty} = k\|\gamma_0''\|_{L^\infty}, \quad \|\gamma_k'''\|_{L^\infty} = k^2\|\gamma_0'''\|_{L^\infty}. \end{gathered} \tag{3.207}$$

Thus, we see that as k increases, the curve γ_k converges to the flat line $\bar{\lambda} x_2 e_2$, but the fine-scale oscillations needed to obtain this convergence result in amplified curvature and higher derivatives (as seen by the dependence on k in the derivatives).

While the canonical construction is illustrative, we do not restrict ourselves to it. Instead, we consider a more generic class of wrinkled curves $\mathcal{A}_k^\tau$ which retains quantitative estimates on the amplification of curvature and higher order derivatives that we see in the examples with (3.207), but does not impose restrictions on the

detailed appearance of the wrinkled curves:

$$\mathcal{A}_k^\tau := \Big\{\gamma_k \in C^3([0,1],\mathbb{R}^3) : \gamma_k \text{ as in (3.196)}, \\ \|\gamma_k - \bar{\lambda} x_2 e_2\|_{L^\infty} \le \tau k^{-1}, \quad \|\gamma_k''\|_{L^\infty} \le \tau k, \quad \|\gamma_k'''\|_{L^\infty} \le \tau k^2\Big\} \tag{3.208}$$

for some $\tau > 0$ and $k \in \mathbb{Z}^+$ (a positive integer). For a given $\tau > 0$ and $k \in \mathbb{Z}^+$, this set encapsulates a rather generic class of wrinkled curves where we think of the index k as denoting essentially the number of wrinkles (or $1/k$ as the approximate wavelength) and τ quantifying the localized features of the wrinkles – with large τ allowing for more localized features. Moreover for fixed $\tau > 0$, any sequence of curves $\gamma_k \in \mathcal{A}_k^\tau$ is assured the convergence in (3.205) (up to a subsequence). Hence, any sequence of midplane deformations y_k in (3.195) with wrinkled curves $\gamma_k \in \mathcal{A}_k^\tau$ has the desired limiting behavior in (3.200).

Incompressible extensions of the tension wrinkling midplane deformations

Having characterized the tension wrinkling deformations of the midplane, we seek to extend them to the entire thin sheet. We have to do so in such a manner that preserves incompressibility and yields low membrane energy. Throughout this section we assume that $\tau > 0$ is fixed and the integer k and thickness are such that $hk < 1$.

Given a midplane deformation y_k of the form (3.195) with $\gamma_k \in \mathcal{A}_k^\tau$, we define

$$b_k := \frac{\partial_1 y_k \times \partial_2 y_k}{|\partial_1 y_k \times \partial_2 y_k|^2} = \delta(\tilde{\nabla} y_k)^{-1} N_{y_k} \quad \text{on } \omega \tag{3.209}$$

in light of the attainment result: equation (3.199) in Theorem 3.8.1. We then extend the midplane deformation to Ω_h by setting

$$y_k^h(x) := y_k(\tilde{x}) + \xi_k^h(x) b_k(\tilde{x}), \quad x \in \Omega_h \tag{3.210}$$

for some $\xi_k^h \in C^1(\overline{\Omega}_h, \mathbb{R}^3)$ satisfying

$$\xi_k^h(\tilde{x}, 0) = 0, \quad \tilde{x} \in \omega. \tag{3.211}$$

By an important result, we can find a function ξ_k^h which yields an incompressible extension if the sheet is sufficiently thin, i.e.,

$$\det(\nabla y_k^h) = 1 \quad \text{on } \Omega_h. \tag{3.212}$$

Specifically:

Theorem 3.8.2 *Fix $\tau > 0$ and $k \in \mathbb{Z}^+$. There exists an $\bar{h} = \bar{h}(\tau) > 0$ with $\bar{h}k < 1$ such that for any y_k in (3.195), b_k in (3.209) and $h \in (0, \bar{h})$, there exists a unique $\xi_k^h \in C^1(\bar{\Omega}_h, \mathbb{R}^3)$ satisfying (3.211) for which y_k^h defined in (3.210) satisfies (3.212) Moreover, we have the following approximation for ∇y_k^h:*

$$\begin{aligned} \nabla y_k^h &= (\tilde{\nabla} y_k | b_k) + x_3 (\tilde{\nabla} b_k | 0) - x_3 Tr(G_k) b_k \otimes e_3 \\ &\quad + \frac{3}{2} x_3^2 Tr(G_k)^2 b_k \otimes e_3 - \frac{1}{2} x_3^2 Tr(G_k)) (\tilde{\nabla} b_k | 0) \\ &\quad + O(k^2 x_3^2) b_k \otimes e_2 + O(k^3 x_3^3) \quad \text{on } \Omega_h, \\ G_k &:= (\tilde{\nabla} y_k | b_k)^{-1} (\tilde{\nabla} b_k | 0) \quad \text{on } \omega. \end{aligned} \tag{3.213}$$

We prove this at the end of the section. This proof makes use of techniques due to Conti and Dolzmann [31, 30]. Finally, the deformation satisfies other properties:

Corollary 3.8.3 *For y_k as in (3.195), b_k as in (3.209) and G_k as in (3.213) we have the following pointwise identities everywhere on ω:*

$$\begin{aligned} &(\tilde{\nabla} y_k | b_k)^T b_k = |b_k|^2 e_3 = \bar{\lambda}_M^{-1} e_3, \\ &(\tilde{\nabla} b_k | 0)^T b_k = 0, \\ &|\tilde{\nabla} b_k|^2 = |II_{y_k}|^2, \\ &Tr((\tilde{\nabla} y_k | b_k)^T (\tilde{\nabla} b_k | 0)) = \bar{\lambda}_M^{-1/2} Tr(II_{y_k}), \\ &Tr(G_k) = \bar{\lambda}_M^{1/2} Tr(II_{y_k}), \\ &Tr(II_{y_k})^2 = |II_{y_k}|^2, \\ &(\lambda_M(\tilde{\nabla} y_k | b_k), \lambda_M(cof(\tilde{\nabla} y_k | b_k))) = (\bar{\lambda}_M, \bar{\lambda}_M^{1/2}) \in S. \end{aligned} \tag{3.214}$$

Further, if kh is sufficiently small, then y_k^h in (3.210) satisfies

$$\lambda_M(\nabla y_k^h) = \bar{\lambda}_M \quad \text{and} \quad (\lambda_M(\nabla y_k^h), \lambda_M(cof \nabla y_k^h)) \in S \quad \text{on } \Omega_h. \tag{3.215}$$

Note that from the proof of the theorem, the form (3.210) can be expanded in x_3 as $y_k^h = y_k + x_3 b_k - \frac{x_3^2}{2} \mathrm{Tr}(G_k) b_k + \ldots$, and so this deformation is consistent with the leading order behavior in (3.189).

The energy of tension wrinkling

We now compute the energy of the deformations (3.210). Throughout, we make the physically reasonable restriction to deformations for which the radius of curvature is large compared to the thickness, which is tantamount to assuming $kh \ll 1$.

In this setting, we first recall the last property in (3.214) and note that if kh is sufficiently small, (3.215) holds. Further, for any $F \in \mathbb{R}^{3\times 3}$ with $(\lambda_M(F), \lambda_M(\mathrm{cof}F)) \in S$,

$$W_{3D}^{qc}(F) = W_{3D}(F) = \frac{\mu}{2}\left(r^{1/3}\left(|F|^2 - \left(\frac{r-1}{r}\right)(\lambda_M(F))^2\right) - 3\right). \tag{3.216}$$

So in setting

$$A_k^h := \nabla y_k^h - (\tilde{\nabla} y_k | b_k) \quad \text{ on } \Omega_h, \tag{3.217}$$

we obtain

$$\begin{aligned}
\mathcal{E}_{3D}^h(y_k^h) &= \frac{\mu}{2}\int_{\Omega_h}\left(r^{1/3}\left(|\nabla y_k^h|^2 - \left(\frac{r-1}{r}\right)(\lambda_M(\nabla y_k^h))^2\right) - 3\right)dx \\
&= \int_{\Omega_h}\left(W_{3D}^{qc}((\tilde{\nabla} y_k|b_k)) + \frac{\mu r^{1/3}}{2}\left(2\mathrm{Tr}((\tilde{\nabla} y_k|b_k)^T A_k^h) + |A_k^h|^2\right)\right)dx \\
&= h\int_\omega W_{ps}(\tilde{\nabla} y_k)d\tilde{x} + \frac{\mu r^{1/3}}{2}\int_{\Omega_h}\left(2\mathrm{Tr}((\tilde{\nabla} y_k|b_k)^T A_k^h) + |A_k^h|^2\right)dx
\end{aligned} \tag{3.218}$$

using (3.215) and Theorem 3.8.1 combined with the definition of b_k in (3.209).

We compare (3.213) and (3.217) to expand A_k^h. Substituting this expansion into (3.218), we see first that

$$\begin{aligned}
&\mu r^{1/3}\int_{\Omega_h}\mathrm{Tr}((\tilde{\nabla} y_k|b_k)^T A_k^h)dx = \\
&\qquad \frac{r^{1/3}\mu h^3}{24}\int_\omega\left(3\mathrm{Tr}(G_k)^2|b_k|^2 - \mathrm{Tr}(G_k)\mathrm{Tr}((\tilde{\nabla} y_k|b_k)^T(\tilde{\nabla} b_k|0))\right)d\tilde{x} \\
&\qquad\qquad + O(k^3h^4)
\end{aligned} \tag{3.219}$$

using the fact that the terms linear in x_3 vanish upon integration through the thickness and also using the first identity in Corollary 3.8.3. By a similar argument and with the second identity in this corollary, we arrive at

$$\begin{aligned}
&\frac{\mu r^{1/3}}{2}\int_{\Omega_h}|A_k^h|^2dx = \\
&\qquad \frac{\mu r^{1/3}h^3}{24}\int_\omega\left(|\tilde{\nabla} b_k|^2 + \mathrm{Tr}(G_k)^2|b_k|^2\right)d\tilde{x} + O(k^3h^4).
\end{aligned} \tag{3.220}$$

Making use of the remaining identities in the corollary, we find that the two energies (3.219) and (3.220) combine to form a term penalizing the second fundamental form of the midplane deformation y_k,

$$\begin{aligned}
&\frac{\mu r^{1/3}}{2}\int_{\Omega_h}\left(2\mathrm{Tr}((\tilde{\nabla} y_k|b_k)^T A_k^h) + |A_k|^2\right)dx = \\
&\qquad \frac{\mu r^{1/3}h^3}{6}\int_\omega |\mathrm{II}_{y_k}|^2 d\tilde{x} + O(k^3h^4).
\end{aligned} \tag{3.221}$$

Finally in combining (3.218) and (3.221), we obtain

$$\mathcal{E}^h_{3D}(y^h_k) = \mathcal{E}^h_K(y_k) + O(k^3h^4). \tag{3.222}$$

Observe that the stretching term in $\mathcal{E}^h_K$ is $O(h)$ while the bending part is $O(k^2h^3)$. Thus, with the radius of curvature large compared to the thickness, $kh \ll 1$ and therefore the term $O(k^3h^4)$ is negligible compared to the rest.

Proof of Theorem 3.8.1.

Recall that the Koiter theory for nematic elastomer sheets has two terms: a membrane term and $O(h)$ and a bending term at $O(h^3)$. Here, we show that the explicit form of the membrane term in this theory arises as a minimization of the out-of-plane deformation gradient of the relaxed three dimensional energy of DeSimone and Dolzmann [37]:

Proof of Theorem 3.8.1. Let $\tilde{F} \in \mathbb{R}^{3\times 2}$ and $b \in \mathbb{R}^3$. We may assume that $\tilde{F}$ is full-rank as the equality holds trivially otherwise (with $W^{qc}_{3D} = (W^{qc}_{3D})_{2D} = +\infty$). By the singular value decomposition, we can set

$$\begin{aligned} \tilde{F} = Q\tilde{D}\tilde{R}, \quad \text{for} \quad Q \in SO(3), \quad \tilde{R} \in O(2), \\ \tilde{D} = \operatorname{diag}(\bar{\lambda}_M, \bar{\delta}/\bar{\lambda}_M) \in \mathbb{R}^{3\times 2}. \end{aligned} \tag{3.223}$$

Here $\bar{\lambda}_M = \lambda_M(\tilde{F}) > 0$ is the maximum singular value of $\tilde{F}$, and $\bar{\delta} = \delta(\tilde{F}) > 0$ is the areal stretch of $\tilde{F}$ as defined below (3.7). Both are positive since $\tilde{F}$ is full-rank. In addition, we let

$$\bar{b} := (\det \tilde{R})Q^T b. \tag{3.224}$$

By the frame invariance and isotropy of W^{qc}_{3D}, we observe that

$$W^{qc}_{3D}(\tilde{F}|b) = W^{qc}_{3D}(Q(\tilde{D}|\bar{b})(\tilde{R}|(\det \tilde{R})e_3)) = W^{qc}_{3D}(\tilde{D}|\bar{b}) \tag{3.225}$$

since Q and $(\tilde{R}|(\det \tilde{R})e_3)$ are both in $SO(3)$. Given this equality and recalling that $\tilde{F}$ is an arbitrary full-rank $\mathbb{R}^{3\times 2}$ matrix and b is arbitrary, we see that to prove the equality (3.198) it suffices to optimize W^{qc}_{3D} amongst the deformation

$$F(\bar{b}_1, \bar{b}_2) := \begin{pmatrix} \bar{\lambda}_M & 0 & \bar{b}_1 \\ 0 & \bar{\delta}/\bar{\lambda}_M & \bar{b}_2 \\ 0 & 0 & \bar{\delta}^{-1} \end{pmatrix}. \tag{3.226}$$

Indeed, since $\bar{b}$ in (3.224) is a bijective function of b, we have given (3.225)

$$\begin{aligned}(W_{3D}^{qc})_{2D}(\tilde{F}) &:= \inf_{b\in\mathbb{R}^3} W_{3D}^{qc}(\tilde{F}|b) \\ &= \inf_{\bar{b}\in\mathbb{R}^3} W_{3D}^{qc}(\tilde{D}|\bar{b}) = \inf_{(\bar{b}_1,\bar{b}_2)\in\mathbb{R}^2} W_{3D}^{qc}(F(\bar{b}_1,\bar{b}_2)).\end{aligned} \tag{3.227}$$

For the last equality, as the infimum is necessarily incompressible, we enforce $\det(\tilde{D}|\bar{b}) = 1$ (which is only true if $\bar{b}\cdot e_3 = \delta^{-1}$ as in (3.226)).

Now, we claim that for any full-rank $\tilde{F}$,

$$(W_{3D}^{qc})_{2D}(\tilde{F}) = W_{3D}^{qc}(F_0) \quad \text{where} \quad F_0 := F(0,0). \tag{3.228}$$

To show this, we will make use of the fact that $W_{3D}^{qc}(F) = \psi_{3D}(\lambda_M(F), \lambda_M(\operatorname{cof} F))$ and the fact that ψ_{3D} is a monotonically increasing function in both of its arguments (this can be seen from the contour plot in Figure 2.4(b)). In this direction, we first observe that

$$\lambda_M^2(F(\bar{b}_1,\bar{b}_2)) \geq \max_{i\in\{1,2,3\}} |F(\bar{b}_1,\bar{b}_2)e_i|^2 \geq \max_{i\in\{1,2,3\}} |F_0 e_i|^2 = \lambda_M^2(F_0). \tag{3.229}$$

This is deduced from the parameterization in (3.226); as is the fact that

$$\operatorname{cof} F(\bar{b}_1,\bar{b}_2) = \begin{pmatrix} \bar{\lambda}_M^{-1} & 0 & 0 \\ 0 & \bar{\lambda}_M\bar{\delta}^{-1} & 0 \\ -\bar{b}_1\bar{\delta}/\bar{\lambda}_M & -\bar{\lambda}_M\bar{b}_2 & \delta \end{pmatrix}. \tag{3.230}$$

With (3.230), we find that

$$\begin{aligned}\lambda_M^2(\operatorname{cof} F(\bar{b}_1,\bar{b}_2)) &\geq \max_{i\in\{1,2,3\}} |\operatorname{cof} F(\bar{b}_1,\bar{b}_2)e_i|^2 \\ &\geq \max_{i\in\{1,2,3\}} |\operatorname{cof} F_0 e_i|^2 = \lambda_M^2(\operatorname{cof} F_0)\end{aligned} \tag{3.231}$$

as well. Finally, combining (3.229) and (3.231) and using the fact that ψ_{3D} is a monotonically increasing function in both its arguments, we find that

$$\begin{aligned}W_{3D}^{qc}(F(\bar{b}_1,\bar{b}_2)) &= \psi_{3D}(\lambda_M(F(\bar{b}_1,\bar{b}_2)), \lambda_M(\operatorname{cof} F(\bar{b}_1,\bar{b}_2))) \\ &\geq \psi_{3D}(\lambda_M(F_0), \lambda_M(\operatorname{cof} F_0)) = W_{3D}^{qc}(F_0).\end{aligned} \tag{3.232}$$

Hence, the infimum is attained by setting $(\bar{b}_1,\bar{b}_2) = 0$, i.e.,

$$\inf_{(\bar{b}_1,\bar{b}_2)\in\mathbb{R}^2} W_{3D}^{qc}(F(\bar{b}_1,\bar{b}_2)) = W_{3D}^{qc}(F_0), \tag{3.233}$$

and combining (3.233) with (3.227), we deduce the claim in (3.228).

The formulas (3.184) and (3.198) are obtained using (3.228) by explicit verification: briefly, if $\bar{\lambda}_M \geq \bar{\delta}^{-1}$ and $\bar{\delta} \geq \bar{\lambda}_M \bar{\delta}^{-1}$, then $(\lambda_M(F_0), \lambda_M(\operatorname{cof} F_0)) = (\bar{\lambda}_M, \bar{\delta})$ and

$$\begin{aligned} W_{3D}^{qc}(F_0) = \psi_{3D}(\bar{\lambda}_M, \bar{\delta}) = \psi_{2D}(\bar{\lambda}_M, \bar{\delta}) = W_{2D}^{qc}(\tilde{F}), \\ (\lambda_M(\tilde{F}), \delta(\tilde{F})) \in \mathcal{M} \cup \mathcal{S} \cup (\mathcal{L}_M \cap L); \end{aligned} \tag{3.234}$$

if $\bar{\lambda}_M \geq \bar{\delta}^{-1}$ and $\bar{\lambda}_M \bar{\delta}^{-1} > \bar{\delta}$, then $(\lambda_M(F_0), \lambda_M(\operatorname{cof} F_0)) = (\bar{\lambda}_M, \bar{\lambda}_M \bar{\delta}^{-1})$ and

$$\begin{aligned} W_{3D}^{qc}(F_0) &= \psi_{3D}(\bar{\lambda}_M, \bar{\lambda}_M \bar{\delta}^{-1}) \\ &= \begin{cases} \psi_{2D}(\bar{\lambda}_M, \bar{\delta}) = W_{2D}^{qc}(\tilde{F}) & \text{if } (\lambda_M(\tilde{F}), \delta(\tilde{F})) \in \mathcal{L}_m \setminus L \\ \varphi_{2D}(\bar{\lambda}_M, \bar{\delta}) = W_{2D}(\tilde{F}) & \text{if } (\lambda_M(\tilde{F}), \delta(\tilde{F})) \in C \cap \tilde{C} \end{cases} \end{aligned} \tag{3.235}$$

where $\tilde{C} := \{(s,t) \in \mathbb{R}^+ \times \mathbb{R}^+ : t \geq s^{-1}\}$; if $\bar{\lambda}_M < \bar{\delta}^{-1}$ and $\bar{\lambda}_M \bar{\delta}^{-1} > \bar{\delta}$, then $(\lambda_M(F_0), \lambda_M(\operatorname{cof} F_0)) = (\bar{\delta}^{-1}, \bar{\lambda}_M \bar{\delta}^{-1})$ and

$$\begin{aligned} W_{3D}^{qc}(F_0) = \psi_{3D}(\bar{\delta}^{-1}, \bar{\lambda}_M \bar{\delta}^{-1}) = \varphi_{2D}(\bar{\lambda}_M, \bar{\delta}) = W_{2D}(\tilde{F}), \\ (\lambda_M(\tilde{F}), \delta(\tilde{F})) \in C \setminus \tilde{C}. \end{aligned} \tag{3.236}$$

This exhausts all possible cases, as any other case is actually incompatible with the fact that $\bar{\delta} = \bar{\lambda}_M \bar{\lambda}_m$ where $\bar{\lambda}_m = \lambda_m(\tilde{F})$ is the minimum singular value of $\tilde{F}$. Combining (3.234), (3.235) and (3.236) with the fact that (3.228) holds, we arrive at the representation in (3.198).

To see that the infimum is attained with b^* in (3.199), we notice that actually

$$b^* = \bar{\delta}^{-2} Q(\tilde{D}\tilde{R}\tilde{e}_1 \times \tilde{D}\tilde{R}\tilde{e}_2) = \bar{\delta}^{-1}(\det \tilde{R}) Q e_3. \tag{3.237}$$

for $Q, \tilde{D}$ and $\tilde{R}$ in (3.223). Hence, again using the frame invariance and isotropy of W_{3D}^{qc},

$$W_{3D}^{qc}(\tilde{F}|b^*) = W_{3D}^{qc}(Q(\tilde{D}|\bar{\delta}^{-1}e_3)(\tilde{R}|(\det \tilde{R})e_3)) = W_{3D}^{qc}(F_0). \tag{3.238}$$

So given (3.228), the infimum is attained with b^* as desired. This completes the proof. □

Proof of Theorem 3.8.2.

We now turn to the bending term in the Koiter theory. For this, we provide an explicit characterization of three dimensional deformations which correspond to wrinkling. These incur a *bending* penalty in their three dimensional elastic energy, which (up to higher order effects) is exactly proportional to the second fundamental form of the deformed membrane:

Proof of Theorem 3.8.2. We first consider the naive deformation

$$v_k^h(x) := y_k(\tilde{x}) + x_3 b_k(\tilde{x}), \quad \tilde{x} \in \omega. \tag{3.239}$$

This deformation is not incompressible. However, it is nearly so, as the gradient

$$\nabla v_k^h = (\tilde{\nabla} y_k | b_k) + x_3 (\tilde{\nabla} b_k | 0) \quad \text{on } \Omega_h \tag{3.240}$$

has a determinant which is $O(kx_3)$ close to unity. Indeed, $\det(\tilde{\nabla} y_k | b_k) = 1$ by construction, and so we define

$$G_k := (\tilde{\nabla} y_k | b_k)^{-1} (\tilde{\nabla} b_k | 0) \quad \text{on } \omega, \tag{3.241}$$

and observe that given (3.240) and (3.241) and since $\det((\tilde{\nabla} y_k | b_k)^{-1}) = 1$ on ω,

$$\begin{aligned} \det(\nabla v_k^h) &= \det((\tilde{\nabla} y_k | b_k)^{-1} \nabla v_k^h) \\ &= \det(I_{3\times 3} + x_3 G_k) = 1 + x_3 \operatorname{Tr}(G_k) \quad \text{on } \Omega_h. \end{aligned} \tag{3.242}$$

Here, we used that both $\operatorname{Tr}(\operatorname{cof} G_k)$ and $\det G_k$ are zero on ω. With this relationship, we find that

$$\begin{aligned} &|\det(\nabla v_k^h) - 1| \le C(\tau) k |x_3|, \quad \text{on } \Omega_h, \quad kh < 1, \\ &|\partial_2 \det(\nabla v_k^h)| \le C(\tau) k^2 |x_3|, \quad \text{on } \Omega_h, \quad kh < 1, \\ &\partial_1 \det(\nabla v_k^h) = 0 \quad \text{on } \Omega_h, \end{aligned} \tag{3.243}$$

using the fact that G_k is independent of x_1 and $\gamma_k \in \mathcal{A}_k^\tau$. An interesting observation is that as implied, the constant $C(\tau) > 0$ can be chosen to depend only on τ. In particular, G_k does not depend appreciably on $\bar{\lambda}_M > r^{1/3}$, and so the constant need not depend on this stretch.

Now, as (3.242) shows, the determinant of a generic ∇v_k^h is not unity. Thus, we introduce a $\xi_k^h \in C^1(\bar{\Omega}_h, \mathbb{R})$ (for some $h > 0$ to be chosen later) satisfying $\xi_k^h(\tilde{x}, 0) = 0$ and define y_k^h as in (3.210). Using properties of the determinant, we find that

$$\begin{aligned} &\det(\nabla y_k^h) = 1 \quad \text{on } \Omega_h \\ \Leftrightarrow \quad &\partial_3 \xi_k^h(x) = \frac{1}{\det\left(\nabla v_k^h(\tilde{x}, \xi_k^h(x))\right)}, \quad x \in \Omega_h. \end{aligned} \tag{3.244}$$

Therefore, the incompressibility of ∇y_k^h is equivalent to solving an ordinary differential equation in $\xi_k^h(\tilde{x}, \cdot)$. It turns out that there exists an $\bar{h} = \bar{h}(\tau) > 0$ such that for any $h \in (0, \bar{h})$ and k such that $kh < 1$, there exists a unique $\xi_k^h \in C^1(\bar{\Omega}_h, \mathbb{R})$

satisfying this differential equation subject to the initial condition $\xi_k^h(\tilde{x}, 0) = 0$. Moreover, from (3.243), ξ_k^h has the properties that

$$\begin{aligned} &|\xi_k^h - x_3| \leq C(\tau)k|x_3|^2, \quad |\partial_3 \xi_k^h - 1| \leq C(\tau)k|x_3|, \quad \text{on } \Omega_h \\ &|\partial_2 \xi_k^h| \leq C(\tau)k^2|x_3|^2, \quad \partial_1 \xi_k^h = 0, \quad \text{on } \Omega_h. \end{aligned} \tag{3.245}$$

This result is the consequence of a contraction map principle and some further analysis (presented, for instance, in the next chapter; also in [81] Section 3).

In the remainder, we assume $h \in (0, \bar{h})$, $kh < 1$, and y_k^h as in (3.210) for $\xi_k^h \in C^1(\bar{\Omega}_h, \mathbb{R})$ satisfying $\xi_k^h(\tilde{x}, 0) = 0$, the ordinary differential equation (3.244) and the estimates (3.245). By explicit calculation, we have

$$\begin{aligned} \nabla y_k^h = (\tilde{\nabla} y_k | b_k) + x_3(\tilde{\nabla} b_k | 0) + (\partial_3 \xi_k^h - 1) b_k \otimes e_3 \\ + (\xi_k^h - x_3)(\tilde{\nabla} b_k | 0) + b_k \otimes \tilde{\nabla} \xi_k^h \quad \text{on } \Omega_h. \end{aligned} \tag{3.246}$$

We can extract a more illuminating form by examining closely identities and estimates for ξ_k^h. Indeed, combining the ordinary differential equation (3.244) with the parameterization of $\det(\nabla v_k^h)$ in (3.242), we find that

$$\partial_3 \xi_k^h - 1 = -\partial_3 \xi_k^h \xi_k^h \operatorname{Tr}(G_k) \quad \text{on } \Omega_h. \tag{3.247}$$

In addition, making use of the boundary condition $\xi_k^h(\tilde{x}, 0) = 0$, the fundamental theorem of calculus, and our newfound parameterization (3.247),

$$\xi_k^h - x_3 = -\frac{1}{2}(\xi_k^h)^2 \operatorname{Tr}(G_k) \quad \text{on } \Omega_h. \tag{3.248}$$

Hence, with the estimates (3.245) and these parameterizations, we establish that

$$\begin{aligned} \partial_3 \xi_k^h - 1 &= -x_3 \operatorname{Tr}(G_k) + \frac{3}{2} x_3^2 \operatorname{Tr}(G_k)^2 + O(k^3 x_3^3) \quad \text{on } \Omega_h, \\ \xi_k^h - x_3 &= -\frac{1}{2} x_3^2 \operatorname{Tr}(G_k) + O(k^2 x_3^3) \quad \text{on } \Omega_h. \end{aligned} \tag{3.249}$$

Finally, the results on the planar derivatives of ξ_k^h in (3.245) imply that

$$b_k \otimes \tilde{\nabla} \xi_k^h = O(k^2 x_3^2) b_k \otimes e_2 \quad \text{on } \Omega_h. \tag{3.250}$$

Combining (3.246), (3.248), (3.249) and (3.250), we arrive at the parameterization for ∇y_k^h in (3.213) as desired. □

Now, we turn to the proof of further properties of this deformation, which we have collected in Corollary 3.8.3:

Proof of Corollary 3.8.3. First, we observe that $b_k = \bar{\lambda}_M^{-1/2} N_{y_k}$ where N_{y_k} is the surface normal of y_k. Thus, $(\tilde{\nabla} y_k)^T b_k = 0$ by definition, and the first identity in (3.214) follows. In addition, since N_{y_k} is a unit vector, $\partial_\alpha N_{y_k} \cdot N_{y_k} = (1/2)\partial_\alpha |N_{y_k}|^2 = 0$. So the second identity in (3.214) follows.

Now, for the third equality, we first observe that for tension wrinkling

$$\begin{aligned} \mathrm{II}_{y_k} = (\tilde{\nabla} y_k)^T (\tilde{\nabla} N_{y_k}) &= \begin{pmatrix} \partial_1 y_k \cdot \partial_1 N_{y_k} & \partial_1 y_k \cdot \partial_2 N_{y_k} \\ \partial_2 y_k \cdot \partial_1 N_{y_k} & \partial_2 y_k \cdot \partial_2 N_{y_k} \end{pmatrix} \\ &= \begin{pmatrix} 0 & 0 \\ 0 & \partial_2 y_k \cdot \partial_2 N_{y_k} \end{pmatrix} \end{aligned} \tag{3.251}$$

using the fact that N_{y_k} is independent of x_1 and that $\partial_1 y_k \cdot \partial_2 N_{y_k} = \bar{\lambda}_M e_1 \cdot \partial_2 N_{y_k} = 0$ since $N_{y_k} \cdot e_1 = 0$. Thus, the second fundamental form is greatly simplified in the context of tension wrinkling. In addition, we observe that

$$\begin{aligned} &(\tilde{\nabla} y_k | b_k) = R_k \Lambda_M, \quad \Lambda_M = \mathrm{diag}(\bar{\lambda}_M, \bar{\lambda}_M^{-1/2}, \bar{\lambda}_M^{-1/2}) \\ &R_k := \begin{pmatrix} 1 & 0 & 0 \\ 0 & (\gamma_k' \cdot e_2) & -(\gamma_k' \cdot e_3) \\ 0 & (\gamma_k' \cdot e_3) & (\gamma_k' \cdot e_2) \end{pmatrix} \in SO(3). \end{aligned} \tag{3.252}$$

Consequently,

$$|\tilde{\nabla} b_k|^2 = |R_k^T (\tilde{\nabla} b_k)|^2 = |\Lambda_M^{-1} (\tilde{\nabla} y_k | b_k)^T \tilde{\nabla} b_k|^2 = (\partial_2 y_k \cdot \partial_2 N_{y_k})^2. \tag{3.253}$$

Combining (3.251) and (3.253), we obtain the third identity in (3.214) as desired. The calculation for the fourth is similar. For the fifth, we can deduce from (3.252) that

$$(\tilde{\nabla} y_k | b_k)^{-1} = \Lambda_M^{-1} R_k^T = \Lambda_M^{-2} (\tilde{\nabla} y_k | b_k)^T. \tag{3.254}$$

Consequently,

$$\mathrm{Tr}(G_k) = \mathrm{Tr}(\Lambda_M^{-2} (\tilde{\nabla} y_k | b_k)^T (\tilde{\nabla} b_k | 0)) = \bar{\lambda}_M^{1/2} (\partial_2 y_k \cdot \partial_2 N_{y_k}), \tag{3.255}$$

and the fifth identity in (3.214) follows from (3.251). Note also the sixth identity in (3.214) also follows from (3.251).

For the last identity in (3.214) and also (3.215), we note that the functions $\{e_1, \gamma_k', N_{y_k}\}$ form an orthonormal basis of $\mathbb{R}^3$, and $b_k = \bar{\lambda}_M^{-1/2} N_{y_k}$ and is independent of x_1. Further, y_k^h is as in Proposition 3.8.2, so in particular the representations (3.246) and

(3.213) hold. Combining all this, we conclude that

$$\begin{aligned}
(\nabla y_k^h)^T e_1 &= (\tilde{\nabla} y_k | b_k)^T e_1 = \bar{\lambda}_M e_1 \quad \text{on } \Omega_h, \\
(\nabla y_k^h)^T \gamma_k' &= (\tilde{\nabla} y_k | b_k)^T \gamma_k' + O(x_3)(\tilde{\nabla} b_k | 0)^T \gamma_k' \\
&= \left(\bar{\lambda}_M^{-1/2} + O(kx_3)\right) e_2 \quad \text{on } \Omega_h, \\
(\nabla y_k^h)^T N_{y_k} &= (\tilde{\nabla} y_k | b_k)^T N_{y_k} + O(kx_3)(e_3 \otimes b_k) N_{y_k} + O(k^2 x_3^2)(e_2 \otimes b_k) N_{y_k} \\
&= \left(\bar{\lambda}_M^{-1/2} + O(kx_3)\right) e_3 + O(k^2 x_3^2) e_2 \quad \text{on } \Omega_h,
\end{aligned} \tag{3.256}$$

where the first result uses that e_1 is orthogonal to b_k and $\tilde{\nabla} b_k$, the second result uses that γ_k' is orthogonal to b_k and the last result uses that N_{y_k} is orthogonal the $\tilde{\nabla} b_k$. Since $\bar{\lambda}_M > \bar{\lambda}_M^{-1/2}$, the first term dominates the other two terms for kh sufficiently small, and we readily conclude that

$$\lambda_M(\nabla y_k^h) = \lambda_M(\tilde{\nabla} y_k | b_k) = \bar{\lambda}_M > r^{1/3} \tag{3.257}$$

as desired.

Now to show the $\lambda_M(\text{cof}(\tilde{\nabla} y_k | b_k)) = \bar{\lambda}_M^{-1/2}$, we note that $\lambda_M(\text{cof}\, F) = \lambda_M(F)\lambda_2(F)$ for any $F \in \mathbb{R}^{3\times 3}$ where λ_2 denotes the middle singular value. Thus, the result follows from the fact that on ω, $(\tilde{\nabla} y_k | b_k)^T \gamma_k' = \bar{\lambda}_M^{-1/2} e_2$, $(\tilde{\nabla} y_k | b_k)^T N_{y_k} = \bar{\lambda}_M^{-1/2} e_3$ and $(\tilde{\nabla} y_k | b_k)^T e_1 = \bar{\lambda}_M e_1$. This proves the last indentity in (3.214).

Now given (3.257) we know that ∇y_k^h cannot lie in L on the energy landscape for W_{3D}^{qc}. So to complete the proof, we simply have to conclude that ∇y_k^h is not in M on this landscape. This is assured if

$$\bar{\lambda}_M > r^{1/2} \lambda_2(\nabla y_k^h), \tag{3.258}$$

again given (3.257) and the definition of the set M in (2.26). It is easy to see that from (3.256) that

$$\lambda_2(\nabla y_k^h) = \bar{\lambda}_M^{-1/2} + O(kx_3). \tag{3.259}$$

In addition, since $\bar{\lambda}_M > r^{1/3}$, we know that $\bar{\lambda}_M > r^{1/2} \bar{\lambda}_M^{-1/2}$. Thus, (3.258) follows from (3.259) for kh sufficiently small, and therefore ∇y_k^h lies in S on the energy landscape. This completes the proof. □

3.9 On the numerical implementation of these theories

The Koiter theory

We implement the commercial software package ABAQUS via a user material model (UMAT) for S4 shell elements. This requires Cauchy stress to be specified as

a function of the 2×2 surface deformation gradient $\tilde{F}_s \in \mathbb{R}^{2\times 2}$ as well as the consistent tangent modulus derived from this Cauchy stress (see, for instance, the Abaqus User Subroutines Reference Manual, the section on UMAT, and the subsection on large volume changes with geometric nonlinearity [90]). For this formulation, we take the energy as in (3.184) restricted to 2×2 matrices $\tilde{F} \equiv \tilde{F}_s$ where $\tilde{F}_{31} = \tilde{F}_{32} = 0$. This corresponds to fixing a frame. Also, $\delta(\tilde{F}) = \det \tilde{F}_s$, $\lambda_M(\tilde{F}) = \lambda_M(\tilde{F}_s)$ and following the formalism established at the end of Section 3.6, the Cauchy stress is given by

$$\sigma_r^K(\tilde{F}_s) := (W_{ps})_{,\tilde{F}_s}\, \tilde{F}_s^T, \tag{3.260}$$

where the subscript r is used to emphasize the dependence of this stress on the anisotropy parameter.

Now, the membrane stress σ_r^K in (3.260) inherits soft elasticity, a feature distinct to nematic elastomers as compared to purely elastic materials. This poses some numerical challenges. At small strains, much of the deformation of these elastomers can be accommodated by either soft or very lightly stressed microstructure (regions $\mathcal{L}_m$ and $\mathcal{M}$ on the energy landscape in Figure 3.5). For these regions, the tangent modulus derived from σ_r^K in (3.260) is positive semi-definite and not strictly positive definite: a nematic elastomer has zero stiffness in region $\mathcal{L}_m$ and it has no stiffness against shear in region $\mathcal{M}$. These features lead to difficulties in numerical convergence at small strains. To combat this, we introduce a small energy regularizer whose Cauchy stress has the form

$$\sigma_\epsilon^{reg}(\tilde{F}_s) := \mu\epsilon \left(\tilde{F}_s\tilde{F}_s^T - I_{2\times 2}\right) \tag{3.261}$$

for $0 \leq \epsilon \ll 1$. The consistent tangent modulus derived from σ_ϵ^{reg} is strictly positive definite for all surface deformation gradients $\tilde{F}_s \in \mathbb{R}^{2\times 2}$ with $\det \tilde{F}_s > 0$. Thus, introducing the regularizer $\epsilon \ll 1$ stabilizes the numerical calculation at small strains. For our calculations we use $\epsilon = 0.05$. We have studied the role of ϵ on our simulations and only present conclusions that are independent of this regularization.

The formulas introduced in Section 3.7 for the Koiter theory take the isotropic state to be the reference. However, notice that identity is deep in the interior of the soft region and $\sigma_r^K = 0$ in a neighborhood of identity for $r > 1$ (identity corresponds to the intersection of the red and dark blue curves on the energy landscape for W_{ps} in Figure 3.5(a)). This is a trivial soft regime, which is not of interest here.[4] We

[4]We refer to Conti et al. [27, 28] for extensive investigations of soft elasticity in a similar framework.

are interested in the interplay of microstructure and tension wrinkling, an interplay which is broached in this setting when a genuine tensile response to stretch is induced in the membrane. Therefore, we take the end of this trivial soft state, one with $\lambda_M = \delta = r^{1/6}$, as the reference state by setting

$$\sigma^{sim}_{r,\epsilon}(\tilde{F}_s) := \sigma^K_r(\tilde{F}_s\tilde{U}^r_s) + \sigma^{reg}_\epsilon(\tilde{F}_s), \quad \tilde{U}^r_s := \begin{pmatrix} r^{1/6} & 0 \\ 0 & 1 \end{pmatrix}. \tag{3.262}$$

Finally, the Abaqus S4 shell element slightly modifies the bending term from that derived in our Koiter theory. Specifically, the shell element is based on a kinematic ansatz of the shell deformation through the thickness (see the Abaqus Theory Manual, 3.6.5 Finite-strain shell element formulation [91]). This formulation, in effect, yields a bending energy which depends on a linearization of the second fundamental form.

To study wrinkling, we use the two part procedure detailed by Wong and Pellegrino [111] and Ling Zheng [113] to capture the wrinkling geometry in Abaqus. This involves first a pre-buckling eigenvalue analysis, and then a post buckling analysis. For the pre-buckling eigenvalue analysis, we introduce a small initial prestress in the form of an edge displacement to the membrane. Then we perform an eigenvalue buckling analysis on this lightly stressed membrane to determine the likely buckling modes. After computing the buckling mode shapes, we introduce a linear combination of one or more selected eigenmodes as a geometric imperfection in the membrane at the start of the post buckling analysis. We then apply an initial prestress to the membrane (as in the pre-buckling analysis) in order to provide an initial out-of-plane stiffness to the membrane. Finally, we use the static stabilization procedure in Abaqus to compute the wrinkled shape of the membrane under the clamped stretching deformation. Our detailed implementation of this procedure follows the input file example (Ling Zheng [113] in Appendix B) modified appropriately to incorporate the user material model (3.262) for nematic elastomer sheets.

The effective membrane theory

We compare the results of simulations under the implementation of the Koiter theory described above with analogous simulations of the membrane theory for nematic elastomers (described in Section 3.2). We implement this once again into ABAQUS via UMAT for plane stress CPS4 element, where we take the Cauchy stress in the implementation to be akin to (3.262), with

$$\sigma^{sim}_r(\tilde{F}_s) := \sigma^{mem}_r(\tilde{F}_s\tilde{U}^r_s), \quad \sigma^{mem}_r(\tilde{F}_s) := (W^{qc}_{2D})_{,\tilde{F}_s}\,\tilde{F}^T_s. \tag{3.263}$$

Notice here that we do not employ the use of a regularizer. For simulating the effective membrane theory, there is no wrinkling bifurcation to compute, as wrinkling is treated through effective deformation. Consequently, we do not need to explore the stretch monotonically from small initial stretch. Instead, we explore a range of stretch which excludes small stretch associated to soft elasticity. This can be done without regularization (i.e., by first deforming the specimen homogeneously from the unstressed reference state to a state of stretch far away from soft elastic behavior with the top and bottom of the sheet fixed in the e_2 direction, and then relaxing the boundary conditions on top and bottom to a sheet which is traction free away from the clamped ends).

3.10 Microstructure-induced suppression of wrinkling

We now study the clamped-stretch experiments of Kundler and Finkelmann [58] via simulation of the Koiter theory and the effective membrane theory for nematic elastomer sheets. These results can also be found in Plucinsky and Bhattacharya [80].

We consider a rectangular sheet with length 254 mm, width 101.6 mm and thickness $h = 0.1$ mm that is clamped on both ends and subject to a stretch along its length in the e_1 direction. We choose these dimensions since purely elastic sheets of this dimension readily wrinkle when stretched as demonstrated experimentally and numerically by Zheng [113] (also confirmed numerically by Nayyar et al. [75] and Taylor et al. [93]). We also fix the shear modulus to be $\mu = 6 \times 10^5$ Pa in accordance to experimental observations [105], though this choice is irrelevant as all terms in the energy and stress scale with μ. We take r to be in the range 1 through 1.45 to explore the entire elastic to nematic range.

We often use the nominal strain

$$\varepsilon_{eng} := \frac{L_{final} - L_{initial}}{L_{initial}} \tag{3.264}$$

to display the results. We also use a microstructure indicator parameter

$$\frac{r^{1/2}\delta}{\lambda_M^2}. \tag{3.265}$$

Recall that the curve $\lambda_M^2 = r^{1/2}\delta$ forms the boundary between the region $\mathcal{M}$ with microstructure and region $\mathcal{S}$ without. So, a microstructure parameter (3.265) larger than 1 indicates the presence of fine-scale microstructure.

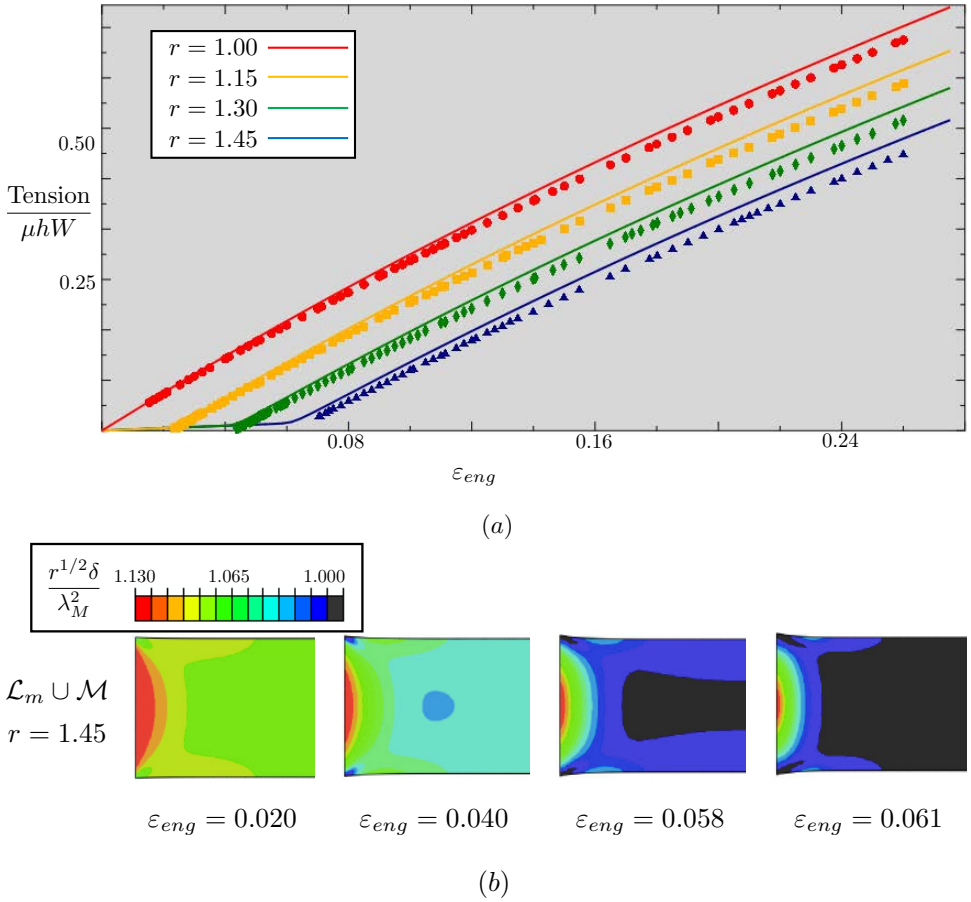

Figure 3.7: (a) Normalized tensile response to stretch (with $W = 101.6$ mm the undeformed width) for nematic elastomer membranes of varying anisotropy: Koiter theory simulations (lines), effective membrane theory simulations (points). (b) Soft elastic response for $r = 1.45$ nematic membrane, and transition to stressed elasticity. Microstructure in $\mathcal{L}_m \cup \mathcal{M}$ indicated by colored regions ($r^{1/2}\delta/\lambda_M^2 > 1$). Note that only the left half of the sheet is shown as the distribution is symmetric

Simulations with Koiter theory

The nominal tensile force of the sheet is plotted in Figure 3.7(a) as a function of the nominal strain. The purely elastic sheet ($r = 1$) is, as expected, immediately tensioned due to the stretch, whereas the nematic sheets ($r > 1$) are soft and nearly stress free during the initial stages of stretch. We call the extent of the soft strain ε_{eng}^{soft}. This depends on the nematic anisotropy r. Recall that we start at $\widehat{U}_r$ or $(\lambda_M, \delta) = (r^{1/6}, r^{1/6})$, the far left point on the boundary between $\mathcal{M}$ and $\mathcal{L}_m$. On the initial application of strain, we expect much of the membrane to traverse this boundary with no stress to the right until it reaches the point $(\lambda_M, \delta) = (r^{1/3}, r^{1/6})$. So we expect to see soft behavior until $\varepsilon_{eng}^{soft} \approx r^{1/6} - 1$. This is consistent with the simulations (e.g., the formula gives $\varepsilon_{eng}^{soft} = 0.063$ in agreement with 0.061 in the

simulations for $r = 1.45$). We note that the soft elastic strain in the Kundler and Finkelmann experiments is $r^{1/2} - 1$ since they start from a state where the director is uniformly vertical instead of $\tilde{U}_s^r$.

The formation of the microstructure is indicated in Figure 3.7(b) for the case $r = 1.45$ by plotting the distribution of the microstructure parameter (3.265) (note that only the left half of the sheet is shown as the distribution is symmetric). Since we start from the state at $\tilde{U}_s^r$, the initial sheet has uniform microstructure. As we stretch, the microstructure evolves differently close to the grips compared to away from them: it is gradually driven out in most of the sheet but persists at the grips. Since the imposed deformation is accommodated by the rearrangement of the microstructure, the response is soft. Eventually, all the microstructure is driven out and the director is uniformly horizontal except close to the grips, signaling an end of the soft behavior. Subsequent stretching leads to proportional increase in load. All of this is consistent with the observations of Kundler and Finkelmann [58] and the simulations of Conti et al. [28].

We show the evolution of wrinkles by plotting the out-of-plane displacement in Figure 3.8 for a variety of r and ε_{eng}. Notice from the top row of Figure 3.8(a) that for the purely elastic sheet ($r = 1$), wrinkles appear almost immediately upon stretch, grow with further stretch, reach a maximum amplitude $u_3/h \approx 3$ and eventually diminish. This, in fact, reproduces the results of Zheng [113] and Nayyar et al. [75]. For a nematic sheet with small nematic order ($r = 1.15$) shown on the second row, we see that wrinkles do not appear until a larger value of stretch, are much smaller in amplitude and disappear faster. For higher values of r shown in the third and fourth rows, wrinkles do not appear. All of this is explored further in Figure 3.8(b), which shows the amplitude of the wrinkles as a function of stretch for various r. We see that wrinkles appear early, have large amplitude and disappear late for the purely elastic sheet ($r = 1$). We also see that wrinkling is suppressed by the introduction of nematic order. In fact, increasing r leads to delayed onset, smaller amplitude and earlier disappearance of wrinkles. Moreover, wrinkling is fully suppressed for values of r greater than 1.2.

Figure 3.9 shows the corresponding evolution of the microstructure. We see from Figure 3.9(a) that microstructure disappears in most of the sheet at small to modest stretch but persists for larger stretch near the grips. We see from Figure 3.9(b) that the maximum microstructure parameter $r^{1/2}\delta/\lambda_M^2$, i.e., the value at the grips, delineates three distinct regions describing microstructure in the sheet for the full

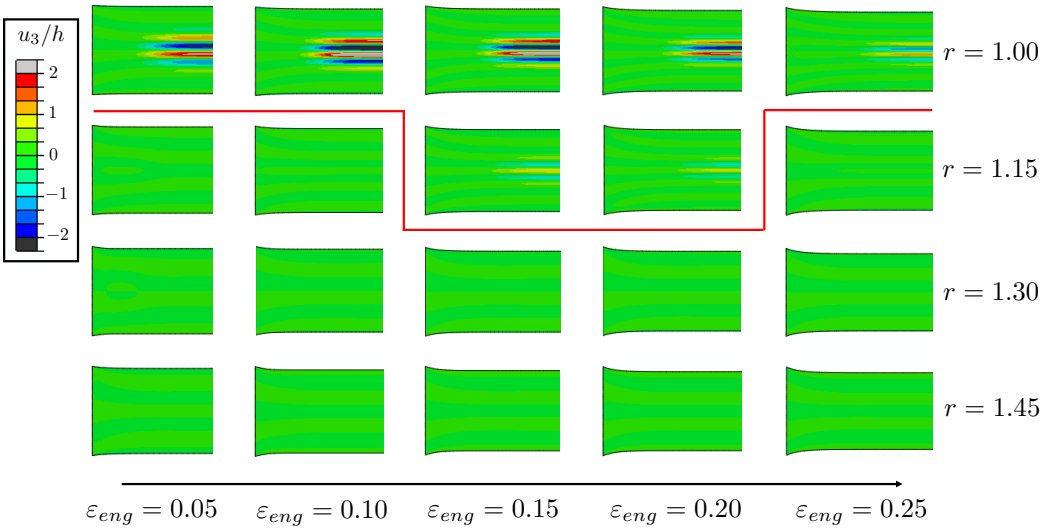

(a)

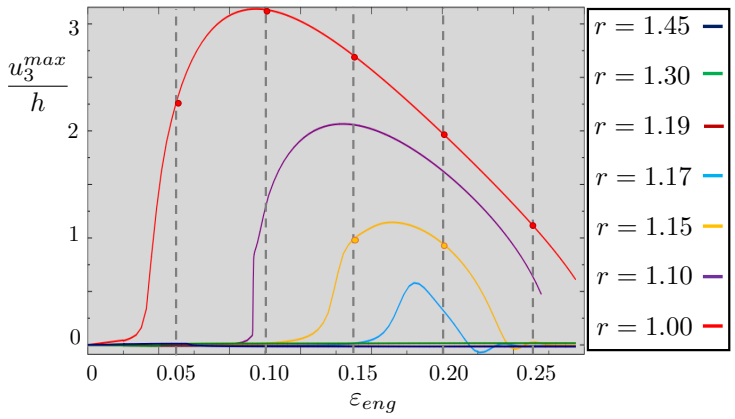

(b)

Figure 3.8: The evolution of wrinkles with applied stretch for a purely elastic material and nematic elastomers with increasing degrees of order. (a) Snapshots of the out-of-plane displacement. (b) The amplitude of wrinkles (i.e., maximum out-of-plane displacement) as a function of stretch for various values of r. We see that wrinkles appear early, have large amplitude and disappear late for the usual elastic material ($r = 1$), but are suppressed with the introduction of nematic order.

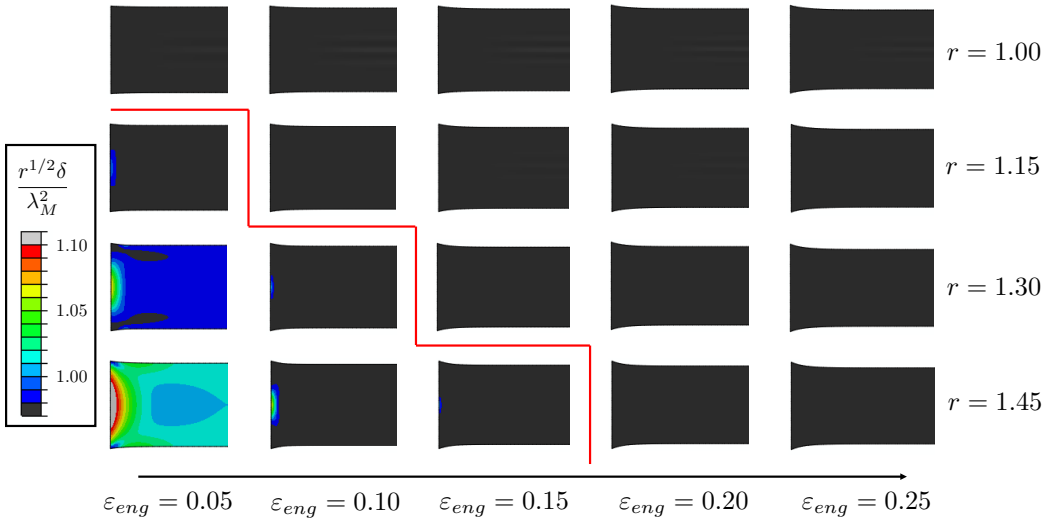

(a)

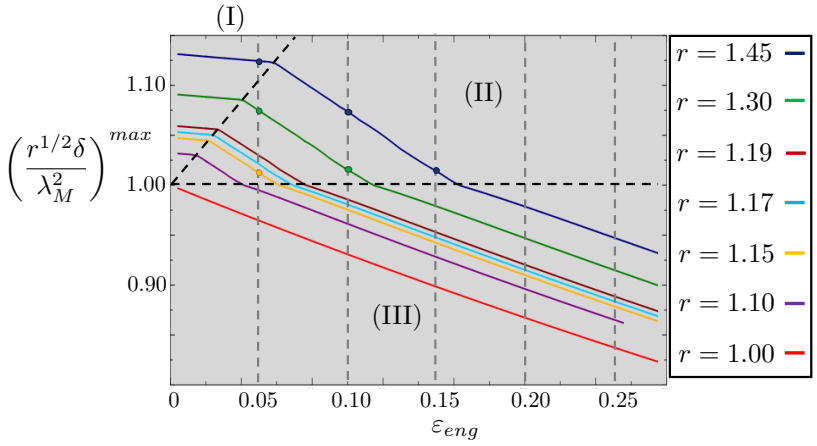

(b)

Figure 3.9: The evolution of microstructure with applied stretch. (a) Snapshots of the microstructure parameter $r^{1/2}\delta/\lambda_M^2$ (values greater than 1 indicate microstructure). (b) The maximum value of the microstructure parameter as a function of stretch for various values of r. This shows three distinct regions: (I) soft; (II) stressed but with microstructure; (III) without microstructure.

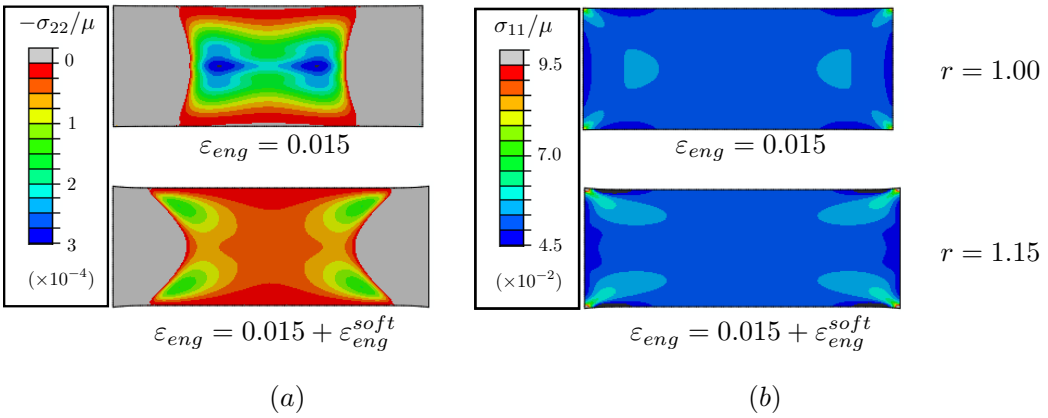

Figure 3.10: The state of stress in a purely elastic sheet ($r = 1$, top row) compared with that in a nematic sheet ($r = 1.15$, bottom row) at comparable values of nominal load but before the onset of wrinkles in the elastic sheet. Note that the purely elastic sheet shows significant transverse compression in the middle, but the nematic sheet does not.

range of stretch: (I) captures soft response to stretch of the sheet, (II) captures the stretch for which the sheet is stressed but with microstructure at the grips and (III) captures the stretch for which there is no longer any microstructure present in the sheet. Thus, larger r implies both a more prolonged soft elastic response and a more prolonged response for which microstructure persists at the clamps.

We turn now to understanding the mechanism by which the presence of nematic microstructure suppresses wrinkling. Figure 3.10 compares the state of stress in a purely elastic sheet ($r = 1$) with that of a nematic sheet ($r = 1.15$) at comparable values of nominal load but before the onset of wrinkles in the elastic sheet (i.e., at a value of ε_{eng} of 0.015 for the elastic sheet and 0.015 beyond the soft strain for the nematic sheet). Notice (top of Figure 3.10(a)) that the purely elastic sheet develops transverse compression. This compressive stress leads to the buckling to a wrinkled state beginning at a stretch $\varepsilon_{eng} \approx 0.025$. However (bottom of Figure 3.10(a)), we notice that there is no transverse compression in the nematic sheet at a comparable value of nominal load. There is some transverse compression closer to the edges, but it is much smaller in magnitude. We see from Figure 3.10(b) that the distribution of longitudinal stress is also different. All of this is a result of the persistence of the microstructure near the grips. In other words, the ability of the nematic material to form microstructure not only gives rise to soft behavior in the bulk, but also qualitatively changes the distribution of stresses near the grips and that in turn suppresses the wrinkling.

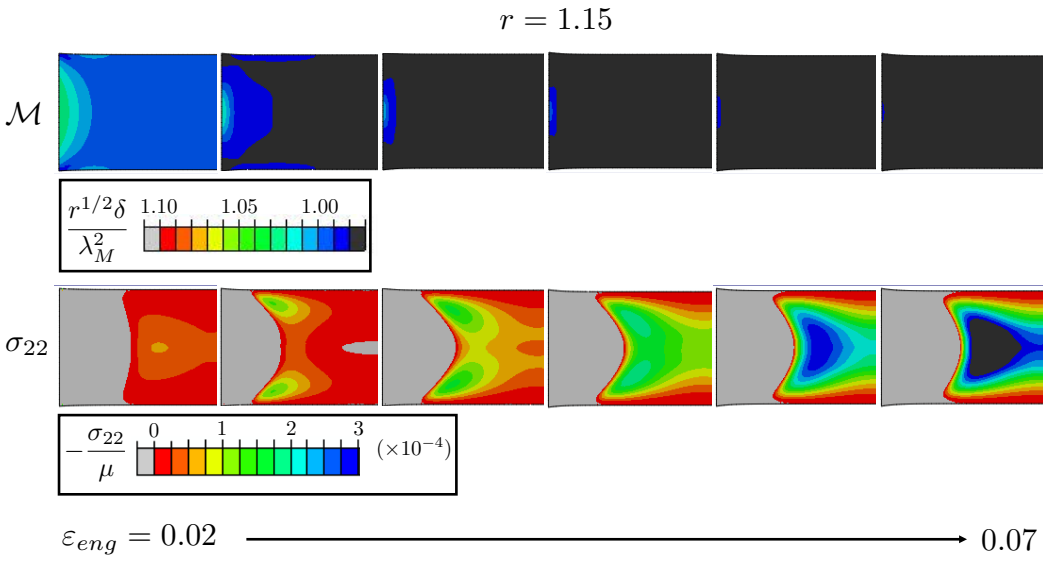

Figure 3.11: The evolution of the microstructure and the lateral compressive stress with increasing stretch in a sheet with $r = 1.15$. Note that there is little to no compression in the middle as long as microstructure persists near the grips.

Mechanistically, note that as the sheet is stretched, it seeks to compress laterally. It is free to do so away from the grips, but is prevented from doing so near the clamped grips. This leads to a shear deformation near the corners extending diagonally into the sheet. This, in turn, leads to the compressive stress in the elastic sheet. In contrast, the ability of the nematic sheet to form microstructure enables it to accommodate the shear strain through equi-biaxial tension at the clamps (recall that nematic sheets can accommodate shear strain without shear stress in the region or microstructure $\mathcal{M}$).

Figures 3.11 and 3.12 elaborate on this. Figure 3.11 shows how the microstructure parameter and transverse compression evolve in the sheet with increasing stretch, starting at the end of soft behavior. We observe that the microstructure persists near the grips but reduces with increasing stretch until it is fully driven out. Additionally, we see small regions of transverse compressive stress form near the free edges, and these regions gradually move inward with increasing magnitude as microstructure is driven out. Finally, when all microstructure is driven out, we have transverse compressive stress in the middle similar to that of the purely elastic sheet (top of Figure 3.10(a)). This compression increases with further stretch and eventually leads to wrinkling (Figure 3.8). However, as shown in Figure 3.12, the ratio of the transverse compression to the longitudinal tension at a value of stretch where all microstructure is driven out decreases with increasing r. As we know from the study

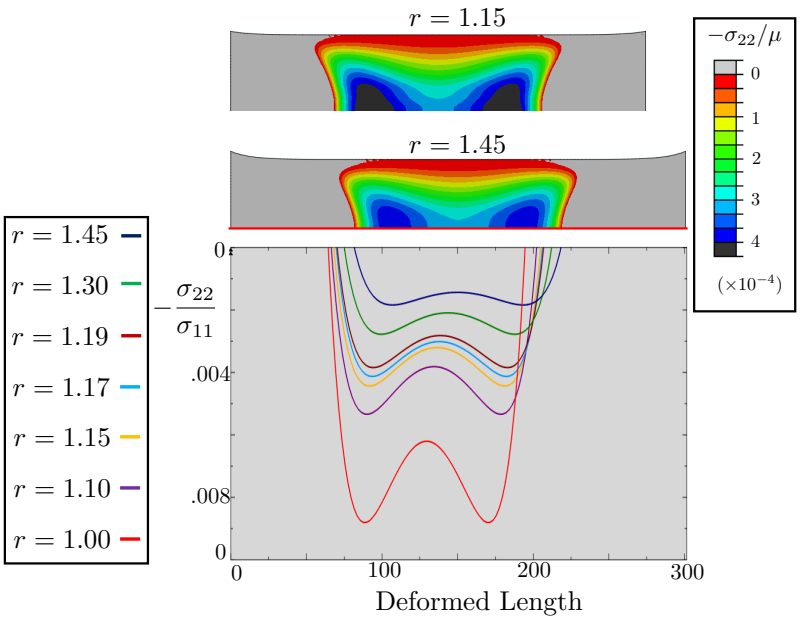

Figure 3.12: The distribution of the lateral compressive stress (top) and the ratio of the lateral compressive stress to longitudinal tensile stress along the middle line in sheets with various r at the stretch where the microstructure just disappears at the clamps.

of elastic sheets, high relative longitudinal tension suppresses wrinkles[5] – note from Figure 3.8(a) that wrinkles disappear in the elastic sheet at high stretch. Thus, the microstructure near the grips delays the formation of a central region of transverse compressive stress and the onset of wrinkles. However, large relative longitudinal tension also suppresses wrinkles; so if the delay is sufficient, as is the case for larger r, then wrinkling is fully suppressed.

Simulations with effective membrane theory and comparison

We repeat the clamped-stretch simulations of purely elastic and nematic sheets using the membrane or tension field theory. The nominal force vs. nominal strain is shown in Figure 3.7(a) as the points. We see that the results agree well with those obtained using the Koiter theory. We show the evolution of the microstructure at $\varepsilon_{eng} = 0.08$ for various values of r, and compare it with those obtained with the Koiter theory in Figure 3.13(a). Again we find striking agreement. Recall that the membrane theory does not describe the details of the wrinkles but relaxes over them, i.e., computes their consequence assuming that they were infinitely fine. So, the results do not show any out-of-plane displacement. However, recall that the curve $\delta = \lambda_M^{1/2}$ is the

[5]This is also evident in the role of aspect ratio as was shown by Ling Zheng [113] and Nayyer et al. [75].

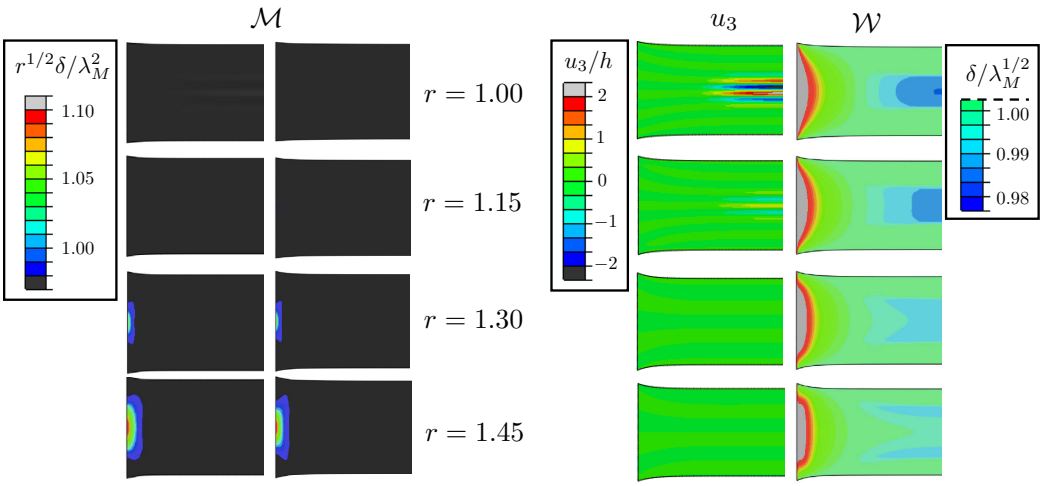

Figure 3.13: Comparison of clamped stretched simulation under the effective membrane theory and Koiter theory for $r = 1, 1.15, 1.30$ and 1.45 nematic sheets. (a) Microstructure comparison at stretch $\varepsilon_{eng} = 0.08$; Koiter (left) and membrane (right). (b) Wrinkling comparison at stretch $\varepsilon_{eng} = 0.20$; Koiter (left) and membrane (right).

boundary between the presence and absence of wrinkling. Therefore, any value of the parameter

$$\frac{\delta}{\lambda_M^{1/2}} \tag{3.266}$$

below 1 indicates the presence of (infinitely) fine scale wrinkles in the simulation with this membrane theory. This indicator is shown in Figure 3.13(b) for $\varepsilon_{eng} = 0.20$, and compared with the wrinkles computed earlier. Again, we see very good agreement.

Thus we conclude that the membrane or tension field theory provides a very good description of the overall behavior of the sheets including nominal stress-strain relation, the formation of microstructure and the formation of wrinkles. Further, the agreement using an independent set of simulations provides confidence in our understanding regarding the suppression of wrinkles by nematic microstructure.

Chapter 4

ACTUATION OF HETEROGENEOUSLY PATTERNED THIN SHEETS

In this chapter, we explain the richness of the shape-changing deformations of nematic elastomers and how this can be exploited to make the material act as a machine [15]. The foundation of our work is the metric constraint governing actuation in these sheets (equation (4.2) below). We start from the established theory for nematic elastomers by Bladon et al. [19, 105] (recall Chapter 2) and show that designs and deformations that satisfy (4.2) arise naturally from energy minimization.

This metric constraint is a generalization of the metric constraint underlying Aharoni et al. [2] with two novel features which dramatically expand the design landscape for shape-changing deformation in these sheets. First, smoothness is not a requirement here. With this, we explore *nonisometric origami* where heterogeneity is programmed in a piecewise constant pattern so that thermal actuation leads to complex folding patterns (Figures 4.2-4.3). Second, the constraint is amenable to three dimensional programming. With this, we explore *lifted surfaces* where heterogeneity is programmed so that thermal actuation leads to a prescribed surface of arbitrary complexity as long as it is smooth and has limited slope (Figure 4.4).

In Section 4.1, we provide a summary which (i) introduces the key metric constraint, (ii) discusses the novel designs amenable to this constraint and (iii) sketches of the derivation of the constraint. This summary is analogous to our short paper: Plucinsky et al. [82], written with a view towards applications. In the remaining sections, we turn to a precise justification of the constraint and its corresponding design landscape; thus, taking the more mathematical perspective. These results can be found in Plucinsky et al. [81].

4.1 Programming complex shapes in thin nematic elastomer sheets

The metric constraint

To introduce the metric constraint, we recall that n_0 (which maps to $\mathbb{S}^2$) denotes the nematic director or the direction of anisotropy in the undeformed sheet, and $r(T) \geq 1$ is the temperature-dependent anisotropy parameter which captures the

stretch along the director and contraction transversely. This parameter is assumed to be monotonically decreasing for temperatures below the isotropic-nematic transition temperature and equal to 1 in the isotropic regime. For a nematic-genesis elastomer formed at temperature T_0 and subjected to a new temperature T_f, a spontaneous distortion with stretch $\ell_{n_0}^{1/2}$ is the preferred state, where

$$\ell_{n_0} := \bar{r}^{-1/3}(I_{3\times 3} + (\bar{r} - 1)n_0 \otimes n_0) \tag{4.1}$$

is the step-length tensor (see Chapter 2) and $\bar{r} = r(T_f)/r(T_0)$, so that $\bar{r} > 1$ for cooling and $\bar{r} \in (0, 1)$ for heating.

For actuation, we consider a thin sheet of thickness h occupying an initially undeformed flat three dimensional region $\Omega_h := \omega \times (-h/2, h/2) \subset \mathbb{R}^3$ where $\omega \subset \mathbb{R}^2$ denotes the two dimensional midplane of the sheet. In the synthesis of nematic elastomer sheets (e.g., the experiments of Ware et al. [102])), typically $h \sim 10\mu m$ whereas the lateral dimensions of the sheet are much larger, typically $\sim cm$. Hence, we assume $h \ll 1$ and the characteristic length scale of ω is $O(1)$ in non-dimensional units. Let $x := (x_1, x_2, x_3)$ denote the position on Ω_h in a Cartesian frame with $\{e_1, e_2, e_3\}$ denoting the basis and e_3 pointing normal to ω. We will identify a point $\tilde{x} := (x_1, x_2) \in \omega$ with $(x_1, x_2, 0) \in \Omega_h$. By a program or design, we mean the prescription of a non-uniform director field on the sheet $n_0 : \Omega_h \to \mathbb{S}^2$. In this letter, we only consider directors that are uniform through the thickness, i.e., $n_0 \equiv n_0(\tilde{x})$. When the sheet is heated or cooled, non-uniform spontaneous distortion forces a possible out-of-plane deformation of the sheet. If the sheet is thin enough (we return to this later), it suffices to study the deformation of the midplane, $y : \omega \to \mathbb{R}^3$. In particular, we are interested in midplane deformations which are *stress-free*. These are characterized by the metric constraint

$$(\tilde{\nabla} y)^T \tilde{\nabla} y = r^{-1/3}(I_{2\times 2} + (r - 1)\tilde{n}_0 \otimes \tilde{n}_0) =: \tilde{\ell}_{n_0}, \qquad \text{a.e. on } \omega. \tag{4.2}$$

Here, $I_{2\times 2} \in \mathbb{R}^{2\times 2}$ is the identity, $\tilde{\nabla}$ is the planar gradient (i.e., with respect to $\tilde{x}$) so that $\tilde{\nabla} y$ is a 3×2 matrix, $\tilde{n}_0 := (n_0 \cdot e_1, n_0 \cdot e_2)^T$ is the projection of n_0 onto the plane ω and $\tilde{\ell}_{n_0}$ is the 2×2 submatrix of ℓ_{n_0} associated to this projection. Note that since $\tilde{n}_0$ is a projection, it need not be a unit vector.

As already intimated, the metric constraint (4.2) generalizes the constraint of Aharoni et al. [2] in two directions; by relaxing the smoothness requirement and by extending the constraint to three dimensional programming. Indeed, for the former, the metric constraint (4.2) need only hold almost everywhere (i.e., except on sets of

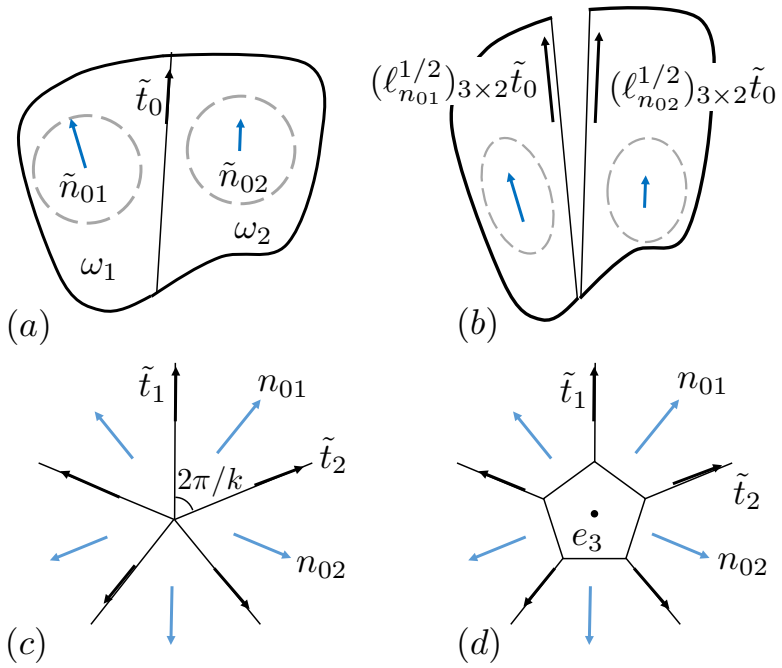

Figure 4.1: Interfaces and junctions on cooling. (a,b) If each half of the sheet (a) is allowed to independently deform spontaneously, it has the shape in (b) where $(\ell^{1/2}_{n_{0i}})_{3\times2} := \bar{r}^{-1/6}(I_{3\times2} + (\bar{r}^{1/2} - 1)n_{0i} \otimes \tilde{n}_{0i})$. The interface can be unbroken by rotating one side relative to the other if and only if (4.3) holds. (c) Symmetric junction. (d) Truncated junction.

zero measure in $\mathbb{R}^2$), and this allows for piecewise constant director designs. For the latter, (4.2) allows for three dimensional programming while reducing to the constraint of [2] in the case of a planar director. To see this, if n_0 is planar, then $n_0 \equiv \tilde{n}_0$ and we can write $n_0 \cdot e_1 = \cos(\theta)$ and $n_0 \cdot e_2 = \sin(\theta)$. It follows that $(\tilde{\nabla} y)^T \tilde{\nabla} y = \tilde{\ell}_{n_0} = \tilde{R}(\theta)\text{diag}\,(\bar{r}^{2/3}, \bar{r}^{-1/3})\tilde{R}(\theta)^T = g_y$ for $\tilde{R}(\theta) \in SO(2)$, a rotation of θ about the normal to the initially flat sheet as required by [2].

Examples

We turn now to examples which highlight the richness of designable surfaces satisfying the metric constraint (4.2). In addition, these examples serve to motivate the appropriate compatibility conditions consistent with (4.2) for a general class of smooth and non-smooth designable surfaces. Finally, an important attribute of these designable surfaces is that the actuation is extremely robust since the entire sheet participates in the deformation. This was observed experimentally by Ware et al. [102], and it is in marked contrast to other attempts at foldable structures and origami where the actuation is limited to folds [47, 84], or bendable structures where through thickness non-uniformity results in complex shape but with little ability to

carry load [1, 104].

Nonisometric origami

We begin with *nonisometric origami* where the director is programmed in a piecewise constant pattern (also see [69, 68]). To start, assume the sheet ω is the union of two regions ω_1 and ω_2 separated by a straight interface assigned a tangent vector $\tilde{t}_0 \in \mathbb{S}^1$. Suppose we program this sheet with the director n_{01} in ω_1 and n_{02} in ω_2. Then, it is possible to satisfy (4.2) via a continuous piecewise affine deformation y on all of ω if and only if

$$|\tilde{n}_{01} \cdot \tilde{t}_0| = |\tilde{n}_{02} \cdot \tilde{t}_0|, \tag{4.3}$$

where again $\tilde{n}_{0i}$ denotes the projection of n_{0i} onto ω. This is the consequence of a geometric argument for constructing continuous piecewise affine deformations with prescribed metric or stretch tensor provided in Figures 4.1(a) and (b)—an argument that has been applied previously in the study of active martensitic sheets [14, 15].

Now consider a sheet of k sectors $\omega_i, i = 1, \dots k$, with the interfaces $\tilde{t}_i$ meeting at a junction and with the sheet programmed with the director n_{0i} in the sector ω_i. While the condition (4.3) is necessary at each interface, it is not sufficient to satisfy (4.2) via a continuous piecewise affine deformation. One needs an additional global condition to ensure that all the rotations match up as one goes around the junction. This is extremely rich in general: for example, the case of three sectors with fixed distinct planar directors $n_{0i} \equiv \tilde{n}_{0i}$ for $i = 1, 2, 3$ can have up to 32 non-trivial compatible junctions for various $\bar{r}$ and n_{0i} (we detail this in Appendix A.3). For now though, we focus on a simple case of a junction with all sectors spanning the same angle and with the director programmed to be planar. In this case, it is possible to satisfy (4.2) via a continuous piecewise affine deformation on cooling (respectively heating) if the director n_{0i} is programmed to bisect the angle between $\tilde{t}_i$ and $\tilde{t}_{i+1}$ (respectively is normal to the bisector) as shown in Figure 4.1(c). Indeed, on cooling, the angle to each sector reduces, but all the sectors can be brought into contact by rotating them out-of-plane to form a $k-$sided pyramid. Note that there is a symmetry here and one can form two possible pyramids (going up or down). However, one can break this symmetry in practice by adding a small inhomogeneity though the thickness to bias bending in one direction. One can form a truncated pyramid by replacing the junction with a regular $k-$sided polygon as shown in Figure 4.1(d); each sector is programmed with a planar director as before while the central polygon is programmed with the director to be fully out-of-plane.

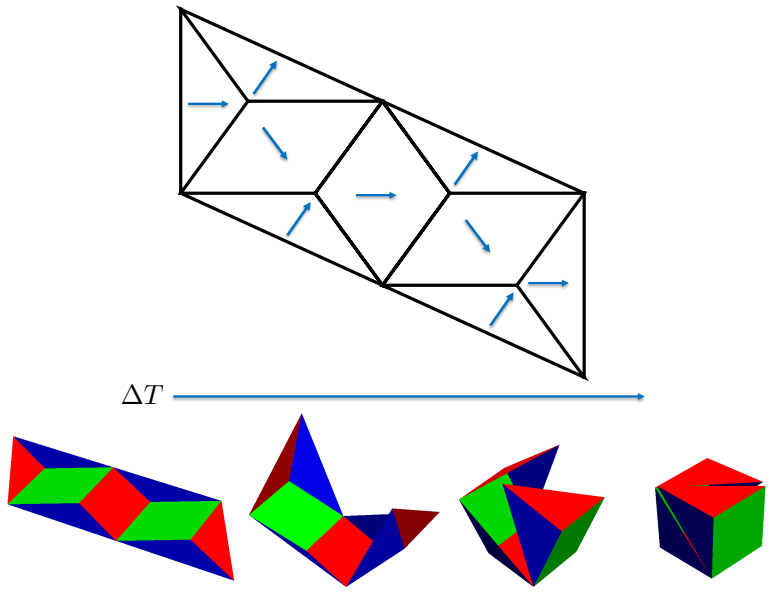

(a) Box

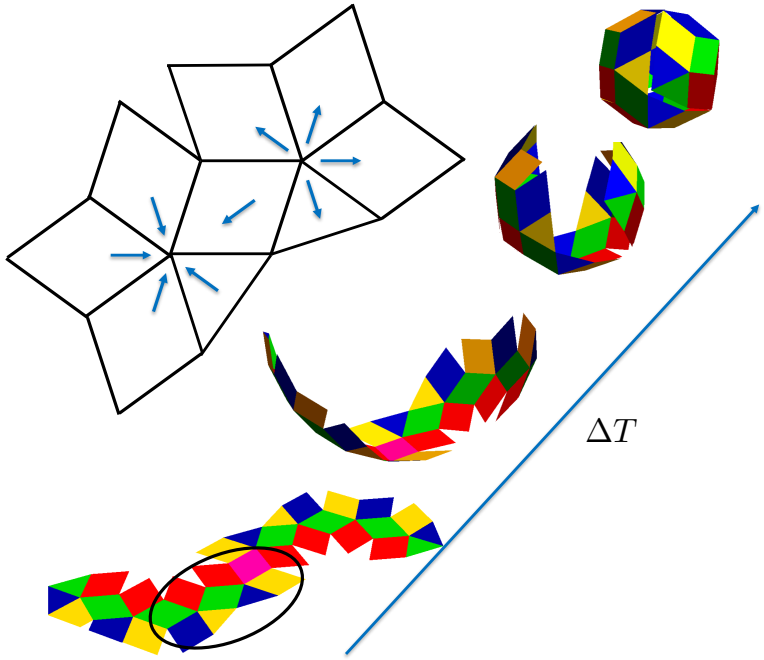

(b) Rhombic triacontahedron

Figure 4.2: Polyhedra examples of nonisometric origami: The line diagrams show the design with the arrows representing the constant director prescribed in each region. The color images show the deformed shape upon cooling. We note that the designs in (a) and (b) are compositions of a number of symmetric junctions shown in Figure 4.1(c) ($k = 3$ in (a) and $k = 5$ in (b)).

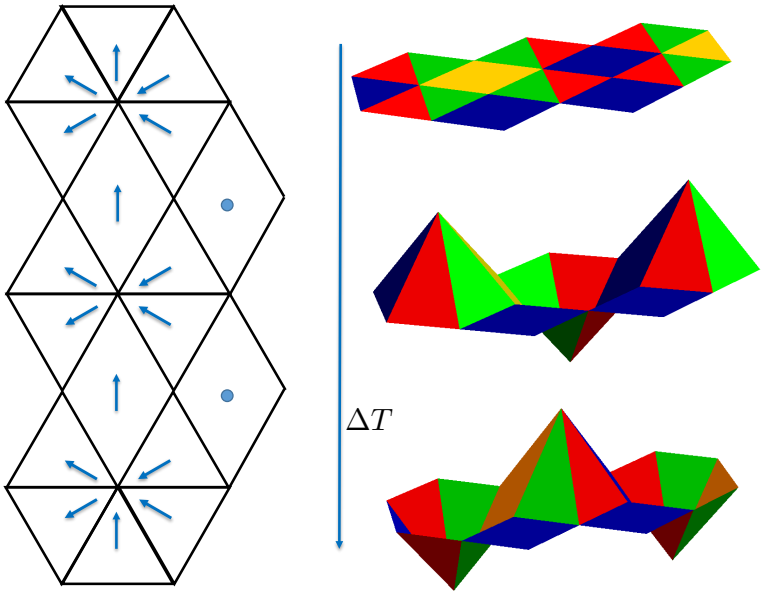

(a) Devil's Golfcourse

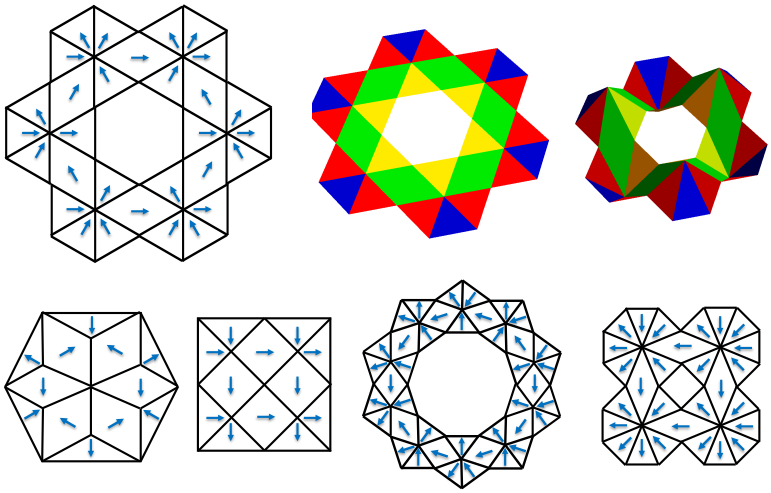

(b) Periodic flower(ish) designs

Figure 4.3: Periodic examples of nonisometric origami: The line diagrams show the design with the arrows representing the constant director prescribed in each region. The color images show the deformed shape upon cooling. We note that the designs in (a) incorporate a truncated junction (Figure 4.1(d)). The designs in (b) connect symmetric junctions azimuthally about an axis.

Importantly, it is possible to arrange a number of these junctions and truncated junctions to form complex shapes as we explain with four examples. First, we can put together a number of three-sided junctions to form a cube as in Figure 4.2(a) (also see [69]). As the temperature decreases and thus $\bar{r}$ increases each junction becomes a pyramid and eventually becomes the corner of a cube at $\bar{r} = 3$. Our next example in Figure 4.2(b) shows a rhombic triacontahedron. This design is formed by repeating the pattern shown. Next in Figure 4.3(a), we form a Devil's Golfcourse using the design shown. Since this design is periodic, it can be extended ad infinitum. Finally, we emphasize that these are but a small number of exemplars and many generalizations are possible. For instance, in Figure 4.3(b), we patch an even number of regular polygons into a ring and follow a construction to obtain an azimuthally periodic compatible shape. There are an infinite number of these designs.

Lifted surfaces

We now consider our second class of examples, that of *lifted surfaces*. We look for designs where cooling the sheet leads to a surface that can be described by the graph of a function φ. We show that this is possible if function φ is smooth enough (in the Sobolev space $W^{2,\infty}$) and satisfies the constraint

$$\|\tilde{\nabla}\varphi\|^2_{L^\infty} < \lambda_{\bar{r}} := \bar{r} - 1 \tag{4.4}$$

on its domain. Specifically, we show that we can achieve this shape with the director programmed as follows

$$n_0(\tilde{x}) = \frac{1}{\lambda_{\bar{r}}^{1/2}} \begin{pmatrix} \partial_1\varphi(\bar{r}^{-1/6}\tilde{x}) \\ \partial_2\varphi(r^{-1/6}\tilde{x}) \\ (\lambda_{\bar{r}} - |\tilde{\nabla}\varphi(\bar{r}^{-1/6}\tilde{x})|^2)^{1/2} \end{pmatrix} \tag{4.5}$$

and through a deformation y that consists of a uniform contraction followed by a lifting:

$$y(\tilde{x}) = \bar{r}^{-1/6}(x_1 e_1 + x_2 e_2) + \varphi(\bar{r}^{-1/6}\tilde{x})e_3. \tag{4.6}$$

Before we prove that this ansatz satisfies the metric constraint (4.2), we note that one can create a large number of shapes using such an approach. Since $\bar{r}$ can be significantly different from 1 in nematic elastomers, one can form shapes with significant displacement like spherical caps and sinusoidally rough surfaces. Figure 4.4 shows two additional examples with complex surface relief. These are but a

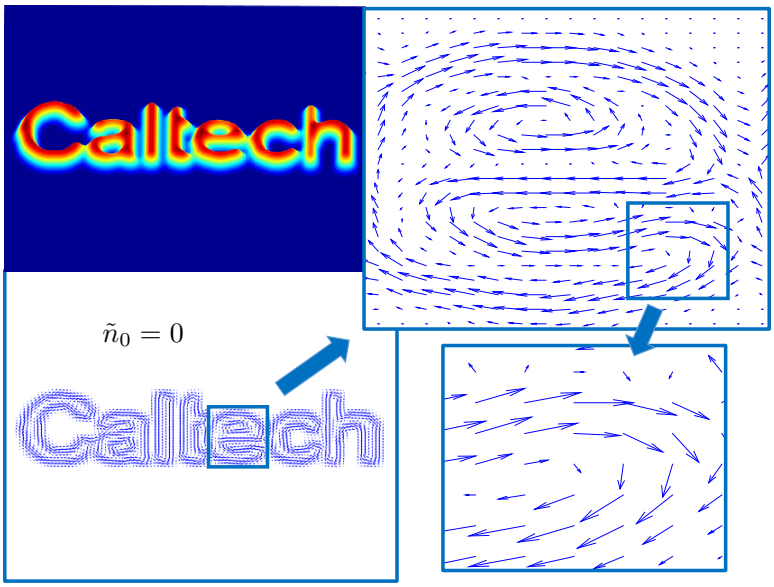

(a) Caltech

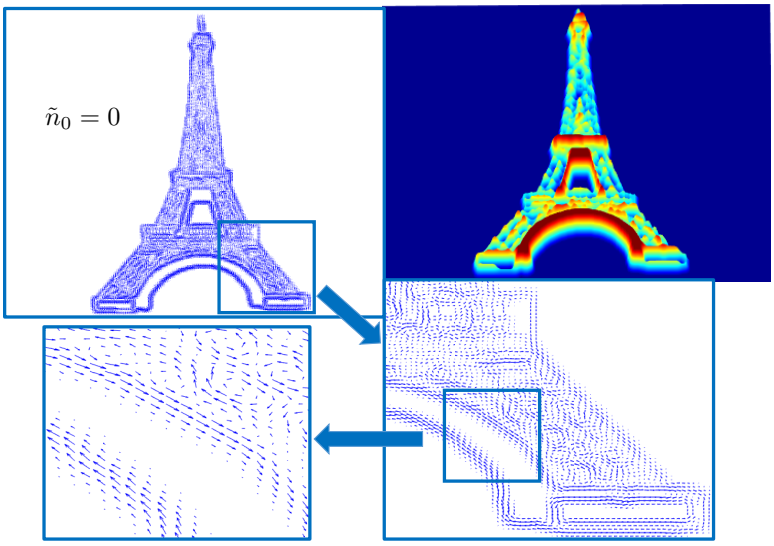

(b) Eiffel tower

Figure 4.4: The deformed shape and designs for lifted surfaces. The vector plots show the director orientation in the design. The amplitude of each vector denotes the planar component n_0' of the director. The color images show the topographic map of the sheet after deformation with the colors representing height (hot colors are high). The designs are generated from equation (4.103) by taking φ to be a smoothened and rescaled greyscale of the desired image.

small sample of the designs amenable to this framework. Indeed, given any arbitrary greyscale image $\mathcal{G}$, we can program a nematic sheet so that the surface of the sheet upon cooling corresponds to this image. We do this by smearing $\mathcal{G}$ (for instance by mollification or by averaging over a small square twice) and taking this as φ.

The fact that the lifted surface ansatz satisfies (4.2) can be verified directly. However to motivate the ansatz, we now rewrite (4.2) in an equivalent form which points to a concrete design scheme. Heuristically, we turn the statement around by first identifying the set of deformation gradients consistent with (4.2) for any director and then identifying the director associated with the deformation gradient. We conclude that the metric constraint (4.2) holds if and only if

$$\tilde{\nabla} y(\tilde{x}) \in \mathcal{D}_{\bar{r}}, \quad n_0(\tilde{x}) \in \mathcal{N}^{\bar{r}}_{\tilde{\nabla} y(\tilde{x})}, \qquad \text{a.e. } \tilde{x} \in \omega. \tag{4.7}$$

Here,

$$\begin{aligned} \mathcal{D}_{\bar{r}} := \Big\{ \tilde{F} \in \mathbb{R}^{3\times 2} : |\tilde{F}|^2 \leq \bar{r}^{-1/3} + \bar{r}^{2/3}, \\ \bar{r}^{-1/3} \leq |\tilde{F} e_\alpha|^2 \leq \bar{r}^{2/3} \ \ \alpha = 1, 2, \\ (\tilde{F}\tilde{e}_1 \cdot \tilde{F}\tilde{e}_2)^2 = (|\tilde{F}\tilde{e}_1|^2 - \bar{r}^{-1/3})(|\tilde{F}\tilde{e}_2|^2 - \bar{r}^{-1/3}) \Big\}, \end{aligned} \tag{4.8}$$

and

$$\begin{aligned} \mathcal{N}^{\bar{r}}_{\tilde{F}} := \Big\{ m \in \mathbb{S}^2 : (m \cdot e_\alpha)^2 = \frac{|\tilde{F}\tilde{e}_\alpha|^2 - \bar{r}^{-1/3}}{\bar{r}^{2/3} - \bar{r}^{-1/3}}, \alpha = 1, 2, \\ \operatorname{sign}((m \cdot e_1)(m \cdot e_2)) = \operatorname{sign}(\tilde{F}\tilde{e}_1 \cdot \tilde{F}\tilde{e}_2) \Big\}, \end{aligned} \tag{4.9}$$

when $\bar{r} > 1$ (the inequalities for $\mathcal{D}_{\bar{r}}$ and the sign in (4.9) are switched when $\bar{r} < 1$). With this description, we seek the restrictions on the class of deformations of the the form (4.101) that satisfy the first condition of (4.7). We find (4.4) is sufficient. We then seek the restrictions on the director n_0 that satisfy the second condition of (4.7) for this deformation, and this yields the formula (4.103).

Naturally, given this analysis, it would be appealing to have a characterization of the geometry of surfaces described by deformations which satisfy (4.7) without the ansatz (4.101). We would then be able to characterize all possible shapes that could be thermally actuated from programing nematic anisotropy into a thin sheet. Unfortunately, such a broad characterization remains open.

Sketch of the derivation of the metric constraint

Finally, we turn to the derivation of the metric constraint (4.2). Our starting point is the well-accepted theory of Bladon et al. [19]. A nematic elastomer formed at

temperature T_0 with initial director $n_0 \in \mathbb{S}^2$, then subjected to a three dimensional deformation gradient $F \in \mathbb{R}^{3\times3}$ and current director $n \in \mathbb{S}^2$ at temperature T_f has a free energy density given by the non-negative quantity

$$W^e(F, n, n_0) := \frac{\mu}{2}\left(\mathrm{Tr}(F^T(\ell_n^f)^{-1}F(\ell_{n_0}^0)) - 3\right), \tag{4.10}$$

where ℓ_n^f and $\ell_{n_0}^0$ are the step-length tensor (4.1) with $\bar{r}$ replaced by $r(T_f)$ and $r(T_0)$ respectively. The incompressibility of elastomers, i.e., $\det F = 1$, is assumed here. Now, given a thin sheet Ω_h of thickness h and a design n_0, we suppose a three dimensional deformation $y^h : \Omega_h \to \mathbb{R}^3$ of this sheet has a strain energy given by

$$\mathcal{I}_{n_0}^h(y^h) := \int_{\Omega_h} W^e\left(\nabla y^h, \frac{\nabla y^h n_0}{|\nabla y^h n_0|}, n_0\right) dx. \tag{4.11}$$

Here, ∇ is the three dimensional gradient as y^h depends on $x = (\tilde{x}, x_3)$, and we introduce a kinematic ansatz on the current director $n^h \colon \Omega_h \to \mathbb{S}^2$ (the middle argument in W^e) justifiable for low energy deformations (i.e., Modes et al. [67]).

To arrive at the metric constraint (4.2), we first observe that due to incompressibility and the kinematic ansatz, $\mathcal{I}_{n_0}^h(y^h)$ is minimized (and equal to 0) if and only if

$$(\nabla y^h)^T \nabla y^h = \ell_{n_0} \quad \text{ a.e. on } \Omega_h \tag{4.12}$$

for the three dimensional step-length tensor ℓ_{n_0} in (4.1). However, this equation is not useful for design since it highly restricts the nature of heterogeneity for said program $n_0 \colon \Omega_h \to \mathbb{S}^2$ (see for instance the discussions in Efrati et al. [39]). Fortunately, it can be relaxed considerably by taking advantage of the thinness of nematic sheets. In fact, if the thickness h is sufficiently small, it suffices to ignore the constraints associated with the out-of-plane deformation gradient $\partial_3 y^h$ entirely, and focus solely on satisfying the constraint at the midplane ω. In doing this, we derive (4.2) from (4.12).

We dedicate the remainder of this chapter to the justification of this simplification and also the justification of the designable actuation this simplification admits.

4.2 The model and the metric constraint

The model

We consider a thin sheet of nematic elastomer of thickness $h \ll 1$. Initially, the sheet occupies a flat region in space,

$$\Omega_h := \omega \times (-h/2, h/2), \qquad \omega \subset \mathbb{R}^2, \tag{4.13}$$

where ω is an open, connected and bounded Lipschitz domain which we call the midplane of the sheet. We envision that the elastomer sheet is patterned heterogeneously by a director field $n_0^h : \Omega_h \to \mathbb{S}^2$ at the initial temperature T_0. Upon changing the temperature from T_0 to the final temperature T_f, the sheet will spontaneously deform by a deformation $y^h : \Omega_h \to \mathbb{R}^3$ which we assume minimizes the entropic elastic energy

$$\mathcal{I}^h_{n_0^h}(y^h) := \int_{\Omega_h} W^e\left(\nabla y^h, \frac{(\nabla y^h)n_0^h}{|(\nabla y^h)n_0^h|}, n_0^h\right) dx. \tag{4.14}$$

Here, following Bladon et al. [19] (see also Warner and Terentjev [105]), we take the *entropic elastic energy density* W^e as in (2.1) (see Chapter 2).

Remark 4.2.1 *(i) W^e satisfies* $\min W^e = 0$. *Further, $W^e(F, \frac{Fn_0}{|Fn_0|}, n_0) = 0$ if and only if $F^TF = \bar{r}^{-1/3}(I_{3\times 3} + (\bar{r} - 1)n_0 \otimes n_0)$ for $\bar{r} = r(T_f)/r(T_0)$ (see the Proposition A.1.7).*

(ii) The elastic energy $\mathcal{I}^h_{n_0^h}$ is defined without any displacement or traction boundary conditions as we are dealing with actuation only.

(iii) In the definition (4.14) *of $\mathcal{I}^h_{n_0^h}(y^h)$, we imposed the kinematic constraint $n^h = \frac{(\nabla y^h)n_0^h}{|(\nabla y^h)n_0^h|}$. The constraint is similar to one that was imposed by Modes et al. [67] in their prediction for conical and saddle like actuation in nematic glass sheets with radial and azimuthal heterogeneity (in fact, both constraints are equivalent for zero energy/stress free states; see Proposition A.1.7).*

There are nematic elastomers which do not satisfy this kinematic constraint (i.e., where the director n^h is allowed to vary more freely). Those materials can show macroscopic deformations which arise from the fine-scale microstructure produced by oscillations of n^h [25, 27, 28, 37] (see also the experiments by Kundler and Finkelmann [58]).

In this chapter, we are interested in actuating complex, yet predictable, shape by programming an initial heterogeneous anisotropy n_0^h in the nematic elastomer. It would be difficult to control actuation for a material that is capable of freely forming microstructure which competes with the shape change driven by the programmed anisotropy, even at low energy. For simplicity, we have chosen the hard kinematic constraint $n^h = \frac{(\nabla y^h)n_0^h}{|(\nabla y^h)n_0^h|}$ here in order to exclude the free formation of microstructure. The results that we prove for this energy (i.e., $\mathcal{I}^h_{n_0^h}$

with this kinematic constraint) can also be proven for a more realistic energy in which the sharp constraint is replaced by a non-ideal energy contribution penalizing deviations from the constraint. (In fact, we use this more realistic model when deriving the metric constraint as a necessary condition; this is discussed in Section 4.6.)

(iv) We are neglecting Frank elasticity (an elasticity thought to play a critical role in the behavior of liquid crystal fluids, i.e., de Gennes and Prost [49]) and related effects in our model, as these are expected to be small in comparison to the entropic elasticity (see discussion in Chapter 3 in Warner and Tarentjev [105]). However, to derive the key metric constraint (introduced below) as a necessary feature of low energy deformations, we add to the energy (4.14) *a small contribution from Frank elasticity for technical reasons. This is discussed in Section 4.6.*

The metric constraint

Our goal is to characterize the class of director fields n_0^h and corresponding deformations y^h which yield small elastic energy $I^h_{n_0^h}(y^h)$ under the assumption of a desired planar director field design $n_0 \equiv n_0(\tilde{x})$. To be precise:

Assumption 4.2.2 *We assume*

$$\begin{aligned} &n_0^h(x) = n_0(\tilde{x}) + O(h), \quad \textit{for a.e. } x \in \Omega_h, \\ &\textit{i.e.,} \quad \|n_0^h - n_0\|_{L^\infty(\Omega_h)} \leq \tau h \quad \textit{for some } \tau > 0. \end{aligned} \tag{4.15}$$

The $O(h)$ term accounts for the following two possible deviations from the desired design. For definiteness, we have fixed the maximum tolerance $\tau > 0$ for these non-idealities.

(a) The assumption accounts for deviations of the director field through the thickness which are of the same order as the thickness. Note that this excludes twisted or splay-bend nematic sheets [47, 104], for which one prescribes the director field on the top surface of the sheet and then differently on the bottom surface, so that the director field has to vary by an $O(1)$ amount through the thickness.

(b) The assumption also accounts for the possibility of planar deviations. In the synthesis techniques employed by Ware et al. [102], the director field is

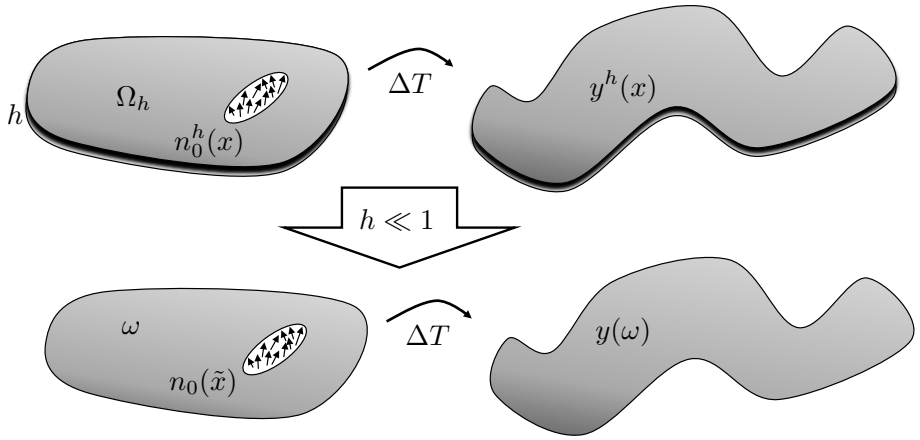

Figure 4.5: Actuation for thin sheets is characterized by the midplane fields.

prescribed in voxels or cubes whose characteristic length is similar to the thickness and we expect the experimental error to be of this order.

Under Assumption 4.2.2, this characterization comes in the form of a two-dimensional effective metric constraint (4.17). The intuition is expressed in Figure 4.5.

To see how the metric constraint arises, we first consider a naive approach by requiring $\mathcal{I}^h_{n_0^h}(y^h) = 0$ (recall that $\min W^e = 0$). In this direction, we note that $\mathcal{I}^h_{n_0^h}(y^h) = 0$ is equivalent to (cf. Remark 4.2.1(i))

$$(\nabla y^h)^T \nabla y^h = \bar{r}^{-1/3}(I_{3\times 3} + (\bar{r} - 1) n_0^h \otimes n_0^h) =: \ell_{n_0^h} \quad \text{a.e. on } \Omega_h, \tag{4.16}$$

where $\bar{r} = r(T_f)/r(T_0)$ so that $\bar{r} \in (0, 1)$ for heating and $\bar{r} > 1$ for cooling. However, (4.16) is too strong a condition to be useful, meaning that there are only few choices of n_0^h for which a y^h satisfying (4.16) exists.

Remark 4.2.3 *Assuming that n_0^h is sufficiently smooth, there exists a y^h satisfying (4.16) if and only if the components of the Riemann curvature tensor of $\ell_{n_0^h}$ vanish. This condition is well-known in the physics literature (e.g., Efrati et al. [39]), and in the language of continuum mechanics, it gives compatibility of the right Cauchy-Green deformation tensor (e.g., Blume [20]). As a consequence, n_0^h has to satisfy a certain nonlinear partial differential equation, and so it must come from a very restricted set of functions. (Note, the non-smooth case is treated in Lewicka and Pakzad [63], and it is similar.)*

Given that (4.16) is too restrictive, we relax the problem and study *approximate minimizers of the elastic energy* $\mathcal{I}^h_{n_0^h}(y^h)$. The key observation is that by making use

of the thinness of the sheet Ω_h and the assumption that n_0^h does not vary too much as a function of x_3, we show that approximate minimizers are characterized (in a sense to be made precise) by the following *effective metric constraint* (4.17). It is a two-dimensional reduction of the three-dimensional constraint (4.16) and reads

$$(\tilde{\nabla} y)^T \tilde{\nabla} y = \bar{r}^{-1/3}(I_{2\times 2} + (\bar{r} - 1)\tilde{n}_0 \otimes \tilde{n}_0) =: \tilde{\ell}_{n_0} \quad \text{a.e. on } \omega. \tag{4.17}$$

Notation. Here and throughout, we denote vector fields which are mappings $\Omega_h \to \mathbb{R}^3$ with a superscript h (e.g., n_0^h, y^h). We also consider vector fields defined on the midplane $\omega \subset \mathbb{R}^2$, (e.g., midplane fields $n_0, y \colon \omega \to \mathbb{R}^3$). Sometime these midplane fields will involve h-dependent smoothings. In such cases, a notation different then the superscript h (often a subscript δ_h) will be used to differentiate these fields from ones mapping from Ω_h. We also use $\tilde{(\cdot)}$ to distinguish two-dimensional quantities from three-dimensional quantities. For instance,

$$x := (x_1, x_2, x_3), \quad \tilde{x} := (x_1, x_2), \qquad \nabla = (\partial_1, \partial_2, \partial_3), \quad \tilde{\nabla} = (\partial_1, \partial_2), \tag{4.18}$$

and $\tilde{n}_0 \in B_1(0) \subset \mathbb{R}^2$ is the projection of n_0 onto ω.

Remark 4.2.4 *(i) If there exists a deformation y which satisfies (4.17) for a given n_0, there may be, in general, multiple such deformations (e.g., the sheet can actuate upward or downwards in different places). We imagine that one can distinguish between these by appropriately breaking additional symmetries, but we do not investigate this further.*

(ii) The constraint (4.17) *generalizes a metric constraint that has been proposed by Aharoni et al. [2] for actuation of nematic sheets. Indeed,* (4.17) *is more general in that (a) it need only hold almost everywhere, allowing for piecewise constant director designs and (b) the director can be programmed out-of-plane. At the same time, it is easy to see that* (4.17) *reduces to the constraint [2] for smooth planar director fields (a proof of this was given in the previous section).*

We justify the use of the metric constraint as a characterization of approximate minimizers of the strain energy through a series of results summarized as follows. We consider two classes of designs: (a) Nonisometric origami and (b) smooth designs. For the former, we show that if the metric constraint holds, then the energy of actuation is $\propto h^2$ and this is optimal. For the latter, we show that the metric constraint is both a necessary and sufficient condition for the energy of actuation to be $O(h^3)$.

4.3 Nonisometric origami constructions under the metric constraint

We first consider *nonisometric origami* under the metric constraint, and show that their strain energy scales at most like h^2.

Definition 4.3.1 (Definition of nonisometric origami) *These are characterized by the following assumptions on the design and deformation respectively:*

(i) (The design). $\omega \subset \mathbb{R}^2$ *is the union of a finite number of polygonal regions* ω_α *which each have constant director field, i.e.,*

$$\begin{aligned} &\omega = \bigcup_{\alpha=\{1,\dots,N\}} \omega_\alpha, \qquad \omega_\alpha \text{ mutually disjoint and polygonal,} \\ &n_0 \colon \omega \to \mathbb{S}^2 \quad \text{satisfies} \quad n_0(\tilde{x}) \equiv n_{0\alpha}, \qquad (\tilde{x} \in \omega_\alpha, \forall \alpha \in \{1,\dots,N\}), \\ &\tilde{n}_{0\alpha} \neq \pm \tilde{n}_{0\beta} \quad \text{when there is an interface between } \omega_\alpha \text{ and } \omega_\beta, \alpha \neq \beta. \end{aligned} \tag{4.19}$$

(ii) (The deformation). $y \in W^{1,\infty}(\omega, \mathbb{R}^3)$ *is a piecewise affine and continuous midplane deformation which satisfies the metric constraint (4.17), i.e.,*

$$y(\tilde{x}) = \tilde{F}_\alpha \tilde{x} + c_\alpha \quad \text{and} \quad (\tilde{F}_\alpha)^T \tilde{F}_\alpha = \tilde{\ell}_{n_{0\alpha}} \tag{4.20}$$

for all $\tilde{x} \in \omega_\alpha$ *and all* $\alpha = \{1,\dots,N\}$.

Note, the last condition in (4.19) is only there to ensure that each interface corresponds to a non-trivial change of the director (otherwise that interface would be superfluous).

For a nonisometric origami design (i.e., ω, n_0 as in (i)) and deformation (i.e., y as in (ii)), we show that we can construct a map $y^h \colon \Omega_h \to \mathbb{R}^3$ which approximately extends y to Ω_h and has strain energy $I^h_{n_0^h}(y^h) = O(h^2)$. In order to do so, we first smooth y. This relies on a technical hypothesis that y has a δ-smoothing:

Definition 4.3.2 *We say that* $y : \omega \to \mathbb{R}^3$ *has a* δ*-smoothing if, for any* $\delta > 0$ *sufficiently small, there exists a map* $y_\delta \in C^3(\bar{\omega}, \mathbb{R}^3)$ *and a subset* $\omega_\delta \subset \omega$ *of area less than* $C\delta$ *such that*

$$\begin{aligned} y_\delta = y \quad &\text{on } \omega \setminus \omega_\delta, \qquad |\partial_1 y_\delta \times \partial_2 y_\delta| \geq c > 0 \quad \text{on } \omega, \\ \|\tilde{\nabla} y_\delta\|_{L^\infty} \leq C, \qquad &\|\tilde{\nabla}\tilde{\nabla} y_\delta\|_{L^\infty} \leq C\delta^{-1}, \qquad \|\tilde{\nabla}^{(3)} y_\delta\|_{L^\infty} \leq C\delta^{-2} \end{aligned} \tag{4.21}$$

for some constants $C, c > 0$ *which can depend on* y *and* ω *but not on* δ.

We have the following theorem:

Theorem 4.3.3 *Let ω and n_0 be as in Definition 4.3.1(i), let y be as in 4.3.1(ii), and let $n_0^h : \Omega_h \to \mathbb{S}^2$ be any vector field that is close to n_0 in the sense of* (4.15)*. Suppose further that for all small enough $\delta > 0$, y has a δ-smoothing y^δ in the sense of Definition 4.3.2 above.*

Then, there exists an $m > 0$ such that if we set $\delta_h = mh$, then for all small enough $h > 0$ there exists a map $y^h : \Omega_h \to \mathbb{R}^3$ with

$$\begin{aligned} y^h(\tilde{x}, 0) =& y_{\delta_h}(\tilde{x}), \quad \tilde{x} \in \omega, \\ I^h_{n_0^h}(y^h) \leq& O(h^2). \end{aligned} \tag{4.22}$$

Moreover, y^h is an approximate extension of y in the sense that $\|y_{\delta_h} - y\|_{W^{1,2}(\omega,\mathbb{R}^3)} = O(h)$.

We prove this theorem in Section 4.5—where we show low energy deformation for smooth and sufficiently smooth surfaces under the metric constraint—as the proofs are similar.

The existence of such a δ-smoothing (of the Lipschitz continuous/origami midplane deformation y) is an important technical tool. It is needed because the global deformation y^h has to satisfy the *incompressibility constraint* $\det \nabla y^h = 1$. (Essentially, the non-degeneracy of the derivatives of y_δ allows one to employ the inverse function theorem to derive a sufficiently well-behaved ordinary differential equation.)

This technical issue has appeared in previous works on incompressibility (also, a $\det F > 0$ constraint) in thin sheets. It was first appreciated by Belgacem [10] and later addressed in some generality by Trabelsi [95] and Conti and Dolzmann [31]. However, their methods are very geometrical in nature (they are largely based on Whitney's ideas on the singularities of functions $\mathbb{R}^n \to \mathbb{R}^{2n-1}$, [107, 108]) and it is not obvious how to extract from them the $\delta-$dependent control of the higher derivatives which we need in the present context.

Importantly though, we prove that all of the examples of nonisometric origami in Figure 4.2 and 4.3 *indeed have a δ-smoothing*, in the sense of Definition 4.3.2. We do this by first showing that the existence of a δ-smoothing can be reduced to a linear algebra constraint on the sets of deformation gradients associated to the origami deformation, and then by explicitly verifying that this constraint holds for all nonisometric origami considered. We introduce the constraint below.

We develop nonisometric origami further in an extensive Section 4.7. Specifically, we discuss in some detail an equivalent formulation of the metric constraint (4.20) for nonisometric origami in terms of *compatibility conditions*. These are akin to the rank-one condition studied in the context of fine-scale twinning during the austenite martensite phase transition (also actuation of active martensitic sheets) [4, 13, 14, 15] and to the recently studied compatibility conditions for the actuation for nematic elastomer and glass sheets using planar programming of the director [68, 69]. We also highlight the rich potential of this class of designable actuation by showing that the case of three sectors with fixed distinct planar directors $n_{0i} \equiv \tilde{n}_{0i}$ for $i = 1, 2, 3$ can have up to 32 non-trivial compatible junctions for various $\bar{r}$ and n_{0i}. We develop this in Appendix A.3.

On δ-smoothings of origami deformations

We consider the smoothing of a piecewise affine and continuous deformation of a polygonal region $\omega \subset \mathbb{R}^2$ containing a single junction.

Definition of a single junction. We fix a right-handed frame with standard basis $\{\tilde{e}_1, \tilde{e}_2\} \subset \mathbb{R}^2$, and we set $\tilde{x} := x_1\tilde{e}_1 + x_2\tilde{e}_2$. We suppose ω contains K interfaces merging at a point $\tilde{p} \in \mathbb{R}^2$, each separating regions of distinct constant deformation gradient. For each $\alpha \in \{1, \dots, K\}$, the vector defining the interface (and pointing away from the junction $\tilde{p}$) is called $\tilde{t}_\alpha \in \mathbb{S}^1$ with $\tilde{t}_\alpha^\perp \in \mathbb{S}^1$ the right-handed vector normal to $\tilde{t}_\alpha$. A schematic of this is shown in Figure 4.6 for (a) an exterior junction (i.e., where the junction $\tilde{p}$ lies on $\partial\omega$) and (b) an interior junction. We write

$$\omega = \bigcup_{\alpha\in\{1,\dots,K\}} \omega_\alpha, \tag{4.23}$$

where each ω_α is a polygonal sector containing the $\tilde{t}_\alpha$ interface whose boundaries merging to $\tilde{p}$ either bisect the angle between $\tilde{t}_{\alpha-1}$ and $\tilde{t}_\alpha$, bisect the angle between $\tilde{t}_\alpha$ and $\tilde{t}_{\alpha+1}$, or form the boundary of ω. A schematic of this is shown in Figure 4.6 for (c) an exterior junction and (d) an interior junction.

Definition of origami deformation of a single junction. We consider a general piecewise affine and continuous deformation $y\colon \omega \to \mathbb{R}^3$ of this single junction at point $\tilde{p}$. This is defined as

$$\begin{aligned} y(\tilde{x}) = \gamma_\alpha((\tilde{x} - \tilde{p}) \cdot \tilde{t}_\alpha^\perp) + ((\tilde{x} - \tilde{p}) \cdot \tilde{t}_\alpha)\tilde{F}_\alpha\tilde{t}_\alpha + y(\tilde{p}) \\ \text{if} \quad \tilde{x} \in \omega_\alpha, \quad \alpha \in \{1, \dots K\}, \end{aligned} \tag{4.24}$$

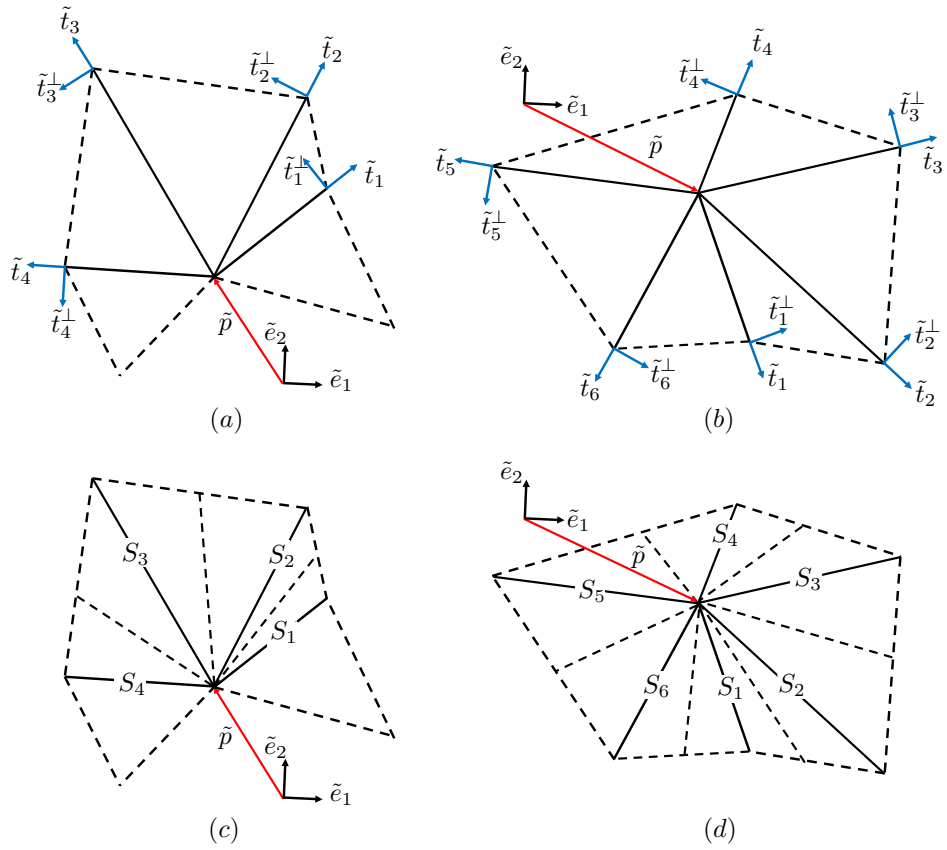

Figure 4.6: Schematic on a single junction at point $\tilde{p}$: Exterior (a)/(c) and interior (b)/(d).

for some $y(\tilde{p}) \in \mathbb{R}^3$, for $\gamma_\alpha : \mathbb{R} \to \mathbb{R}^3$ satisfying

$$\gamma_\alpha(t) = \begin{cases} t\tilde{F}_{\alpha-1}\tilde{t}_\alpha^{\perp} & \text{if } t < 0 \\ t\tilde{F}_\alpha \tilde{t}_\alpha^{\perp} & \text{if } t > 0 \end{cases}, \quad \alpha \in \{1, \dots K\}, \tag{4.25}$$

and for any set of matrices $\tilde{F}_0, \tilde{F}_1, \dots, \tilde{F}_K \in \mathbb{R}^{3\times 2}$ having the properties:

$$\begin{aligned} &\tilde{F}_{\alpha-1} \neq \tilde{F}_\alpha, \quad (\tilde{F}_\alpha - \tilde{F}_{\alpha-1})\tilde{t}_\alpha = 0 \quad \text{and} \\ &\lambda \text{adj}\tilde{F}_{\alpha-1} + (1-\lambda)\text{adj}\tilde{F}_\alpha \neq 0, \quad \forall \ \ \lambda \in [0,1] \end{aligned} \tag{4.26}$$

for each $\alpha \in \{1, \dots K\}$ (if $\tilde{p}$ is an interior junction, then $\tilde{F}_0 = \tilde{F}_K$).

The first condition in (4.26) ensures that each $\tilde{t}_\alpha$ interface is a non-trivial (i.e., there is a jump in the deformation gradient across the interface). The second condition in (4.26) is the rank-one compatibility condition which ensures that y is continuous across each $\tilde{t}_\alpha$ interface. Finally, the latter condition in (4.26) ensures that adjoining regions do not fold into themselves.

We now show the existence of a δ-smoothing for a special class of origami junctions where the F_α satisfy an algebraic condition. The general problem of finding δ-smoothings for any junction that satisfies (4.24)-(4.26) remains open. However, our special class covers the examples of physical interest.

To introduce our result, we recall that the convex hull of a finite collection of $\mathbb{R}^{3\times 2}$ matrices is

$$\mathrm{co}\{\tilde{F}_1, \ldots, \tilde{F}_N\} := \Big\{ \sum_{i=1}^{N} \lambda_i \tilde{F}_i \colon \lambda_i \geq 0 \quad \text{for each } i \text{ and } \quad \sum_{i=1}^{N} \lambda_i = 1 \Big\}. \tag{4.27}$$

In addition, for any collection $\mathcal{S}$ of $\mathbb{R}^{3\times 2}$ matrices, we denote the lower rank of the matrices in this set as

$$\mathrm{rank}_l \mathcal{S} := \min\{\mathrm{rank}\tilde{F} \colon \tilde{F} \in \mathcal{S}\}. \tag{4.28}$$

Our main result on δ-smoothings of generic origami deformation of a single junction is as follows:

Theorem 4.3.4 *Let ω be a single junction (as defined above) and let y be an origami deformation of this junction defined by (4.24), (4.25) and (4.26). Consider the set*

$$\mathcal{A}_y := \left\{ \tilde{F} \in \mathbb{R}^{3\times 2} \colon \mathit{rank}_l \left(\bigcup_{\alpha=1}^{K} \mathit{co}\{\tilde{F}, \tilde{F}_\alpha, \tilde{F}_{\alpha-1}\} \right) = 2 \right\}. \tag{4.29}$$

If $\mathcal{A}_y$ is non-empty, then y has a δ-smoothing.

Proof of Theorem 4.3.4.

The basic idea of our construction is (i) interfaces can be smoothed trivially and (ii) the existence problem at a junction can be reduced to a linear algebra constraint related piecewise constant deformation gradients at each junction. The linear algebra constraint can be found in Theorem 4.3.4 below.

A key step in the proof is to localize the problem to a junction by using a radial cutoff function $\psi(t)$. This produces the *localization error* $s\psi'(s)$. Importantly, this localization error can be made arbitrarily small by choosing ψ to be logarithmic and this observation significantly simplifies our argument. (The intuitive reason for the appearance of the logarithm is that we are considering the scale-invariant operator $t\frac{\mathrm{d}}{\mathrm{d}t}$.)

As it will be useful in the development of the proof of Theorem 4.3.4, we let $\theta_\alpha > 0$ denote the angle between $\tilde{t}_\alpha$ and $\tilde{t}_{\alpha+1}$ for each $\alpha \in \{1, \ldots K-1\}$ (and $\theta_K > 0$ the

angle between $\tilde{t}_K$ and $\tilde{t}_1$ if $\tilde{p}$ is an interior junction) and define

$$\theta^* := \min_{\alpha} \theta_\alpha. \tag{4.30}$$

Now for the proof of this theorem, we first consider a mollification of each γ_α in (4.25), i.e., $\gamma_{\alpha,\delta} \in C^\infty(\mathbb{R}, \mathbb{R}^3)$ given by

$$\gamma_{\alpha,\delta} := \gamma_\alpha * \eta_\delta, \quad \alpha \in \{1, \dots, K\} \tag{4.31}$$

for $\eta_\delta \in C^\infty(\mathbb{R}, \mathbb{R})$, the standard symmetric mollifier supported on the interval $(-\delta/2, \delta/2)$. For any $\delta > 0$, we define the function $y_{0,\delta} \colon \omega \to \mathbb{R}^3$ given by

$$\begin{aligned} y_{0,\delta}(\tilde{x}) &:= \gamma_{\alpha,\delta}((\tilde{x} - \tilde{p}) \cdot \tilde{t}_\alpha^\perp) + ((\tilde{x} - \tilde{p}) \cdot \tilde{t}_\alpha)\tilde{F}_\alpha \tilde{t}_\alpha + y(\tilde{p}) \\ &\text{if} \quad \tilde{x} \in \omega_\alpha, \quad \alpha \in \{1, \dots K\}. \end{aligned} \tag{4.32}$$

This is a δ-smoothing of y outside of a small neighborhood of the junction.

Proposition 4.3.5 *Let ω and y be as in Theorem 4.3.4. Set $m > 1/\sin(\theta^*/2)$ for θ^* in (4.30). For any $\delta > 0$, define $y_{0,\delta}$ as in (4.32). Then $y_{0,\delta}$ restricted to $\omega \setminus B_{m\delta}(\tilde{p})$ is a δ-smoothing of y. Moreover,*

$$\begin{aligned} \tilde{\nabla} y_{0,\delta}(\tilde{x}) &= (1 - \lambda_\delta((\tilde{x} - \tilde{p}) \cdot g_\alpha^\perp))\tilde{F}_{\alpha-1} + \lambda_\delta((\tilde{x} - \tilde{p}) \cdot g_\alpha^\perp)\tilde{F}_\alpha, \\ &\textit{if} \quad \tilde{x} \in \omega_\alpha \setminus B_{m\delta}(\tilde{p}) \end{aligned} \tag{4.33}$$

where $\lambda_\delta \in C^\infty(\mathbb{R}, [0,1])$ is given by $\lambda_\delta(s) := \int_{-\delta/2}^{s} \eta_\delta(t)dt$.

The issue with this construction, however, is that $y_{0,\delta}$ is not even continuous on $B_{m\delta}(\tilde{p})$, so we require a modification of this deformation in a neighborhood of $\tilde{p}$ for a δ-smoothing on all of ω. From now on, we assume that the set $\mathcal{A}_y$ in (4.29) is non-empty. We replace $y_{0,\delta}$ on the $B_{m\delta}(\tilde{p})$ by

$$y_c(\tilde{x}) = \tilde{F}_c(\tilde{x} - \tilde{p}) + y(\tilde{p}), \quad \tilde{F}_c \in \mathcal{A}_y. \tag{4.34}$$

Then for any $\delta > 0$, we define $y_\delta \colon \omega \to \mathbb{R}^3$ as

$$y_\delta(\tilde{x}) = y_{0,\delta}(\tilde{x}) + \psi_\delta(|\tilde{x} - \tilde{p}|)(y_c(\tilde{x}) - y_{0,\delta}(\tilde{x})) \tag{4.35}$$

for some cutoff function ψ_δ such that

$$\begin{aligned} &\psi_\delta \in C^3(\mathbb{R}, [0,1]) \quad \text{such that} \\ &\psi_\delta(s) = \begin{cases} 1 & \text{if } s < m\delta \\ 0 & \text{if } s > M\delta \end{cases}, \quad M > m > 1/\sin(\theta^*/2). \end{aligned} \tag{4.36}$$

We make the following observation about this construction:

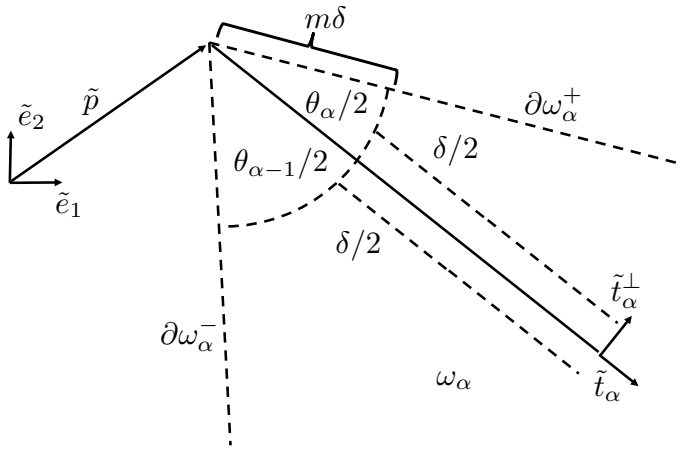

Figure 4.7: Schematic of an arbitrary $\tilde{t}_\alpha$ interface for a junction at point $\tilde{p}$.

Proposition 4.3.6 *Let ω and y be as in Theorem 4.3.4. Let $\mathcal{A}_y$ be non-empty. For any $\delta > 0$ define y_δ as (4.35) for $y_{0,\delta}$ in (4.32) with y_c as in (4.34). There exists a ψ_δ satisfying (4.36) such that y_δ is a δ-smoothing.*

Proof of Theorem 4.3.4. The theorem follows directly from Proposition 4.3.6. □

It remains to prove Propositions 4.3.5 and 4.3.6:

Proof of Proposition 4.3.5. Let $\omega_m := \omega \setminus B_{m\delta}(\tilde{p})$, and consider any δ sufficiently small so that ω_m is non-empty. Since $m \geq 1/\sin(\theta^*/2) \geq 1/\sin(\theta_\alpha/2)$ for each $\alpha \in \{1, \ldots, K-1\}$ (and K if ω is an interior junction), $y_{0,\delta}$ defined in (4.32) is equal to y across each $\partial\omega_\alpha^\pm \cap \omega_m$ (see the schematic in Figure 4.7) and y is smooth across these interfaces. Therefore, we need only to show that $y_{0,\delta}$ is a δ-smoothing of y on each $\omega_m \cap \omega_\alpha$ to prove it is a δ-smoothing of y on ω_m.

Fix an $\omega_\alpha \subset \omega$. Since $\gamma_{\alpha,\delta}$ is a δ-mollification of a piecewise affine and continuous function γ_α as defined by (4.25) and (4.31), it follows that

$$\begin{aligned} &y_{0,\delta} = y \quad \text{ except on a } \delta\text{-strip} \subset \omega_m \cap \omega_\alpha \quad \text{ and} \\ &|\tilde{\nabla} y_{0,\delta}| \leq C, \quad |\tilde{\nabla}\tilde{\nabla} y_{0,\delta}| \leq C\delta^{-1}, \quad |\tilde{\nabla}^{(3)} y_{0,\delta}| \leq C\delta^{-2} \quad \text{ on } \omega_m \cap \omega_\alpha \end{aligned} \tag{4.37}$$

for some $C > 0$ independent of δ. For the lower bound constraint on the cross-product, we observe that

$$\gamma_{\alpha,\delta}(s) = \tilde{F}_\alpha \tilde{t}_\alpha^\perp \int_{-\delta/2}^{s} \eta_\delta(t)(s-t)dt + \tilde{F}_{\alpha-1}\tilde{t}_\alpha^\perp \int_{s}^{\delta/2} \eta_\delta(t)(s-t)dt, \tag{4.38}$$

and thus

$$(\gamma_{\alpha,\delta})'(s) = (1 - \lambda_\delta(s))\tilde{F}_{\alpha-1}\tilde{t}_\alpha^\perp + \lambda_\delta(s)\tilde{F}_\alpha\tilde{t}_\alpha^\perp \tag{4.39}$$

for λ_δ defined in the proposition. Since $\tilde{\nabla} y_{0,\delta}(\tilde{x}) = (\gamma_{\alpha,\delta})'((\tilde{x}-\tilde{p})\cdot\tilde{t}_\alpha^\perp)\otimes\tilde{t}_\alpha^\perp + \tilde{F}_\alpha\tilde{t}_\alpha\otimes\tilde{t}_\alpha$ for $\tilde{x}\in\omega_\alpha$, we obtain (4.33) by direct substitution of $(\gamma_{\alpha,\delta})'$ above and using the fact that $\tilde{F}_{\alpha-1}g_\alpha = \tilde{F}_\alpha g_\alpha$. Finally, noting that $\operatorname{adj}(\tilde{F}\tilde{R}) = \det(\tilde{R})\operatorname{adj}(\tilde{F}) = \operatorname{adj}\tilde{F}$ for any $\tilde{F}\in\mathbb{R}^{3\times 2}$ and $\tilde{R}\in SO(3)$, we find

$$\begin{aligned}\operatorname{adj}(\tilde{\nabla} y_{0,\delta}(\tilde{x})) &= \tilde{\nabla} y_{0,\delta}(\tilde{x})\tilde{t}_\alpha \times \tilde{\nabla} y_{0,\delta}(\tilde{x})\tilde{t}_\alpha^\perp \\ &= \tilde{F}_\alpha\tilde{t}_\alpha \times \Big((1-\lambda_\delta((\tilde{x}-\tilde{p})\cdot\tilde{t}_\alpha^\perp))\tilde{F}_{\alpha-1}\tilde{t}_\alpha^\perp + \lambda_\delta((\tilde{x}-\tilde{p})\cdot\tilde{t}_\alpha^\perp)\tilde{F}_\alpha\Big) \\ &= (1-\lambda_\delta((\tilde{x}-\tilde{p})\cdot\tilde{t}_\alpha^\perp))\operatorname{adj}\tilde{F}_{\alpha-1} + \lambda_\delta((\tilde{x}-\tilde{p})\cdot\tilde{t}_\alpha^\perp)\operatorname{adj}\tilde{F}_\alpha,\end{aligned} \tag{4.40}$$

for any $\tilde{x}\in\omega_m\cap\omega_\alpha$ making repeated use of the fact that $\tilde{F}_{\alpha-1}\tilde{t}_\alpha = \tilde{F}_\alpha\tilde{t}_\alpha$. By hypothesis (4.26), this is bounded away from zero since $\lambda_\delta\in[0,1]$. That is, we conclude $|\operatorname{adj}\tilde{\nabla} y_{0,\delta}|\geq c_\alpha > 0$ on ω_α. Here, $\alpha\in\{1,\dots,K\}$ was arbitrary and so the proof is complete. □

Proof of Proposition 4.3.6. We note that for any m, M such that $M > m > 1/\sin(\theta^*/2)$ and for any $\delta > 0$ sufficiently small,

$$\tilde{\nabla} y_\delta = \tilde{F}_\delta + \tilde{G}_\delta \quad \text{ on } \omega, \tag{4.41}$$

where $\tilde{F}_\delta, \tilde{G}_\delta : \omega\to\mathbb{R}^{3\times 2}$ are given by

$$\begin{aligned}\tilde{F}_\delta(\tilde{x}) &:= (1-\psi_\delta(|\tilde{x}-\tilde{p}|))\tilde{\nabla} y_{0,\delta}(\tilde{x}) + \psi_\delta(|\tilde{x}-\tilde{p}|)\tilde{F}_c, \\ \tilde{G}_\delta(\tilde{x}) &:= |\tilde{x}-\tilde{p}|^{-1}\psi_\delta'(|\tilde{x}-\tilde{p}|)(y_c(\tilde{x})-y_{0,\delta}(\tilde{x}))\otimes(\tilde{x}-\tilde{p}).\end{aligned} \tag{4.42}$$

Focusing first on $\tilde{F}_\delta$, we note that for any $\omega_\alpha\subset\omega$,

$$\begin{aligned}\tilde{F}_\delta(\tilde{x}) = (1-\psi_\delta(|\tilde{x}-\tilde{p}|))\Big((1-\lambda_\delta((\tilde{x}-\tilde{p})\cdot\tilde{t}_\alpha^\perp))\tilde{F}_{\alpha-1} + \lambda_\delta((\tilde{x}-\tilde{p})\cdot\tilde{t}_\alpha^\perp)\tilde{F}_\alpha\Big) \\ + \psi_\delta(|\tilde{x}-\tilde{p}|)\tilde{F}_c, \quad \tilde{x}\in\omega_\alpha\end{aligned} \tag{4.43}$$

using (4.33) from Proposition 4.3.5. Consequently,

$$\tilde{F}_\delta(\tilde{x})\in\operatorname{co}\{\tilde{F}_c, \tilde{F}_{\alpha-1}, \tilde{F}_\alpha\}, \quad \tilde{x}\in\omega_\alpha, \quad \alpha\in\{1,\dots,K-1\} \tag{4.44}$$

(and K if ω is an interior junction) since $\psi_\delta, \lambda_\delta$ map to $[0,1]$. We claim that (4.44) implies

$$|\operatorname{adj}\tilde{F}_\delta|\geq c^* \quad \text{ on } \omega \tag{4.45}$$

for some $c^* > 0$.

To see this, we define $f_\alpha : \Lambda_3\to\mathbb{R}$ as

$$f_\alpha(\lambda_1,\lambda_2,\lambda_3) := |\operatorname{adj}(\lambda_1\tilde{F}_c + \lambda_2\tilde{F}_{\alpha-1} + \lambda_3\tilde{F}_\alpha)|, \tag{4.46}$$

where $\Lambda_3 := \{(\lambda_1, \lambda_2, \lambda_3) \in \mathbb{R}^3 \colon \lambda_i \geq 0 \quad \text{for each } i \text{ and } \sum_{i=1}^3 \lambda_i = 1\}$. Λ_3 is a compact subset of $\mathbb{R}^3$ and each f_α is continuous on Λ_3. Thus, the infimum of each f_α is attained. We denote

$$(\lambda_1^\alpha, \lambda_2^\alpha, \lambda_3^\alpha) := \arg\min_{\Lambda_3} f_\alpha, \quad \alpha \in \{1, \dots, K-1\} \tag{4.47}$$

(and K if ω is an interior junction). Since $\tilde{F}_c \in \mathcal{A}_y$, each $\lambda_1^\alpha \tilde{F}_c + \lambda_2^\alpha \tilde{F}_{\alpha-1} + \lambda_3^\alpha \tilde{F}_\alpha \in \mathbb{R}^{3\times 2}$ is full rank and thus we can take

$$c^* := \min_{\alpha\in\{1,\dots,K-1\}} \min_{\Lambda_3} f_\alpha > 0 \tag{4.48}$$

(again minimizing over K as well if ω is an interior junction) to achieve the identity (4.45).

Now, for the lower bound estimate of a δ-smoothing, we notice that given the representations (4.41) and (4.42),

$$\begin{aligned} |\operatorname{adj} \nabla y_\delta| &\geq |\operatorname{adj} \tilde{F}_\delta| - |\tilde{G}_\delta|(2|\tilde{F}_\delta| + |\tilde{G}_\delta|) \\ &\geq c^* - C|\tilde{G}_\delta|(1 + |\tilde{G}_\delta|) \quad \text{on } \omega. \end{aligned} \tag{4.49}$$

The latter constant C is independent of M, m and δ since $\|\tilde{F}_\delta\|_{L^\infty}$ can be bounded uniformly independent of these quantities following (4.44).

Now, for estimating $\tilde{G}_\delta$ in (4.42) with this cutoff function, we notice first that

$$\begin{aligned} |y_{0,\delta} - y_c| &\leq |y - y(\tilde{p})| + |y_c - y(\tilde{p})| + |y_{0,\delta} - y| \\ &\leq C(\delta + |\tilde{x} - \tilde{p}|) \quad \text{on } B_{M\delta}(\tilde{p}) \setminus B_{m\delta}(\tilde{p}). \end{aligned} \tag{4.50}$$

To obtain this estimate, we used that $|y_{0,\delta} - y| = |\gamma_\alpha^\delta - \gamma_\alpha| \leq C\delta$ on each $\omega_\alpha \setminus B_{m\delta}(\tilde{p})$ since γ_α is Lipschitz continuous, and we used that both y and y_c are equal to $y(\tilde{p})$ at $\tilde{x} = \tilde{p}$ and Lipschtiz continuous with uniform Lipschitz constant on $B_{M\delta}(\tilde{p}) \setminus B_{m\delta}(\tilde{p})$. Moreover, $\tilde{G}_\delta$ is only non-zero on that annulus $B_{M\delta}(\tilde{p}) \setminus B_{m\delta}(\tilde{p})$ since $\psi_\delta'(|\tilde{x}-\tilde{p}|) = 0$ outside this annulus. Hence, we observe that

$$\begin{aligned} |\tilde{G}_\delta(\tilde{x})| &\leq |\psi_\delta'(|\tilde{x} - \tilde{p}|)||y_{0,\delta}(\tilde{x}) - y_c(\tilde{x})| \leq C|\psi_\delta'(|\tilde{x} - \tilde{p}|)|(\delta + |\tilde{x} - \tilde{p}|) \\ &\leq C(1/m + 1)||\tilde{x} - \tilde{p}|\psi_\delta'(|\tilde{x} - \tilde{p}|)| \leq C\|s\psi_\delta'(s)\|_{L^\infty}, \end{aligned} \tag{4.51}$$

where in the second to last estimate we use that $|\tilde{x} - \tilde{p}|/m\delta > 1$ on the annulus $B_{M\delta}(\tilde{p}) \setminus B_{m\delta}(\tilde{p})$, and all constants $C > 0$ above can be chosen uniform independent of δ and $M > m > 1/\sin(\theta^*/2)$. Hence, by applying Lemma 4.3.7 (below), we suitably choose m, M and the cutoff function ψ_δ to establish the estimate

$$|\operatorname{adj} \tilde{\nabla} y_\delta| \geq c^*/2 \quad \text{on } \omega \tag{4.52}$$

for all $\delta > 0$ sufficiently small. Here, we made use of (4.49) and (4.51).

With this lower bound established, the other properties which show y_δ is a δ-smoothing of y are easily verified: Indeed, $y = y_\delta$ except on a set of measure $O(\delta)$ for all δ sufficiently small since y_δ deviates from $y_{0,\delta}$ only on a set of $O(\delta^2)$. Moreover, the derivative estimates follow from the chain rule and using the estimates for the cutoff function ψ_δ established in Lemma 4.3.7 below. This completes the proof. □

Lemma 4.3.7 *Fix $\epsilon > 0$. There is a $\Delta_\epsilon > 0$ such that for any $M > m > 1/\sin(\theta^*/2)$ satisfying $M/m \geq \Delta_\epsilon$ and $M - m > 2$, there exists for all $\delta > 0$ a cutoff function ψ_δ satisfying (4.36) with the properties*

$$\begin{aligned} &\|t\psi_\delta'(t)\|_{L^\infty} \leq \epsilon \\ &\|\psi_\delta'\|_{L^\infty} \leq C\delta^{-1}, \quad \|\psi_\delta''\|_{L^\infty} \leq C\delta^{-2} \quad \text{and} \quad \|\psi_\delta'''\|_{L^\infty} \leq C\delta^{-3} \end{aligned} \tag{4.53}$$

for $C \equiv C(M, m) > 0$ independent of δ.

Proof. Consider the cutoff function $\tilde{\psi}_\delta \colon \mathbb{R} \to [0, 1]$ given by

$$\tilde{\psi}_\delta(s) := \begin{cases} 1 & \text{if } s < (m + 1/2)\delta \\ \frac{\log(s/(M-1/2)\delta)}{\log((m+1/2)/(M-1/2))} & \text{if } s \in [(m + 1/2)\delta, (M - 1/2)\delta] \\ 0 & \text{if } s > (M - 1/2)\delta. \end{cases} \tag{4.54}$$

Here, $\tilde{\psi}_\delta$ is Lipschitz continuous since $M - m > 2$ and equal to 1 in a neighborhood of the origin since $m \geq 1/\sin(\theta^*/2) \geq 1$. This is not a cutoff function with the properties (4.36). However, importantly

$$|t\tilde{\psi}_\delta'(s)| = |\log\Big(\frac{M - 1/2}{m + 1/2}\Big)|^{-1} =: \epsilon_{M,m}, \tag{4.55}$$

which can be made arbitrarily small (independent of δ) by choosing M/m sufficiently large. By mollification, we can retain a similar estimate for a ψ_δ as in (4.36).

Indeed, we let $\psi_\delta := \eta_\delta * \tilde{\psi}_\delta$ for $\eta_\delta \in C^\infty(\mathbb{R}, \mathbb{R})$ the standard symmetric mollifier supported on the interval $(-\delta/2, \delta/2)$. Since $\tilde{\psi}_\delta$ is Lipschitz continuous, equal to 1 for $s < (m + 1/2)\delta$ and equal to 0 for $s > (M - 1/2)\delta$, ψ_δ is a cutoff function satisfying all the properties in (4.36) and it satisfies the latter estimates in (4.53).

It remains to prove the first estimate in (4.53). To this end, note $\psi'_\delta = \eta_\delta * \tilde{\psi}'_\delta$, and so explicitly

$$|t\psi'_\delta(s)| \leq \epsilon_{M,m} \begin{cases} \int_{(m+1/2)\delta}^{s+\delta/2} \eta_\delta(s-t)|\frac{s}{t}|dt & \text{if } s \in (m\delta, (m+1)\delta] \\ \int_{s-\delta/2}^{s+\delta/2} \eta_\delta(s-t)|\frac{s}{t}|dt & \text{if } s \in ((m+1)\delta, (M-1)\delta] \\ \int_{s-\delta/2}^{(M-1/2)\delta} \eta_\delta(s-t)|\frac{s}{t}|dt & \text{if } s \in ((M-1)\delta, M\delta] \\ 0 & \text{otherwise.} \end{cases} \tag{4.56}$$

From this, we deduce that

$$\|s\psi'_\delta(s)\|_{L^\infty} \leq \left(\frac{m+1}{m+1/2}\right)\epsilon_{M,m} \leq 2\epsilon_{M,m}. \tag{4.57}$$

Thus, there is a Δ_ϵ such that if $M/m \geq \Delta_\epsilon$, $\epsilon_{M,m} \leq \epsilon/2$. This completes the proof given (4.57). □

Examples of noniosmetric origami and their δ-smoothings.

In this section, we examine the nonisometric origami to actuate a box, rhombic dodecahedron and rhombic triacontahedron. We will show that each of these designs has a corresponding δ-smoothing. In this direction, consider Figure 4.8 showing for the case of cooling a nematic elastomer sheet: (a) the design to actuate a box, (b) part of the design to actuate the rhombic dodecahedron and (c) part of the design to actuate the rhombic triacontahedron. In each case, there are only two non-trivial junctions to consider, each highlighted in red. That is, once the deformations (both the origami and δ-smoothing deformations) are constructed for these junctions, then the entire deformation can be built as rotations and translations of these constructions.

As a first step towards constructing a δ-smoothing for these actuations, we identify the deformation gradients associated with the origami. This makes use of the notion of compatibility discussed in Section 4.7.

Proposition 4.3.8 *Consider the designs depicted in Figure 4.8. Up to a rigid body rotation, the deformation gradients corresponding to each region are given by*

(a) For the box

$$\tilde{F}_\alpha = \begin{cases} R_{n_{0\alpha}}(\ell^{1/2}_{n_{0\alpha}})_{3\times 2}, & \alpha \in \{1,2,3\} \\ R^2_{n_{01}} R_{n_{04}}(\ell^{1/2}_{n_{04}})_{3\times 2} & \alpha = 4 \\ R^2_{n_{03}} R_{n_{05}}(\ell^{1/2}_{n_{05}})_{3\times 2} & \alpha = 5; \end{cases} \tag{4.58}$$

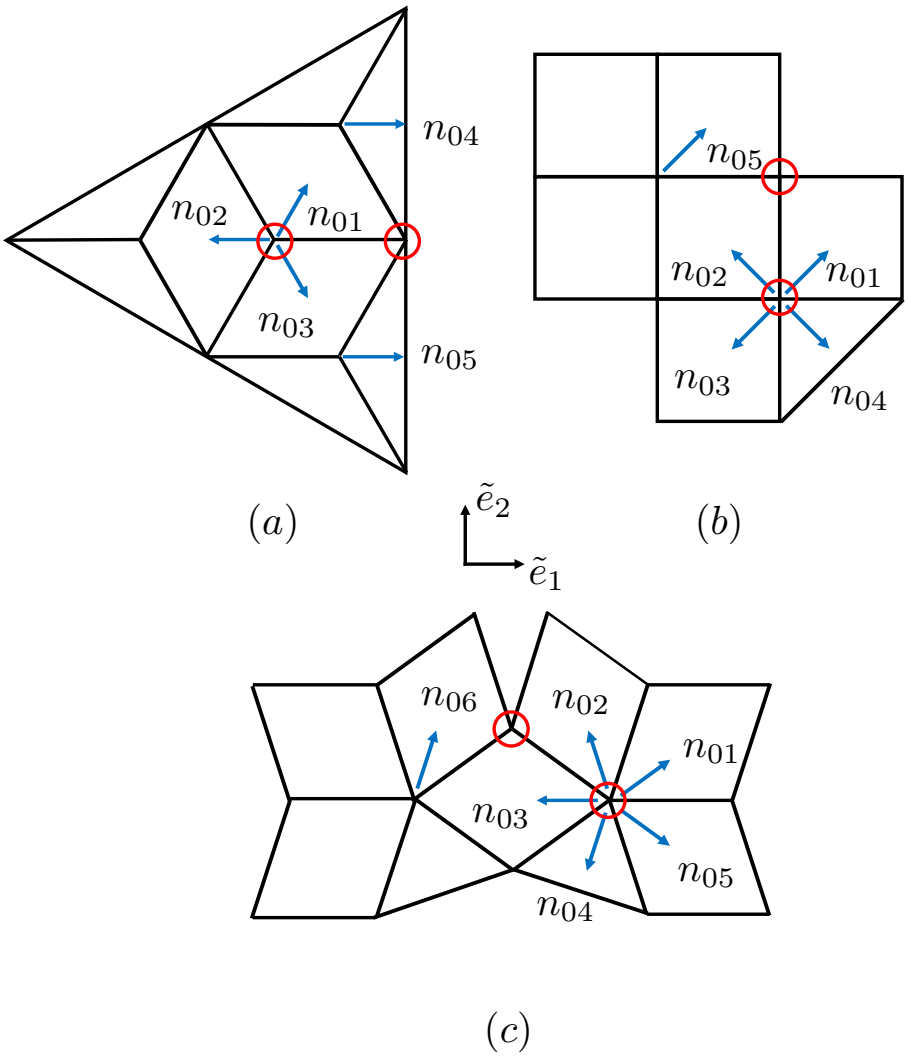

Figure 4.8: Designs to actuate a box (a), rhombic dodecahedron (b) and rhombic triacontahedron (c) upon cooling (i.e., $\bar{r} > 1$). Only a portion of the design is shown in (b) and (c).

(b) for the rhombic dodecahedron

$$\tilde{F}_\alpha = \begin{cases} R_{n_{0\alpha}}(\ell_{n_{0\alpha}}^{1/2})_{3\times 2} & \alpha \in \{1,\dots,4\} \\ R_{n_{02}}^2 R_{n_{05}}(\ell_{n_{05}}^{1/2})_{3\times 2} & \alpha = 4; \end{cases} \tag{4.59}$$

(c) for the rhombic triacontahedron

$$\tilde{F}_\alpha = \begin{cases} R_{n_{0\alpha}}(\ell_{n_{0\alpha}}^{1/2})_{3\times 2} & \alpha \in \{1,\dots,5\} \\ R_{n_{03}}^2 R_{n_{06}}(\ell_{n_{06}}^{1/2})_{3\times 2} & \alpha = 4. \end{cases} \tag{4.60}$$

Here, each $R_{n_{0\alpha}} \in SO(3)$ *satisfies* $R_{n_{0\alpha}} n_{0\alpha} = \bar{r}^{-1/2} n_{0\alpha} + \sqrt{1-\bar{r}^{-1}}\, e_3$ *for* $r \in [1, \bar{r}_{max}]$.

Clearly in each region $\tilde{F}_\alpha^T \tilde{F}_\alpha = \tilde{\ell}_{n_{0\alpha}}$. Thus, we need only to show that the deformation gradients are rank-one compatible at each interface. Let $\tilde{t}_\alpha \in \mathbb{S}^1$ denote the outward normal (to the junction) for the interface separating $n_{0\alpha}$ and $n_{0(\alpha-1)}$ for the interior junctions as depicted in Figure 4.8 (i.e., $\alpha \in \{1, \dots, K\}$ with $K = 3$ (box), 4 (rhombic dodecahedron), 5 (rhombic triacontahedron) and $0 = K$ in each case). We have that $\tilde{n}_{0\alpha} = \cos(\theta)\tilde{t}_\alpha + \sin(\theta)\tilde{t}_\alpha^\perp$ where $\theta \in \{\pi/3, \pi/4, \pi/5\}$ for the box, rhombic dodecahedron and rhombic triacontahedron, respectively, with $\tilde{t}_\alpha^\perp$ being the right-hand orthonormal vector to $\tilde{t}_\alpha$.

Now, to verify interface compatibility, let us first assume only that $R_{n_{0\alpha}} n_{0\alpha} = \cos(\varphi_{\bar{r}}) n_{0\alpha} + \sin(\varphi_{\bar{r}}) e_3$. By explicit computation, we find that

$$\begin{aligned} \left(R_{n_{0\alpha}}(\ell^{1/2}_{n_{0\alpha}})_{3\times 2} - R_{n_{0(\alpha-1)}}(\ell^{1/2}_{n_{0(\alpha-1)}})_{3\times 2}\right)\tilde{t}_\alpha = \\ 2\cos(\theta)\sin(\theta)(\bar{r}^{1/3}\cos(\varphi_{\bar{r}}) - \bar{r}^{-1/6}) g_\alpha^\perp. \end{aligned} \tag{4.61}$$

Thus, interface compatibility (i.e., this quantity being equal to zero) is achieved with $\cos(\varphi_{\bar{r}}) = \bar{r}^{-1/2}$, and this gives the condition on each $R_{n_{0\alpha}} \in SO(3)$ defined in the proposition.

It remains to verify compatibility for the exterior junctions. Let us focus on the n_{04} case for the box in (a). Notice that if we consider the interior junction which contains the n_{04} sector without compatibility of the entire origami structure, by the previous argument on interior junctions, we find that the junction in isolation is compatible given

$$\tilde{F}_1^* = R_{n_{01}}^T (\ell^{1/2}_{n_{01}})_{3\times 2}, \quad \tilde{F}_4^* = R_{n_{04}} (\ell^{1/2}_{n_{04}})_{3\times 2}. \tag{4.62}$$

The transpose for $\tilde{F}_1^*$ is since n_{01} points toward this junction and not away from it. For compatability of the whole structure, we notice that $\tilde{F}_1 = R_{n_{01}}^2 \tilde{F}_1^*$, and so rigidily rotating this isolated compatible junction by $R_{n_{01}}^2$ achieves a fully compatible structure. This gives $\tilde{F}_4$ in the proposition for (a). An analogous argument holds for all the other exterior junction cases. □

Now, for a δ-smoothing of the deformation, we claim first:

Proposition 4.3.9 *Each interior junction in (a), (b) and (c) has a δ-smoothing.*

Proof. By Proposition 4.3.8 and Theorem 4.3.4, we prove this result if we can find a $\tilde{F}_K \in \mathbb{R}^{3\times 2}$ such that the set

$$\mathcal{S}_{int}^K := \bigcup_{\alpha=1}^{K} \operatorname{co}\{\tilde{F}_K, R_{n_{0\alpha}}(\ell^{1/2}_{n_{0\alpha}})_{3\times 2}, R_{n_{0(\alpha-1)}}(\ell^{1/2}_{n_{0(\alpha-1)}})_{3\times 2}\} \tag{4.63}$$

contains only matrices of full rank. Here, $K \in \{3, 4, 5\}$ is for the box, rhombic dodecahedron and rhombic triacontahedron respectively and $n_{00} = n_{0K}$ for each K.

The choice of $\tilde{F}_K$ which gives $\text{rank}_l(\mathcal{S}^K_{int}) = 2$ is facilitated by the following observation. Consider $\tilde{v} := \beta_1 \tilde{n}_{0\alpha} + \beta_2 \tilde{n}^{\perp}_{0\alpha}$ for any $(\beta_1, \beta_2) \in \mathbb{R}^2$ (i.e., $\tilde{v}$ is an arbitrary vector on $\mathbb{R}^2$). We observe that

$$\begin{aligned} R_{n_{0\alpha}}(\ell^{1/2}_{n_{0\alpha}})_{3\times 2}\tilde{v} &= R_{n_{0\alpha}}(\bar{r}^{1/3}\beta_1 n_{0\alpha} + \bar{r}^{-1/6}\beta_2 n^{\perp}_{0\alpha}) \\ &= \bar{r}^{-1/6}(\beta_1 n_{0\alpha} + \beta_2 n^{\perp}_{0\alpha}) + \bar{r}^{1/3}\sqrt{1-\bar{r}^{-1}}e_3 \\ &= \bar{r}^{-1/6}v + \bar{r}^{1/3}\sqrt{1-\bar{r}^{-1}}e_3. \end{aligned} \tag{4.64}$$

Thus, since $\tilde{v}$ was arbitrary and α was arbitrary, we conclude that

$$\mathbb{P}_{e_3}(R_{n_{0\alpha}}(\ell^{1/2}_{n_{0\alpha}})_{3\times 2}) = \bar{r}^{-1/6} I_{2\times 2}, \qquad \text{for each } \alpha \text{ and } K, \tag{4.65}$$

where $\mathbb{P}_{e_3} : \mathbb{R}^{3\times 2} \to \mathbb{R}^{2\times 2}$ projects any $\mathbb{R}^{3\times 2}$ matrix to that plane normal to e_3.

Now, if we choose $\tilde{F}_K = \bar{r}^{-1/6} I_{3\times 2}$ for each $K \in \{3, 4, 5\}$, we notice that for any $\lambda, \mu \in [0, 1]$

$$\begin{aligned} &\mathbb{P}_{e_3}\left(\lambda \bar{r}^{-1/6} I_{3\times 2} + (1-\lambda)\left(\mu R_{n_{0\alpha}}(\ell^{1/2}_{n_{0\alpha}})_{3\times 2} + (1-\mu)R_{n_{0(\alpha-1)}}(\ell^{1/2}_{n_{0(\alpha-1)}})_{3\times 2}\right)\right) \\ &\quad = \lambda \bar{r}^{-1/6}\mathbb{P}_{e_3}(I_{3\times 2}) + (1-\lambda)\left(\mu \mathbb{P}_{e_3}(R_{n_{0\alpha}}(\ell^{1/2}_{n_{0\alpha}})_{3\times 2}) + \mathbb{P}_{e_3}(R_{n_{0(\alpha-1)}}(\ell^{1/2}_{n_{0(\alpha-1)}})_{3\times 2})\right) \\ &\quad = \lambda \bar{r}^{-1/6} I_{2\times 2} + (1-\lambda)(\mu \bar{r}^{-1/6} I_{2\times 2} + (1-\mu)\bar{r}^{-16} I_{2\times 2}) = \bar{r}^{-1/6} I_{2\times 2}. \end{aligned} \tag{4.66}$$

That is, this $\mathbb{R}^{2\times 2}$ projection of any convex combination of these $\mathbb{R}^{3\times 2}$ matrices is full-rank. Therefore, any convex combination is also full-rank. This result did not depend on α or K, so in particular, it shows that $\text{rank}_l(\mathcal{S}^K_{int}) = 2$ for each K. Thus, these interior junctions have a δ-smoothing. □

Now, with regard to the exterior junctions, the case of only two interfaces is trivial. In particular:

Proposition 4.3.10 *For any $\bar{r} \geq 1$ prior to self-intersection, each exterior junction for (b) the rhombic dodecahedron and (c) the rhombic triacontahedron has a δ-smoothing.*

Proof. By Proposition 4.3.8 and Theorem 4.3.4, we prove this result if we can find a $\tilde{F}_{b,c} \in \mathbb{R}^{3\times 2}$ such that the sets

$$\begin{aligned} \mathcal{S}^{(b)}_{ext} &:= \text{co}\,\{\tilde{F}_b, \tilde{F}_2, \tilde{F}_5\} \cup \text{co}\,\{\tilde{F}_b, \tilde{F}_2, \tilde{F}_1\} \\ \mathcal{S}^{(c)}_{ext} &:= \text{co}\,\{\tilde{F}_c, \tilde{F}_6, \tilde{F}_3\} \cup \text{co}\,\{\tilde{F}_c, \tilde{F}_3, \tilde{F}_2\} \end{aligned} \tag{4.67}$$

contain only matrices of full rank where the $\tilde{F}_\alpha$ are as described in Proposition 4.3.8 for (b) and (c). Hence, we choose $\tilde{F}_b = \tilde{F}_2$ and $\tilde{F}_c = \tilde{F}_3$. With these choices, actually

$$\begin{aligned} \mathcal{S}_{ext}^{(b)} &= \text{co}\,\{\tilde{F}_2, \tilde{F}_5\} \cup \text{co}\,\{\tilde{F}_2, \tilde{F}_1\}, \\ \mathcal{S}_{ext}^{(c)} &= \text{co}\,\{\tilde{F}_3, \tilde{F}_6\} \cup \text{co}\,\{\tilde{F}_3, \tilde{F}_2\}. \end{aligned} \tag{4.68}$$

Focusing on (b), we note that since $\tilde{F}_2$ and $\tilde{F}_5$ are rank-one compatible by Proposition 4.3.8 and since actuating the rhombic dodecahedron prior to self intersection $\lambda \,\text{adj}\,\tilde{F}2 \times (1-\lambda)\,\text{adj}\,\tilde{F}_5 \neq 0$ for all $\lambda \in [0,1]$), $\text{rank}_l(\text{co}\{\tilde{F}_2, \tilde{F}_5\}) = 2$. The same argument applies to other convexified set in $\mathcal{S}_{ext}^{(b)}$. Thus, $\text{rank}_l(\mathcal{S}_{ext}^{(b)}) = 2$. The argument is the same also for $\mathcal{S}_{ext}^{(c)}$. This completes the proof. □

The exterior junction for the box has three interfaces separating four regions of distinct deformation gradient. Therefore, the previous proof technique is not applicable. Instead, we resort to explicit computation of the deformation gradients. Nevertheless:

Proposition 4.3.11 *For any $\bar{r} \geq 1$ prior to self-intersection at $r > 3$, the exterior junction for (a) the box also has a δ-smoothing.*

Proof. By explicit computation in the $\{\tilde{e}_1, \tilde{e}_2\}$ basis shown (with e_3 the outward normal) in Figure 4.8,

$$\begin{aligned} \tilde{F}_{1,3} &= \bar{r}^{-1/6} \begin{pmatrix} 1 & 0 \\ 0 & 1 \\ \frac{1}{2}\sqrt{\bar{r}-1} & \pm\frac{\sqrt{3}}{2}\sqrt{\bar{r}-1} \end{pmatrix}, \\ \tilde{F}_{4,5} &= \bar{r}^{-1/6} \begin{pmatrix} \frac{3-\bar{r}}{2\bar{r}} & \mp\frac{\sqrt{3}}{2}\left(\frac{\bar{r}-1}{\bar{r}}\right) \\ \mp 3\frac{\sqrt{3}}{2}\left(\frac{\bar{r}-1}{\bar{r}}\right) & \frac{3-\bar{r}}{2\bar{r}} \\ (3-r)\frac{\sqrt{\bar{r}-1}}{\bar{r}} & \pm\sqrt{3}\frac{\sqrt{\bar{r}-1}}{\bar{r}} \end{pmatrix}. \end{aligned} \tag{4.69}$$

Now, we claim that the set

$$\mathcal{S}_{ext}^{(a)} := \text{co}\{\tilde{F}_a, \tilde{F}_1, \tilde{F}_4\} \cup \text{co}\{\tilde{F}_a, \tilde{F}_3, \tilde{F}_5\} \cup \text{co}\{\tilde{F}_a, \tilde{F}_1, \tilde{F}_3\} \tag{4.70}$$

contains only matrices of full-rank if $\tilde{F}_a = \bar{r}^{-1/6} I_{3\times 2}$.

To see this, first we note that we need only consider the first two sets since $\text{rank}_l(\text{co}\{\bar{r}^{-1/6} I_{3\times 2}, \tilde{F}_1, \tilde{F}_3\}) = 2$ from Proposition 4.3.9. In addition, we notice

by explicit calculation that

$$\begin{aligned}\tilde{F}^{\mp}(\lambda,\mu,\bar{r}) &:= \lambda\left((1-\mu)\bar{r}^{-1/6}I_{3\times 2}+\mu\tilde{F}_{1,3}\right)+(1-\lambda)\tilde{F}_{4,5}\\ &= \begin{pmatrix} \xi(\lambda,\bar{r}) & \mp\kappa(\lambda,\bar{r}) \\ \mp 3\kappa(\lambda,\bar{r}) & \xi(\lambda,\bar{r}) \\ \gamma(\lambda,\mu,\bar{r}) & \pm\phi(\lambda,\mu,\bar{r}) \end{pmatrix},\end{aligned} \tag{4.71}$$

where $\xi,\kappa,\gamma,\phi\geq 0$ for all $\lambda,\mu\in[0,1]$ and $\bar{r}\in[1,3]$. Thus,

$$\operatorname{adj}\tilde{F}^{\mp} = \begin{pmatrix} -(3\kappa\phi+\xi\gamma) \\ \mp(\gamma\kappa+\xi\phi) \\ \xi^2-3\kappa^2 \end{pmatrix}, \tag{4.72}$$

where we have suppressed the dependence on λ,μ and r. We will simply require the non-negativity of each parameter as stated above for our argument.

Suppose for the sake of a contradiction that $\operatorname{adj}\tilde{F}^{\mp}=0$. Using the non-negativity of the parameters, we have

$$\begin{aligned}\operatorname{adj}\tilde{F}^{\mp}=0 \quad &\Rightarrow \quad \xi=\sqrt{3}\kappa\\ &\Rightarrow \text{either: } \begin{cases}\gamma=-\sqrt{3}\phi \quad \Rightarrow \quad \phi,\gamma=0\\ \xi,\kappa=0.\end{cases}\end{aligned} \tag{4.73}$$

Let us assume it is the case $\xi,\kappa=0$, and notice that $\xi=0$ implies $\bar{r}=3$ and $\lambda=0$. However, in this case $\tilde{F}^{\mp}=\tilde{F}_{4,5}$, and $\tilde{F}_{4,5}$ is full-rank. Thus if $\operatorname{adj}\tilde{F}^{\mp}=0$, it must be that $\phi,\gamma=0$. However, we find additionally that

$$\phi(\lambda,\mu,\bar{r}) = \left(\lambda\mu\frac{1}{2}+(1-\lambda)\frac{1}{\bar{r}}\right)\sqrt{3(\bar{r}-1)}. \tag{4.74}$$

Thus, we see that $\phi=0$ for $\lambda,\mu\in[0,1]$ and $\bar{r}\in[1,3]$ in only two cases: if $\lambda=1$ and $\mu=0$ or if $\bar{r}=1$. For the first case though, $\tilde{F}^{\mp}=\tilde{F}_{1,3}$, which is full-rank. For the second case, $\tilde{F}^{\mp}=I_{3\times 2}$, which is also full-rank. So ϕ is only equal to zero on full-rank matrices. This is the desired contradiction. Indeed given this fact, $\operatorname{adj}\tilde{F}^{\pm}$ can never be zero due to (4.73). □

4.4 On the optimality of nonisometric origami

From Theorem 4.3.3, we can construct approximations to nonisometric origami (under the hypothesis (4.21)) with energy $O(h^2)$. Thus, it is natural to ask whether these constructions are energetically optimal for a prescribed director field.

We prove that this is the case (not for $\mathcal{I}^h_{n_0^h}$, but) for a two-dimensional analogue of the three-dimensional entropic strain energy,

$$\tilde{\mathcal{I}}^h_{n_0}(y) = h \int_\omega \left(|(\tilde{\nabla} y)^T \tilde{\nabla} y - \tilde{\ell}_{n_0}|^2 + h^2 |\tilde{\nabla}\tilde{\nabla} y|^2 \right) d\tilde{x}. \tag{4.75}$$

The first term here represents the membrane stretching part and is minimized exactly when the metric constraint (4.17) is satisified. The second term approximates bending. Such a two-dimensional energy is a widely used proxy to describe the elasticity of non-Euclidean plates (e.g., Efrati et al. [39] and Bella and Kohn [11]). In a broader context, these proxies often agree in h-dependent optimal energy scaling with that of the three dimensional elastic energy, and deformations which achieve this scaling in this two dimensional setting tend to form the midplane deformations for optimal three dimensional constructions (e.g., Bella and Kohn [12] and the single fold approximation of Conti and Maggi [32]).

Theorem 4.4.1 *Let $\bar{r} > 0$ and $\neq 1$, and let ω and n_0 as in Definition 4.3.1(i). For $h > 0$ sufficiently small*

$$\inf \left\{ \tilde{\mathcal{I}}^h_{n_0}(y) \colon y \in W^{2,2}(\omega, \mathbb{R}^3) \right\} \geq c_L h^2.$$

Here, $c_L = c_L(n_0, \bar{r}, \omega) > 0$ is independent of h.

Remark 4.4.2 *(i) If, in addition to the assumptions of the theorem, there exists a y as in Definition 4.3.1(ii), then for $h > 0$ sufficiently small, there exists a $y_{\delta_h} \in C^3(\bar{\omega}, \mathbb{R}^3)$ such that*

$$\|y_{\delta_h} - y\|_{W^{1,2}} \leq O(h) \quad \text{and} \quad \tilde{\mathcal{I}}^h_{n_0}(y_{\delta_h}) = O(h^2). \tag{4.76}$$

Hence, nonisometric origami is optimal in this two dimensional setting. The proof of this is straightforward. Indeed, the estimates (4.21), with the exception of the full-rank condition, can be obtained by standard mollification. Setting $\delta = h$ for these estimates yields a y_{δ_h} satisfying (4.76).

(ii) Let us discuss some of the heuristics behind the lower bound in Theorem 4.4.1. At an interface separating two regions of distinct constant director, an energetic penalty associated with membrane stretching at $O(h)$ drives the deformation to be piecewise affine with a fold precisely at the interface connecting the two regions, whereas an energetic penalty associated with bending at $O(h^3)$ cannot accommodate sharp folds, and thus a smoothing is necessitated. This

interplay gives rise to an intermediate energetic scaling between $O(h)$ and $O(h^3)$. For isometric origami, folds can be smoothed to mostly preserve the isometric condition, leading to approximate constructions and (under suitable hypotheses) lower bounds which scale as $O(h^{8/3})$ (see, for instance, Conti and Maggi [32]). For nonisometric origami, the preferred metric jumps across a possible fold and this leads to a larger membrane stretching term.

(iii) For the proof, we show that it is possible to reduce this estimate to a canonical problem localized at a single interface. Further, we show that a lower bound for this canonical problem is described by a one-dimensional Modica-Mortola type functional. In their result, Modica and Mortola [71] (see also Modica [70]) prove that such functionals (under suitable hypotheses) Γ-converge to functionals which are proportional to the number of jumps of their argument. In our setting, these jumps correspond to the jump in the preferred metric over the interface. That these "jumps" have finite energy in the Γ-convergence setting implies the estimate in the theorem.

Proof of Theorem 4.4.1.

We now prove Theorem 4.4.1. Specifically, we show that for the two-dimensional analog to the entropic energy given by $\tilde{I}^h_{n_0}$ in (4.75), a piecewise constant director design in the sense of Definition 4.3.1(i) necessarily implies an energy of at least $O(h^2)$ upon actuation. In section 4.4, we show that this estimate can be reduced to a canonical problem localized at a single interface. Further, we show that a lower bound for this canonical problem is described by a one-dimensional Modica-Mortola type functional [71, 70]. In Section 4.4, we present a self-contained argument which shows that the minimum of our Modica-Mortola type functional is necessarily bounded away from zero for $h > 0$ sufficiently small. This is the key result we use to prove Theorem 4.4.1.

The canonical problem

We assume ω and $n_0 \colon \omega \to \mathbb{S}^2$ satisfy (4.19). Then there exists a straight interface $\tilde{t}_{\alpha\beta} \in \mathbb{S}^1$ adjoining two regions ω_α and ω_β such that $\tilde{n}_{0\alpha} \neq \pm\tilde{n}_{0\beta}$. We let $\tilde{t}^\perp_{\alpha\beta} \in \mathbb{S}^1$ be the right-handed vector normal to $\tilde{t}_{\alpha\beta}$. Focusing on this single interface, we have two cases to consider:

1. *Case 1.* $(\tilde{n}_{0\alpha} \cdot \tilde{t}_{\alpha\beta})^2 \neq (\tilde{n}_{0\beta} \cdot \tilde{t}_{\alpha\beta})^2$ or $(\tilde{n}_{0\alpha} \cdot \tilde{g}^\perp_{\alpha\beta})^2 \neq (\tilde{n}_{0\beta} \cdot \tilde{g}^\perp_{\alpha\beta})^2$;
2. *Case 2.* $(\tilde{n}_{0\alpha} \cdot \tilde{t}_{\alpha\beta})^2 = (\tilde{n}_{0\beta} \cdot \tilde{t}_{\alpha\beta})^2$ and $(\tilde{n}_{0\alpha} \cdot \tilde{g}^\perp_{\alpha\beta})^2 = (\tilde{n}_{0\beta} \cdot \tilde{g}^\perp_{\alpha\beta})^2$.

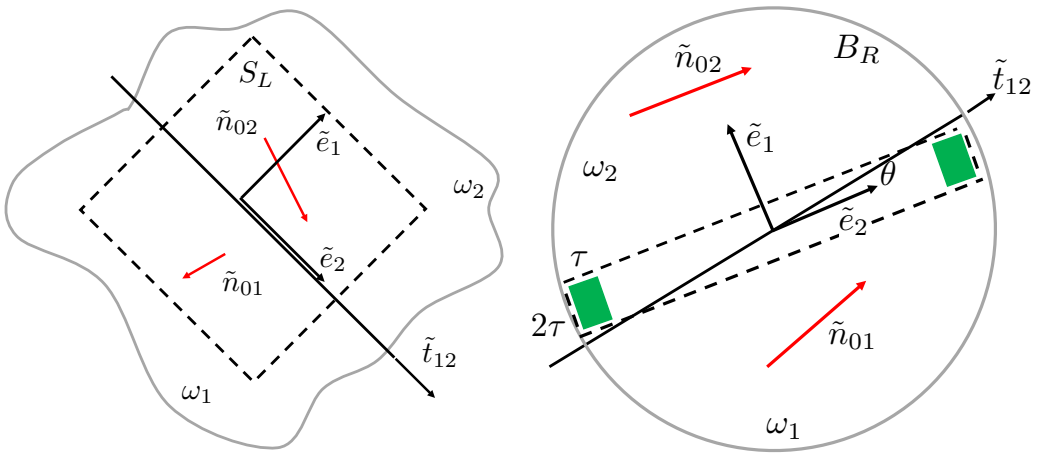

(a) Case 1 (b) Case 2

Figure 4.9: Schematic for canonical problem of Theorem 4.4.1

Definition for Case 1: In this case, we relabel so that $\alpha = 1$ and $\beta = 2$. We fix a global frame so that $\tilde{e}_2$ lies on the $\tilde{g}_{12}$ interface and $\tilde{e}_1$ points in the direction of ω_2. We let the origin of this frame lie on the $\tilde{g}_{12}$ interface such that for some $L > 0$ there exists a $S_L := (-L, L)^2 \subset \omega_1 \cup \omega_2$. A schematic of this description is provided in Figure 4.9a. We make the following observation in this case:

Proposition 4.4.3 *If ω and n_0 have an interface as in the definition of Case 1 (see Figure 4.9a), then for any $y \in W^{2,2}(\omega, \mathbb{R}^3)$,*

$$\tilde{I}^h_{n_0}(y) \geq 2L^2 h M^h_1, \tag{4.77}$$

where

$$M^h_1 := \inf \left\{ \int_{-1}^{1} \left((u^2 - \sigma(t))^2 + \frac{h^2}{L^2}(u')^2 \right) dt \right. \\ \left. \text{subject to } \ u \in W^{1,2}((-1,1),\mathbb{R}) \quad \text{with } \ u \geq 0 \text{ a.e.} \right\} \tag{4.78}$$

$$\alpha(t) = \begin{cases} \alpha_1 & \text{if } t < 0 \\ \alpha_2 & \text{if } t > 0. \end{cases}$$

Here $\alpha_1, \alpha_2 \geq 0$ and $\alpha_1 \neq \alpha_2$.

Proof. Let $y \in W^{2,2}(\omega, \mathbb{R}^3)$. Since $S_L \subset \omega_1 \cup \omega_2 \subset \omega$ and the integrand in (4.75) is

non-negative, we have

$$\begin{aligned}\tilde{\mathcal{I}}^h_{n_0}(y) &\geq h\int_{S_L}\left(|(\tilde{\nabla}y)^T\tilde{\nabla}y-\tilde{\ell}_{n_0}|^2+h^2|\tilde{\nabla}\tilde{\nabla}y|^2\right)d\tilde{x}\\ &\geq h\int_{S_L}\left(|\tilde{e}_i\cdot((\tilde{\nabla}y)^T\tilde{\nabla}y-\tilde{\ell}_{n_0})\tilde{e}_i|^2+h^2|\partial_1\partial_i y|^2\right)d\tilde{x}\\ &= h\int_{S_L}\left(||\partial_i y|^2-\sigma(x_1)|^2+h^2|\partial_1\partial_i y|^2\right)d\tilde{x},\end{aligned} \tag{4.79}$$

where $i\in\{1,2\}$ is chosen such that $(\tilde{n}_{01}\cdot\tilde{e}_i)^2\neq(\tilde{n}_{02}\cdot\tilde{e}_i)^2$. We see then that σ is given by

$$\sigma(t)=\begin{cases}\bar{r}^{-1/3}(1+(\bar{r}-1)(\tilde{n}_{01}\cdot\tilde{e}_i)^2) & \text{if } t<0\\ \bar{r}^{-1/3}(1+(\bar{r}-1)(\tilde{n}_{02}\cdot\tilde{e}_i)^2) & \text{if } t>0.\end{cases} \tag{4.80}$$

Thus, we set $\sigma_1:=\bar{r}^{-1/3}(1+(\bar{r}-1)(\tilde{n}_{01}\cdot\tilde{e}_i)^2)$ and $\sigma_2:=\bar{r}^{-1/3}(1+(\bar{r}-1)(\tilde{n}_{02}\cdot\tilde{e}_i)^2)$, and note that $\sigma_1\neq\sigma_2$ by definition of this case, and $\sigma_1,\sigma_2>0$ since $\bar{r}>0$.

Given the chain of inequalities (4.79), we deduce that

$$\begin{aligned}\tilde{\mathcal{I}}^h_{n_0}(y) &\geq 2Lh\inf\left\{\int_{-L}^{L}\left((|w|^2-\sigma(t))^2+h^2|w'|^2\right)dt\colon w\in W^{1,2}((-L,L),\mathbb{R}^3)\right\}\\ &\geq 2Lh\inf\left\{\int_{-L}^{L}\left((|w|^2-\sigma(t))^2+h^2(|w|')^2\right)dt\colon w\in W^{1,2}((-L,L),\mathbb{R}^3)\right\}\\ &= 2Lh\inf\left\{\int_{-L}^{L}\left((v^2-\sigma(t))^2+h^2(v')^2\right)dt\right.\\ &\qquad\left.\text{subject to}\quad v\in W^{1,2}((-L,L),\mathbb{R})\quad\text{with}\quad v\geq 0\text{ a.e.}\right\}\\ &= 2L^2hM^h_1.\end{aligned} \tag{4.81}$$

The first inequality follows by replacing $\partial_2 y$ with a function w which depends only on x_1 and taking the infimum amongst $W^{1,2}$ functions, and the second follows by noting $(|w|')^2\leq|w'|^2$. Finally, we simply replace $|w|$ by a function $v\geq 0$ for the first equality, and the second equality follows by a change of variables $v(t)=u(t/L)$. This completes the proof. □

Definition for Case 2: In this case, we again relabel so that $\alpha=1$ and $\beta=2$. We note that $\tilde{n}_{02}\neq 0$ (otherwise, following the definition of Case 2, $\tilde{n}_{01}=0$ and therefore $\tilde{n}_{01}=\tilde{n}_{02}$ which is not allowed). Hence, we again fix a global Cartesian frame so that $\tilde{e}_2=\tilde{n}_{02}/|\tilde{n}_{02}|$ and $\tilde{e}_1$ points in the direction of region ω_2. Next, for some $R>0$, we find a ball $B_R\subset\omega_1\cup\omega_2$ whose center intersects the interface $\tilde{g}_{12}$.

Note that $R = R(\omega)$ depends only on ω. We set $\theta \in (0, \pi/2]$ to be the acute angle between $\tilde{n}_{02}$ and $\tilde{g}_{12}$ (which is non-zero by definition of this case) and define

$$L_1 := R\cos(\theta), \qquad \tau := L_1 \frac{\tan(\theta)}{1+\tan(\theta)}. \tag{4.82}$$

We note that by their very definition, L_1 and τ depend only on ω and n_0. Further, $\tau \in (0, L_1]$. In particular, it cannot be zero since $\theta \neq 0$. A schematic of this case is provided in Figure 4.9b. We make the following observation for this case:

Proposition 4.4.4 *If ω and n_0 have an interface as in the definition of Case 2 (see Figure 4.9b), then for any $y \in W^{2,2}(\omega, \mathbb{R}^3)$,*

$$\tilde{\mathcal{I}}^h_{n_0}(y) \geq L_1 h \int_{-\tau}^{\tau} M_2^h(s) ds, \tag{4.83}$$

where

$$\begin{aligned} M_2^h(s) := \inf \Bigg\{ \int_{-1}^{1} \left((u^2 - \sigma(s,t))^2 + \frac{h^2}{L_1^2}(u')^2 \right) dt \\ \text{subject to} \quad u \in W^{1,2}((-1,1),\mathbb{R}) \quad \text{with} \quad u \geq 0 \text{ a.e.} \Bigg\} \end{aligned} \tag{4.84}$$

$$\sigma(s,t) = \begin{cases} \sigma_1 & \text{if } t < \max\{-1 + \tau/L_1, (1-\tau/L_1)(s/\tau)\} \\ \sigma_2 & \text{if } t > \min\{1 - \tau/L_1, (1-\tau/L_1)(s/\tau)\}. \end{cases}$$

Here $\sigma_1, \sigma_2 \geq 0$ and $\sigma_1 \neq \sigma_2$.

Proof. Let $y \in W^{2,2}(\omega, \mathbb{R}^3)$. Akin to the estimate in (4.79), we reason that

$$\tilde{\mathcal{I}}^h_{n_0}(y) \geq 2h \int_{-\tau}^{\tau} \int_{-L_1}^{L_1} \left(||\partial_2 y|^2 - \sigma(\tilde{x})|^2 + h^2 |\partial_2^2 y|^2 \right) d\tilde{x} \tag{4.85}$$

for $\sigma(\tilde{x})$ depending on both coordinates and given by

$$\sigma(\tilde{x}) = \begin{cases} \bar{r}^{-1/3}(1 + (\bar{r}-1)|\tilde{n}_{02}|^2) & \text{if } x_2 < \max\{-L_1 + \tau, (L_1 - \tau)(x_1/\tau)\} \\ \bar{r}^{-1/3}(1 + (\bar{r}-1)\frac{(\tilde{n}_{01}\cdot\tilde{n}_{02})^2}{|\tilde{n}_{02}|^2}) & \text{if } x_2 > \min\{L_1 - \tau, (L_1 - \tau)(x_1/\tau)\}. \end{cases} \tag{4.86}$$

Since $\tilde{n}_{01} \neq \pm\tilde{n}_{02}$ by definition, $(\tilde{n}_{01} \cdot \tilde{n}_{02}) \neq |\tilde{n}_{02}|^2$. Therefore, $\sigma_2 := \bar{r}^{-1/3}(1 + (\bar{r}-1)|\tilde{n}_{02}|^{-2}(\tilde{n}_{01}\cdot\tilde{n}_{02})^2)$ does not equal $\sigma_1 := \bar{r}^{-1/3}(1 + (\bar{r}-1)|\tilde{n}_{02}|^2)$. Moreover, $\sigma_1, \sigma_2 > 0$ since $\bar{r} > 0$.

Now, given the inequality in (4.85), we again see that in this case

$$\begin{aligned}\mathcal{I}^h_{n_0}(y) &\geq h\int_{-\tau}^{\tau} \inf\left\{\int_{-L_1}^{L_1}\left((|w|^2-\sigma(s,t))^2+h^2|w'|^2\right)dt \right. \\ &\qquad\qquad \left. \text{subject to } \ w\in W^{1,2}((-L_1,L_1),\mathbb{R}^3)\right\}ds \qquad (4.87)\\ &\geq L_1 h\int_{-\tau}^{\tau} M^h_2(s)ds\end{aligned}$$

as desired. This part of the argument is completely analogous to that of Proposition 4.4.3. This completes the proof. □

The Modica-Mortola analog and proof of optimal scaling

We have shown that, given any design described by flat sheet $\omega \subset \mathbb{R}^2$ and $n_0\colon \omega \to \mathbb{S}^2$ satisfying (4.19), the problem of deducing a lower bound on the energy (4.75) reduces to a canonical problem which has at most two flavors: Case 1 and Case 2 in Section 4.4. Actually though, following Proposition 4.4.3 and 4.4.4, we find for the lower bound that one only needs to consider the variational problem given by the one dimensional functionals

$$\mathcal{I}^h_s(u) := \int_{-1}^{1}\frac{1}{h}\left((u^2-\sigma(s,t))^2+c_1h(u')^2\right)dt, \quad s\in[-c_2,c_2] \qquad (4.88)$$

minimized amongst the functions $\{u\in W^{1,2}((-1,1),\mathbb{R})\colon u\geq 0\}$, where

$$\sigma(s,t)=\begin{cases}\sigma_1 & \text{if } t<\max\{-1+c_3,c_4s\}\\ \sigma_2 & \text{if } t>\min\{1-c_3,c_4s\}\end{cases} \qquad (4.89)$$

for $c_1,c_2>0, c_3\in(0,1]$ and $c_4\in[0,(1-c_3)/c_2]$. In fact, the proof of Theorem 4.4.1 follows from the observation that the infimum of $\mathcal{I}^h_s$ is bounded away from zero. Precisely:

Lemma 4.4.5 *For any $c_1,c_2>0, c_3\in(0,1]$ and $c_4\in[0,(1-c_3)/c_2]$, and for $h>0$ sufficiently small*

$$\inf\left\{\mathcal{I}^h_s(u)\colon u\in W^{1,2}((-1,1),\mathbb{R}) \text{ with } u\geq 0 \text{ a.e.}\right\}\geq c_L, \qquad (4.90)$$

where $c_L=c_L(c_1,c_2,c_3,c_4)>0$ is independent of s and h.

This is the crucial observation for the theorem. Indeed:

Proof of Theorem 4.4.1. We note following Section 4.4 that it suffices to restrict to the canonical problem given by the two cases in Figure 4.9. From Proposition 4.4.3 and 4.4.4, we have that for any $y \in W^{2,2}(\omega, \mathbb{R}^3)$,

$$\mathcal{I}^h_{n_0}(y) \geq \begin{cases} 2L^2 h M^h_1 & \text{for Case 1} \\ L_1 h \int_{-\tau}^{\tau} M^h_2(s)dx & \text{for Case 2.} \end{cases} \tag{4.91}$$

In addition, we observe that

$$\begin{aligned} M^h_1 &= h \inf \left\{ \mathcal{I}^h_s(u) \colon u \in W^{1,2}((-1,1),\mathbb{R}) \text{ with } u \geq 0 \text{ a.e.} \right\} \\ &\quad \text{when} \quad c_1 = L^{-1},\ c_3 = 1,\ c_4 = 0; \\ M^h_2(s) &= h \inf \left\{ \mathcal{I}^h_s(u) \colon u \in W^{1,2}((-1,1),\mathbb{R}) \text{ with } u \geq 0 \text{ a.e.} \right\} \\ &\quad \text{when} \quad c_1 = L_1^{-1},\ c_2 = \tau,\ c_3 = \tau/L_1,\ c_4 = (1/\tau - 1/L_1). \end{aligned} \tag{4.92}$$

Thus, by these observations and given Lemma 4.4.5,

$$\mathcal{I}^h_{n_0}(y) \geq \begin{cases} 2L^2 c_L h^2 & \text{for Case 1} \\ 2L_1 \tau c_L h^2 & \text{for Case 2} \end{cases} \tag{4.93}$$

for $c_L = c_L(c_1, c_2, c_3, c_4) > 0$ as in the lemma. This completes the proof. □

To close the argument, it remains to prove Lemma 4.4.5:

Proof of Lemma 4.4.5. By the direct methods in the calculus of variations (see, for instance, Dacorogna [33]), we find that for any $s \in [-c_2, c_2]$ and $h > 0$, there exists a minimizer to $\mathcal{I}^h_s$ in the space $\{u \in W^{1,2}((-1,1),\mathbb{R}) \colon u \geq 0 \text{ a.e.}\}$. For the lower bound, it suffices to restrict our attention to any such minimizer, which we label as u^h_s. Further, we may assume for some fixed constant $M > 0$ that

$$\mathcal{I}^h_s(u^h_s) < M. \tag{4.94}$$

Indeed, if for some $s \in [-c_2, c_2]$ and $h > 0$ this does not hold, then we immediately establish a lower bound for this case since the reverse inequality holds.

Now, since $c_4 \in [0, (1 - c_3)/c_2]$, we have that $\sigma(s,t) = \sigma_1$ when $t < -1 + c_3$ and $\sigma(s,t) = \sigma_2$ when $t > 1 - c_3$. Without loss of generality, we assume $\sigma_1 < \sigma_2$. We let $\langle\sigma\rangle = (\sigma_1 + \sigma_2)/2$, and we claim that for any $h > 0$ sufficiently small,

$$\begin{cases} \text{for some} \quad t \in [-1, -1 + c_3/2], & u^h_s(t)^2 \in (\frac{1}{2}\sigma_1, \frac{1}{2}(\sigma_1 + \langle\sigma\rangle)); \\ \text{for some} \quad t \in [1 - c_3/2, 1], & u^h_s(t)^2 \in (\frac{1}{2}(\sigma_2 + \langle\sigma\rangle), \frac{3}{2}\sigma_2). \end{cases} \tag{4.95}$$

Indeed, suppose the first condition does not hold. Then $(u_s^h(t)^2-\sigma_1)^2 \geq \frac{1}{4}\min\{\sigma_1^2, (\langle\sigma\rangle-\sigma_1)^2\} > 0$ on the interval $[-1,-1+c_3/2]$, which gives

$$\mathcal{I}_s^h(u_s^h) \geq \int_{-1}^{-1+c_3/2} \frac{1}{h}((u_s^h)^2-\sigma_1)^2 dt \geq \frac{c_3}{8h}\min\{\sigma_1^2, (\langle\sigma\rangle-\sigma_1)^2\}. \tag{4.96}$$

Taking $h > 0$ sufficiently small, we eventually arrive at a contradiction to (4.94). The second condition in (4.95) holds by an identical argument.

Now, by the Sobolev embedding theorem $u_s^h \in W^{1,2}((-1,1),\mathbb{R})$ has a continuous representative. This continuity and the observation that (4.95) holds leads to the non-zero lower bound on the energy. Indeed, we have the estimate

$$\mathcal{I}_s^h(u_s^h) \geq 2\sqrt{c_1}\int_{-1}^{1} |(u_s^h)^2-\sigma(s,t)||(u_s^h)'|dt. \tag{4.97}$$

Hence, we define

$$\begin{aligned} a &:= \max\{t\in[-1,1]\colon u_s^h(t)^2 = \frac{1}{2}(\sigma_1+\langle\sigma\rangle)\},\\ b &:= \min\{t\in(a,1]\colon u_s^h(t)^2 = \frac{1}{2}(\sigma_2+\langle\sigma\rangle)\}. \end{aligned} \tag{4.98}$$

By the continuity of u_s^h and the observation (4.95), these quantities (as asserted) do, in fact, exist. Moreover,

$$\begin{aligned} &\int_{-1}^{1} |(u_s^h)^2-\sigma(s,t)||(u_s^h)'|dt\\ &\quad\geq \int_a^b |(u_s^h)^2-\sigma(s,t)||(u_s^h)'|dt \geq \frac{1}{2}\min_{1,2}\{|\langle\sigma\rangle-\sigma_i|\}\int_a^b |(u_s^h)'|dt\\ &\quad\geq \frac{1}{2}\min_{1,2}\{|\langle\sigma\rangle-\sigma_i|\}\Big|\int_a^b (u_s^h)'dt\Big| = \frac{1}{2}\min_{1,2}\{|\langle\sigma\rangle-\sigma_i|\}|u_s^h(b)-u_s^h(a)|\\ &\quad= \frac{1}{2\sqrt{2}}\min_{1,2}\{|\langle\sigma\rangle-\sigma_i|\}|(\sigma_2+\langle\sigma\rangle)^{1/2}-(\sigma_1+\langle\sigma\rangle)^{1/2}| \end{aligned} \tag{4.99}$$

by the fundamental theorem of calculus. Since this lower bound is positive and independent of s and h, combining (4.97) and (4.99) completes the proof. □

4.5 Examples of pure bending actuation under the metric constraint

We turn now to the case of smooth or sufficiently smooth surfaces and programs satisfying the metric constraint (4.17). For these configurations, we will show the actuation is pure bending, i.e., $O(h^3)$ in the entropic strain energy after actuation.

Theorem 4.5.1 (Smooth Surfaces) *Let $\bar{r} \in (0,1)$ or $\bar{r} > 1$. Let n_0^h and n_0 satisfy (4.15). If $y \in C^3(\bar{\omega}, \mathbb{R}^3)$ and $n_0 \in C^2(\bar{\omega}, \mathbb{S}^2)$ such that $(\tilde{\nabla} y)^T \tilde{\nabla} y = \tilde{\ell}_{n_0}$ everywhere on ω, then for $h > 0$ sufficiently small, there exists a $y^h \in C^1(\overline{\Omega}_h, \mathbb{R}^3)$ such that*

$$y^h(\tilde{x}, 0) = y(\tilde{x}), \quad \tilde{x} \in \omega \qquad \mathcal{I}^h_{n_0^h}(y^h) = O(h^3). \tag{4.100}$$

Notice that for this theorem we assume y and n_0 are C^3 and C^2 respectively. Such smoothness is not always necessary. To highlight this, we introduce a large class of y, n which *automatically satisfy the two-dimensional metric constraint* (4.17). These surfaces are given as the graph of a function, combined with an appropriate contraction (here we consider cooling, so $\bar{r} > 1$). We call these "lifted surfaces". They are defined by

$$y(\tilde{x}) = \bar{r}^{-1/6}(x_1 e_1 + x_2 e_2) + \varphi(\bar{r}^{-1/6}\tilde{x}) e_3, \tag{4.101}$$

where the function φ is from the following set

$$\{\phi \in W^{2,\infty}(\bar{r}^{-1/6}\omega, \mathbb{R}) \colon \|\tilde{\nabla}\phi\|_{L^\infty} < \lambda_{\bar{r}} := \bar{r} - 1, \quad \operatorname{supp}\phi \subset \bar{r}^{-1/6}\omega_m\}. \tag{4.102}$$

Here, we set $\omega_m := \{\tilde{x} \in \omega \colon \operatorname{dist}(\tilde{x}, \partial\omega) > m > 0\}$ (recall that $\omega \subset \mathbb{R}^2$ is the midplane of the sheet, a bounded Lipschitz domain). The corresponding director field of a lifted surface is

$$n_0(\tilde{x}) = \frac{1}{\lambda_{\bar{r}}^{1/2}} \begin{pmatrix} \partial_1 \varphi(\bar{r}^{-1/6}\tilde{x}) \\ \partial_2 \varphi(\bar{r}^{-1/6}\tilde{x}) \\ (\lambda_{\bar{r}} - |\tilde{\nabla}\varphi(\bar{r}^{-1/6}\tilde{x})|^2)^{1/2} \end{pmatrix}. \tag{4.103}$$

We emphasize that any such choice of y, n_0 satisfies (4.17). This fact can be proved by rewriting (4.17) in an equivalent form, which is in fact more practical from the perspective of design, and we discuss this in Section 4.7, which has a focus towards applications.. The first main result is then that lifted surfaces have entropic energy of $O(h^3)$ (and therefore they are good candidates for designable actuation).

Corollary 4.5.2 (Lifted Surfaces) *Let $\bar{r} > 1$ and $m > 0$. Given a midplane deformation y as in (4.101) with φ taken from the set (4.102), define the director field n_0 as in (4.103). Let n_0^h be close to n_0 in the sense of (4.15).*

Then, for every $h > 0$ sufficiently small, there exists a $y_{\delta_h} \in C^3(\bar{\omega}, \mathbb{R}^3)$ and an extension $y^h \in C^1(\overline{\Omega}_h, \mathbb{R}^3)$ such that

$$\begin{aligned} &y^h(\tilde{x}, 0) = y_{\delta_h}(\tilde{x}), \quad \tilde{x} \in \omega, \qquad \|y_{\delta_h} - y\|_{W^{1,\infty}(\omega)} = O(h), \\ &\mathcal{I}^h_{n_0^h}(y^h) = O(h^3). \end{aligned} \tag{4.104}$$

The key reason why the lifted surface configurations satisfy the $O(h^3)$ scaling is that they satisfy the metric constraint, they are sufficiently smooth and (for our proof technique) they can be approximated by even smoother configurations which satisfy the metric constraint (see Remark 4.5.3(ii)). Thus, we can generalize the proof of Theorem 4.5.1 to obtain this result.

Remark 4.5.3 *(i) The surfaces of revolution in Aharoni et al. [2] and the designs exploring Gaussian curvature in Mostajeran [72] satisfy the conditions of Corollary 4.5.2. Thus, these designs and their predicted actuation are pure bending configurations in that they have entropic energy of $O(h^3)$ (which justifies that they are good candidates to be realized in actuation).*

(ii) To arrive at the results presented in this section, we employ techniques of Conti and Dolzmann [30, 31] to construct incompressible three dimensional deformations $y^h \in C^1(\overline{\Omega}_h, \mathbb{R}^3)$. These techniques rely on the ability to approximate Sobolev functions by sufficiently smooth functions (see the details of Section 2 in Plucinsky et al. [81]). In this direction, an important feature of lifted surfaces is that given any y as in (4.101) with φ as in (4.102), there exists a smooth y_{δ_h} approximating y in the $W^{2,2}(\omega, \mathbb{R}^3)$ norm which additionally satisfies $\tilde{\nabla} y_{\delta_h} \in \mathcal{D}_{\bar{r}}$ on ω (see Theorem 4.7.1 for the context for which the space $\mathcal{D}_{\bar{r}}$ arises). The space $\mathcal{D}_{\bar{r}}$ can be thought of as the appropriate generalization to nematic anisotropy of the space of matrices representing isometries. Specifically, in the isotropic case $\bar{r} = 1$, $\mathcal{D}_{\bar{r}}$ reduces to $\mathcal{D}_1 = \{\tilde{F} \in \mathbb{R}^{3\times 2} : \tilde{F}^T \tilde{F} = I_{2\times 2}\}$. The corresponding function space

$$W^{2,2}_{iso}(\omega, \mathbb{R}^3) := \{y \in W^{2,2}(\omega, \mathbb{R}^3) : (\tilde{\nabla} y)^T \tilde{\nabla} y = I_{2\times 2} \quad a.e.\} \tag{4.105}$$

has been studied extensively in the literature as this is the space of all bending deformations for isotropic sheets (as detailed rigorously by Friesecke et al. [46]). For instance, Pakzad [77] showed that smooth isometric immersions are dense in $W^{2,2}_{iso}$ as long as the initially flat sheet ω is a convex regular domain. This was later generalized by Hornung [52] for flat sheets which belong to a much larger class of bounded and Lipschitz domains. For nematic elastomers, an appealing analogue to these results would be a similar density result for the space

$$W^{2,2}_{\bar{r}}(\omega, \mathbb{R}^3) := \{y \in W^{2,2}(\omega, \mathbb{R}^3) : \tilde{\nabla} y \in \mathcal{D}_{\bar{r}} \quad a.e.\}. \tag{4.106}$$

For instance, this space arises in compactness at the bending scale for the combined entropic and Frank energy studied in section 4.6. It does not appear that a result of this type has been considered so far. Our result for non-smooth midplane deformations satisfying $\tilde{\nabla} y \in \mathcal{D}_{\bar{r}}$ a.e. is only stated for lifted surfaces, as these are the examples we can explicitly construct and approximate.

Proof of Theorems 4.3.3 & 4.5.1.

Each of the idealized two dimensional actuations detailed in this work (i.e., nonisometric origami, sufficiently smooth surface, and lifted surfaces) satisfy the effective metric constraint: $(\tilde{\nabla} y)^T \tilde{\nabla} y = \tilde{\ell}_{n_0}$ a.e. on ω. For extending these to three dimensional deformations with low energy, the basic idea is to construct an incompressible extension y^h which satisfies $y^h(x) \approx y(\tilde{x}) + x_3 b(\tilde{x})$, where $b\colon \omega \to \mathbb{R}^3$ is chosen so that $(\tilde{\nabla} y|b)^T(\tilde{\nabla} y|b) = \ell_{n_0}$ a.e. on ω. The energy of the constructions depends on the regularity of the idealized two dimensional fields y, b and n_0. (The energy is $O(h^2)$ for nonisometric origami and $O(h^3)$ for lifted surfaces and sufficiently smooth surfaces).

The importance of regularity considerations is reflected in the construction of y^h. Indeed, if the fields are not regular enough, as is the case with nonisometric origami and some lifted surfaces, we develop δ-dependent approximations y_δ and b_δ that satisfy $(\tilde{\nabla} y_\delta|b_\delta)^T(\tilde{\nabla} y_\delta|b_\delta) \approx \ell_{n_0}$ for small δ. In extending these approximations to a three dimensional incompressible deformation (by parameterizing δ by h), the *low* energy argument emerges as a balance between deviations from the metric constraint and a *bending* penalty related to localized deformation induced by nearly satisfying the metric constraint.

First, we construct three dimensional *incompressible* deformations starting from sufficiently smooth two dimensional deformations. These constructions cover all cases of idealized actuation considered in this work. Then, we use these constructions to prove the $O(h^3)$ energy statement for lifted surfaces and sufficiently smooth surfaces. As part of the proof, we develop two dimensional approximations to the lifted surface ansatz as needed. Finally, we follow analogous steps to prove the $O(h^2)$ energy statement for nonisometric origami.

Incompressible extensions

We begin with extensions of the deformations of a planar domain to three dimensional incompressible deformations of a thin domain based on the techniques of

Conti and Dolzmann[30, 31].

Lemma 4.5.4 *Let $\alpha \in \{-1, 0, 1\}$. Suppose for any $\delta > 0$ sufficiently small we have $y_\delta \equiv y_\delta(\alpha) \in C^3(\bar{\omega}, \mathbb{R}^3)$ and $b_\delta \equiv b_\delta(\alpha) \in C^2(\bar{\omega}, \mathbb{R}^3)$ satisfying*

$$\begin{aligned} &\det(\tilde{\nabla} y_\delta | b_\delta) = 1 \quad \text{on } \omega, \\ &\|\tilde{\nabla} y_\delta\|_{L^\infty} + \|b_\delta\|_{L^\infty(\omega)} \leq M, \\ &\|\tilde{\nabla}\tilde{\nabla} y_\delta\|_{L^\infty} + \|\tilde{\nabla} b_\delta\|_{L^\infty} \leq M\delta^{\min\{-\alpha,0\}}, \\ &\|\tilde{\nabla}^{(3)} y_\delta\|_{L^\infty} + \|\tilde{\nabla}\tilde{\nabla} b_\delta\|_{L^\infty} \leq M\delta^{-\alpha-1} \end{aligned} \tag{4.107}$$

for some uniform constant $M > 0$. Then there exists an $m \equiv m(M, \alpha) \geq 1$ such that for any $h > 0$ sufficiently small, there exists a unique $\xi^h \equiv \xi^h(\alpha) \in C^1(\overline{\Omega}_h, \mathbb{R})$ and an extension $y^h \equiv y^h(\alpha) \in C^1(\overline{\Omega}_h, \mathbb{R}^3)$ satisfying

$$\begin{aligned} &y^h = y_{\delta_h} + \xi^h b_{\delta_h}, \quad \text{with} \quad \delta_h = mh \\ &\quad \text{and} \quad \det \nabla y^h = 1 \quad \text{on } \Omega_h. \end{aligned} \tag{4.108}$$

In addition, ξ^h satisfies the pointwise estimates

$$\begin{aligned} &|\xi^h - x_3| \leq Ch^{\min\{-\alpha,0\}}|x_3|^2, \\ &|\partial_3 \xi^h - 1| \leq Ch^{\min\{-\alpha,0\}}|x_3|, \\ &|\tilde{\nabla}\xi^h| \leq Ch^{-\alpha-1}|x_3|^2. \end{aligned} \tag{4.109}$$

everywhere on Ω_h. Here, each $C \equiv C(M)$ and does not depend on h.

We prove this lemma at the end of the section.

Remark 4.5.5 *(i) The $\alpha \in \{-1, 0, 1\}$ dependent hypotheses (4.107) is related to the (sufficiently) smooth approximations to midplane fields y and b which satisfy $(\tilde{\nabla} y|b)^T(\tilde{\nabla} y|b) = \ell_{n_0}$ a.e. on ω for idealized actuation. These approximations depend on the regularity of the midplane field y, b and n_0. If the fields are smooth enough, then no approximation is required, and this is reflected in the hypotheses with $\alpha = -1$. Lifted surfaces need not be smooth (i.e., we can have $y \in W^{2,\infty}(\omega, \mathbb{R}^3) \setminus C^3(\bar{\omega}, \mathbb{R}^3)$). Consequently, approximations in this case (i.e., $y_\delta(\alpha)$) correspond to $\alpha = 0$. Finally, nonisometric origami actuations are strictly Lipschitz continuous, and as such, the approximations correspond to $\alpha = 1$.*

(ii) We will show below that the three dimensional extensions y^h defined in (4.108) have low energy for appropriate choices of y_δ and b_δ. Moreover, the estimates (4.109) precisely quantify the approximation $\xi^h \approx x_3$, and these are crucial for the energy argument.

(iii) We can choose $m = 1$ for $\alpha = \{-1, 0\}$. For $\alpha = 1$, we generally have to choose m such that $m \geq \max\{C(M), 1\}$ where $C(M)$ is a constant that depends on M but is independent of h.

The $O(h^3)$ energy argument for lifted surfaces and sufficiently smooth surfaces We begin with the case of sufficiently smooth surfaces and programs which satisfy the metric constraint. In this case, we do not have to approximate the midplane fields associated to idealized actuation, and so the approach is straightforward.

Definition of three dimensional deformation for smooth surfaces: Let $\bar{r} > 0$. We suppose that $n_0 \in C^2(\bar{\omega}, \mathbb{S}^2)$ and $y \in C^3(\bar{\omega}, \mathbb{R}^3)$ such that $(\tilde{\nabla} y)^T \tilde{\nabla} y = \tilde{\ell}_{n_0}$ on ω. Following Proposition A.1.9, there exists a $b \in C^2(\bar{\omega}, \mathbb{R}^3)$ such that $(\tilde{\nabla} y|b)^T (\tilde{\nabla} y|b) = \ell_{n_0}$ and $\det(\tilde{\nabla} y|b) = 1$. The smoothness is due to the regularity of n_0 and y by explicit differentiation of the parameterization in (A.24). Now y and b satisfy the hypotheses of Lemma 4.5.4 with $\alpha = -1$ since these fields are δ-independent. Hence, for $h > 0$ sufficiently small there exists a $\xi^h \in C^1(\overline{\Omega}_h, \mathbb{R})$ and an extension $y^h \in C^1(\overline{\Omega}_h, \mathbb{R}^3)$ with the properties:

$$\begin{cases} y^h := y + \xi^h b, \quad \det \nabla y^h = 1 \quad \text{on } \Omega_h, \\ |\xi^h - x_3| \leq C|x_3|^2, \quad |\partial_3 \xi^h - 1| \leq C|x_3|, \quad |\tilde{\nabla} \xi^h| \leq C|x_3|^2 \quad \text{on } \Omega_h. \end{cases} \tag{4.110}$$

Proof of Theorem 4.5.1. We first note the $y^h(\tilde{x}, 0) = y(\tilde{x})$ for $\tilde{x} \in \omega$ since $\xi^h(\tilde{x}, 0) = 0$ by the first estimate for ξ^h in (4.110). So it remains to prove only the $O(h^3)$ scaling of the energy $I_{n_0^h}(y^h)$.

We compute explicitly

$$\begin{aligned} \nabla y^h = (\tilde{\nabla} y|b) + x_3(\tilde{\nabla} b|0) + (\xi^h - x_3)(\tilde{\nabla} b|0) \\ + (\partial_3 \xi^h - 1) b \otimes e_3 + b \otimes \tilde{\nabla} \xi^h. \end{aligned} \tag{4.111}$$

Hence, by the estimates on ξ^h in (4.110), we conclude

$$\nabla y^h = (\tilde{\nabla} y|b) + O(x_3). \tag{4.112}$$

By hypothesis, $(\tilde{\nabla} y|b)^T(\tilde{\nabla} y|b) = \ell_{n_0}$, and so we find that

$$W^e((\tilde{\nabla} y|b), n, n_0) = W_{nH}((\ell^f_n)^{-1/2}(\tilde{\nabla} y|b)(\ell^0_{n_0})^{1/2}) = 0 \quad \text{on } \omega \tag{4.113}$$

following Proposition A.1.7 and the identity (2.3). Here, we have set

$$n := \frac{(\tilde{\nabla} y|b)n_0}{|(\tilde{\nabla} y|b)n_0|} \quad \text{on } \omega. \tag{4.114}$$

Since the energy density (4.113) vanishes, we deduce from Proposition A.1.4 that

$$(\ell^f_n)^{-1/2}(\tilde{\nabla} y|b)(\ell^0_{n_0})^{1/2} =: R \in SO(3) \quad \text{on } \omega. \tag{4.115}$$

Now, we let $n^h := (\nabla y^h)n^h_0/|(\nabla y^h)n^h_0|$ on Ω_h, and observe that

$$(\ell^0_{n^h_0})^{1/2} = (\ell^0_{n_0})^{1/2} + O(h), \tag{4.116}$$

where the equality follows from the scaling of the non-ideal terms in (4.15). Additionally given (4.112), we conclude

$$(\ell^f_{n^h})^{-1/2} = (\ell^f_n)^{-1/2} + O(x_3) + O(h). \tag{4.117}$$

Hence, combining the estimates (4.112), (4.116) and (4.117), we find

$$\begin{aligned} W^e(\nabla y^h, n^h, n^h_0) &= W_{nH}((\ell^f_n)^{-1/2}(\tilde{\nabla} y|b)(\ell^0_{n_0})^{1/2} + O(x_3) + O(h)) \\ &= W_{nH}(R^T(\ell^f_n)^{-1/2}(\tilde{\nabla} y|b)(\ell^0_{n_0})^{1/2} + O(x_3) + O(h)) \\ &= W_{nH}(I_{3\times 3} + O(x_3) + O(h)) = O(h^2) \quad \text{on } \omega. \end{aligned} \tag{4.118}$$

For the last equality, we used the definition of R in (4.115) and for the inequality, we used the estimate in Proposition A.1.3. Since this inequality holds on all of ω,

$$\mathcal{I}^h_{n^h_0}(y^h) = \int_{-h/2}^{h/2}\int_\omega W^e(\nabla y^h, n^h, n^h_0)dx = O(h^3). \tag{4.119}$$

This completes the proof. □

We now apply Lemma 4.5.4 to the case of lifted surfaces.

Definition of three dimensional deformations for lifted surfaces: Let $\bar{r} > 1$. We suppose $\{\varphi, y, n_0\}$ are as in the lifted surface ansatz (i.e., y satsifying (4.101) and n_0 satisfying (4.103) for φ as in (4.102) for some $m > 0$) and n^h_0 is as in (4.15). For $\delta > 0$ sufficiently small, there exist $\delta-$dependent functions $\{\varphi_\delta, y_\delta, n_{0,\delta}, b_\delta\}$ approximating this ansatz as detailed in Propositions 4.5.6-4.5.8 at the end of this section. The approximations satisfy $(\tilde{\nabla} y_\delta|b_\delta)^T(\tilde{\nabla} y_\delta|b_\delta) \approx \ell_{n_0}$, and they are sufficiently smooth

so that we can apply Lemma 4.5.4 with $\alpha = 0$ when we set $\delta_h \equiv \delta = h$ (see Remark 4.5.5(iii)). Thus for $h > 0$ sufficiently small, there exists a $\xi^h \in C^1(\overline{\Omega}_h, \mathbb{R})$ and an extension $y^h \in C^1(\overline{\Omega}_h, \mathbb{R}^3)$ with the properties:

$$\begin{cases} y^h := y_{\delta_h} + \xi^h b_{\delta_h}, \quad \det \nabla y^h = 1 \quad \text{on } \Omega_h, \\ |\xi^h - x_3| \leq C|x_3|^2, \quad |\partial_3 \xi^h - 1| \leq C|x_3|, \quad |\tilde{\nabla} \xi^h| \leq Ch^{-1}|x_3|^2 \quad \text{on } \Omega_h \end{cases} \tag{4.120}$$

for $C = C(\tilde{\nabla} y) > 0$ independent of h. With this construction, we prove Corollary 4.5.2:

Proof of Corollary 4.5.2. We first note the $y^h(\tilde{x}, 0) = y_{\delta_h}(\tilde{x})$ for $\tilde{x} \in \omega$ since $\xi^h(\tilde{x}, 0) = 0$ by the first estimate for ξ^h in (4.120). Moreover, $\|y_{\delta_h} - y\|_{W^{1,\infty}} = O(h)$ is shown in Proposition 4.5.7. So it remains to prove only the $O(h^3)$ scaling of the energy $\mathcal{I}_{n_0^h}(y^h)$.

For this, we note that given the estimates and properties established in Proposition 4.5.6-4.5.8, the fact that we are smoothing on a length scale $\delta_h \equiv \delta = h$ and the estimates for ξ^h in (4.120), the proof here follows exactly the same line of arguments as in the theorem above by replacing $\{y, n_0, n, b, R\}$ with $\{y_{\delta_h}, n_{0,\delta_h}, n_{\delta_h}, b_{\delta_h}, R_{\delta_h}\}$. □

It remains to construct the δ-dependent smoothings $\{\varphi_\delta, n_{0,\delta}, y_\delta, b_\delta\}$ asserted in the definition of three dimensional deformations for lifted surfaces.

Construction of φ_δ. Consider any φ as in (4.102) for $m > 0$. We extend φ to all of $\mathbb{R}^2$ yielding $\varphi \in W^{2,\infty}(\mathbb{R}^2, \mathbb{R}^3)$ (the extension is not relabeled), and we set

$$\varphi_\delta := \eta_\delta * \varphi \quad \text{ on } \bar{r}^{-1/6}\omega \tag{4.121}$$

for a standard mollifier η_δ supported on a ball of radius $\delta/2$. For this mollification, we have:

Proposition 4.5.6 *For $\delta > 0$ sufficiently small, φ_δ in (4.121) belongs to $C_0^\infty(\bar{r}^{-1/6}\omega, \mathbb{R})$ and satisfies the estimates*

$$\begin{aligned} &\|\varphi - \varphi_\delta\|_{W^{1,\infty}} = O(\delta), \quad \|\tilde{\nabla}\varphi_\delta\|_{L^\infty} < \lambda_r, \\ &\|\tilde{\nabla}^{(n)}\varphi_\delta\|_{L^\infty} = O(\delta^{2-n}), \quad \textit{for any integer } n \geq 2. \end{aligned} \tag{4.122}$$

Proof. φ_δ is smooth by mollification. It vanishes on the boundary of $\bar{r}^{-1/6}\omega$ for $\delta > 0$ sufficiently small since by (4.102), $\text{spt}\varphi \subset \bar{r}^{-1/6}\omega_m := \bar{r}^{-1/6}\{\tilde{x} \in \omega\colon \text{ dist}(\tilde{x}, \omega) >$

$m\}$ and since η_δ is supported on a ball of radius $\delta/2$. From standard manipulation of the mollification (4.121), the estimate on the $W^{1,\infty}$ norm follows from the Lipschitz continuity of φ and $\tilde{\nabla}\varphi$, the estimate on $\tilde{\nabla}\varphi_\delta$ follows from that fact that $\|\tilde{\nabla}\varphi\|_{L^\infty} < \lambda_r$, and the estimates on the higher derivatives follow from the fact that $\tilde{\nabla}\tilde{\nabla}\varphi \in L^\infty$. □

Construction of $n_{0,\delta}$ and y_δ. We replace φ in the lifted surface ansatz (4.101) and (4.103) with φ_δ from the proposition above and define $n_{0,\delta}$ as in (4.103) and y_δ as in (4.101) with this replacement. We make the following observations:

Proposition 4.5.7 *Let $\delta > 0$ sufficiently small. Let $n_{0,\delta}$ and y_δ be as defined above for φ_δ as in (4.121), φ as in (4.102), n_0 as in (4.103) and y as in (4.101). Then $n_{0,\delta} \in C^\infty(\bar{\omega}, \mathbb{S}^2)$ and $y_\delta \in C^\infty(\bar{\omega}, \mathbb{R}^3)$ and they satisfy*

$$\begin{aligned}
&(\tilde{\nabla} y_\delta)^T(\tilde{\nabla} y_\delta) = \tilde{\ell}_{n_{0,\delta}} \quad \text{on } \omega \\
&\|n_{0,\delta} - n_0\|_{L^\infty} = O(\delta), \quad \|y_\delta - y\|_{W^{1,\infty}} = O(\delta), \\
&\|\tilde{\nabla} y_\delta\|_{L^\infty} + \|\tilde{\nabla}\tilde{\nabla} y_\delta\|_{L^\infty} + \|\tilde{\nabla} n_{0,\delta}\|_{L^\infty} \leq C, \\
&\|\tilde{\nabla}^{(3)} y_\delta\|_{L^\infty} + \|\tilde{\nabla}\tilde{\nabla} n_{0,\delta}\|_{L^\infty} \leq C\delta^{-1}
\end{aligned} \tag{4.123}$$

for C independent of δ.

Proof. These properties are a consequence of the properties on φ_δ established in Proposition 4.5.6. In particular, smoothness follows since φ_δ is a mollification; the metric constraint holds by the equivalence (4.205) since $\|\tilde{\nabla}\varphi_\delta\|_{L^\infty} < \lambda_r$; the estimates on the approximations $n_{0,\delta} - n_0$ and $y_\delta - y$ follow from the $W^{1,\infty}$ estimate of $\varphi_\delta - \varphi$ using the explicit definition of each field; and the δ-dependent derivative estimates follow from the δ-dependent derivative estimates of φ_δ again using the explicit definition of each field. □

Construction of b_δ. We construct the out-of-plane vector $b_\delta \colon \omega \to \mathbb{R}^3$ to ensure the metric constraint is satisfied at the midplane:

Proposition 4.5.8 *Let $\delta > 0$ sufficiently small. Let n_0^δ and y_δ as in Proposition 4.5.7. There exists a $b_\delta \in C^\infty(\bar{\omega}, \mathbb{R}^3)$ such that*

$$\begin{aligned}
&(\tilde{\nabla} y_\delta | b_\delta)^T(\tilde{\nabla} y_\delta | b_\delta) = \ell_{n_0^\delta}, \quad \det(\tilde{\nabla} y_\delta | b_\delta) = 1, \\
&\|b_\delta\|_{L^\infty} + \|\tilde{\nabla} b_\delta\|_{L^\infty} \leq C, \quad \|\tilde{\nabla}\tilde{\nabla} b_\delta\|_{L^\infty} \leq C\delta^{-1}
\end{aligned} \tag{4.124}$$

for C independent of δ.

Proof. Since by Proposition 4.5.7, we have $(\tilde{\nabla} y_\delta)^T \tilde{\nabla} y_\delta = \tilde{\ell}_{n_{0,\delta}}$ everywhere on ω, we apply Proposition A.1.9 pointwise everywhere on ω. Thus, we define the vector $b_\delta \colon \omega \to \mathbb{R}^3$ as in (A.24) with $\tilde{\nabla} y_\delta$ replacing $\tilde{F}$ and $n_{0,\delta}$ replacing n_0 in these relations. Hence, (4.124) holds on ω. Smoothness follows since $n_{0,\delta}$, y_δ and the parameterization (A.24) are each themselves smooth. The estimates on the derivatives of b_δ follow from the estimates on the derivative of y_δ and n_0^δ in Proposition 4.5.7 by explicit differentiation of the parameterization in (A.24). □

The $O(h^2)$ energy argument for nonisometric origami

We now apply Lemma 4.5.4 to the case of nonisometric origami. This requires the existence of a δ-smoothing of y in the sense of Definition 4.3.2.

Definition of three dimensional deformations for nonisometric orgiami: Let $\bar{r} > 0$. We suppose $\omega \subset \mathbb{R}^2$ and n_0 satisfy Definition 4.3.1(i), y satsifies Definition 4.3.1(ii) and n_0^h satisfies (4.15). In addition, we assume there exists a δ-smoothing $y^\delta \in C^3(\bar{\omega}, \mathbb{R}^3)$ as in Definition 4.3.2.

In Proposition 4.5.9 below, we prove that the existence of a δ-smoothing y_δ also guarantees the existence of a vector field b_δ that complements y_δ. (By this, we mean that it satisfies $(\tilde{\nabla} y_\delta | b_\delta)^T (\tilde{\nabla} y_\delta | b_\delta) \approx \ell_{n_0}$, and it is sufficiently smooth so that we can apply Lemma 4.5.4 with $\alpha = 1$.) Thus by Lemma 4.5.4, there exists a $m = m(\tilde{\nabla} y) \geq 1$ such that for $h > 0$ sufficiently small there exists a $\xi^h \in C^1(\overline{\Omega}_h, \mathbb{R})$ and an extension $y^h \in C^1(\overline{\Omega}_h, \mathbb{R}^3)$ with the properties:

$$\begin{cases} y^h := y_{\delta_h} + \xi^h b_{\delta_h} \quad \text{with} \quad \delta_h = mh, \quad \det \nabla y^h = 1 \quad \text{on } \Omega_h, \\ |\xi^h - x_3| \leq Ch^{-1}|x_3|^2, \quad |\partial_3 \xi^h - 1| \leq Ch^{-1}|x_3|, \quad |\tilde{\nabla} \xi^h| \leq Ch^{-2}|x_3|^2 \quad \text{on } \Omega_h \end{cases} \tag{4.125}$$

for $C = C(\tilde{\nabla} y) > 0$ independent of h. With this construction, we prove Theorem 4.3.3.

Proof of Theorem 4.3.3. We first remark that $y^h(\tilde{x}, 0) = y_{\delta_h}(\tilde{x})$ for every $\tilde{x} \in \omega$ since $\xi^h(\tilde{x}, 0) = 0$ following the first estimate for ξ^h in (4.125). Further since y_{δ_h} is a δ_h-smoothing of y (recall definition 4.3.2), we find $\|y_{\delta_h} - y\|_{W^{1,2}} = O(h)$. Thus, it remains only to show that the energy scales as $O(h^2)$ for this deformation.

To this end, we first compute ∇y^h explicitly. We find that

$$\nabla y^h = (\tilde{\nabla} y_{\delta_h} | 0) + \xi^h (\tilde{\nabla} b_{\delta_h} | 0) + (\partial_1 \xi^h b_{\delta_h} | \partial_2 \xi^h b_{\delta_h} | \partial_3 \xi^h b_{\delta_h}), \tag{4.126}$$

and note that from Proposition 4.5.9, $\tilde{\nabla} b_{\delta_h} = 0$ on the set $\omega \setminus \tilde{\omega}_{\delta_h}$ where $|\tilde{\omega}_{\delta_h}| = O(\delta_h) = O(h)$. It follows that $\xi^h = x_3$ on this set. Indeed, since $\det \nabla y^h = 1$, we find that on $\omega \setminus \tilde{\omega}_{\delta_h}$,

$$1 = \det((\tilde{\nabla} y_{\delta_h}|0) + (\partial_1 \xi^h b_{\delta_h}|\partial_2 \xi^h b_{\delta_h}|\partial_3 \xi^h b_{\delta_h})) = \partial_3 \xi^h \det(\tilde{\nabla} y_{\delta_h}|b_{\delta_h}). \quad (4.127)$$

Also from Proposition 4.5.9, $\det(\tilde{\nabla} y_{\delta_h}|b_{\delta_h}) = 1$. Thus, $\partial_3 \xi^h = 1$ on $\omega \setminus \tilde{\omega}_{\delta_h}$. Consequently, $\xi^h = x_3$ on this set since we have the condition $\xi^h(\tilde{x}, 0) = 0$.

To recap, we find that

$$\nabla y^h = (\tilde{\nabla} y_{\delta_h}|b_{\delta_h}) \quad \text{on } \omega \setminus \tilde{\omega}_{\delta_h}. \quad (4.128)$$

On the exceptional set $\tilde{\omega}_{\delta_h}$, we find that

$$\begin{aligned} |\nabla y^h| &= \Big|(\tilde{\nabla} y_{\delta_h}|b_{\delta_h}) + (\partial_3 \xi^h - 1) b_{\delta_h} \otimes e_3 \\ &\quad + x_3(\tilde{\nabla} b_{\delta_h}|0) + (\xi^h - x_3)(\tilde{\nabla} b_{\delta_h}|0) + b_{\delta_h} \otimes \tilde{\nabla} \xi^h \Big| \\ &\leq |(\tilde{\nabla} y_{\delta_h}|b_{\delta_h})| + |\partial_3 \xi^h - 1||b_{\delta_h}| \\ &\quad + |x_3||\tilde{\nabla} b_{\delta_h}| + |\xi^h - x_3||\tilde{\nabla} b_{\delta_h}| + |b_{\delta_h}||\tilde{\nabla} \xi^h| \\ &\leq C\left(1 + h^{-1}|x_3| + h^{-2}|x_3|^2\right) \leq C, \end{aligned} \quad (4.129)$$

where each $C = C(\tilde{\nabla} y, m(\tilde{\nabla} y)) > 0$ is independent of h. These estimates follow from the estimates (4.21), (4.139) in Proposition 4.5.9, and (4.125).

Now, we recall from Proposition 4.5.9 that $(\tilde{\nabla} y_{\delta_h}|b_{\delta_h})^T (\tilde{\nabla} y_{\delta_h}|b_{\delta_h}) = \ell_{n_0}$ on $\omega \setminus \tilde{\omega}_{\delta_h}$. Thus,

$$\begin{aligned} &W^e((\tilde{\nabla} y_{\delta_h}|b_{\delta_h}), n_{\delta_h}, n_0) \\ &\quad = W_{nH}((\ell^f_{n_{\delta_h}})^{-1/2} (\tilde{\nabla} y_{\delta_h}|b_{\delta_h})(\ell^0_{n_0})^{1/2}) = 0 \quad \text{on } \omega \setminus \tilde{\omega}_{\delta_h} \end{aligned} \quad (4.130)$$

following Proposition A.1.7 and the identity (2.3). Here, we have set

$$n_{\delta_h} := \frac{(\tilde{\nabla} y_{\delta_h}|b_{\delta_h}) n_0}{|(\tilde{\nabla} y_{\delta_h}|b_{\delta_h}) n_0|} \quad \text{on } \omega. \quad (4.131)$$

Since the energy density (4.130) vanishes, we deduce from Proposition A.1.4 that

$$(\ell^f_{n_{\delta_h}})^{-1/2} (\tilde{\nabla} y_{\delta_h}|b_{\delta_h})(\ell^0_{n_0})^{1/2} =: R^h \in SO(3) \quad \text{on } \omega \setminus \tilde{\omega}_{\delta_h}. \quad (4.132)$$

We have yet to account for the non-ideal terms on this set as n_0^h in (4.15) is the appropriate argument for the energy density, not n_0. To do this, we exploit the observation in (4.132). Indeed, we set

$$n^h := \frac{(\nabla y^h) n_0^h}{|(\nabla y^h) n_0^h|} \quad \text{on } \Omega_h \quad (4.133)$$

and observe

$$\begin{aligned}(\ell^0_{n^h_0})^{1/2} &= (\ell^0_{n_0})^{1/2} + O(h),\\ (\ell^f_{n^h})^{-1/2} &= (\ell^f_{n_{\delta_h}})^{-1/2} + O(h) \quad \text{ on } \omega \setminus \tilde{\omega}_{\delta_h}\end{aligned} \tag{4.134}$$

following (4.128) and the scaling of the non-ideal term in (4.15). Hence on $\omega \setminus \tilde{\omega}_{\delta_h}$, we find

$$\begin{aligned}W^e(\nabla y^h, n^h, n^h_0) &= W_{nH}((\ell^f_{n_{\delta_h}})^{-1/2}(\tilde{\nabla} y_{\delta_h}|b_{\delta_h})(\ell^0_{n_0})^{1/2} + O(h))\\ &= W_{nH}((R^h)^T((\ell^f_{n_{\delta_h}})^{-1/2}(\tilde{\nabla} y_{\delta_h}|b_{\delta_h})(\ell^0_{n_0})^{1/2} + O(h)))\\ &= W_{nH}(I_{3\times 3} + O(h)) = O(h^2).\end{aligned} \tag{4.135}$$

For the equalities, we used (4.128), (4.134), the frame invariance of W_{nH}, and (4.132). For the inequality, we used the estimate in Proposition A.1.3.

Now, on the exceptional set $\tilde{\omega}_{\delta_h}$, we have

$$W^e(\nabla y^h, n^h, n^h_0) \le c(|\nabla y^h|^2 + 1) \le C \tag{4.136}$$

given the estimate in Proposition A.1.2 and (4.129). Thus, on the set $\tilde{\omega}_{\delta_h}$, the energy is $|O(1)|$ compared to h but this set is small for nonisometric origami, i.e., $|\tilde{\omega}_{\delta_h}| = O(\delta_h) = O(h)$ given $\delta_h = mh$ in (4.125). Hence, combining the estimates (4.135) and (4.136), we conclude

$$\begin{aligned}\mathcal{I}^h_{n^h_0}(y^h) &= \int_{-h/2}^{h/2}\int_{\tilde{\omega}_{\delta_h}} W^e(\nabla y^h, n^h, n^h_0)dx\\ &\quad + \int_{-h/2}^{h/2}\int_{\omega\setminus\tilde{\omega}_{\delta_h}} W^e(\nabla y^h, n^h, n^h_0)dx\\ &\le Ch|\tilde{\omega}_{\delta_h}| + O(h^3) = O(h^2).\end{aligned} \tag{4.137}$$

This completes the proof. □

Proposition 4.5.9 *Let $\bar{r} > 0$. Let ω and n_0 satisfy Definition 4.3.1(i) and $y \in W^{1,\infty}(\omega, \mathbb{R}^3)$ satisfy Definition 4.3.1(ii). If there exists a δ-smoothing y_δ of y as in definition 4.3.2, then for $\delta > 0$ sufficiently small, there exists a $b_\delta \in C^2(\bar{\omega}, \mathbb{R}^3)$ such that*

$$\begin{aligned}(\tilde{\nabla} y_\delta|b_\delta)^T(\tilde{\nabla} y_\delta|b_\delta) = \ell_{n_0} \quad &\textit{and} \quad \tilde{\nabla} b_\delta = 0\\ \textit{on } \omega \setminus \tilde{\omega}_\delta \quad &\textit{with } |\tilde{\omega}_\delta| = O(\delta),\\ \det(\tilde{\nabla} y_\delta|b_\delta) = 1 \quad &\textit{everywhere on } \omega.\end{aligned} \tag{4.138}$$

Moreover, b_δ satisfies

$$\|b_\delta\|_{L^\infty} \le C, \quad \|\tilde{\nabla} b_\delta\|_{L^\infty} \le C\delta^{-1}, \quad \|\tilde{\nabla}\tilde{\nabla} b_\delta\|_{L^\infty} \le C\delta^{-2} \tag{4.139}$$

everywhere on ω for some $C > 0$ which can depend on y and n_0 but is independent of δ.

Proof. From Proposition A.1.9, if $\tilde{F} \in \mathbb{R}^{3\times 2}$ and $n_0 \in \mathbb{S}^2$ such that $\tilde{F}^T\tilde{F} = \tilde{\ell}_{n_0}$, then there exists a $b \equiv b(\tilde{F}, n_0) \in \mathbb{R}^3$ such that $(\tilde{F}|b)^T(\tilde{F}|b) = \ell_{n_0}$ and $\det(\tilde{F}|b) = 1$. The parameterization is explicit, i.e., (A.24). Hence, we set

$$b_\delta := b(\tilde{\nabla} y_\delta, n_{0,\delta}) \quad \text{ on } \omega \tag{4.140}$$

for the δ-smoothing y_δ and the director $n_{0,\delta} \in C^\infty(\bar{\omega}, \mathbb{S}^2)$ given below in Proposition 4.5.10. The parameterization $b(\tilde{F}, n_0)$ is smooth in its arguments when $|\tilde{F}\tilde{e}_1 \times \tilde{F}\tilde{e}_2|$ is bounded away from zero. Consequently, (4.139) holds by the chain rule given the properties of the δ-smoothing y_δ and that $n_{0,\delta}$ satisfies (4.141). Further $\det(\tilde{\nabla} y_\delta | b_\delta) = 1$ everywhere on ω as the parameterization ensures this (even when the metric constraint is not satisfied).

It remains to verify the first two properties in (4.138). To this end, note for δ sufficiently small we have that $y_\delta = y$ except on a set of measure $O(\delta)$ (by hypothesis of a δ-smoothing) and that $n_{0,\delta} = n_0$ except on (perhaps a different) set of measure $O(\delta)$ (Proposition 4.5.10 below). Therefore, we conclude that there is a set $\tilde{\omega}_\delta$ of measure $O(\delta)$ such that $y_\delta = y$ and $n_{0,\delta} = n_0$ on $\omega \setminus \tilde{\omega}_\delta$. Moreover, $\tilde{\nabla} y = const.$, $n_0 = const.$ and $(\tilde{\nabla} y)^T \tilde{\nabla} y = \tilde{\ell}_{n_0}$ in any connected region in $\omega \setminus \omega_\delta$. Hence, we conclude the first two properties in (4.138) given (4.140) for b as in Proposition A.1.9. □

To construct b_δ, we utilized a smoothing approximation for the piecewise constant direction design $n_0 \colon \omega \to \mathbb{S}^2$ akin to a construction of DeSimone (Assertion 1 [36]). Precisely:

Proposition 4.5.10 *Let $\bar{r} > 0$. Let ω and n_0 satisfy (4.19). For any $\delta > 0$ sufficiently small, there exists an $n_{0,\delta} \in C^\infty(\bar{\omega}, \mathbb{S}^2)$ which satisfies*

$$\begin{aligned} &n_{0,\delta} = n_0 \quad \text{ on } \omega \setminus \omega_\delta \quad \text{ with } \quad |\omega_\delta| = O(\delta), \\ &\|\tilde{\nabla} n_{0,\delta}\|_{L^\infty} \leq C\delta^{-1} \quad \text{ and } \quad \|\tilde{\nabla}\tilde{\nabla} n_{0,\delta}\|_{L^\infty} \leq C\delta^{-2}. \end{aligned} \tag{4.141}$$

Here $C \equiv C(n_0) > 0$ is independent of δ.

Proof. Given that $\omega = \cup_{\alpha=1,\dots,N}\omega_\alpha$ for connected polygonal regions ω_α and $n_0 \colon \omega \to \mathbb{S}^2$ satisfies $n_0 = n_{0\alpha}$ on each ω_α, there exists a $\nu \in \mathbb{S}^2$ such that $B_\epsilon(\nu) \cap \text{range}\{n_0\} = \emptyset$

for some $\epsilon > 0$. We let $\Pi_\nu \colon \mathbb{S}^2 \setminus \{\nu\} \to \mathbb{R}^2$ denote the stereographic projection with projection point ν. This map is bijective (i.e., there exists a $\Pi_\nu^{-1} \colon \mathbb{R}^2 \to \mathbb{S}^2 \setminus \{\nu\}$). Thus, we extend n_0 to all of $\mathbb{R}^2$ by setting $n_0 = n_{01}$ for $\mathbb{R}^2 \setminus \omega$ (we do not relabel) and we define

$$n_{0,\delta}(\tilde{x}) = (\Pi_\nu^{-1} \circ (\eta_\delta * (\Pi_\nu \circ n_0)))(\tilde{x}), \quad \tilde{x} \in \omega. \tag{4.142}$$

Here $\eta_\delta \in C^\infty(\mathbb{R}^2, \mathbb{R})$ is the standard mollifier on $\mathbb{R}^2$ supported on a ball of radius $\delta/2$.

We claim that this map has all the properties stated in the proposition. Indeed, $\Pi_\nu \circ n_0$ maps to a compact subset of $\mathbb{R}^2$ given that ν is at least ϵ away from any $n_{0\alpha}$. Thus, $\|\Pi_\nu \circ n_0\|_{L^\infty} \leq C$ for $C \equiv C(n_0) > 0$. Consequently, $\eta_\delta * (\Pi_\nu \circ n_0) \in C^\infty(\mathbb{R}^2, \mathbb{R}^2)$ with

$$\begin{aligned} \|\tilde{\nabla}(\eta_\delta * (\Pi_\nu \circ n_0))\|_{L^\infty} &\leq C\delta^{-1} \\ \|\tilde{\nabla}\tilde{\nabla}(\eta_\delta * (\Pi_\nu \circ n_0))\|_{L^\infty} &\leq C\delta^{-2} \end{aligned} \tag{4.143}$$

given that η_δ is the mollifier as above. Here $C \equiv C(n_0) > 0$ is independent of $\delta > 0$. Now Π_ν^{-1} is smooth. Thus, $n_{0,\delta} \in \mathbb{C}^\infty(\bar{\omega}, \mathbb{S}^2)$ and by the chain rule, we deduce the estimates in (4.141).

For the equality condition in (4.141), we set $\omega_\delta = \{\tilde{x} \in \omega \colon \operatorname{dist}(\tilde{x}, \partial\omega_\alpha) \leq \delta/2 \quad \text{for some } \alpha \in \{1, \dots, N\})\}$. Clearly this set has measure $O(\delta)$ for $\delta > 0$ sufficiently small. Moreover, we observe that

$$\eta_\delta * (\Pi_\nu \circ n_0) = \Pi_\nu \circ n_0 \quad \text{ on } \omega \setminus \omega_\delta \tag{4.144}$$

since $n_0 = const.$ on $B_{\delta/2}(\tilde{x})$ for any $\tilde{x} \in \omega \setminus \omega_\delta$. Given this and the definition of $n_{0,\delta}$ in (4.142), we deduce the equality in (4.141). This completes the proof. □

Proof of Lemma 4.5.4. (On incompressibility)

Here we prove Lemma 4.5.4, which develops (and catalogues properties associated with) explicit constructions of incompressible deformations for thin elastomer sheets. *Proof of Lemma 4.5.4.* We set $\delta_h = mh$ for $m \geq 1$ to be determined in Proposition 4.5.11 below. We consider the function $v^h \equiv v^h(\alpha)$ given by

$$v^h(\tilde{x}, x_3) := y_{\delta_h}(\tilde{x}) + x_3 b_{\delta_h}(\tilde{x}) \tag{4.145}$$

and assume $x_3 \in (-h/2, h/2)$. Since $\nabla v^h = (\tilde{\nabla} y_{\delta_h} | b_{\delta_h}) + x_3(\tilde{\nabla} b_{\delta_h} | 0)$ and $\det(\tilde{\nabla} y_{\delta_h} | b_{\delta_h}) = 1$, we let $S^h \equiv S^h(\alpha) := (\tilde{\nabla} y_{\delta_h} | b_{\delta_h})^{-1}(\tilde{\nabla} b_{\delta_h} | 0)$ and find

$$\begin{aligned} \det \nabla v^h &= \det((\tilde{\nabla} y_{\delta_h} | b_{\delta_h})^{-1} \nabla v^h) = \det(I + x_3 S^h) \\ &= 1 + x_3 \operatorname{Tr}(S^h) + x_3^2 \operatorname{Tr}(\operatorname{cof} S^h) + x_3^3 \det(S^h). \end{aligned} \tag{4.146}$$

For the estimates below, $C \equiv C(M)$. We note that $\|(\tilde{\nabla} y_{\delta_h}|b_{\delta_h})^{-1}\|_{L^\infty(\omega)} \leq C$ since the determinant is unity, and therefore $|S^h| \leq C\delta_h^{\min\{-\alpha,0\}}$ by hypothesis and

$$\begin{aligned} |\det \nabla v^h - 1| &\leq C\left(|x_3|\delta_h^{\min\{-\alpha,0\}} + |x_3|^2\delta_h^{2\min\{-\alpha,0\}} + |x_3|^3\delta_h^{3\min\{-\alpha,0\}}\right) \\ &\leq C|x_3|\delta_h^{\min\{-\alpha,0\}} \quad \text{for} \quad \alpha \in \{-1,0,1\}, \quad m \geq 1. \end{aligned} \tag{4.147}$$

In addition, for $\beta = 1,2$, since $\|\partial_\beta S^h\|_{L^\infty(\omega)} \leq C(\delta_h^{2\min\{-\alpha,0\}} + \delta_h^{-\alpha-1}) \leq C\delta_h^{-\alpha-1}$ for $\alpha \in \{-1,0,1\}$ and since $|\partial_\beta \operatorname{Tr}(S^h)| \leq |\partial_\beta S^h|$, $|\partial_\beta \operatorname{Tr}(\operatorname{cof} S^h)| \leq 2|S^h||\partial_\beta S^h|$ and $|\partial_\beta \det(S^h)| \leq |S^h|^2|\partial_\beta S^h|$, we conclude that

$$\begin{aligned} |\partial_\beta \det \nabla v^h| &\leq C\Big(|x_3|\delta_h^{-\alpha-1} + |x_3|^2\delta_h^{\min\{-\alpha,0\}}\delta_h^{-\alpha-1} \\ &\qquad + |x_3|^3\delta_h^{2\min\{-\alpha,0\}}\delta_h^{-\alpha-1}\Big) \\ &\leq C|x_3|\delta_h^{-\alpha-1} \quad \text{for} \quad \beta \in \{1,2\}, \quad \alpha \in \{-1,0,1\}, \quad m \geq 1. \end{aligned} \tag{4.148}$$

Now since v^h is not incompressible, we modify it through a non-linear change in coordinates. We let $\Xi^h(\tilde{x}, x_3) = (\tilde{x}, \xi^h(\tilde{x}, x_3))$ for $\xi^h \in C^1(\overline{\Omega}_h, \mathbb{R})$ to be determined, and we define $y^h \equiv y^h(\alpha) := v^h \circ \Xi^h$. Hence, by the column linearity of the determinant, we find that

$$\det \nabla y^h = \det(\nabla v^h \circ \Xi^h)\partial_3 \xi^h. \tag{4.149}$$

Thus, satisfying the determinant constraint on ∇y^h amounts to satisfying the ordinary differential equation

$$\partial_3 \xi^h = \frac{1}{\det(\nabla v^h \circ \Xi^h)} \quad \text{on} \quad \Omega_h \tag{4.150}$$

for some ξ^h. There is an $m = m(\alpha, M) \geq 1$ such that for $h > 0$ sufficiently small, there is a solution to (4.150), i.e., $\xi^h \equiv \xi^h(\alpha)$ for a $\xi^h \in C^1(\overline{\Omega}_h, \mathbb{R})$ with the initial condition $\xi^h(\tilde{x}, 0) = 0$, see Proposition 4.5.11.

It remains to prove the estimates in (4.109). By Proposition 4.5.11, the map ξ^h satisfies pointwise

$$|\xi^h| \leq 2|x_3|, \quad |\partial_3 \xi^h| \leq 2 \tag{4.151}$$

everywhere on Ω_h. Thus, given (4.150),(4.147) and the estimates above, we deduce

$$\begin{aligned} |\partial_3 \xi^h - 1| &\leq |\partial_3 \xi^h||\det(\nabla v^h \circ \Xi^h) - 1| \\ &\leq Ch^{\min\{-\alpha,0\}}|\xi^h| \leq Ch^{\min\{-\alpha,0\}}|x_3| \end{aligned} \tag{4.152}$$

everywhere on Ω_h. Similarly,

$$\begin{aligned} |\xi^h - x_3| &\le \Big| \int_0^{x_3} (\partial_3 \xi^h - 1) d\bar{x}_3 \Big| \\ &\le \int_0^{|x_3|} |\partial_3 \xi^h - 1| d\bar{x}_3 \le C h^{\min\{-\alpha, 0\}} |x_3|^2 \end{aligned} \tag{4.153}$$

everywhere on Ω_h. Finally, to estimate the first and second derivative of ξ_h, we define $F_h(\tilde{x}, t) := \int_0^s \det(\nabla v^h(\tilde{x}, s)) ds$, and notice that the ordinary differential equation in (4.150) is equivalent to the implicit equation $F_h(\tilde{x}, \xi^h(x)) = x_3$. Differentiating this equation with respect to x_β, $\beta = 1$, or 2, we find

$$\int_0^{\xi^h} \partial_\beta \det(\nabla v^h) ds + \det(\nabla v^h \circ \Xi^h) \partial_\beta \xi^h = 0. \tag{4.154}$$

Hence using (4.150), (4.148) and (4.151),

$$\begin{aligned} |\partial_\beta \xi^h| &\le |\partial_3 \xi^h| \int_0^{|\xi^h|} |\partial_\beta \det \nabla v^h| ds \\ &\le C h^{-\alpha - 1} \int_0^{|\xi^h|} |s| ds \le C h^{-\alpha - 1} |x_3|^2 \end{aligned} \tag{4.155}$$

everywhere on Ω_h for $\beta = 1, 2$. These are the desired estimates. □

Proposition 4.5.11 *Let $\alpha \in \{-1, 0, 1\}$. Let $v^h \equiv v^h(\alpha)$ as defined in (4.145) with y_{δ_h} and b_{δ_h} as in Lemma 4.5.4 with $\delta_h = mh$. There is an $m = m(\alpha, M) \ge 1$ such that for any $h > 0$ sufficiently small, there exists a $\xi^h \equiv \xi^h(\alpha) \in C^1(\overline{\Omega}_h, \mathbb{R})$ such that*

$$\partial_3 \xi^h = \frac{1}{\det(\nabla v^h \circ \Xi^h)} \quad \text{on } \Omega_h, \quad \text{with} \quad \xi^h(\tilde{x}, 0) = 0. \tag{4.156}$$

Moreover ξ^h satisfies pointwise the estimate

$$|\xi^h| \le 2|x_3|, \quad |\partial_3 \xi^h| \le 2 \quad \text{on } \Omega_h. \tag{4.157}$$

Proof. For $\alpha \in \{-1, 0, 1\}$ and $h > 0$, we consider the mapping $T^h \equiv T^h(\alpha) \colon \mathcal{M}^h \to C(\bar{\Omega}_h)$ given by

$$T^h(\phi)(\tilde{x}, x_3) = \int_0^{x_3} \frac{1}{\det(\nabla v^h(\tilde{x}, \phi(\tilde{x}, s)))} ds \quad \text{for each} \quad (\tilde{x}, x_3) \in \Omega_h, \tag{4.158}$$

where $\mathcal{M}^h \equiv \mathcal{M}^h(\alpha)$ is given by

$$\begin{aligned} \mathcal{M}^h := \Big\{ \phi \in C(\overline{\Omega}_h) \colon \phi(\tilde{x}, 0) = 0, \ \ |\phi(\tilde{x}, x_3)| \le 2|x_3|, \\ \det(\nabla v^h(\tilde{x}, \phi(\tilde{x}, x_3))) \ge 1/2 \text{ for each } (\tilde{x}, x_3) \in \Omega_h \Big\}. \end{aligned} \tag{4.159}$$

This is a (non-empty) complete space under the infinity norm. Thus, we aim to show that there is an appropriate choice of $m = m(\alpha, M)$ in δ_h such that for $h > 0$ sufficiently small, the mapping T^h is, in fact, a contraction map in the space $\mathcal{M}^h$ under the infinity norm. The proposition will follow by the equivalence of the integral representation of (4.156).

We first prove that T^h is an operator (i.e., $T^h \colon \mathcal{M}^h \to \mathcal{M}^h$) for an appropriate choice of $m = m(\alpha, M)$ and small enough h. For the estimates below, $C \equiv C(M)$. Since $\phi \in \mathcal{M}^h$, we have

$$|T^h(\phi)(\tilde{x}, x_3)| \leq 2|x_3|, \qquad \text{for each} \quad (\tilde{x}, x_3) \in \Omega_h. \tag{4.160}$$

In addition, using a similar estimate to (4.147), we obtain

$$\begin{aligned} |\det \nabla v^h(\tilde{x}, T^h(\tilde{x}, x_3)) - 1| &\leq C|T^h(\tilde{x}, x_3)|\delta_h^{\min\{-\alpha,0\}} \\ &\leq C|x_3|h^{\min\{-\alpha,0\}} m^{\min\{-\alpha,0\}} \end{aligned} \tag{4.161}$$

for $\alpha \in \{-1, 0, 1\}$. Thus, for $\alpha \in \{-1, 0\}$, we need only enforce $m \geq 1$ and for $\alpha = 1$ we enforce $m = m(\alpha, M) \geq \max\{2C, 1\}$ to ensure $T^h \equiv T^h(\alpha)$ is an operator for small h.

It remains to prove that T^h is a contraction under the L^∞ norm. Observe for $\phi, \psi \in \mathcal{M}^h$,

$$\begin{aligned} &|T^h(\phi)(\tilde{x}, x_3) - T^h(\psi)(\tilde{x}, x_3)| \\ &\quad \leq 4 \int_0^{|x_3|} |\det(\nabla v^h(\tilde{x}, \psi(\tilde{x}, s)) - \det(\nabla v^h(\tilde{x}, \phi(\tilde{x}, s))| ds \\ &\quad \leq C\delta_h^{\min\{-\alpha,0\}} \int_0^{|x_3|} |\psi(\tilde{x}, s) - \phi(\tilde{x}, s)| ds \\ &\quad \leq C m^{\min\{-\alpha,0\}} h^{\min\{-\alpha,0\}} h \|\psi - \phi\|_{L^\infty(\Omega_h)} \end{aligned} \tag{4.162}$$

for any $(\tilde{x}, x_3) \in \Omega_h$. Here the first inequality uses the determinant constraint on $\mathcal{M}^h$, the second uses the equation (4.146), and the third uses that $\delta_h = mh$. Finally, from this estimate, it is clear that we can choose $m = m(\alpha, M) \geq 1$ independent of h (in fact $m = 1$ suffices for $\alpha = -1, 0$ as in the remark), such that for h sufficiently small

$$\|T^h(\phi) - T^h(\psi)\|_{L^\infty(\Omega_h)} < \|\psi - \phi\|_{L^\infty(\Omega_h)}, \tag{4.163}$$

i.e., it is a contraction map.

We now fix this $m = m(\alpha, M)$ and an $h > 0$ sufficiently small. Since $T^h \equiv T^h(\alpha)$ is a contraction map, there exists a $\xi^h \equiv \xi^h(\alpha)$ such that

$$\xi^h = T^h(\xi^h) = \int_0^{x_3} \frac{1}{\det(\nabla v^h(\tilde{x}, \xi^h(\tilde{x}, s)))} ds \quad \text{for each} \quad (\tilde{x}, x_3) \in \Omega_h. \quad (4.164)$$

This is equivalent to the ordinary differential equation (4.156). The regularity $\xi^h \in C^1(\overline{\Omega}_h, \mathbb{R})$ follows from the regularity of y_{δ_h} and b_{δ_h}. The estimates (4.157) follow from the fact that $\xi^h \in \mathcal{M}^h$. This completes the proof. □

4.6 The metric constraint as a necessary condition for bending

We come to our last main result. So far, we exhibited constructions (nonisometric origami and smooth surfaces) which satisfy the metric constraint (4.17) and this guarantees that they have small entropic strain energy ($O(h^2)$ and $O(h^3)$ respectively). Now, we assume that the strain energy of a sequence of y^h is of order h^3 (i.e., is small) and we prove a suitable rescaling of y^h converges to a map $y : \omega \to \mathbb{R}^3$ satisfying the metric constraint. For this, we augment the entropic elastic energy from before.

We no longer require the deformed director n^h to be constrained as $n^h = \frac{(\nabla y^h) n_0^h}{|(\nabla y^h n_0^h|}$ (see the discussion in Remark 4.2.1(iii)). Instead, we introduce the *non-ideal* elastic energy associated to nematic elastomers. Following Biggins et al. [17, 18] and others [27, 76, 101, 100], we take $W^{ni} : \mathbb{R}^{3\times 3} \times \mathbb{S}^2 \times \mathbb{S}^2 \to \mathbb{R} \cup \{+\infty\}$ to be as in (2.8) (see Remark 4.6.2 below). Moreover, we set $\widehat{W} := (\mu/2)^{-1}(W^e + W^{ni})$, and study the combined energy

$$\mathcal{I}^{h,\sqrt{\kappa/\mu}}_{n_0^h}(y^h, n^h) := \int_{\Omega_h} \left(\widehat{W}(\nabla y^h, n^h, n_0^h) + \frac{\kappa}{\mu} |\nabla n^h|^2 \right) dx. \quad (4.165)$$

Here, we also introduce a Frank elastic term (see Remark 4.6.3 below) for which $\kappa > 0$ is the modulus of this elasticity.

For the compactness result, we rescale the x_3 variable via a change of coordinates $z(x) = (\tilde{x}, h^{-1}x_3)$. This allows us to consider sequences on the fixed domain $\Omega = \omega \times (-1/2, 1/2)$, i.e.,

$$\begin{aligned} &v^h(z(x)) = y^h(x), \quad m_0^h(z(x)) = n_0^h(x), \\ &h^{-3}\mathcal{I}^{h,\varepsilon}_{n_0^h}(y^h, n^h) \equiv \mathcal{J}^{h,\varepsilon}_{m_0^h}(v^h, m^h), \end{aligned} \quad (4.166)$$

where the rescaled energy $\mathcal{J}^{h,\varepsilon}_{m_0^h} : W^{1,2}(\Omega, \mathbb{R}^3) \times W^{1,2}(\Omega, \mathbb{S}^2) \to \mathbb{R} \cup \{+\infty\}$ is given by

$$\mathcal{J}^{h,\varepsilon}_{m_0^h}(v^h, m^h) := \int_\Omega \left(\frac{1}{h^2} \widehat{W}(\nabla_h v^h, m^h, m_0^h) + \frac{\varepsilon^2}{h^2} |\nabla_h m^h|^2 \right) dz. \quad (4.167)$$

Here, for $f:\Omega\to\mathbb{R}^3$, we denote $\nabla_h f$ as $(\tilde{\nabla} f|\frac{1}{h}\partial_3 f)$, which reflects the rescaling of x_3 by $1/h$.

Given these rescalings, we have:

Theorem 4.6.1 (Compactness) *Let $r>0$. Let $n_0\in W^{1,2}(\omega,\mathbb{S}^2)$ and let*

$$c_l h\le \varepsilon\equiv\varepsilon_h\le c_u h, \tag{4.168}$$

for some constants $c_u\ge c_l>0$. Moreover, let m_0^h satisfy

$$m_0^h(z)=n_0(\tilde{z})+O(h),\quad \text{for a.e. } z\in\Omega,\quad i.e.,\ \ \|m_0^h-n_0\|_{L^\infty(\Omega)}\le\tau h. \tag{4.169}$$

For every sequence $\{v^h,m^h\}\subset W^{1,2}(\Omega,\mathbb{R}^3)\times W^{1,2}(\Omega,\mathbb{S}^2)$ with $\mathcal{J}^{h,\varepsilon_h}_{m_0^h}(v^h,m^h)\le C$ as $h\to 0$, there exists a subsequence (not relabeled) and a $y\in W^{2,2}(\Omega,\mathbb{R}^3)$ independent of z_3 such that as $h\to 0$

$$\left(v^h-\frac{1}{|\Omega|}\int_\Omega v^h dz\right)\to y\quad \text{in } W^{1,2}(\Omega,\mathbb{R}^3)\quad \text{with}\quad (\tilde{\nabla}y)^T\tilde{\nabla}y=\tilde{\ell}_{n_0}\ \text{a.e. on } \omega. \tag{4.170}$$

Moreover as $h\to 0$, $\|m^h-\sigma\frac{(\nabla v^h)m_0^h}{|(\nabla v^h)m_0^h|}\|_{L^2(\Omega)}\to 0$ for some σ a fixed constant from the set $\{1,-1\}$.

In the energy (4.165) above, we introduced two new terms compared to the strain energy (4.14): the non-ideal term (2.8) (which replaces the hard kinematic constraint) and the Frank elastic term $|\nabla n^h|^2$. We now discuss the physical background behind these energetic contributions.

Remark 4.6.2 (The non-ideal energy density) *(i) The energy density W^{ni} in (2.8) for this contribution is well-established in the physics literature [18, 17, 76] (though, in these works it is written out in a different but nevertheless completely equivalent form). It has microscopic origins as detailed by Verwey and Warner [100], and a slight variant of this energy has been used to explain the semi-soft behavior of clamped-stretched nematic elastomer sheets [27, 101]. This was discussed further in Chapter 2.*

(ii) The non-ideal term prevents the material from freely forming microstructure at low energy. As we discussed in Remark 4.2.1(iii), some control on microstructure is necessary for predictable shape actuation. Nematic elastomers

heterogeneously patterned for actuation are typically cross-linked in the nematic phase (e.g., the samples of Ware et al. [102]), and thus encode some memory of their patterned director n_0. The non-ideal term (2.8) is modeling this memory. (This is in contrast to nematic elastomers which are cross-linked in the high temperature isotropic phase as in the samples of Kundler and Finkelmann [58], and which do readily form microstructure.)

(iii) During thermal actuation, the entropic energy density W^e is minimized (and equal to zero) when $F = (\ell_n^f)^{1/2} R (\ell_{n_0}^0)^{-1/2}$ for any $R \in SO(3)$ and any $n \in \mathbb{S}^2$. That is, there is a degenerate set of shape-changing soft deformations since n is unconstrained by the deformation. Introducing the non-ideal term breaks this degeneracy. Specifically, if W^e and W^{ni} are both minimized (and equal to zero), then $n = \sigma R \nu_0 = \sigma F n_0 / |F n_0|$ for $\sigma \in \{-1, 1\}$ in addition to the identity above (we make this precise in Proposition A.1.8 in the appendix). That is, ν is no longer unconstrained, but instead the initial director ν_0 gets convected by the deformation to ν (or $-\nu_0$ gets convected to ν since the energies are invariant under a change of sign of the director). This observation underlies the fact that the director is approximately convected by the deformation at low enough energies (and therefore, we recover the sharp kinematic constraint in (4.14) up to a trivial change in the sign in the limit $h \to 0$). As a result, the metric constraint emerges rigorously at the bending scale.

Remark 4.6.3 (Frank elasticity) *(i) Our augmented energy also considers Frank elasticity as a contribution. The presence of this term allows us to employ the geometric rigidity result of Friesecke, James and Müller [46]. Geometric rigidity is the central technical tool for deriving a compactness result for bending theories from three dimensional elastic energies (compare [16, 45, 62, 63]). The choice $\varepsilon \propto h$ is dictated by the desire to have Frank elasticity be comparable to the entropic elasticity (and thus to get a non-trivial limit) at the bending scale. We discuss this further below.*

(ii) Following de Gennes and Prost [49], Frank elasticity is a phenomenological continuum model for an energy penalizing distortions in the alignment of the current director n which can be bounded from above an below as

$$\frac{1}{2}\kappa_l |\mathrm{grad}\, n|^2 \leq W_{Fr} \leq \frac{1}{2}\kappa_u |\mathrm{grad}\, n|^2 \tag{4.171}$$

for $\kappa_l \leq \kappa_u$ (recall the discussion on Frank elasticity in Chapter 2).

We are interested foremost in how Frank energy may compete with the entropic energy at the bending scale. Thus, we consider only the simplified model penalizing $|grad\ n|^2$ *since the detailed model is sandwiched energetically by models of this type (4.171). We make a further assumption regarding how distortions in nematic alignment are accounted in the energetic framework. To elaborate, a model for Frank elasticity should ideally penalize spatial distortions in the alignment of the director field, i.e., the grad operator should be with respect to the current frame. Unfortunately, this seems quite technical to capture in a variational setting, as notions of invertibility of Sobolev maps must be carefully considered. It is, however, an active topic of mathematical research. For instance, we refer the interested reader to the works of Barchiesi and DeSimone [8] and Barchiesi et al. [9] for Frank elasticity and nematic elastomers in this context. Nevertheless, for our purpose in understanding whether the metric constraint (4.17) is necessitated by a smallness in the energy, we find it sufficiently interesting to consider the simplified model*

$$W_{Fr} \approx \frac{\kappa}{2}|\nabla n^h|^2, \quad n^h \colon \Omega_h \to \mathbb{S}^2 \tag{4.172}$$

where n^h *refers to the current director field as a mapping from the initially flat sheet* Ω_h *and* ∇ *is the gradient with respect to this reference state. The term* (4.172) *is the one that appears in the energy* (4.165).

(iii) The parameter $\varepsilon = \sqrt{\kappa/\mu}$ *is likely quite small in nematic elastomers, typiccally* $\varepsilon \sim 10 - 100nm$ *(recall the discussion on Frank elasiticy in Chapter 2). Thus, entropic elasticity will often dominate Frank elasticity in these elastomers. However, a typical thin sheet will have a thickness* $h \sim 10 - 100\mu m$*. So there are two small length scales to consider in this problem. For mechanical boundary conditions which induce stretch and stress in these sheets, the entropic energy does appear to dominate the Frank term. For instance, stripe domains of oscillating nematic orientation would be suppressed by a large Frank energy, and yet these have been observed by Kundler and Finkelmann [58] in the clamped stretch experiments on thin sheets. Mathematically, this dominance under stretch is made precise, for instance, by Cesana et al. [25] in studying an energy which includes Frank and entropic elastic contributions. The resulting membrane theory does not depend on Frank elasticity. These results notwithstanding, actuation of nematic sheets with controlled heterogeneity occurs at a much lower energy state. Therefore, it is possible that the actuated configuration emerges from a non-trivial competition between*

entropic and Frank elasticity at these small energy scales. Hence, we study this competition in an asymptotic sense by taking h and $\varepsilon \to 0$.

Proof of Theorem 4.6.1.

In this section, we prove that the metric constraint (4.17) is necessary for a configuration in pure bending when Frank elasticity is comparable to entropic elasticity at the bending scale (Theorem 4.6.1). First, we address some key preliminary results for this compactness, including a crucial lemma which is a consequence of geometric rigidity. Then, we prove Theorem 4.6.1.

Preliminaries for compactness

The key lemma which enables a proof of compactness in this setting is based on the result of geometric rigidity by Friesecke, James and Müller [46], and generalization to non-Euclidean plates by Lewicka and Pakzad [63].

Lemma 4.6.4 *Let $\omega \subset \mathbb{R}^2$ bounded and Lipschitz, and $r_f, r_0 > 1$ and $\tau \geq 0$. There exists a $C = C(\omega, r_f, r_0, \tau) > 0$ with the following property: For every $h > 0$, $\Omega_h := \omega \times (-h/2, h/2)$, $y^h \in W^{1,2}(\Omega_h, \mathbb{R}^3)$, $n^h \in W^{1,2}(\Omega_h, \mathbb{S}^2)$ and n_0^h as in (4.15) with $n_0 \in W^{1.2}(\omega, \mathbb{S}^2)$, there exists an associated matrix field $G^h : \omega \to \mathbb{R}^{3\times 3}$ satisfying the estimates*

$$\begin{aligned}
&\frac{1}{h}\int_{\Omega_h} |G^h - (\ell^f_{n^h})^{-1/2}(\nabla y^h)(\ell^0_{n_0^h})^{1/2}|^2 dx \\
&\qquad \leq \frac{C}{h}\int_{\Omega_h} \Big(\operatorname{dist}^2((\ell^f_{n^h})^{-1/2}(\nabla y^h)(\ell^0_{n_0^h})^{1/2}, SO(3)) \\
&\qquad\qquad + h^2(|\nabla n^h|^2 + |\tilde{\nabla} n_0|^2 + 1)\Big) dx, \\
&\int_\omega |\tilde{\nabla} G^h|^2 d\tilde{x} \\
&\qquad \leq \frac{C}{h^3}\int_{\Omega_h} \Big(\operatorname{dist}^2((\ell^f_{n^h})^{-1/2}(\nabla y^h)(\ell^0_{n_0^h})^{1/2}, SO(3)) \\
&\qquad\qquad + h^2(|\nabla n^h|^2 + |\tilde{\nabla} n_0|^2 + 1)\Big) dx.
\end{aligned} \tag{4.173}$$

We address this result at the end of the section. For similar results related to non-Euclidean plates in a different context, see Lewicka et al. [16, 62].

Recall the rescaled variables v^h and m_0^h defined at the start of this section. We have:

Proposition 4.6.5 *Let $\omega \subset \mathbb{R}^2$ bounded and Lipschitz, $r_f, r_0 > 1$, $\tau \geq 0$, and ε_h as in (4.168). Let $v^h \in W^{1,2}(\Omega, \mathbb{R}^3)$, $m^h \in W^{1,2}(\Omega, \mathbb{S}^2)$ and m_0^h as in (4.169) for $n_0 \in W^{1,2}(\omega, \mathbb{S}^2)$. There exists an associated matrix field $G^h \colon \omega \to \mathbb{R}^{3\times 3}$ such that*

$$\begin{aligned} &\int_\Omega |G^h - (\ell^f_{m^h})^{-1/2}(\nabla_h v^h)(\ell^0_{m_0^h})^{1/2}|^2 dz \\ &\qquad \leq Ch^2(\mathcal{J}^{h,\varepsilon_h}_{m_0^h}(v^h, m^h) + \|\tilde{\nabla} n_0\|^2_{L^2(\omega)} + 1) \\ &\int_\Omega |\tilde{\nabla} G^h|^2 d\tilde{z} \leq C(\mathcal{J}^{h,\varepsilon_h}_{m_0^h}(v^h, m^h) + \|\tilde{\nabla} n_0\|^2_{L^2(\omega)} + 1) \end{aligned} \tag{4.174}$$

for ε_h, c_l as in (4.168) and some uniform $C = C(\omega, r_f, r_0, c_l, \tau)$ which is independent of h.

Proof. Using Proposition A.1.4 and the identity (2.3), we find that

$$\begin{aligned} &\int_\Omega \operatorname{dist}^2((\ell^f_{m^h})^{-1/2}(\nabla_h v^h)(\ell^0_{m_0^h})^{1/2}, SO(3))dz \\ &\qquad \leq \int_\Omega \widehat{W}_{nH}((\ell^f_{m^h})^{-1/2}(\nabla_h v^h)(\ell^0_{m_0^h})^{1/2})dz, \\ &\qquad \leq \int_\Omega \widehat{W}^e(\nabla_h v^h, m^h, m_0^h)dz \leq \int_\Omega \widehat{W}(\nabla_h v^h, m^h, m_0^h)dz, \end{aligned} \tag{4.175}$$

where $\widehat{(\cdot)} = (2/\mu)(\cdot)$ and the last inequality follows given W^{ni} in (2.8) is ≥ 0. Since ε_h as in (4.168), we also find that

$$\int_\Omega h^2 |\nabla_h m^h|^2 dz \leq \frac{1}{c_l^2} \int_\Omega \varepsilon_h^2 |\nabla_h m^h|^2 dz. \tag{4.176}$$

Combining these two estimates, we find that

$$\begin{aligned} &\int_\Omega \left(\operatorname{dist}^2((\ell^f_{m^h})^{-1/2}(\nabla_h v^h)(\ell^0_{m_0^h})^{1/2}, SO(3)) + h^2 |\nabla_h m^h|^2 \right) dz \\ &\qquad \leq Ch^2 \mathcal{J}^{h,\varepsilon_h}_{m_0^h}(v^h, m^h) \end{aligned} \tag{4.177}$$

for some uniform $C = C(c_l)$.

To obtain the desired estimates in (4.174), we change variables via $z(x) := (x_1, x_2, \frac{x_3}{h})$ for $x \in \Omega_h$, set the functions as defined in (4.166), apply Lemma 4.6.4, and the estimates follow from the bound (4.177). □

Compactness for comparable entropic and Frank elasticity in bending

We turn now to the proof of Theorem 4.6.1. For clarity, we break up the proof into several steps.

Recall that for this theorem, we suppose m_0^h as in (4.169) with $n_0 \in W^{1,2}(\omega, \mathbb{S}^2)$ and ε_h as in (4.168). We consider a sequence $\{v^h, m^h\} \subset W^{1,2}(\Omega, \mathbb{R}^3) \times W^{1,2}(\Omega, \mathbb{S}^2)$ such that

$$\mathcal{J}^{h,\varepsilon_h}_{m_0^h}(v^h, m^h) \leq C, \tag{4.178}$$

for all h small and for some C independent of h. The convergences stated in each step are for a suitably chosen subsequence as $h \to 0$.

Step 1. $m_0^h \to n_0$ *in* $L^2(\Omega, \mathbb{S}^2)$, *and* $(\ell^0_{m_0^h})^{\pm 1/2} \to (\ell^0_{n_0})^{\pm 1/2}$ *in* $L^2(\Omega, \mathbb{R}^{3\times 3})$.

The first convergence is a trivial consequence of the definition of m_0^h in (4.169). The second follows from the estimate $|(\ell^0_{\nu_1})^{\pm 1/2} - (\ell^0_{\nu_2})^{\pm 1/2}| \leq C(r_0)|\nu_1 - \nu_2|$ for $\nu_{1,2} \in \mathbb{S}^2$ and the first convergence. □

Step 2. $m^h \rightharpoonup n$ *in* $W^{1,2}(\Omega, \mathbb{S}^2)$ *for some* n *independent of* z_3 *and* $(\ell^f_{m^h})^{\pm 1/2} \to (\ell^f_n)^{\pm 1/2}$ *in* $L^2(\Omega, \mathbb{R}^{3\times 3})$.

For h sufficiently small, we have

$$\begin{aligned} \frac{1}{c_l^2}\int_\Omega |\nabla m^h|^2 dz &\leq \frac{1}{c_l^2}\int_\Omega \left(|\tilde{\nabla} m^h|^2 + \frac{1}{h^2}|\partial_3 m^h|^2\right) dz \\ &\leq \mathcal{J}^{h,\varepsilon_h}_{m_0^h}(v^h, m^h) \leq C \end{aligned} \tag{4.179}$$

for C independent of h by (4.178). Thus, up to a subsequence, $m^h \rightharpoonup n$ in $W^{1,2}(\Omega, \mathbb{R}^3)$. By Rellich's theorem, taking a further subsequence (if necessary), we have strong convergence, $m^h \to n$ in $L^2(\Omega, \mathbb{R}^3)$. Since $m^h \in \mathbb{S}^2$ a.e., we deduce that $n \in \mathbb{S}^2$ a.e. by this strong convergence. Further, n is independent of z_3 since by the estimate (4.179), we find $\partial_3 m^h \to 0$ in $L^2(\Omega, \mathbb{R}^3)$, and therefore $\partial_3 n = 0$ a.e. by the uniqueness of the weak $W^{1,2}$ limit. The convergences of $(\ell^f_{m^h})^{\pm 1/2}$ follow by an argument similar to the convergences of $(\ell^0_{m_0^h})^{\pm 1/2}$ in Step 1. □

Step 3. $(v^h - \frac{1}{|\Omega|}\int_\Omega v^h dz) \rightharpoonup y$ *in* $W^{1,2}(\Omega, \mathbb{R}^3)$ *for some* y *independent of* z_3. *Also,* $h^{-1}\partial_3 v^h \rightharpoonup b$ *in* $L^2(\Omega, \mathbb{R}^3)$.

For h sufficiently small, we have

$$\begin{aligned} &\frac{1}{c}\int_\Omega (|\tilde{\nabla} v^h|^2 + |h^{-1}\partial_3 v^h|^2 - 1) dz \\ &\qquad \leq \int_\Omega \widehat{W}^e(\nabla_h v^h, m^h, m_0^h) dz \leq \mathcal{J}^{h,\varepsilon_h}_{m_0^h}(v^h, m^h) \leq C \end{aligned} \tag{4.180}$$

by Proposition A.1.2 and (4.178). Thus, since $|\nabla v^h| \leq |\nabla_h v^h|$ for h small, we conclude the first convergence (up to a subsequence) given the estimate (4.180) and

an application of the Poincaré inequality. We again use (4.180) to conclude that up to a subsequence, $h^{-1}\partial_3 v^h \rightharpoonup b$ in $L^2(\Omega, \mathbb{R}^3)$ for some vector valued function b, and that the limit y is independent of z_3 (exactly the same argument as in Step 2 for n independent of z_3). □

Step 4. There exists a sequence of matrix fields $\{G^h\}$ with $G^h : \omega \to \mathbb{R}^{3\times 3}$ such that

$$\int_\Omega |G^h - (\ell^f_{m^h})^{-1/2}(\nabla_h v^h)(\ell^0_{m^h_0})^{1/2}|^2 dz \le Ch^2, \qquad \int_\omega |\tilde{\nabla} G^h|^2 d\tilde{z} \le C \tag{4.181}$$

for C independent of h. Moreover, $G^h \rightharpoonup R$ in $W^{1,2}(\omega, \mathbb{R}^{3\times 3})$ with $R \in SO(3)$ a.e.

To obtain the estimates in (4.181), we first apply Proposition 4.6.5 to obtain each matrix field G^h, and then observe that the estimates follow from the bound on the energy (4.178) and the fact that by hypothesis $n_0 \in W^{1,2}(\omega, \mathbb{S}^2)$.

For the convergence, we note the first estimate in (4.181) implies

$$\int_\omega |G^h|^2 d\tilde{z} \le Ch^2 + 2c(r_f, r_0) \int_\Omega |\nabla_h v^h|^2 dz. \tag{4.182}$$

The constant $c(r_f, r_0)$ is from estimating the step-length tensors. From Step 3, $\nabla_h v^h$ is bounded uniformly in L^2, and therefore using the above estimate and the second estimate in (4.181), we conclude that up to a subsequence $G^h \rightharpoonup R$ in $W^{1,2}(\omega, \mathbb{R}^{3\times 3})$. Now, to deduce that $R \in SO(3)$ a.e., we estimate via two applications of the triangle inequality

$$\begin{aligned}
\int_\omega \operatorname{dist}^2(R, SO(3)) d\tilde{z} &\le 2 \int_\Omega \left(\operatorname{dist}^2(G^h, SO(3)) dz + |G_h - R|^2 \right) dz \\
&\le C \left(h^2 + \int_\Omega (\operatorname{dist}^2((\ell^f_{m^h})^{-1/2}(\nabla_h v^h)(\ell^0_{m^h_0})^{1/2}, SO(3)) + |G_h - R|^2) dz \right) \\
&\le C \left(h^2 + h^2 \mathcal{J}^{h,\varepsilon_h}_{m^h_0}(v^h, m^h) + \int_\omega |G_h - R|^2 d\tilde{z} \right).
\end{aligned} \tag{4.183}$$

In the second estimate, we also use the first estimate in (4.181). For the third estimate, we recall (4.177). Now, by Rellich's theorem, we have $G^h \to R$ in $L^2(\Omega, \mathbb{R}^{3\times 3})$ for a subsequence. Thus, it is clear given (4.178) that the upperbound above vanishes as $h \to 0$. This implies $R \in SO(3)$ a.e. as desired. □

Step 5. $(\ell^f_{m^h})^{-1/2}(\nabla_h v^h)(\ell^0_{m^h_0})^{1/2} \to R$ in $L^2(\Omega, \mathbb{R}^{3\times 3})$ for R from Step 4.

Since

$$\begin{aligned}
&\int_\Omega |(\ell^f_{m^h})^{-1/2}(\nabla_h v^h)(\ell^0_{m^h_0})^{1/2} - R|^2 dz \\
&\qquad \le 2 \int_\Omega \left(|G^h - R|^2 + |G^h - (\ell^f_{m^h})^{-1/2}(\nabla_h v^h)(\ell^0_{m^h_0})^{1/2}|^2 \right) dz,
\end{aligned} \tag{4.184}$$

we conclude that $(\ell^f_{m^h})^{-1/2}(\nabla_h v^h)(\ell^0_{m^h_0})^{1/2} \to R$ in $L^2(\Omega, \mathbb{R}^{3\times 3})$ using Step 4. □

Step 6. Actually, $R = (\ell^f_n)^{-1/2}(\tilde{\nabla} y|b)(\ell^0_{n_0})^{-1/2}$ a.e. for the limiting fields above. In particular, $(\ell^f_n)^{-1/2}(\tilde{\nabla} y|b)(\ell^0_{n_0})^{1/2} \in W^{1,2}(\omega, SO(3))$.

We observe that $\|(\ell^f_{m^h})^{-1/2}(\nabla_h v^h)\|_{L^2(\Omega)} \leq c(r_f)\|\nabla_h v^h\|_{L^2(\Omega)} \leq C$ by the compactness of the step-length tensor on $\mathbb{S}^2$ and following Step 3. So up to a subsequence $(\ell^f_{m^h})^{-1/2}(\nabla_h v^h)$ converges weakly in $L^2(\Omega, \mathbb{R}^{3\times 3})$. In addition, the results of Step 2 and 3 imply $(\ell^f_{m^h})^{-1/2}(\nabla_h v^h) \rightharpoonup (\ell^f_n)^{-1/2}(\tilde{\nabla} y|b)$ in $L^1(\Omega, \mathbb{R}^{3\times 3})$. Hence, in combination and by the uniqueness of the L^1 limit, we also have weak convergence to this limiting field in L^2 (rather than just L^1).

Given the weak-L^2 convergence just established and the convergence in Step 1, we deduce

$$(\ell^f_{m^h})^{-1/2}(\nabla_h v^h)(\ell^0_{m^h_0})^{1/2} \rightharpoonup (\ell^f_n)^{-1/2}(\tilde{\nabla} y|b)(\ell^0_{n_0})^{1/2} \quad \text{in } L^1(\Omega, \mathbb{R}^{3\times 3}). \tag{4.185}$$

By the convergence in Step 5 and the uniqueness of the weak-L^1 limit $R = (\ell^f_n)^{-1/2}(\tilde{\nabla} y|b)(\ell^0_{n_0})^{1/2}$ a.e. To complete the proof, we recall from Step 4 that $R \in W^{1,2}(\omega, \mathbb{R}^{3\times 3})$ and that $R \in SO(3)$ a.e. □

Step 7. The sequences in Step 3 actually converge strongly in their respective spaces. In addition, we have improved regularity: $y \in W^{2,2}(\omega, \mathbb{R}^3)$ and b is independent of z_3 and in $W^{1,2}(\omega, \mathbb{R}^3)$.

For the strong L^2 convergence, we have the estimate

$$\begin{aligned}
&\int_\Omega |\nabla_h v^h - (\tilde{\nabla} y|b)|^2 dz \\
&\leq 2\int_\Omega \left(|\nabla_h v^h - (\ell^f_{m^h})^{1/2} R (\ell^0_{m^h_0})^{-1/2}|^2 + |(\ell^f_{m^h})^{1/2} R (\ell^0_{m^h_0})^{-1/2} - (\tilde{\nabla} y|b)|^2 \right) dz \\
&\leq C\int_\Omega \Big(|(\ell^f_{m^h})^{-1/2}(\nabla_h v^h)(\ell^0_{m^h_0})^{-1/2} - R|^2 \\
&\qquad + |(\ell^f_{m^h})^{1/2} - (\ell^f_n)^{1/2}|^2 + |(\ell^0_{m^h_0})^{-1/2} - (\ell^0_{n_0})^{-1/2}|^2 \Big) dz
\end{aligned} \tag{4.186}$$

using that $R = (\ell^f_n)^{-1/2}(\tilde{\nabla} y|b)(\ell^0_{n_0})^{1/2}$ a.e. from Step 6, and that the step-length tensors are compact and invertible on $\mathbb{S}^2$. It's clear that the upper bound $\to 0$ as $h \to 0$ due to the strong-L^2 convergences of each term (established in the previous steps). Thus, $\nabla_h v^h \to (\tilde{\nabla} y|b)$ in $L^2(\Omega, \mathbb{R}^{3\times 3})$ as desired.

For the improved regularity, we see that

$$(\tilde{\nabla} y|b) = (\ell_n^f)^{1/2} R (\ell_{n_0}^0)^{-1/2} \quad \text{a.e. on } \omega. \tag{4.187}$$

Note that $R \in W^{1,2}$ from Step 4, $n \in W^{1,2}$ from Step 2, and $n_0 \in W^{1,2}$ by assumption. By the structure of the step-length tensors, we also have that $(\ell_{n_0}^0)^{-1/2}, (\ell_n^f)^{1/2} \in W^{1,2}$. Thus, the improved regularity is clear from differentiating the right side using the product rule for these Sobolev functions. Finally, b is independent of z_3 since $(\ell_n^f)^{1/2} R (\ell_{n_0}^0)^{-1/2} e_3$ is independent of z_3. □

Step 8. Actually,

$$\left\| m^h - \sigma \frac{(\nabla_h v^h) m_0^h}{|(\nabla_h v^h) m_0^h|} \right\|_{L^2(\Omega)} \to 0, \quad \textit{and} \quad n = \sigma \frac{(\tilde{\nabla} y|b) n_0}{|(\tilde{\nabla} y|b) n_0|} \textit{ a.e. on } \omega, \tag{4.188}$$

for σ a fixed constant from the set $\{1, -1\}$.

Since $m_0^h \in \mathbb{S}^2$ a.e. by definition and $\|(\tilde{\nabla} y|b) n\|_{L^\infty} \leq C(r_f, r_0)$ given Step 6,

$$\begin{aligned} &\int_\Omega |(I_{3\times 3} - m_0^h \otimes m_0^h)(\nabla_h v^h)^T m^h - (I_{3\times 3} - n_0 \otimes n_0)(\tilde{\nabla} y|b)^T n|^2 dz \\ &\quad \leq C(r_f, r_0) \int_\Omega \Big(|(\nabla_h v^h)^T m^h - (\tilde{\nabla} y|b)^T n|^2 \\ &\qquad\qquad + |m_0^h \otimes m_0^h - n_0 \otimes n_0|^2 \Big) dz. \end{aligned} \tag{4.189}$$

Given the convergences from the previous steps, we conclude $(\nabla_h v^h)^T m^h \to (\tilde{\nabla} y|b)^T n$ and $m_0^h \otimes m_0^h \to n_0 \otimes n_0$ both in $L^2(\Omega)$. Thus following the estimate above,

$$\begin{aligned} &(I_{3\times 3} - m_0^h \otimes m_0^h)(\nabla_h v^h)^T m^h \\ &\qquad \to (I_{3\times 3} - n_0 \otimes n_0)(\tilde{\nabla} y|b)^T n \quad \text{in } L^2(\Omega, \mathbb{R}^3). \end{aligned} \tag{4.190}$$

Notice also that

$$\int_\Omega \widehat{W}^{ni}(\nabla v^h, m^h, m_0^h) dz \leq h^2 \mathcal{J}_{m_0^h}^{h,\varepsilon_h}(v^h, m^h) \leq C h^2. \tag{4.191}$$

Consequently, $(I_{3\times 3} - m_0^h \otimes m_0^h)(\nabla_h v^h)^T m^h$ actually converges strongly to zero in L^2. Hence, by the uniqueness of the L^2 limit, and using the identity for $(\tilde{\nabla} y|b)$ in Step 6,

$$\begin{aligned} &r_f^{1/3} r_0^{1/6} (I_{3\times 3} - n_0 \otimes n_0) R^T n = \\ &\qquad (I_{3\times 3} - n_0 \otimes n_0)(\tilde{\nabla} y|b)^T n = 0 \quad \text{a.e. on } \omega \end{aligned} \tag{4.192}$$

for $R \in SO(3)$ a.e. defined from Step 6. Thus, it must be that $n = Rn_0$ or $n = -Rn_0$ a.e. on ω (note, the sign cannot flip since $R \in W^{1,2}$, $n_0 \in W^{1,2}$ and $n \in W^{1,2}$ from the previous steps). We denote this sign by σ as in the statement. Again using the identity for R in Step 6, we conclude the a.e. equality in (4.188). As a consequence, $m^h \to \sigma(\tilde{\nabla} y|b)n_0/|(\tilde{\nabla} y|b)n_0|$ in $L^2(\Omega, \mathbb{S}^2)$. Further, $(\nabla_h v^h)m_0^h/|(\nabla_h v^h)m_0^h| \to (\tilde{\nabla} y|b)n_0/|(\tilde{\nabla} y|b)n_0|$ in $L^2(\Omega, \mathbb{S}^2)$ (using, for instance, the incompressibility of $\nabla_h v^h$, the fact that $m_0^h \in \mathbb{S}^2$ a.e., the L^2/pointwise a.e. convergence of $(\nabla v^h)m_0^h$, and the Lebesgue dominated convergence theorem). The convergence in (4.188) follows since σ is 1 or -1. □

Step 9. Finally,

$$(\tilde{\nabla} y)^T \tilde{\nabla} y = \ell_{n_0} \text{ a.e. on } \omega. \tag{4.193}$$

From Step 6, $(\ell_n^f)^{-1/2}(\tilde{\nabla} y|b)(\ell_{n_0}^0)^{1/2} \in W^{1,2}(\omega, SO(3))$, and from Step 7, n as in (4.188). Hence,

$$\begin{aligned}\int_\omega W^e\Big((\tilde{\nabla} y|b), \frac{(\tilde{\nabla} y|b)n_0}{|(\tilde{\nabla} y|b)n_0|}, n_0\Big)d\tilde{z} &= \int_\omega W^e\Big((\tilde{\nabla} y|b), \sigma\frac{(\tilde{\nabla} y|b)n_0}{|(\tilde{\nabla} y|b)n_0|}, n_0\Big)d\tilde{z} \\ &= \int_\omega W_{nH}((\ell_n^f)^{-1/2}(\tilde{\nabla} y|b)(\ell_{n_0}^0)^{1/2})d\tilde{z} = 0\end{aligned} \tag{4.194}$$

using that σ from Step 8 is either 1 or -1, using the definitions of W^e and W_{nH}, and since W_{nH} vanishes on $SO(3)$. The conclusion (4.193) follows by Proposition A.1.7. □

Proof of Theorem 4.6.1. The proof follows by the collection of steps above. In particular, Step 7 shows the strong convergence of $\{v^h\}$ and the desired regularity of the limiting field y as a consequence of (4.178). Step 8 shows the convergence of the director $\{m^h\}$ as required. Step 9 shows that the metric constraint must also be satisfied. This is the proof. □

Proof of Lemma 4.6.4

First, we derive the key estimate which relates geometric rigidity [46] to the setting of nematic elastomers.

Proposition 4.6.6 *Let $\omega \subset \mathbb{R}^3$ bounded and Lipschitz. There exists a constant $C = C(r_0, r_f, \tau)$ with the following property: for all $h > 0$, $Q_{\tilde{x}^*,h} := (-h/2, h/2)^3 \subset \Omega_h$,*

$v^h \in W^{1,2}(\Omega_h, \mathbb{R}^3)$, $n^h \in W^{1,2}(\Omega_h, \mathbb{S}^2)$, and n_0^h as in (4.15) with $n_0 \in W^{1,2}(\omega, \mathbb{R}^3)$, there exists an associated constant rotation $R^h_{\tilde{x}^*} \in SO(3)$ such that

$$\begin{aligned}\int_{Q_{\tilde{x}^*,h}} &|(\ell^f_{n^h})^{-1/2}\nabla y^h(\ell^0_{n_0^h})^{1/2} - R^h_{\tilde{x}^*}|^2 dx \\ &\leq C\int_{Q_{\tilde{x}^*,h}} \Big(\operatorname{dist}^2((\ell^f_{n^h})^{-1/2}\nabla y^h(\ell^0_{n_0^h})^{1/2}, SO(3)) \\ &\qquad + h^2(|\nabla n^h|^2 + |\tilde{\nabla} n_0|^2 + 1)\Big) dx.\end{aligned} \tag{4.195}$$

Proof. Let $y^h \in W^{1,2}(\Omega_h, \mathbb{R}^3)$, $n^h \in W^{1,2}(\Omega_h, \mathbb{S}^2)$ and $n_0 \in W^{1,2}(\omega, \mathbb{S}^2)$ with n_0^h as in (4.15). we fix $\tilde{x}^*$ such that $Q_{\tilde{x}^*,h} \subset \Omega_h$ and set

$$A^f_h := \frac{1}{|Q_{\tilde{x}^*,h}|}\int_{Q_{\tilde{x}^*,h}} (\ell^f_{n^h})^{1/2} dx, \quad A^0_h := \frac{1}{|Q_{\tilde{x}^*,h}|}\int_{Q_{\tilde{x}^*,h}} (\ell^0_{n_0})^{-1/2} dx. \tag{4.196}$$

Because of the structure of the step-length tensors, these averages are positive definite, and each of the eigenvalues lives in a compact set of the positive real numbers depending only on r_f and r_0 (in particular, this set does not depend on h). Hence, these linear maps belong to a family of h-indepdent bi-Lipschtiz maps with controlled Lipschitz constant, and so we write $A^f \equiv A^f_h$ and $A^0 \equiv A^0_h$ in sequel.

Now, we set

$$v^h(s) = (A^f)^{-1} y^h((A^0)^{-1}s), \quad s \in (A^0)Q_{\tilde{x}^*,h}. \tag{4.197}$$

We observe that $v^h \in W^{1,2}((A^0)Q_{\tilde{x},h}, \mathbb{R}^3)$ by the regularity of y^h. Therefore by geometric rigidity [46], there exists a constant rotation $R^h_{\tilde{x}} \in SO(3)$ such that

$$\begin{aligned}\int_{Q_{\tilde{x}^*,h}} &|(A^f)^{-1}\nabla y^h(x)(A^0)^{-1} - R^h_{\tilde{x}^*}|^2 dx \\ &= |\det A^0|^{-1}\int_{(A^0)Q_{\tilde{x}^*,h}} |\nabla v^h(s) - R^h_{\tilde{x}^*}|^2 ds \\ &\leq |\det A^0|^{-1} C((A^0)Q_{\tilde{x}^*,h})\int_{(A^0_\omega)Q_{\tilde{x}^*,h}} \operatorname{dist}^2(\nabla v^h(s), SO(3)) ds \\ &= C((A^0)Q_{\tilde{x}^*,h})\int_{Q_{\tilde{x}^*,h}} \operatorname{dist}^2((A^f)^{-1}\nabla y^h(x)(A^0)^{-1}, SO(3)) dx.\end{aligned} \tag{4.198}$$

The constant $C((A^0)Q_{\tilde{x}^*,h})$ can be chosen uniformly for a family of domains which are bi-Lipschitz equivalent with controlled Lipschitz constant. Hence, actually we can choose $C(r_0, Q_{\tilde{x}^*,h}) \geq C((A^0)Q_{\tilde{x}^*,h})$. Moreover, the constant is invariant under

translation and dilatation. Hence, actually we have $C(r_0, Q_{\tilde{x}^*,h}) = C(r_0)$ for any $Q_{\tilde{x}^*,h} \subset \Omega_h$. These properties are given in Friesecke, James and Müller, Theorem 9 [45]. Since r_0 is fixed in this calculation, we write $C(r_0) \equiv C$, and thus

$$\begin{aligned}\int_{Q_{\tilde{x}^*,h}} |(A^f)^{-1}\nabla y^h(x)(A^0)^{-1} - R^h_{\tilde{x}^*}|^2 dx \\ \leq C \int_{Q_{\tilde{x}^*,h}} \mathrm{dist}^2((A^f)^{-1}\nabla y^h(x)(A^0)^{-1}, SO(3))dx\end{aligned} \tag{4.199}$$

from (4.198).

Since we will no longer be dealing with a change of variables in this proof, we now drop the explicit dependence on x inside the integrals. We observe by the key estimate (4.199) that

$$\begin{aligned}\int_{Q_{\tilde{x}^*,h}} |\nabla y^h - (A^f)R^h_{\tilde{x}^*}(A^0)|^2 dx &\leq C \int_{Q_{\tilde{x}^*,h}} |(A^f)^{-1}\nabla y^h(A^0)^{-1} - R^h_{\tilde{x}^*}|^2 dx \\ &\leq C \int_{Q_{\tilde{x}^*,h}} \mathrm{dist}^2((A^f)^{-1}\nabla y^h(A^0)^{-1}, SO(3))dx \\ &\leq C \int_{Q_{\tilde{x}^*,h}} \mathrm{dist}^2(\nabla y^h, (A^f)SO(3)(A^0))dx \\ &\leq C \int_{Q_{\tilde{x}^*,h}} \Big(\mathrm{dist}^2(\nabla y^h, (\ell^f_{n^h})^{1/2} SO(3)(\ell^0_{n^h_0})^{-1/2}) \\ &\qquad + |(\ell^f_{n^h})^{1/2} - A^f|^2 + |(\ell^0_{n^h_0})^{-1/2} - A^0|^2 \Big) dx \\ &\leq C \int_{Q_{\tilde{x}^*,h}} \Big(\mathrm{dist}^2((\ell^f_{n^h})^{-1/2}\nabla y^h(\ell^0_{n^h_0})^{1/2}, SO(3)) + h^2|\nabla n^h|^2 \\ &\qquad + |(\ell^0_{n_0})^{-1/2} - A^0|^2 + |(\ell^0_{n^h_0})^{-1/2} - (\ell^0_{n_0})^{-1/2}|^2 \Big) dx \\ &\leq C \int_{Q_{\tilde{x}^*,h}} \Big(\mathrm{dist}^2((\ell^f_{n^h})^{-1/2}\nabla y^h(\ell^0_{n^h_0})^{1/2}, SO(3)) \\ &\qquad + h^2(|\nabla n^h|^2 + |\tilde{\nabla} n_0|^2 + 1) \Big) dx.\end{aligned} \tag{4.200}$$

Here, the constant $C = C(r_0, r_f, \tau)$ is due to several applications of the triangle inequality and the fact that the norm of the step-length tensors, inverses and averages are compact and this depends only on r_f,r_0. We have also applied the standard Poincaré inequality given the averages (4.196), and used that the diameter of $Q_{\tilde{x}^*,h}$ is h and that the gradients of the step-length tensors are controlled by the gradients of the directors. Finally, from the assumed control of non-idealities for n^h_0 in (4.15), we

have the estimate $\|(\ell^0_{n^h_0})^{-1/2} - (\ell^0_{n_0})^{-1/2}\|_{L^\infty} \leq c(r_0)\tau h$. This gives the dependence on τ in the constant.

Now using (4.200), we find that

$$\begin{aligned}
&\int_{Q_{\bar{x}^*,h}} |(\ell^f_{n^h})^{-1/2}\nabla y^h (\ell^0_{n^h_0})^{1/2} - R^h_{\tilde{x}^*}|^2 dx \\
&\quad \leq C \int_{Q_{\bar{x}^*,h}} |\nabla y^h - (\ell^f_{n^h})^{1/2} R^h_{\tilde{x}^*} (\ell^0_{n^h_0})^{-1/2}|^2 dx \\
&\quad \leq C \int_{Q_{\bar{x}^*,h}} \Big(|\nabla y^h - (\ell^f_{n^h})^{1/2} R^h_{\tilde{x}^*} (\ell^0_{n_0})^{-1/2}|^2 \\
&\qquad\qquad + |(\ell^0_{n^h_0})^{-1/2} - (\ell^0_{n_0})^{-1/2}|^2 \Big) dx \\
&\quad \leq C \int_{Q_{\bar{x}^*,h}} \Big(|\nabla y^h - (A^f) R^h_{\tilde{x}^*} (A^0)|^2 \\
&\qquad\qquad + h^2 + |(\ell^f_{n^h})^{1/2} - A^f|^2 + |(\ell^0_{n_0})^{-1/2} - A^0|^2 \Big) dx \\
&\quad \leq C \int_{Q_{\bar{x}^*,h}} \Big(\mathrm{dist}^2((\ell^f_{n^h})^{-1/2}\nabla y^h (\ell^0_{n_0})^{1/2}, SO(3)) \\
&\qquad\qquad + h^2(|\nabla n^h|^2 + |\tilde{\nabla} n_0|^2 + 1) \Big) dx
\end{aligned} \tag{4.201}$$

as desired. □

Now we note that the approximations in Lemma 4.6.4 are not new. They essentially follow from the same argument as that of Theorem 10 in Friesecke et al. [45], modified appropriately for nematic elastomers using the estimate in Proposition 4.6.6. In the general context of non-Euclidean plates, there is a recent body of literature on such estimates (e.g., Lewicka and Pakzad (Lemma 4.1) [63] and Lewicka et al. (Theorem 1.6) [62], (Lemma 2.3) [16]). Thus briefly:

Proof of Lemma 4.6.4 We repeat steps 1-3 in the proof of Theorem 10 in [45] with some modification due to our nematic elastomer setting. The lemma follows by the estimate in Proposition 4.6.6. □

4.7 Applications

Nonisometric Origami: Compatibility and examples

The actuation of complex origami shapes stems from satisfying the nonisometric condition in Definition 4.3.1, hence the term *nonisometric origami*. In particular, the compatibility of interfaces separating regions of distinct constant director (Figure

(a) A single interface

(b) Three-faced junction

Figure 4.10: Schematic of interfaces and junctions in nonisometric origami

4.10(a)) combined with the compatibility of junctions where these interfaces merge at a single point (Figure 4.10(b)) play the key role in actuation. To address this with mathematical precision, we note that the nonisometric condition in Definition 4.3.1(ii) is equivalent to

$$\tilde{F}_\alpha = R_\alpha(\ell^{1/2}_{n_{0\alpha}})_{3\times 2} \quad \text{for some } R_\alpha \in SO(3)\,, \quad \alpha \in \{1,\dots,N\}, \tag{4.202}$$

where $(\ell^{1/2}_{n_{0\alpha}})_{3\times 2} = r^{-1/6}(I_{3\times 2} + (r^{1/2}-1)n_{0\alpha}\otimes\tilde{n}_{0\alpha})$ for the projection $\tilde{n}_{0\alpha} \in B_1(0) \subset \mathbb{R}^2$ (see Proposition A.1.10). Thus for compatibility, the deformation y in (4.20) must be continuous across each interface separating regions of distinct constant director. This occurs if and only if

$$R_\alpha(\ell^{1/2}_{n_{0\alpha}})_{3\times 2}\tilde{t}_{\alpha\beta} = R_\beta(\ell^{1/2}_{n_{0\beta}})_{3\times 2}\tilde{t}_{\alpha\beta} \tag{4.203}$$

for every interface tangent $\tilde{t}_{\alpha\beta} \in \mathbb{S}^1$. Explicitly, $\tilde{t}_{\alpha\beta}$ represents the tangent vector to the interface separating regions ω_α with director $n_{0\alpha}$ and ω_β with director $n_{0\beta}$ as depicted in Figure 4.10. This condition is akin to the rank-one condition studied in the context of fine-scale twinning during the austenite martensite phase transition and actuation active martensitic sheets [4, 13, 14]. More recently, this compatibility has been appreciated as a means of actuation for nematic elastomer and glass sheets [68, 69] using planar programming of the director. Here though, (4.203) describes the most general case of compatibility in thin nematic sheets as $n_{0\alpha}, n_{0\beta} \in \mathbb{S}^2$ need not be planar.

While (4.203) encodes a complete description of nonisometric origami as defined by Definition 4.3.1, more useful criterion are gleaned from examining necessary and sufficient conditions associated with this constraint. In particular, taking the norm of both sides of (4.203) yields, after some manipulation, a necessary condition for nonisometric origami,

$$|\tilde{n}_{0\alpha}\cdot\tilde{t}_{\alpha\beta}| = |\tilde{n}_{0\beta}\cdot\tilde{t}_{\alpha\beta}| \tag{4.204}$$

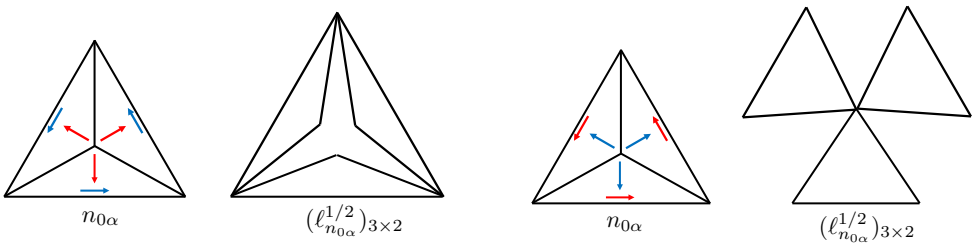

(a) Incompatible Junction (b) Compatible Junction

Figure 4.11: Two junctions with director programs satisfying (4.204). Blue represents the design for cooling and red represents the design for heating. The stretch part of the deformation upon thermal actuation is plotted.

for every interface tangent $\tilde{t}_{\alpha\beta}$ (when $\bar{r} \neq 1$). We emphasize again that $\tilde{n}_{0\alpha} \in B_1(0) \subset \mathbb{R}^2$ is the projection of $n_{0\alpha}$ onto the tangent plane of ω. That this need not be a unit vector is a direct consequence of allowing for non-planar programming.

A director program satisfying (4.204) is not, however, sufficient to ensure the existence of a continuous piecewise affine deformation y as in Definition 4.3.1(ii). To illustrate this point, consider the design in Figure 4.11(a). Here, we have a junction with three sectors of equal angle $2\pi/3$, and the director is programmed to bisect the sector angle (respectively, perpendicular to the bisector) on heating (respectively, cooling). This program satisfies the necessary condition (4.204). However in this case, due to the stretching part of the deformation upon actuation, the base of each triangle expands while the height contracts. Thus, it is clear geometrically that no series of rotations and/or translations of the three deformed triangles can bring about a continuous piecewise affine deformation of the entire junction. Conversely, if thermal actuation is reversed, as illustrated in Figure 4.11(b) with the color change of the director program, then the base of each triangle contracts and the height expands. In this case, a continuous piecewise affine deformation is realized by rotating each of the deformed triangles out-of-plane to form a 3-sided pyramid.

Figure 4.11(b), by way of example, also highlights a simple scheme to form a compatible pyramidal junction. Indeed, if a junction has $K \geq 3$ sectors of equal angle $2\pi/K$ as in Figure 4.12, then programming the director to bisect this angle upon cooling (respectively, perpendicular to the bisector on heating) alway leads to a compatible K-sided pyramid. There are, of course, an infinite number of these types of junction, as emphasized with the designs in the right part of Figure 4.12. Most importantly though, these junctions can be used as unit cells to actuate more complex structures from nematic sheets. This is shown in Figures 4.2 and 4.3. Each

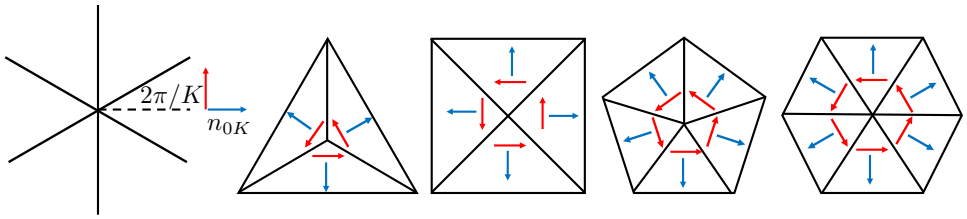

Figure 4.12: Simple scheme for compatible junction.

design incorporates a unit cell in Figure 4.12 as the building block.

The examples highlighted illustrate that for even the simplest of building blocks, there is a richness of shape-changing deformations of nematic elastomer sheets described by nonisometric origami. It should be noted, however, that these structures are in general degenerate. This is shown in Figure 4.13 where we design a program to actuate a rhombic dodecahedron upon cooling. Here though, we have done nothing to break the reflection symmetry associated with the building block. Thus, each interior junction is free to actuate either up or down. Therefore, in addition to possibly actuating the rhombic dodecahedron, the actuation of four alternative surfaces is a completely equivalent outcome given this framework. Such degeneracy was observed actuating conical defects by Ware et al. [102], where it was shown that each defect could actuate either up or down. However, it may be possible to suppress these degeneracies by introducing a slight bias in the through-thickness director orientation via twisted nematic prescription. This was seen, for instance, in Fuchi et al. [47] (see also Gimenez-Pinto et al. [50]), where actuation of a box-like structure was achieved through folds biased in the appropriate direction using such a prescription. Thus, biasing would appear a promising means of breaking the reflection symmetry. Nevertheless, we did not address this here as it is difficult to analyze to the level of rigor intended for this work.

As a final comment on the design landscape for these constructions, recall that the relations associated with (4.203) provide a complete, but not particularly transparent, description of nonisometric origami. Further, the more useful condition (4.204) is only necessary as we provided a counterexample to sufficiency in Figure 4.11(a). In fact, to our knowledge, a complete characterization of the geometry of configurations satisfying (4.203) remains open. Nevertheless, we do expect an immense richness to such a characterization. To highlight this, we work out a characterization of compatible three-faced junctions in Appendix A.3.

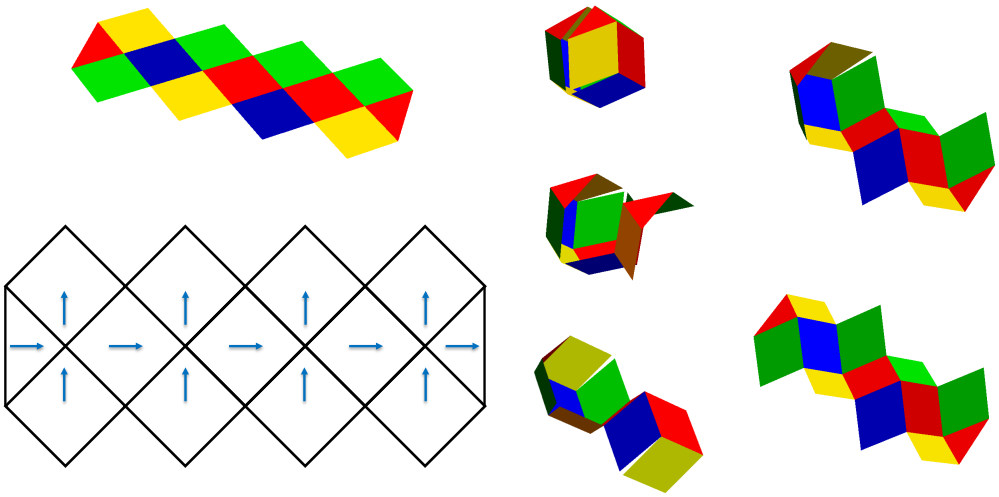

Figure 4.13: Program to actuate a rhombic dodecahedron upon cooling. Due to reflection symmetry, four other shapes are possible

Lifted surfaces, and a recipe for design

The idea for lifted surfaces (i.e., the ansatz (4.101), (4.102) and (4.103)) is based on an equivalent rewriting of the metric constraint $(\tilde{\nabla} y)^T \tilde{\nabla} y = \tilde{\ell}_{n_0}$. (This equivalent form also yields a concrete design scheme for the actuation of nematic elastomer sheets in general.) Essentially, we take the picture of y being a solution to $(\tilde{\nabla} y)^T \tilde{\nabla} y = \tilde{\ell}_{n_0}$ defined by a predetermined n_0 and turn it on its head. That is, we first identify the set of deformation gradients that are consistent with (4.17) for any director field and then we identify the director associated with that deformation gradient.

Theorem 4.7.1 *Let $\bar{r} > 1$. The metric constraint (4.17) holds if and only if*

$$\tilde{\nabla} y(\tilde{x}) = (\partial_1 y | \partial_2 y)(\tilde{x}) \in \mathcal{D}_{\bar{r}}, \quad n_0(\tilde{x}) \in \mathcal{N}^{r}_{\tilde{\nabla} y(\tilde{x})} \quad \text{a.e. } \tilde{x} \in \omega. \tag{4.205}$$

Here, $\mathcal{D}_{\bar{r}}$ and $\mathcal{N}^{\bar{r}}_{\tilde{F}}$ are defined in (4.8) and (4.9) respectively. (For $\bar{r} < 1$, the inequalities in (4.8) and the sign in (4.9) are reversed, i.e., $sign(\tilde{F}\tilde{e}_1 \cdot \tilde{F}\tilde{e}_2) \mapsto -sign(\tilde{F}\tilde{e}_1 \cdot \tilde{F}\tilde{e}_2)$.)

In addition, if $y : \omega \to \mathbb{R}^3$ such that $\tilde{\nabla} y(\tilde{x}) \in \mathcal{D}_{\bar{r}}$ a.e., then there exists an $n : \omega \to \mathbb{S}^2$ such that $n(\tilde{x}) \in \mathcal{N}^{\bar{r}}_{\tilde{\nabla} y(\tilde{x})}$ a.e.

We prove this equivalence below. Regarding the last point of the theorem (i.e., if $y : \omega \to \mathbb{R}^3$ such that $\tilde{\nabla} y(\tilde{x}) \in \mathcal{D}_{\bar{r}} \ldots$), we note that this means that for characterizing the geometry of surfaces which satisfy the metric constraint (4.17), we need only to consider the set of deformation gradients from a flat sheet ω which satisfy

$\tilde{\nabla} y(\tilde{x}) \in \mathcal{D}_{\bar{r}}$ a.e. $\tilde{x} \in \omega$. Unfortunately, such a broad characterization remains open. Of particular difficulty is the fact that this condition on the deformation gradient implies the equality

$$(\partial_1 y \cdot \partial_2 y)^2 = (|\partial_1 y|^2 - \bar{r}^{-1/3})(|\partial_2 y|^2 - \bar{r}^{-1/3}), \quad \text{a.e. on } \omega. \tag{4.206}$$

Lifted surfaces constitute a broad class of deformations such that this constraint holds trivially.

Regarding applications, the lifted surfaces ansatz allows for actuation of a large variety of shapes, since the limitations imposed by (4.102) are not very restrictive. Since r can be significantly different from 1 in nematic elastomers, one can form shapes with significant displacement like spherical caps and sinusoidally rough surfaces. Figure 4.4 shows two additional examples with complex surface relief. These are but a small sample of the designs amenable to this framework. Indeed, given any arbitrary greyscale image $\mathcal{G}$, we can program a nematic sheet so that the surface of the sheet upon cooling corresponds to this image. We do this by smearing $\mathcal{G}$ (for instance by mollification or by averaging over a small square twice) and taking this as φ.

Nevertheless, the key ingredient to the design of lifted surfaces is the ability to program the director three dimensionally. To our knowledge, experimental studies on nematic elastomer sheets such as Ware et al. [102] have examined planar inscription of the director only. We hope that promising designs such as lifted surfaces will inspire future experimentation to realize three dimensional programming. In any case, the theory and design scheme are easily adapted to the planar case. Specifically in the case of a *planar program*, the metric constraint (4.17) reduces to the metric underlying Aharoni et al. [2], and the spaces described above in the theorem reduce to

$$\begin{aligned}
\mathcal{D}_{\bar{r}>1} \equiv \tilde{\mathcal{D}}_{\bar{r}>1} &:= \Big\{ \tilde{F} \in \mathbb{R}^{3\times 2} \colon |\tilde{F}|^2 = \bar{r}^{2/3} + \bar{r}^{-1/3}, \\
&\qquad \bar{r}^{-1/3} \le |\tilde{F}\tilde{e}_1|^2 \le \bar{r}^{2/3}, \ \ \det((\tilde{F})^T \tilde{F}) = r^{1/3} \Big\}, \\
\mathcal{N}_{\tilde{F}}^{\bar{r}>1} \equiv \tilde{\mathcal{N}}_{\tilde{F}}^{\bar{r}>1} &:= \Big\{ \tilde{n}_0 \in \mathbb{S}^1 \colon (\tilde{n}_0 \cdot \tilde{e}_1)^2 = \frac{|\tilde{F}\tilde{e}_1|^2 - \bar{r}^{1/3}}{\bar{r}^{2/3} - \bar{r}^{-1/3}}, \\
&\qquad \operatorname{sign}((\tilde{n}_0 \cdot \tilde{e}_1)(\tilde{n}_0 \cdot \tilde{e}_2)) = \operatorname{sign}(\tilde{F}\tilde{e}_1 \cdot \tilde{F}\tilde{e}_2) \Big\},
\end{aligned} \tag{4.207}$$

where again the inequalities above and the sign in $\tilde{\mathcal{N}}_{\tilde{F}}^{\bar{r}}$ are reversed for $\bar{r} < 1$ (as in the theorem).

The proof of this theorem is simply an exercise in linear algebra:

Proof of Theorem 4.7.1. Let $\tilde{F} \in \mathbb{R}^{3\times 2}$ and $n_0 \in \mathbb{S}^2$ satisfy $\tilde{F}^T\tilde{F} = \tilde{\ell}_{n_0}$. Equivalently,

$$\begin{pmatrix} |\tilde{F}\tilde{e}_1|^2 & (\tilde{F}\tilde{e}_1 \cdot \tilde{F}\tilde{e}_2) \\ (\tilde{F}\tilde{e}_1 \cdot \tilde{F}\tilde{e}_2) & |\tilde{F}\tilde{e}_2|^2 \end{pmatrix} = \\ \bar{r}^{-1/3}\begin{pmatrix} 1 + (\bar{r}-1)(n_0 \cdot e_1)^2 & (\bar{r}-1)(n \cdot e_1)(m \cdot e_2) \\ (\bar{r}-1)(m \cdot e_1)(n_0 \cdot e_2) & 1 + (\bar{r}-1)(n_0 \cdot e_2)^2 \end{pmatrix} \tag{4.208}$$

for $\{\tilde{e}_1, \tilde{e}_2\}$ and $\{e_1, e_2, e_3\}$ the standard basis on $\mathbb{R}^2$ and $\mathbb{R}^3$ respectively. Now, since $n_0 \in \mathbb{S}^2$, $(n_0 \cdot e_\alpha)^2 \in [0, 1]$ and

$$\begin{aligned} |\tilde{F}\tilde{e}_\alpha|^2 \in [\bar{r}^{-1/3}, \bar{r}^{2/3}] \quad \text{if} \quad \bar{r} > 1, \\ \in [\bar{r}^{2/3}, \bar{r}^{-1/3}] \quad \text{if} \quad \bar{r} < 1, \end{aligned} \tag{4.209}$$

from (4.208) for $\alpha = 1, 2$. In addition, $(n_0 \cdot e_1)^2 + (n_0 \cdot e_2)^2 \leq 1$, and so

$$\begin{aligned} |\tilde{F}|^2 = |\tilde{F}\tilde{e}_1|^2 + |\tilde{F}\tilde{e}_2|^2 \leq r^{2/3} + r^{-1/3} \quad \text{if} \quad \bar{r} > 1, \\ \geq \bar{r}^{2/3} + \bar{r}^{-1/3} \quad \text{if} \quad \bar{r} < 1, \end{aligned} \tag{4.210}$$

also from (4.208). Now note that substituting the diagonal terms into the square of the off diagonal term in (4.208) results in

$$(\tilde{F}\tilde{e}_1 \cdot \tilde{F}\tilde{e}_2)^2 = (|\tilde{F}\tilde{e}_1|^2 - \bar{r}^{-1/3})(|\tilde{F}\tilde{e}_2|^2 - \bar{r}^{-1/3}). \tag{4.211}$$

Combining (4.209), (4.210) and (4.211), we conclude $\tilde{F} \in \mathcal{D}_{\bar{r}}$ as desired. To prove $n_0 \in \mathcal{N}_{\tilde{F}}^{\bar{r}}$, note that since $\bar{r} \neq 1$, rearranging the diagonal terms in (4.208) gives

$$(n_0 \cdot e_\alpha)^2 = \frac{|\tilde{F}\tilde{e}_\alpha|^2 - \bar{r}^{-1/3}}{\bar{r}^{2/3} - \bar{r}^{-1/3}}, \quad \alpha = 1, 2. \tag{4.212}$$

Further, since $\bar{r} > 0$ and $\neq 1$, taking the sign of the off diagonal term in (4.208) gives

$$\operatorname{sign}((n_0 \cdot e_1)(n_0 \cdot e_2)) = \operatorname{sign}(\bar{r} - 1)\operatorname{sign}(\tilde{F}\tilde{e}_1 \cdot \tilde{F}\tilde{e}_2). \tag{4.213}$$

Since $n_0 \in \mathbb{S}^2$, combining (4.212) and (4.213) yields $n_0 \in \mathcal{N}_{\tilde{F}}^{\bar{r}}$.

Now, let $\tilde{F} \in \mathcal{D}_{\bar{r}}$ and $n_0 \in \mathcal{N}_{\tilde{F}}^{\bar{r}}$. To prove $\tilde{F}^T\tilde{F} = \tilde{\ell}_{n_0}$, we need to show (4.208). By hypothesis, we have (4.212). By rearranging this formula, we obtain the diagonal terms in (4.208). For the off diagonal term, we note that in addition to (4.212), we have (4.211) by hypothesis. Combining these relations, we find

$$(\tilde{F}\tilde{e}_1 \cdot \tilde{F}\tilde{e}_2)^2 = (\bar{r}^{2/3} - \bar{r}^{-1/3})^2(n_0 \cdot e_1)^2(n_0 \cdot e_2)^2. \tag{4.214}$$

Taking the square root, we have the off diagonal term up to the sign. The correct choice of sign is guaranteed since n_0 and $\tilde{F}$ satisfy (4.213), again by hypothesis.

Finally, we let $\tilde{F} \in \mathcal{D}_{\bar{r}}$, and show $\mathcal{N}_{\tilde{F}}^{\bar{r}}$ is non-empty. Indeed by definition, $\tilde{F}$ satisfies (4.209) and (4.210). Thus, the right side of (4.212) is non-negative. From this, we may find an $n_0 \in \mathbb{R}^3$ satisfying (4.212) and (4.213). Further by (4.210), $(n_0 \cdot e_1)^2 + (n_0 \cdot e_2)^2 \leq 1$. Thus, we can choose $(n_0 \cdot e_3)$ such that $n_0 \in \mathbb{S}^2$. It follows that $\mathcal{N}_{\tilde{F}}^{\bar{r}}$ is non-empty.

For functions, $\tilde{\nabla} y(\tilde{x}) \equiv \tilde{F}$ and $n_0(\tilde{x}) \equiv n_0$, and so all these results should hold pointwise a.e. □

Chapter 5

SUMMARY AND OUTLOOK

5.1 Summary

A summary: On the mechanical response and instabilities in thin sheets

Nematic elastomers are composed of rigid rod-like liquid crystal molecules pendent to a soft polymer network. The liquid crystals tend to align at low temperature, with the average alignment at each point in a continuum sample described by a unit vector n called the director field. These elastomers deform anisotropically due to this alignment; essentially, the soft polymer network wants to stretch along and contract transverse to this director field. At the same time, the director field wants to reorient to align with the maximum stretch of the deformation. This interplay gives rise to a nematic-elastic coupling captured by the free energy density of nematic elastomers. With this coupling, a thin mono-domain nematic elastomer, which is clamped and stretched transverse to the initial alignment of the director field, forms fine-scale stripe domains of oscillating nematic director (i.e., "microstructure") to accommodate deformation. This is shown in Figure 5.1(a) where the clear regions describe uniform director alignment as indicated and the cloudy regions, which emerge under stretch, are the result of fine-scale microstructure (depicted to the left). Interestingly, this thin clamped stretched nematic elastomer sheet does not wrinkle, even though wrinkling is pervasive in thin sheets of normal elastomer under this boundary condition.

All this begs the question: does material microstructure suppress wrinkling in these sheets? To understand this, we derived theories for thin nematic elastomer sheets which capture both the wrinkling and microstructure instabilities and their possible competition in mechanical equilibrium, and we explored these theories analytically and numerically.

Starting from the three dimensional variational model incorporating the free energy of nematic elastomers, we rigorously derived the effective theory of a membrane as the Γ-limit of a suitably normalized functional as the thickness is taken to zero. This theory captures the energy and stress of both instabilities through effective planar deformation. We proved it is completely characterized by four regimes which depend only on the maximum planar stretch λ_M and areal stretch δ in Figure 3.2: $\mathcal{L}$ where

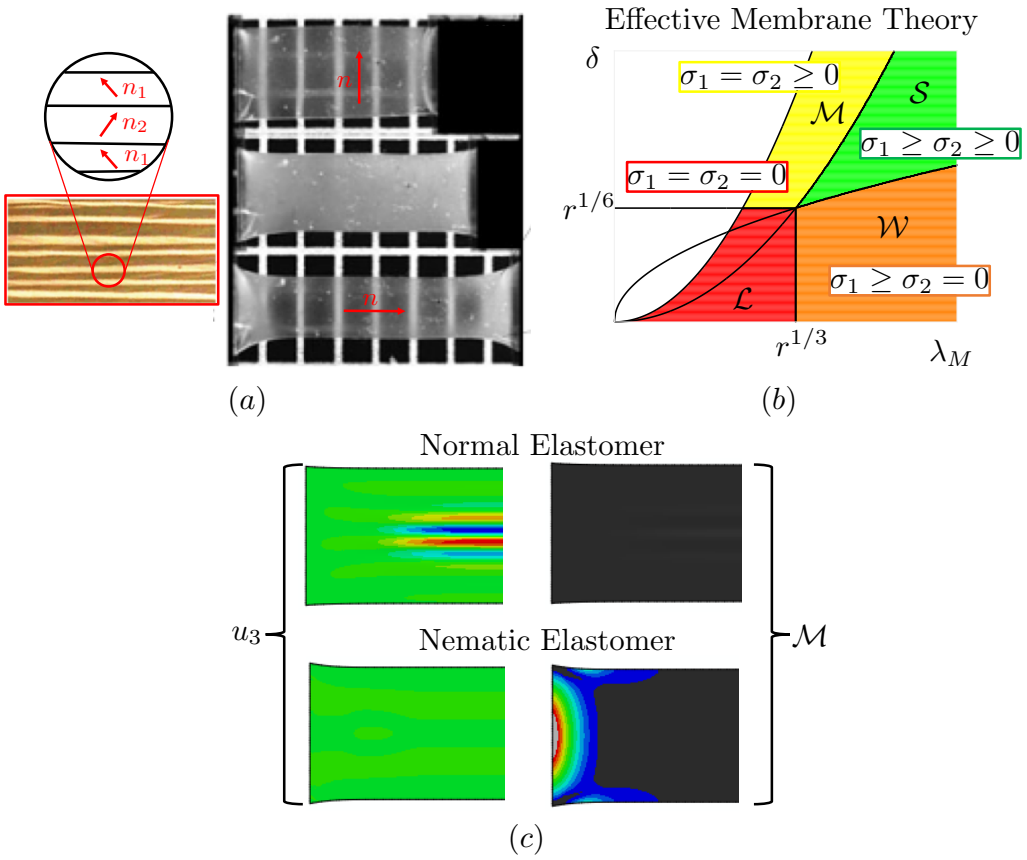

Figure 5.1: (a). Clamped stretched experiments of Kundler and Finkelmann [58] on nematic elastomer membrane show the formation of material microstructure, i.e., the cloudy regions in the sheet. (b). A membrane theory to account for both microstructure and wrinkling in nematic elastomer membranes. (c) Simulations show a normal elastomer sheet wrinkles, but a nematic elastomer sheet forms microstructure at the clamps (just as in the experiment) and this suppresses wrinkling.

both wrinkling and microstructure reduce the effective membrane energy and stress to zero, $\mathcal{W}$ where wrinkling leads to uniaxial tension, $\mathcal{M}$ where microstructure leads to equi-biaxial tension, and $\mathcal{S}$ with no fine scale features and biaxial tension. Importantly, a nematic membrane can form microstructure, and thus relax shear stresses that would otherwise be pervasive in membranes of normal elastomer. This has dramatic implications for the deformation states achieved at equilibrium.

To study this numerically, we derived a Koiter theory which captures microstructure through effective deformation, as in the effective membrane theory, and captures the geometry of wrinkles (i.e., amplitude and frequency of wrinkles) through a bending term systematically obtained from the free energy of nematic elastomers. In simulating the clamped stretched deformation under this theory, we found that

nematic membranes suppress wrinkling precisely due to the microstructure present at the clamps. This is highlighted in Figure 5.1(c). We observed large amplitude wrinkles in a sheet of normal elastomer, but the analogous simulation for a nematic elastomer sheet yielded microstructure at the clamps and no wrinkling (just as in the experiment 5.1(a)).

A summary: On actuation of heterogeneously patterned thin sheets

Nematic elastomers deform spontaneously by thermal actuation due to the temperature-dependent orientational order of liquid crystals: they align at low temperatures, this alignment is suppressed by thermal fluctuations at high temperatures, and the transition between these states is accompanied by distortion of the surrounding polymer network. This property can be exploited in the design of heterogeneously patterned thin sheets that deform into a non-trivial shape when heated or cooled. Given this capability, we set out to develop the general theoretical framework for designable actuation in these sheets as well as classify examples amenable to this framework.

Starting from a variational formulation for the elastic energy of nematic elastomer, we derived from it an effective two-dimensional metric constraint, which links the deformation and the heterogeneous director field. We showed that satisfying the metric constraint is both necessary and sufficient for the director profile and corresponding deformation to approximately minimize the energy. Consequently, these metric-restricted configurations are good candidates for designable actuation.

Importantly, we relaxed two assumptions common to the metric description of non-Euclidean plate theories, and in doing so, I arrived at two novel and broad classes of designable actuation in these sheets: First, we showed that smoothness is not a requirement in this framework, and thus nonisometric origami—where heterogeneity is programmed in a piecewise constant pattern so that thermal actuation leads to complex folding patterns—is a class of designable actuation. Second, we showed that the metric constraint is amenable to three dimensional programming, and thus lifted surfaces—where heterogeneity is programmed so that thermal actuation leads to a prescribed surface of arbitrary complexity as long as it is smooth and has limited slope—is also a class of desigable actuation. Figure 5.2 highlights selected examples of nonisometric origami and lifted surfaces, as well as an experimental realization of simple nonisometric origami junctions.

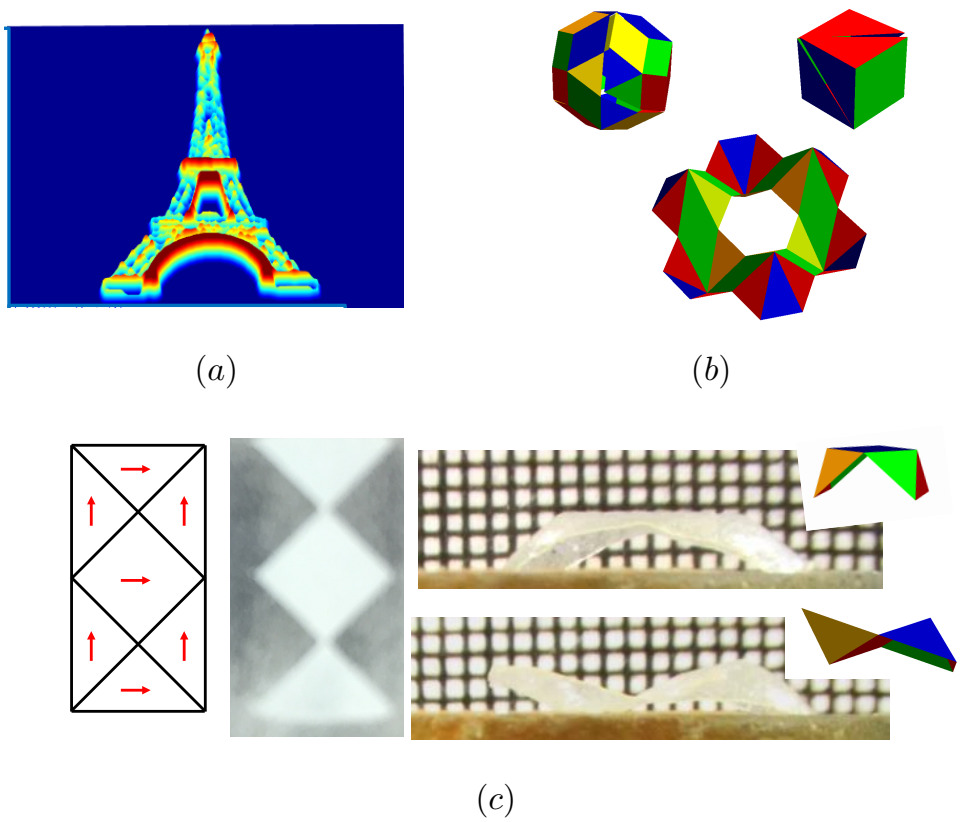

(a) (b) (c)

Figure 5.2: Examples of designable actuation in nematic elastomers. (a) The Eiffel tower can lift from a flat sheet. (b) Nonisometric origami to actuate a box, rhombic triacontahedron and many periodic type designs. (c) Experimental collaboration with Tim White's group at AFRL to realize nonisometric origami junctions. Both the experiment and prediction are shown.

5.2 Outlook

Wrinkling-suppressing membranes

Membrane structures—often with thickness of the order of micrometers and lateral dimension of the order of meters—are increasingly being exploited in space applications due to their high surface to volume ratio, light weight, and easy deployability. However, membranes offer little resistance to out-of-plane deformation and wrinkle under the typical (non-ideal) boundary conditions required to pull membranes taut (see Figure 5.3). This is undesirable. For instance, the effectiveness of solar sails, which exploit large surface area to capture radiation pressure for propulsion, is diminished—by as much as 5 to 15%—by wrinkling. This has motivated a number of structural mechanisms to suppress wrinkling such as catenaries and shear compliant borders. Nevertheless, wrinkling continues to be a challenge in the design of these

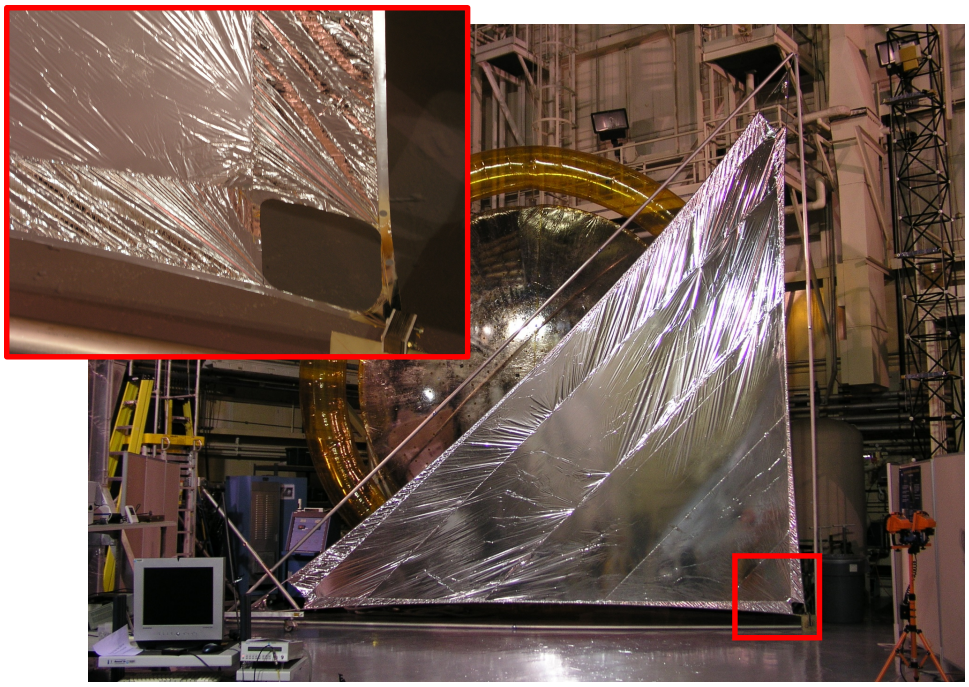

Figure 5.3: Full-scale solar sail with a shear compliant border designed and developed at NASA Langley Research Center. Despite the shear compliant border, wrinkling is still pervasive in this membrane.

systems.

In Chapter 3, we showed that taut and appreciably stressed sheets of nematic elastomer could suppress wrinkling by modifying the state of stress at the clamps through the formation of microstructure. Precisely, we showed that thin sheets of this material can deform in shear without shear stress for a certain range of deformations. Further, we showed that the reason for this is that the director is free to rotate through the material and form stripe domains of material microstructure. It is this capability and the relaxations of shear stress that emerges from this capability that is enabling wrinkle suppression.

Now, the surface area of membrane structures for space applications is large (at the scale of meters), whereas nematic elastomers currently can only be synthesized in small quantities (at the scale of centimeters). Thus, these systems are not directly applicable. Importantly though, we learned that if a material is capable of relaxing shear stress, then it is capable of suppressing wrinkling. Further, we know exactly the types of microstructures that enable such relaxation. Hence building on this theory, can we *engineer* larger-scale membrane structures which mimic the behavior of nematic elastomer?

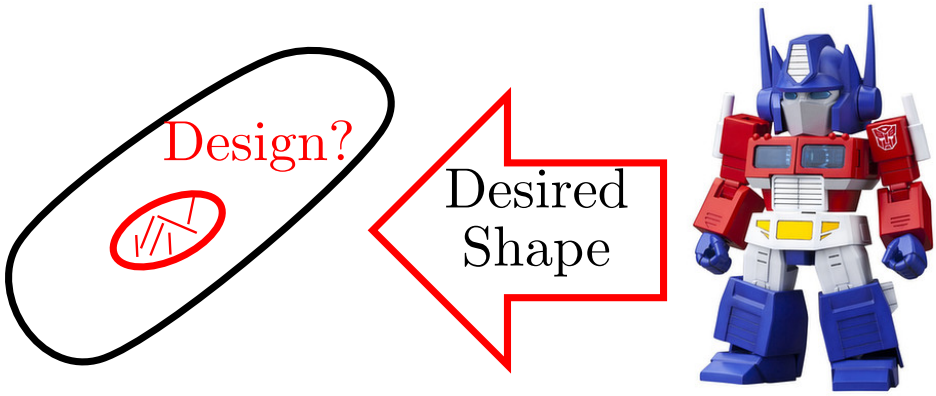

Figure 5.4: We have searched for designs which satisfy the metric constraint, and seen that these can give rise to complex shapes. However, a designer will want a desired shape. Therefore, to close the loop, the shape should be the input, and the design which satisfies the metric constraint to attain this shape should be the output (i.e., we need to solve an inverse problem).

Shapes by design with active sheets.

For soft actuators, medical devices and robotics to emerge as a disruptive technology, they need to be capable of a diverse array of shapes. Hence, can we make *the material the machine* [15]?

With nematic elastomers, we showed in Chapter 4 that thermal actuation of a sheet is governed by a metric constraint. Further, as the experiment in Figure 5.2(c) highlights, we can actuate complex shapes in nematic elastomer sheets under this metric constraint. However, an important inverse problem remains: if one desires a particular non-trivial three dimensional shape (say "Optimus Prime" in Figure 5.4), can one pattern an initially flat sheet to obtain the shape upon actuation? If we can understand this, then we can close the loop between theory, design and experimentally realization; thus, hopefully bridging the gap between the theory on actuation and the promise of technological innovation in soft robotics and medical devices.

BIBLIOGRAPHY

[1] V. Agostiniani, A. DeSimone, and K. Koumatos. "Shape Programming for Narrow Ribbons of Nematic Elastomers". In: *Journal of Elasticity* 127.1 (2017), pp. 1–24. DOI: 10.1007/s10659-016-9594-1. URL: http://dx.doi.org/10.1007/s10659-016-9594-1.

[2] H. Aharoni, E. Sharon, and R. Kupferman. "Geometry of Thin Nematic Elastomer Sheets". In: *Phys. Rev. Lett.* 113 (25 Dec. 2014), p. 257801. DOI: 10.1103/PhysRevLett.113.257801. URL: http://link.aps.org/doi/10.1103/PhysRevLett.113.257801.

[3] O. Anza Hafsa and J-P. Mandallena. "Relaxation theorems in nonlinear elasticity". In: *Annales de l'Institut Henri Poincare (C) Non Linear Analysis* 25.1 (2008), pp. 135–148. ISSN: 0294-1449. DOI: http://dx.doi.org/10.1016/j.anihpc.2006.11.005. URL: http://www.sciencedirect.com/science/article/pii/S0294144906001235.

[4] J.M. Ball and R.D. James. "Fine phase mixtures as minimizers of energy". In: *Archive for Rational Mechanics and Analysis* 100.1 (1987), pp. 13–52.

[5] J.M. Ball and R.D. James. "Incompatible Sets of Gradients and Metastability". In: *Archive for Rational Mechanics and Analysis* 218.3 (2015), pp. 1363–1416. DOI: 10.1007/s00205-015-0883-9. URL: http://dx.doi.org/10.1007/s00205-015-0883-9.

[6] J.M. Ball, B. Kirchheim, and J. Kristensen. "Regularity of quasiconvex envelopes". In: *Calculus of Variations and Partial Differential Equations* 11.4 (2000), pp. 333–359. ISSN: 1432-0835. DOI: 10.1007/s005260000041. URL: http://dx.doi.org/10.1007/s005260000041.

[7] J.M. Ball and F. Murat. "W1,p-quasiconvexity and variational problems for multiple integrals". In: *Journal of Functional Analysis* 58.3 (1984), pp. 225–253. ISSN: 0022-1236. DOI: http://dx.doi.org/10.1016/0022-1236(84)90041-7. URL: http://www.sciencedirect.com/science/article/pii/0022123684900417.

[8] M. Barchiesi and A. DeSimone. "Frank energy for nematic elastomers: a nonlinear model". In: *ESAIM: COCV* 21.2 (2015), pp. 372–377. DOI: 10.1051/cocv/2014022. URL: https://doi.org/10.1051/cocv/2014022.

[9] M. Barchiesi, D. Henao, and C. Mora-Corral. "Local invertibility in Sobolev spaces with applications to nematic elastomers and magnetoelasticity". In: *preprint* (2015).

[10] H.B. Belgacem. “Une méthode de Γ-convergence pour un modele de membrane non linéaire”. In: *Comptes Rendus de l'Académie des Sciences-Series I-Mathematics* 324.7 (1997), pp. 845–849.

[11] P. Bella and R.V. Kohn. “Metric-Induced Wrinkling of a Thin Elastic Sheet”. In: *Journal of Nonlinear Science* 24.6 (2014), pp. 1147–1176. DOI: 10.1007/s00332-014-9214-9. URL: http://dx.doi.org/10.1007/s00332-014-9214-9.

[12] P. Bella and R.V. Kohn. “Wrinkles as the Result of Compressive Stresses in an Annular Thin Film”. In: *Communications on Pure and Applied Mathematics* 67.5 (2014), pp. 693–747. ISSN: 1097-0312. DOI: 10.1002/cpa.21471. URL: http://dx.doi.org/10.1002/cpa.21471.

[13] K. Bhattacharya. *Microstructure of martensite: why it forms and how it gives rise to the shape-memory effect*. Vol. 2. Oxford University Press, 2003.

[14] K. Bhattacharya and R.D. James. “A theory of thin films of martensitic materials withapplications to microactuatorsfn2”. In: *Journal of the Mechanics and Physics of Solids* 47.3 (1999), pp. 531–576. ISSN: 0022-5096. DOI: http://dx.doi.org/10.1016/S0022-5096(98)00043-X. URL: http://www.sciencedirect.com/science/article/pii/S002250969800043X.

[15] K. Bhattacharya and R.D. James. “The Material Is the Machine”. In: *Science* 307.5706 (2005), pp. 53–54. ISSN: 0036-8075. DOI: 10.1126/science.1100892. URL: http://science.sciencemag.org/content/307/5706/53.

[16] K. Bhattacharya, M. Lewicka, and M. Schäffner. “Plates with Incompatible Prestrain”. In: *Archive for Rational Mechanics and Analysis* 221.1 (2016), pp. 143–181. ISSN: 1432-0673. DOI: 10.1007/s00205-015-0958-7. URL: http://dx.doi.org/10.1007/s00205-015-0958-7.

[17] J.S. Biggins, M. Warner, and K. Bhattacharya. “Elasticity of polydomain liquid crystal elastomers”. In: *Journal of the Mechanics and Physics of Solids* 60.4 (2012), pp. 573–590. DOI: http://doi.org/10.1016/j.jmps.2012.01.008. URL: http://www.sciencedirect.com/science/article/pii/S0022509612000166.

[18] J.S. Biggins, M. Warner, and K. Bhattacharya. “Supersoft Elasticity in Polydomain Nematic Elastomers”. In: *Phys. Rev. Lett.* 103 (3 July 2009), p. 037802. DOI: 10.1103/PhysRevLett.103.037802. URL: https://link.aps.org/doi/10.1103/PhysRevLett.103.037802.

[19] P. Bladon, E.M. Terentjev, and M. Warner. “Transitions and instabilities in liquid crystal elastomers”. In: *Phys. Rev. E* 47 (6 June 1993), R3838–R3840. DOI: 10.1103/PhysRevE.47.R3838. URL: http://link.aps.org/doi/10.1103/PhysRevE.47.R3838.

[20] J.A. Blume. “Compatibility conditions for a left Cauchy-Green strain field”. In: *Journal of Elasticity* 21.3 (1989), pp. 271–308. ISSN: 1573-2681. DOI: 10.1007/BF00045780. URL: http://dx.doi.org/10.1007/BF00045780.

[21] S. Boyd and L. Vandenberghe. *Convex optimization*. Cambridge university press, 2004.

[22] A. Braides. *Gamma-convergence for Beginners*. Vol. 22. Clarendon Press, 2002.

[23] B.N. Bridgens, P.D. Gosling, and M.J.S. Birchall. “Tensile fabric structures: concepts, practice & developments”. In: *Structural Engineer* 82.14 (2004), pp. 21–27.

[24] E. Cerda and L. Mahadevan. “Geometry and Physics of Wrinkling”. In: *Phys. Rev. Lett.* 90 (7 Feb. 2003), p. 074302. DOI: 10.1103/PhysRevLett.90.074302. URL: http://link.aps.org/doi/10.1103/PhysRevLett.90.074302.

[25] P. Cesana, P. Plucinsky, and K. Bhattacharya. “Effective Behavior of Nematic Elastomer Membranes”. In: *Archive for Rational Mechanics and Analysis* 218.2 (2015), pp. 863–905. ISSN: 1432-0673. DOI: 10.1007/s00205-015-0871-0. URL: http://dx.doi.org/10.1007/s00205-015-0871-0.

[26] F. Cirak et al. “Computational analysis of liquid crystalline elastomer membranes: Changing Gaussian curvature without stretch energy”. In: *International Journal of Solids and Structures* 51.1 (2014), pp. 144–153. ISSN: 0020-7683. DOI: http://doi.org/10.1016/j.ijsolstr.2013.09.019. URL: http://www.sciencedirect.com/science/article/pii/S0020768313003740.

[27] S. Conti, A. DeSimone, and G. Dolzmann. “Semisoft elasticity and director reorientation in stretched sheets of nematic elastomers”. In: *Phys. Rev. E* 66 (6 Dec. 2002), p. 061710. DOI: 10.1103/PhysRevE.66.061710. URL: http://link.aps.org/doi/10.1103/PhysRevE.66.061710.

[28] S. Conti, A. DeSimone, and G. Dolzmann. “Soft elastic response of stretched sheets of nematic elastomers: a numerical study”. In: *Journal of the Mechanics and Physics of Solids* 50.7 (2002), pp. 1431–1451. ISSN: 0022-5096. DOI: http://dx.doi.org/10.1016/S0022-5096(01)00120-X. URL: http://www.sciencedirect.com/science/article/pii/S002250960100120X.

[29] S. Conti and G. Dolzmann. “Analytical and Numerical Tools for Relaxation in Crystal Plasticity”. In: *Procedia IUTAM* 20 (2017), pp. 56–65.

[30] S. Conti and G. Dolzmann. “Γ-convergence for incompressible elastic plates”. In: *Calculus of Variations and Partial Differential Equations* 34.4 (2008), p. 531. DOI: 10.1007/s00526-008-0194-1. URL: http://dx.doi.org/10.1007/s00526-008-0194-1.

[31] S. Conti and G. Dolzmann. “Derivation of Elastic Theories for Thin Sheets and the Constraint of Incompressibility”. In: *Analysis, Modeling and Simulation of Multiscale Problems*. Ed. by Alexander Mielke. Berlin, Heidelberg: Springer Berlin Heidelberg, 2006, pp. 225–247. ISBN: 978-3-540-35657-8. DOI: 10.1007/3-540-35657-6_9. URL: http://dx.doi.org/10.1007/3-540-35657-6_9.

[32] S. Conti and F. Maggi. “Confining Thin Elastic Sheets and Folding Paper”. In: *Archive for Rational Mechanics and Analysis* 187.1 (2008), pp. 1–48. DOI: 10.1007/s00205-007-0076-2. URL: http://dx.doi.org/10.1007/s00205-007-0076-2.

[33] B. Dacorogna. *Direct methods in the calculus of variations*. Vol. 78. Springer Science & Business Media, 2007.

[34] G. Dal Maso. *An introduction to* Γ*-convergence*. Vol. 8. Springer Science & Business Media, 2012.

[35] J. Dervaux and M. Ben Amar. “Morphogenesis of Growing Soft Tissues”. In: *Phys. Rev. Lett.* 101 (6 Aug. 2008), p. 068101. DOI: 10.1103/PhysRevLett.101.068101. URL: https://link.aps.org/doi/10.1103/PhysRevLett.101.068101.

[36] A. DeSimone. “Energy minimizers for large ferromagnetic bodies”. In: *Archive for rational mechanics and analysis* 125.2 (1993), pp. 99–143.

[37] A. DeSimone and G. Dolzmann. “Macroscopic Response of Nematic Elastomers via Relaxation of a Class of SO(3)-Invariant Energies”. In: *Archive for Rational Mechanics and Analysis* 161.3 (2002), pp. 181–204. ISSN: 1432-0673. DOI: 10.1007/s002050100174. URL: http://dx.doi.org/10.1007/s002050100174.

[38] Efrati E., Sharon E., and Kupferman R. “Elastic theory of unconstrained non-Euclidean plates”. In: *Journal of the Mechanics and Physics of Solids* 57.4 (2009), pp. 762–775. ISSN: 0022-5096. DOI: http://doi.org/10.1016/j.jmps.2008.12.004. URL: http://www.sciencedirect.com/science/article/pii/S0022509608002160.

[39] E. Efrati, E. Sharon, and R. Kupferman. “The metric description of elasticity in residually stressed soft materials”. In: *Soft Matter* 9 (34 2013), pp. 8187–8197. DOI: 10.1039/C3SM50660F. URL: http://dx.doi.org/10.1039/C3SM50660F.

[40] S. Eran et al. “Mechanics: Buckling cascades in free sheets”. English. In: *Nature* 419.6907 (Oct. 2002), p. 579. URL: https://clsproxy.library.caltech.edu/docview/89109123?accountid=9841.

[41] L.C. Evans. “Partial differential equations”. In: (2010).

[42] I. Fonseca. “The lower quasiconvex envelope of the stored energy function for an elastic crystal”. In: *Journal de Mathématiques Pures et Appliquées* 67.2 (1988), pp. 175–195.

[43] I. Fonseca and G. Leoni. *Modern Methods in the Calculus of Variations: L^ p Spaces*. Springer Science & Business Media, 2007.

[44] F.C. Frank. “Liquid crystals on the theory of liquid crystals”. In: *Crystals That Flow: Classic Papers from the History of Liquid Crystals*. CRC Press, 2004, pp. 389–399.

[45] G. Friesecke, R.D. James, and S. Müller. “A Hierarchy of Plate Models Derived from Nonlinear Elasticity by Gamma-Convergence”. In: *Archive for Rational Mechanics and Analysis* 180.2 (2006), pp. 183–236. DOI: 10.1007/s00205-005-0400-7. URL: http://dx.doi.org/10.1007/s00205-005-0400-7.

[46] G. Friesecke, R.D. James, and S. Müller. “A theorem on geometric rigidity and the derivation of nonlinear plate theory from three-dimensional elasticity”. In: *Communications on Pure and Applied Mathematics* 55.11 (2002), pp. 1461–1506. ISSN: 1097-0312. DOI: 10.1002/cpa.10048. URL: http://dx.doi.org/10.1002/cpa.10048.

[47] K. Fuchi et al. “Topology optimization for the design of folding liquid crystal elastomer actuators”. In: *Soft Matter* 11 (37 2015), pp. 7288–7295. DOI: 10.1039/C5SM01671A. URL: http://dx.doi.org/10.1039/C5SM01671A.

[48] P.G. de Gennes. “Phenomenology of short-range-order effects in the isotropic phase of nematic materials”. In: *Physics Letters A* 30.8 (1969), pp. 454–455. ISSN: 0375-9601. DOI: http://dx.doi.org/10.1016/0375-9601(69)90240-0. URL: http://www.sciencedirect.com/science/article/pii/0375960169902400.

[49] P.G. de Gennes and J. Prost. *The physics of liquid crystals*. 83. Oxford university press, 1995.

[50] V. Gimenez-Pinto et al. “Modeling out-of-plane actuation in thin-film nematic polymer networks: From chiral ribbons to auto-origami boxes via twist and topology”. In: *Scientific Reports* 7 (2017).

[51] L.T. de Haan et al. “Engineering of Complex Order and the Macroscopic Deformation of Liquid Crystal Polymer Networks”. In: *Angewandte Chemie International Edition* 51.50 (2012), pp. 12469–12472. ISSN: 1521-3773. DOI: 10.1002/anie.201205964. URL: http://dx.doi.org/10.1002/anie.201205964.

[52] P. Hornung. “Approximation of Flat W 2,2 Isometric Immersions by Smooth Ones”. In: *Archive for Rational Mechanics and Analysis* 199.3 (2011), pp. 1015–1067. DOI: 10.1007/s00205-010-0374-y. URL: http://dx.doi.org/10.1007/s00205-010-0374-y.

[53] C.H.M. Jenkins. “Gossamer spacecraft(membrane and inflatable structures technology for space applications)”. In: *Progress in Astronautics and Aeronautics* (2001).

[54] D. Kinderlehrer and P. Pedregal. “Characterizations of young measures generated by gradients”. In: *Archive for Rational Mechanics and Analysis* 115.4 (1991), pp. 329–365. ISSN: 1432-0673. DOI: 10.1007/BF00375279. URL: http://dx.doi.org/10.1007/BF00375279.

[55] D. Kinderlehrer and P. Pedregal. “Weak Convergence of Integrands and the Young Measure Representation”. In: *SIAM Journal on Mathematical Analysis* 23.1 (1992), pp. 1–19. DOI: 10.1137/0523001. URL: http://dx.doi.org/10.1137/0523001.

[56] Y. Klein, E. Efrati, and E. Sharon. “Shaping of Elastic Sheets by Prescription of Non-Euclidean Metrics”. In: *Science* 315.5815 (2007), pp. 1116–1120. DOI: 10.1126/science.1135994. URL: http://science.sciencemag.org/content/315/5815/1116.

[57] P. Krulevitch et al. “Thin film shape memory alloy microactuators”. In: *Journal of Microelectromechanical Systems* 5.4 (Dec. 1996), pp. 270–282. ISSN: 1057-7157. DOI: 10.1109/84.546407.

[58] I. Kundler and H. Finkelmann. “Strain-induced director reorientation in nematic liquid single crystal elastomers”. In: *Macromolecular Rapid Communications* 16.9 (1995), pp. 679–686. ISSN: 1521-3927. DOI: 10.1002/marc.1995.030160908. URL: http://dx.doi.org/10.1002/marc.1995.030160908.

[59] J. Küpfer and H. Finkelmann. “Liquid crystal elastomers: influence of the orientational distribution of the crosslinks on the phase behaviour and reorientation processes”. In: *Macromolecular chemistry and physics* 195.4 (1994), pp. 1353–1367.

[60] J. Küpfer and H. Finkelmann. “Nematic liquid single crystal elastomers”. In: *Die Makromolekulare Chemie, Rapid Communications* 12.12 (1991), pp. 717–726. DOI: 10.1002/marc.1991.030121211. URL: http://dx.doi.org/10.1002/marc.1991.030121211.

[61] H. Le Dret and A. Raoult. “The nonlinear membrane model as variational limit of nonlinear three-dimensional elasticity”. In: *Journal de mathématiques pures et appliquées* 74.6 (1995), pp. 549–578.

[62] M. Lewicka, L. Mahadevan, and M.R. Pakzad. “The Föppl-von Kármán equations for plates with incompatible strains”. In: *Proceedings of the Royal Society of London A: Mathematical, Physical and Engineering Sciences* 467.2126 (2010), pp. 402–426. ISSN: 1364-5021. DOI: 10.1098/rspa.2010.0138. URL: http://rspa.royalsocietypublishing.org/content/467/2126/402.

[63] M. Lewicka and M.R. Pakzad. "Scaling laws for non-Euclidean plates and the W2,2 isometric immersions of Riemannian metrics". In: *ESAIM: COCV* 17.4 (2011), pp. 1158–1173. DOI: 10.1051/cocv/2010039. URL: https://doi.org/10.1051/cocv/2010039.

[64] E.H. Mansfield. "Load Transfer Via a Wrinkled Membrane". In: *Proceedings of the Royal Society of London A: Mathematical, Physical and Engineering Sciences* 316.1525 (1970), pp. 269–289. ISSN: 0080-4630. DOI: 10.1098/rspa.1970.0079. URL: http://rspa.royalsocietypublishing.org/content/316/1525/269.

[65] C.R. McInnes. *Solar Sailing*. Technology, Dynamics, and Mission Applications. Chichester, UK: Springer-Praxis, 1999. ISBN: 185233102X.

[66] C.D. Modes, K. Bhattacharya, and M. Warner. "Disclination-mediated thermo-optical response in nematic glass sheets". In: *Phys. Rev. E* 81 (6 June 2010), p. 060701. DOI: 10.1103/PhysRevE.81.060701. URL: https://link.aps.org/doi/10.1103/PhysRevE.81.060701.

[67] C.D. Modes, K. Bhattacharya, and M. Warner. "Gaussian curvature from flat elastica sheets". In: *Proceedings of the Royal Society of London A: Mathematical, Physical and Engineering Sciences* 467.2128 (2011), pp. 1121–1140. ISSN: 1364-5021. DOI: 10.1098/rspa.2010.0352. URL: http://rspa.royalsocietypublishing.org/content/467/2128/1121.

[68] C.D. Modes and M. Warner. "Blueprinting nematic glass: Systematically constructing and combining active points of curvature for emergent morphology". In: *Phys. Rev. E* 84 (2 Aug. 2011), p. 021711. DOI: 10.1103/PhysRevE.84.021711. URL: https://link.aps.org/doi/10.1103/PhysRevE.84.021711.

[69] C.D. Modes and M. Warner. "Shape-programmable materials". In: *Physics Today* 69.1 (2016), pp. 32–38.

[70] L. Modica. "The gradient theory of phase transitions and the minimal interface criterion". In: *Archive for Rational Mechanics and Analysis* 98.2 (1987), pp. 123–142. ISSN: 1432-0673. DOI: 10.1007/BF00251230. URL: http://dx.doi.org/10.1007/BF00251230.

[71] L. Modica and S. Mortola. "Un esempio di Γ-convergenza". In: *Boll. Un. Mat. Ital. B (5)* 14.1 (1977), pp. 285–299.

[72] C. Mostajeran. "Curvature generation in nematic surfaces". In: *Phys. Rev. E* 91 (6 June 2015), p. 062405. DOI: 10.1103/PhysRevE.91.062405. URL: http://link.aps.org/doi/10.1103/PhysRevE.91.062405.

[73] C. Mostajeran et al. "Encoding Gaussian curvature in glassy and elastomeric liquid crystal solids". In: *Proceedings of the Royal Society of London A: Mathematical, Physical and Engineering Sciences* 472.2189 (2016). ISSN: 1364-5021. DOI: 10.1098/rspa.2016.0112. URL: http://rspa.royalsocietypublishing.org/content/472/2189/20160112.

[74] S. Müller. "Variational models for microstructure and phase transitions". In: *Calculus of Variations and Geometric Evolution Problems: Lectures given at the 2nd Session of the Centro Internazionale Matematico Estivo (C.I.M.E.) held in Cetraro, Italy, June 15–22, 1996*. Ed. by S. Hildebrandt and M. Struwe. Berlin, Heidelberg: Springer Berlin Heidelberg, 1999, pp. 85–210. DOI: 10.1007/BFb0092670. URL: http://dx.doi.org/10.1007/BFb0092670.

[75] V. Nayyar, K. Ravi-Chandar, and R. Huang. "Stretch-induced stress patterns and wrinkles in hyperelastic thin sheets". In: *International Journal of Solids and Structures* 48.25–26 (2011), pp. 3471–3483. ISSN: 0020-7683. DOI: http://dx.doi.org/10.1016/j.ijsolstr.2011.09.004. URL: http://www.sciencedirect.com/science/article/pii/S0020768311003040.

[76] T.S. Nguyen and J.V. Selinger. "Theory of Liquid Crystal Elastomers: From Polymer Physics to Differential Geometry". In: *arXiv preprint arXiv:1612.06486* (2016).

[77] M.R. Pakzad. "On the Sobolev Space of Isometric Immersions". In: *J. Differential Geom.* 66.1 (Jan. 2004), pp. 47–69. DOI: 10.4310/jdg/1090415029. URL: http://dx.doi.org/10.4310/jdg/1090415029.

[78] A.C. Pipkin. "The Relaxed Energy Density for Isotropic Elastic Membranes". In: *IMA Journal of Applied Mathematics* 36.1 (1986), p. 85. DOI: 10.1093/imamat/36.1.85. URL: +%20http://dx.doi.org/10.1093/imamat/36.1.85.

[79] L. Pismen and A.P. Zakharov. "Textures and shapes in nematic elastomers under the action of dopant concentration gradients". In: *Soft Matter* (2017).

[80] P. Plucinsky and K. Bhattacharya. "Microstructure-enabled control of wrinkling in nematic elastomer sheets". In: *Journal of the Mechanics and Physics of Solids* 102 (2017), pp. 125–150. ISSN: 0022-5096. DOI: http://dx.doi.org/10.1016/j.jmps.2017.02.009. URL: http://www.sciencedirect.com/science/article/pii/S0022509616308572.

[81] P. Plucinsky, M. Lemm, and K. Bhattacharya. "Actuation of thin nematic elastomer sheets with controlled heterogeneity". In: *arXiv:1611.00729 (submitted)* (2017).

[82] P. Plucinsky, M. Lemm, and K. Bhattacharya. "Programming complex shapes in thin nematic elastomer and glass sheets". In: *Phys. Rev. E* 94 (1 July 2016), p. 010701. DOI: 10.1103/PhysRevE.94.010701. URL: http://link.aps.org/doi/10.1103/PhysRevE.94.010701.

[83] L. Qi and R.S. Womersley. "On extreme singular values of matrix valued functions". In: *Journal of Convex Analysis* 3 (1996), pp. 153–166.

[84] J. Rogers et al. "Origami mems and nems". In: *Mrs Bulletin* 41.02 (2016), pp. 123–129.

[85] E. Sharon and E. Efrati. “The mechanics of non-Euclidean plates”. In: *Soft Matter* 6.22 (2010), pp. 5693–5704.

[86] E. Sharon, M. Marder, and H. Swinney. “Leaves, Flowers and Garbage Bags: Making Waves Rippled fractal patterns on thin plastic sheets and biological membranes offer elegant examples of the spontaneous breaking of symmetry”. In: *American Scientist* 92.3 (2004), pp. 254–261.

[87] Y.C. Shu. “Heterogeneous Thin Films of Martensitic Materials”. In: *Archive for Rational Mechanics and Analysis* 153.1 (2000), pp. 39–90. DOI: 10.1007/s002050000088. URL: http://dx.doi.org/10.1007/s002050000088.

[88] D.J. Steigmann. “Tension-Field Theory”. In: *Proceedings of the Royal Society of London A: Mathematical, Physical and Engineering Sciences* 429.1876 (1990), pp. 141–173. ISSN: 0080-4630. DOI: 10.1098/rspa.1990.0055. URL: http://rspa.royalsocietypublishing.org/content/429/1876/141.

[89] D.J. Steigmann and A.C. Pipkin. “Finite deformations of wrinkled membranes”. In: *Quarterly Journal of Mechanics and Applied Mathematics* 42.3 (1989), pp. 427–440.

[90] Dassault Systèmes. “Abaqus 6.10 online documentation”. In: *Abaqus User Subroutines Reference Manual* (2010).

[91] Dassault Systèmes. “ABAQUS 6.12 Theory manual”. In: *Dassault Systèmes Simulia Corp., Providence, Rhode Island* (2012).

[92] A.R. Tajbakhsh and E.M. Terentjev. “Spontaneous thermal expansion of nematic elastomers”. In: *The European Physical Journal E* 6.2 (2001), pp. 181–188. ISSN: 1292-8941. DOI: 10.1007/s101890170020. URL: http://dx.doi.org/10.1007/s101890170020.

[93] M. Taylor, K. Bertoldi, and D.J. Steigmann. “Spatial resolution of wrinkle patterns in thin elastic sheets at finite strain”. In: *Journal of the Mechanics and Physics of Solids* 62 (2014). Sixtieth anniversary issue in honor of Professor Rodney Hill, pp. 163–180. ISSN: 0022-5096. DOI: http://dx.doi.org/10.1016/j.jmps.2013.09.024. URL: http://www.sciencedirect.com/science/article/pii/S0022509613002081.

[94] K. Trabelsi. “Incompressible nonlinearly elastic thin membranes”. In: *Comptes Rendus Mathematique* 340.1 (2005), pp. 75–80. ISSN: 1631-073X. DOI: http://dx.doi.org/10.1016/j.crma.2004.11.005. URL: http://www.sciencedirect.com/science/article/pii/S1631073X04005291.

[95] K. Trabelsi. “Modeling of a membrane for nonlinearly elastic incompressible materials via gamma-convergence”. In: *Analysis and Applications* 04.01 (2006), pp. 31–60. DOI: 10.1142/S0219530506000693. URL: http://www.worldscientific.com/doi/abs/10.1142/S0219530506000693.

[96] K. Urayama. “Selected issues in liquid crystal elastomers and gels”. In: *Macromolecules* 40.7 (2007), p. 2277.

[97] K. Urayama, S. Honda, and T. Takigawa. “Deformation Coupled to Director Rotation in Swollen Nematic Elastomers under Electric Fields”. In: *Macromolecules* 39.5 (2006), pp. 1943–1949. DOI: 10.1021/ma052762q. URL: http://dx.doi.org/10.1021/ma052762q.

[98] K. Urayama, S. Honda, and T. Takigawa. “Electrooptical effects with anisotropic deformation in nematic gels”. In: *Macromolecules* 38.9 (2005), pp. 3574–3576.

[99] K. Urayama et al. “Polydomain-Monodomain Transition of Randomly Disordered Nematic Elastomers with Different Cross-Linking Histories”. In: *Macromolecules* 42.12 (2009), pp. 4084–4089. DOI: 10.1021/ma9004692. URL: http://dx.doi.org/10.1021/ma9004692.

[100] G.C. Verwey and M. Warner. “Compositional Fluctuations and Semisoftness in Nematic Elastomers”. In: *Macromolecules* 30.14 (1997), pp. 4189–4195. DOI: 10.1021/ma961801i. URL: http://dx.doi.org/10.1021/ma961801i.

[101] G.C. Verwey, M. Warner, and E.M. Terentjev. “Elastic Instability and Stripe Domains in Liquid Crystalline Elastomers”. In: *J. Phys. II France* 6.9 (1996), pp. 1273–1290. DOI: 10.1051/jp2:1996130. URL: https://doi.org/10.1051/jp2:1996130.

[102] T.H. Ware et al. “Voxelated liquid crystal elastomers”. In: *Science* 347.6225 (2015), pp. 982–984. ISSN: 0036-8075. DOI: 10.1126/science.1261019. URL: http://science.sciencemag.org/content/347/6225/982.

[103] M. Warner, P. Bladon, and E.M. Terentjev. ““Soft elasticity” — deformation without resistance in liquid crystal elastomers”. In: *J. Phys. II France* 4.1 (1994), pp. 93–102. DOI: 10.1051/jp2:1994116. URL: https://doi.org/10.1051/jp2:1994116.

[104] M. Warner, C.D. Modes, and D. Corbett. “Curvature in nematic elastica responding to light and heat”. In: *Proceedings of the Royal Society of London A: Mathematical, Physical and Engineering Sciences* 466.2122 (2010), pp. 2975–2989. DOI: 10.1098/rspa.2010.0135. URL: http://rspa.royalsocietypublishing.org/content/466/2122/2975.

[105] M. Warner and E.M. Terentjev. *Liquid crystal elastomers*. Vol. 120. OUP Oxford, 2003.

[106] T.J. White and D.J. Broer. “Programmable and adaptive mechanics with liquid crystal polymer networks and elastomers”. In: *Nature materials* 14.11 (2015), pp. 1087–1098.

[107] H. Whitney. “The Self-Intersections of a Smooth n-Manifold in 2n-Space”. In: *Annals of Mathematics* 45.2 (1944), pp. 220–246. URL: http://www.jstor.org/stable/1969265.

[108] H. Whitney. “The Singularities of a Smooth n-Manifold in (2n - 1)-Space”. In: *Annals of Mathematics* 45.2 (1944), pp. 247–293. URL: http://www.jstor.org/stable/1969266.

[109] W. Wong and S. Pellegrino. “Wrinkled membranes I: experiments”. In: *Journal of Mechanics of Materials and Structures* 1.1 (2006), pp. 3–25. DOI: 10.2140/jomms.2006.1.3.

[110] W. Wong and S. Pellegrino. “Wrinkled membranes II: analytical models”. In: *Journal of Mechanics of Materials and Structures* 1.1 (2006), pp. 27–61. DOI: 10.2140/jomms.2006.1.27.

[111] W. Wong and S. Pellegrino. “Wrinkled membranes III: numerical simulations”. In: *Journal of Mechanics of Materials and Structures* 1.1 (2006), pp. 63–95. DOI: 10.2140/jomms.2006.1.63.

[112] A.P. Zakharov and L.M. Pismen. “Reshaping nemato-elastic sheets”. In: *The European Physical Journal E* 38.7 (2015), p. 75. DOI: 10.1140/epje/i2015-15075-6. URL: http://dx.doi.org/10.1140/epje/i2015-15075-6.

[113] L. Zheng. “Wrinkling of dielectric elastomer membranes”. In: *Thesis* (2008).

Appendix A

LOOSE ENDS AND OTHER MATTERS

A.1 Some useful linear algebra applied to nematic elastomers

Frame indifference and isotropy

Proposition A.1.1 *The energy densities W^e in (2.1) and W^e_{iso} in (2.19) are frame-indifferent and isotropic in the sense that*

$$\begin{aligned} W^e(RF, Rn, n_0) &= W^e(F, n, n_0), \\ W^e_{iso}(RFQ, Rn) &= W^e(F, n), \end{aligned} \tag{A.1}$$

for all $R, Q \in SO(3)$, for all $F \in \mathbb{R}^{3\times 3}$ and for all $n, n_0 \in \mathbb{S}^2$.

Proof. Pick any R, Q, F, n, n_0 as above. We have

$$\begin{aligned} W^e(RFQ, Rn, Q^T n_0) &= W_{nH}(R(\ell^f_n)^{-1/2} R^T RF(\ell^0_{n_0})^{1/2}) \\ &= W_{nH}\left((\ell^f_n)^{-1/2} F(\ell^0_{n_0})^{1/2}\right) = W^e_{iso}(F, n, n_0) \end{aligned} \tag{A.2}$$

since W_{nH} is frame-indifferent and isotropic. The case W^e_{iso} is similar. □

Some estimates on the energy densities

Proposition A.1.2 *If $F \in \mathbb{R}^{3\times 3}$ such that $\det F = 1$ and $n_0, n \in \mathbb{S}^2$, then*

$$\begin{aligned} \frac{1}{c}(|F|^2 - 1) \le W^e(F, n, n_0) \le c(|F|^2 + 1), \\ \frac{1}{c}(|F|^2 - 1) \le W^e_{iso}(F, n) \le c(|F|^2 + 1) \end{aligned} \tag{A.3}$$

for some $c = c(r_f, r_0) > 0$.

Proof. Since $\det F = 1$ and $n_0 \in \mathbb{S}^2$, we have $n = Fn_0/|Fn_0| \in \mathbb{S}^2$ and

$$\begin{aligned} W^e(F, n, n_0) &= W_{nH}((\ell^f_n)^{-1/2} F(\ell^0_{n_0})^{1/2}) \\ &\ge \frac{\mu}{2}\left(\frac{1}{3}\sigma^2_{min}((\ell^0_{n_0})^{1/2})|(\ell^f_n)^{-1/2}F|^2 - 3\right) \\ &\ge \frac{\mu}{2}\left(\frac{1}{9}\sigma^2_{min}((\ell^0_{n_0})^{1/2})\sigma^2_{min}((\ell^f_n)^{-1/2})|F|^2 - 3\right). \end{aligned} \tag{A.4}$$

We note that $\sigma_{min}((\ell^0_{n_0})^{1/2})$ is nonzero and depends only on r_0. Similarly, $\sigma_{min}((\ell^f_n)^{-1/2})$ is nonzero and depends only on r_f. Thus, the lower bound in (A.3) follows. The upperbound is similar. The inequalities hold for W^e_{iso} by an analogous argument. □

Proposition A.1.3 *Let $G \in \mathbb{R}^{3\times 3}$ such that $\det(I_{3\times 3} + G) = 1$. We find*

$$W_{nH}(I_{3\times 3} + G) \leq C(|G|^2 + |G|^3), \tag{A.5}$$

for W_{nH} in (2.5) and for some uniform constant $C > 0$.

Proof. For the inequality on W_{nH}, we note that since $\det(I_{3\times 3} + G) = 1$,

$$\operatorname{Tr}(G) = -\operatorname{Tr}(\operatorname{cof} G) - \det(G) \tag{A.6}$$

and W_{nH} is finite. Hence,

$$\begin{aligned} W_{nH}(I_{3\times 3} + G) &= \frac{\mu}{2}\left(|I_{3\times 3} + G|^2 - 3\right) \\ &= \frac{\mu}{2}\left(|G|^2 + 2\operatorname{Tr}(G)\right) \\ &= \frac{\mu}{2}\left(|G|^2 - 2\operatorname{Tr}(\operatorname{cof} G) - 2\det(G)\right). \end{aligned} \tag{A.7}$$

Since there exists a $C > 0$ independent of G such that $|\operatorname{Tr}(\operatorname{cof} G)| \leq C|G|^2$ and $|\det(G)| \leq C|G|^3$, we conclude (A.5) following the identity (A.7). □

Proposition A.1.4 *The energy density W_{nH} in (2.5) satisfies*

$$W_{nH}(F) \geq \frac{\mu}{2}\operatorname{dist}^2(F, SO(3)) \tag{A.8}$$

for all $F \in \mathbb{R}^{3\times 3}$.

Proof. We may assume $\det F = 1$ as the bound holds trivially otherwise. Consequently and by the polar decomposition theorem, $F = RU$ for $R \in SO(3)$ and U positive definite. Hence, we find $\operatorname{dist}(F, SO(3)) = |U - I_{3\times 3}|$. In addition, since $\det U = 1$ we conclude

$$\begin{aligned} \frac{\mu}{2}\operatorname{dist}^2(F, SO(3)) &= \frac{\mu}{2}|U - I_{3\times 3}|^2 \\ &= \frac{\mu}{2}(|U|^2 - 2\operatorname{Tr}(U) + 3) \\ &\leq \frac{\mu}{2}(|U|^2 - \inf\{\operatorname{Tr}(G) : G \text{ pos. def.}, \det G = 1\} + 3) \\ &= \frac{\mu}{2}(|U|^2 - 3) = W_{nH}(F). \end{aligned} \tag{A.9}$$

Here, we used that the infimum above is attained at $G = I_{3\times 3}$. □

Some results on the out-of-plane component of the deformation gradient

Proposition A.1.5 *If* $\tilde{F} \in \mathbb{R}^{3\times 2}$ *such that* $\operatorname{rank} \tilde{F} = 2$*, then*

$$b_0 := \arg\min_{b\in\mathbb{R}^3} W_{nH}(\tilde{F}|b) = \frac{\operatorname{adj} \tilde{F}}{|\operatorname{adj} \tilde{F}|^2}. \tag{A.10}$$

Proof. Let $f_{\tilde{F}}(b) := W_{nH}(\tilde{F}|b)$ and recognize that the minimization can be posed as

$$\inf\left\{ f_{\tilde{F}}(b) \colon b \cdot \operatorname{adj} \tilde{F} = 1, b \in \mathbb{R}^3 \right\}. \tag{A.11}$$

This is a standard convex optimization problem with an affine equality constraint (see, for instance, Boyd and Vandenberghe [21], Section 5.5.3). That is, there is a global minimizer of this optimization if and only if there exists a $\lambda \in \mathbb{R}$ such that $\nabla f_{\tilde{F}}(b_0) + \lambda \operatorname{adj} \tilde{F} = 0$; explicitly, such that

$$\mu b_0 - \lambda \operatorname{adj} \tilde{F} = 0. \tag{A.12}$$

Applying the constraint leads to $\lambda = \frac{\mu}{|\operatorname{adj} \tilde{F}|^2}$ (which is well-defined since $\operatorname{rank} \tilde{F} = 2$, and b_0 as in (A.10)). □

Proposition A.1.6 *If* $\tilde{F} \in \mathbb{R}^{3\times 2}$ *such that* $\operatorname{rank} \tilde{F} = 2$ *and* $n \in \mathbb{S}^2$*, then*

$$b_0 := \arg\min_{b\in\mathbb{R}^3} W^e_{iso}(\tilde{F}|b, n) = \frac{(\ell^*_n) \operatorname{adj} \tilde{F}}{|(\ell^*_n)^{1/2} \operatorname{adj} \tilde{F}|^2}. \tag{A.13}$$

Proof. Recall that $W^e_{iso}(\tilde{F}|b, n) = W_{nH}((\ell^*_n)^{-1/2}\tilde{F}|(\ell^*_n)^{-1/2}b)$ Thus, we set $\tilde{G} = (\ell^*_n)^{-1/2}\tilde{F}$ (which is full-rank) and $c = (\ell^*_n)^{-1/2}b$. Hence, it follows from Proposition A.1.5 that

$$c_0 := \arg\min_{c\in\mathbb{R}^3} W_{nH}(\tilde{G}|c) = \frac{\operatorname{adj} \tilde{G}}{|\operatorname{adj} \tilde{G}|^2}. \tag{A.14}$$

Therefore, $b_0 = ((\ell^*_n)^*)^{1/2}c_0$, and so

$$b_0 = \frac{(\ell^*_n)^{1/2} \operatorname{adj}((\ell^*_n)^{-1/2}\tilde{F})}{|\operatorname{adj}((\ell^*_n)^{-1/2}\tilde{F})|^2}. \tag{A.15}$$

Finally, $\operatorname{adj}((\ell^*_n)^{-1/2}\tilde{F}) = (\ell^*_n)^{1/2} \operatorname{adj} \tilde{F}$ since $\det(\ell^*_n) = 1$ and given the definition of adj in (3.1). This is the proof. □

Relating the metric and the step-length tensor

Proposition A.1.7 *The energy density W^e in (2.1) satisfies $W^e(F, Fn_0/|Fn_0|, n_0) = 0$ if and only if* $\det F = 1$ *and $F^TF = \ell_{n_0}$ for ℓ_{n_0} defined in (4.16). In addition, if these identities hold, then $Fn_0/|Fn_0| = Rn_0$ where $R \in SO(3)$ is the unique rotation associated with the polar decomposition of F.*

Proof. We first assume $W^e(F, Fn_0/|Fn_0|, n_0) = 0$. Then $\det F = 1$, $n_0 \in \mathbb{S}^2$ and $|Fn_0| \neq 0$. We set $n := Fn_0/|Fn_0| \in \mathbb{S}^2$ and observe from (2.3),

$$0 = W^e(F, Fn_0/|Fn_0|, n_0) = W_{nH}((\ell_n^f)^{-1/2} F (\ell_{n_0}^0)^{1/2}).$$

Thus, we deduce from Proposition A.1.4 that $(\ell_n^f)^{-1/2} F (\ell_{n_0}^0)^{1/2} = R$ for some $R \in SO(3)$. Evidently then,

$$F = (\ell_n^f)^{1/2} R (\ell_{n_0}^0)^{-1/2}. \tag{A.16}$$

Further,

$$\begin{aligned} r_f^{1/6} n = (\ell_n^f)^{-1/2} n &= (\ell_n^f)^{-1/2} \left(\frac{Fn_0}{|Fn_0|} \right) \\ &= (\ell_n^f)^{-1/2} \left(\frac{(\ell_n^f)^{1/2} R (\ell_{n_0}^0)^{-1/2} n_0}{|Fn_0|} \right) = r_0^{-1/6} \left(\frac{Rn_0}{|Fn_0|} \right). \end{aligned} \tag{A.17}$$

Here, we used the definition of n, the result in (A.16) and properties of the step-length tensors (2.4). Since both n and $Rn_0 \in \mathbb{S}^2$, it follows from this equality chain that actually $n = Rn_0$. Substituting this into (A.16) yields

$$F = R(\ell_{n_0}^f)^{1/2} R^T R (\ell_{n_0}^0)^{-1/2} = R(\ell_{n_0}^f)^{1/2} (\ell_{n_0}^0)^{-1/2} = R\ell_{n_0}^{1/2}, \tag{A.18}$$

noting that $(\ell_{Rn_0}^f)^{1/2} = R(\ell_{n_0}^f)^{1/2} R^T$ and $(\ell_{n_0}^f)^{1/2} (\ell_{n_0}^0)^{-1/2} = \ell_{n_0}^{1/2}$. Consequently, $F^TF = \ell_{n_0}$ as desired.

For the other direction, we assume $\det F = 1$ and $F^TF = \ell_{n_0}$. This implies $F = R\ell_{n_0}^{1/2}$ for some $R \in SO(3)$ and $n := Fn_0/|Fn_0| \in \mathbb{S}^2$. Thus,

$$n = \frac{Fn_0}{|Fn_0|} = \frac{R\ell_{n_0}^{1/2} n_0}{|Fn_0|} = r^{-1/6} \frac{Rn_0}{|Fn_0|}, \tag{A.19}$$

and since both n and $Rn_0 \in \mathbb{S}^2$, we deduce $n = Rn_0$. Then, by definition (2.1), $W^e(F, Fn_0/|Fn_0|, n_0 = W^e(F, Rn_0, n_0)$ and clearly this is finite. Further, given

(2.3), we find

$$\begin{aligned} W^e(F, Rn_0, n_0) &= W_{nH}((\ell^f_{Rn_0})^{-1/2} F (\ell^0_{n_0})^{1/2}) \\ &= W_{nH}(R(\ell^f_{n_0})^{-1/2} R^T R \ell^{1/2}_{n_0} (\ell^0_{n_0})^{1/2}) \\ &= W_{nH}(R(\ell^f_{n_0})^{-1/2} (\ell^f_{n_0})^{1/2} (\ell^0_{n_0})^{-1/2} (\ell^0_{n_0})^{1/2}) = W_{nH}(R). \end{aligned} \tag{A.20}$$

For this, we have exploited properties of the step-length tensors (see previous paragraph). Hence since $R \in SO(3)$, by Proposition A.1.4 we find $W_{nH}(R) = 0$ as desired.

Finally for the implication, we note that in the proof of both directions, we found $F = R\ell^{1/2}_{n_0}$ and $n = Rn_0$ for $R \in SO(3)$. Consequently, since $\ell^{1/2}_{n_0}$ is positive definite, R is actually the unique rotation in the polar decomposition of F. □

Proposition A.1.8 *Set $\widehat{W}(F, n, n_0) := (\mu/2)^{-1}(W^e(F, n, n_0) + W^{ni}(F, n, n_0))$ for W^e in (2.1) and W^{ni} in (2.8). $\widehat{W}$ is minimized (and equal to zero) if and only if*

$$\det F = 1, \quad F^T F = \ell_{n_0} \quad \text{and} \quad n = \sigma \frac{Fn_0}{|Fn_0|} \quad \text{for } \sigma \in \{-1, 1\}. \tag{A.21}$$

Proof. ($\Rightarrow$.) Given $\widehat{W} = 0$, $W^e = 0$ and $W^{ni} = 0$ since both are non-negative. The former equality implies $(\ell^f_n)^{-1/2} F (\ell^0_{n_0})^{1/2} = R \in SO(3)$ gives Proposition A.1.4. Hence, we observe that

$$\begin{aligned} W^{ni}(F, n, n_0) &= \frac{\mu\alpha}{2} r_f^{2/3} |(I_{3\times 3} - n_0 \otimes n_0) F^T (\ell^f_n)^{-1/2} n|^2 \\ &= \frac{\mu\alpha}{2} (r_0^{1/3} r_f^{2/3}) |(I_{3\times 3} - n_0 \otimes n_0)(\ell^0_{n_0})^{1/2} F^T (\ell^f_n)^{-1/2} n|^2 \\ &= \frac{\mu\alpha}{2} (r_0^{1/3} r_f^{2/3}) |(I_{3\times 3} - n_0 \otimes n_0) R^T n|^2, \end{aligned} \tag{A.22}$$

and this must vanish. Consequently, $n = \sigma R n_0 = \sigma F n_0 / |F n_0|$ for some $\sigma \in \{-1, 1\}$ (the latter equality follows from $R = (\ell^f_n)^{-1/2} F (\ell^0_{n_0})^{1/2}$). Thus by Proposition A.1.7, $\det F = 1$ and $F^T F = \ell_{n_0}$.

($\Leftarrow$.) Given (A.21), $W^e = 0$, $n = \sigma R n_0$ and $F = R(\ell_{n_0})^{1/2}$ by Proposition A.1.7. Thus with $(I_{3\times 3} - n_0 \otimes n_0)\ell^{1/2}_{n_0} = r^{1/6}(I_{3\times 3} - n_0 \otimes n_0)$, it is easy to see that W^{ni} also vanishes. This completes the proof. □

Proposition A.1.9 *If $\tilde{F} \in \mathbb{R}^{3\times 2}$ and $n_0 \in \mathbb{S}^2$ such that $\tilde{F}^T \tilde{F} = \tilde{\ell}_{n_0}$, then there exists a $b \in \mathbb{R}^3$ such that*

$$(\tilde{F}|b)^T (\tilde{F}|b) = \ell_{n_0}, \quad \det(\tilde{F}|b) = 1. \tag{A.23}$$

In particular,

$$
\begin{aligned}
b &= \bar{b}_1 \tilde{F}\tilde{e}_1 + \bar{b}_2 \tilde{F}\tilde{e}_2 + \bar{b}_3 (\tilde{F}\tilde{e}_1 \times \tilde{F}\tilde{e}_2), \\
\begin{pmatrix} \bar{b}_1 \\ \bar{b}_2 \end{pmatrix} &= (\tilde{\ell}_{n_0})^{-1} I_{2\times 3} \ell_{n_0} e_3, \quad \bar{b}_3 = \frac{1}{|\tilde{F}\tilde{e}_1 \times \tilde{F}\tilde{e}_2|^2}, \\
(\tilde{\ell}_{n_0})^{-1} &= \bar{r}^{1/3} \left(I_{2\times 2} + \left(\frac{1-\bar{r}}{1 + |\tilde{n}_0|^2(\bar{r}-1)} \right) \tilde{n}_0 \otimes \tilde{n}_0 \right)
\end{aligned}
\tag{A.24}
$$

for $\tilde{n}_0 = (n_0 \cdot e_1, n_0 \cdot e_2) \in B_1(0) \subset \mathbb{R}^2$.

Proof. We remark that $\det(\tilde{\ell}_{n_0}) = \bar{r}^{-2/3}(1 + (\bar{r}-1)|\tilde{n}_0|^2) > 0$ for $\bar{r} > 0$. Thus rank $\tilde{F} = 2$, since by hypothesis $\tilde{F}^T\tilde{F} = \tilde{\ell}_{n_0}$. Therefore, $\operatorname{span}\{\tilde{F}e_1, \tilde{F}e_2, \tilde{F}e_1 \times \tilde{F}e_2\} = \mathbb{R}^3$. Hence, (A.24) simply rewrites $b \in \mathbb{R}^3$ equivalently in terms of $(\bar{b}_1, \bar{b}_2, \bar{b}_3) \in \mathbb{R}^3$. The proof follows by explicitly verifying the formula.

To be explicit, we set

$$
b = (\tilde{F} | \tilde{F}\tilde{e}_1 \times \tilde{F}\tilde{e}_2)\bar{b} \tag{A.25}
$$

for some $\bar{b} \in \mathbb{R}^3$ and observe that

$$
\begin{aligned}
(\tilde{F}|b)^T b = \tilde{F}^T\tilde{F} \begin{pmatrix} \bar{\bar{b}} \\ 0 \end{pmatrix} + |b|^2 e_3 &= \begin{pmatrix} \tilde{\ell}_{n_0}\bar{\bar{b}} \\ \bar{b} \cdot \begin{pmatrix} \tilde{\ell}_{n_0} & 0 \\ 0 & |\tilde{F}\tilde{e}_1 \times \tilde{F}\tilde{e}_2|^2 \end{pmatrix} \bar{b} \end{pmatrix} \\
&= \begin{pmatrix} \tilde{\ell}_{n_0}\bar{\bar{b}} \\ \bar{\bar{b}} \cdot \tilde{\ell}_{n_0}\bar{\bar{b}} + (\bar{b} \cdot e_3)^2 |\tilde{F}\tilde{e}_1 \times \tilde{F}\tilde{e}_2|^2 \end{pmatrix}
\end{aligned}
\tag{A.26}
$$

Note that given $\tilde{F}^T\tilde{F} = \tilde{\ell}_{n_0}$, $(\tilde{F}|b)^T(\tilde{F}|b) = \ell_{n_0}$ if and only if $(\tilde{F}|b)^T b = \ell_{n_0} e_3$. Thus clearly, we require $\bar{\bar{b}} = (\tilde{\ell}_{n_0})^{-1} I_{2\times 3} \ell_{n_0} e_3$, as we have denoted above in (A.24). Moreover,

$$
\det(\tilde{F}|b) = 1 \quad \Rightarrow b \cdot (\tilde{F}\tilde{e}_1 \times \tilde{F}\tilde{e}_2) = (\bar{b} \cdot e_3)|\tilde{F}\tilde{e}_1 \times \tilde{F}\tilde{e}_2|^2 = 1. \tag{A.27}
$$

Thus, we also require that

$$
\bar{b} \cdot e_3 = \frac{1}{|\tilde{F}\tilde{e}_1 \times \tilde{F}\tilde{e}_2|^2} = \frac{1}{|\tilde{F}\tilde{e}_1|^2 |\tilde{F}\tilde{e}_2|^2 - (\tilde{F}\tilde{e}_1 \cdot \tilde{F}\tilde{e}_2)^2} = \frac{1}{\det \tilde{\ell}_{n_0}}. \tag{A.28}
$$

as, again, we have denoted above with (A.24).

Now, notice that we have solved for $\bar{b}$, and but we still require

$$
e_3 \cdot \ell_{n_0} e_3 = \bar{\bar{b}} \cdot \tilde{\ell}_{n_0}\bar{\bar{b}} + (\bar{b} \cdot e_3)^2 |\tilde{F}\tilde{e}_1 \times \tilde{F}\tilde{e}_2|^2 \tag{A.29}
$$

for the lemma to hold. This would appear to be very bad, but in fact, this equality holds trivially. Indeed,

$$e_3 \cdot \ell_{n_0} e_3 = \bar{r}^{1/3}(1 + (\bar{r} - 1)(n_0 \cdot e_3)^2). \tag{A.30}$$

For the other side, after some algebra, one eventually finds that

$$\tilde{\bar{b}} \cdot \tilde{\ell}_{n_0} \tilde{\bar{b}} + (\bar{b} \cdot e_3)^2 |\tilde{F}\tilde{e}_1 \times \tilde{F}\tilde{e}_2|^2 = \bar{r}^{-1/3} \left(\frac{|\tilde{n}_0|^2 (n_0 \cdot e_3)^2 (\bar{r} - 1)^2 + \bar{r}}{1 + |\tilde{n}_0|^2 (\bar{r} - 1)} \right) \tag{A.31}$$

using all of these relations for $\bar{b}$. Using the fact that $|\tilde{n}_0|^2 + (n_0 \cdot e_3)^2 = 1$, it is easy to show that (A.30) equals (A.31). □

Proposition A.1.10 *Let $\tilde{F} \in \mathbb{R}^{3\times 2}$ and $n_0 \in \mathbb{S}^2$. Then,*

$$(\tilde{F})^T \tilde{F} = \tilde{\ell}_{n_0} \quad \Leftrightarrow \quad \tilde{F} = R(\ell_{n_0}^{1/2})_{3\times 2} \quad \text{for some } R \in SO(3). \tag{A.32}$$

Here, $\tilde{\ell}_{n_0} = \bar{r}^{-1/3}(I_{2\times 2} + (\bar{r} - 1)\tilde{n}_0 \otimes \tilde{n}_0)$ and $(\ell_{n_0}^{1/2})_{3\times 2} = \bar{r}^{-1/6}(I_{3\times 2} + (\bar{r}^{1/2} - 1)n_0 \otimes \tilde{n}_0)$.

Proof. ($\Leftarrow$.) This is obviously true. ($\Rightarrow$.) Since $(\tilde{F})^T \tilde{F} = \tilde{\ell}_{n_0}$, we can find a b such that $(\tilde{F}|b)^T(\tilde{F}|b) = \ell_{n_0}$ and $\det(\tilde{F}|b) = 1$. Further, owing to the positivity of the determinant here, by the polar decomposition theorem there exists a unique $R \in SO(3)$ and a unique $U \in \mathbb{R}^{3\times 3}$ positive-definite such that $(\tilde{F}|b) = RU$. Given the metric condition, we have that $U^2 = \ell_{n_0}$, and so actually $U = \ell_{n_0}^{1/2}$. Consequently,

$$(\tilde{F}|b) = R\ell_{n_0}^{1/2} = (R(\ell_{n_0}^{1/2})_{3\times 2} | R\ell_{n_0}^{1/2} e_3), \tag{A.33}$$

and so $\tilde{F} = R(\ell_{n_0}^{1/2})_{3\times 2}$ for some $R \in SO(3)$. □

A.2 On the two-dimensional theories for monodomain sheets

In both the effective membrane theory for nematic elastomers and the Koiter theory, the deformation is taken as a mapping from an isotropic reference configuration. We now show that theories can be equivalently written with respect to the monodomain reference configuration (as long as the director in the monodomain sample is in the plane of the sheet).

For this, we consider an initial monodomain nematic elastomer sheet Ω_h of thickness $h \ll 1$ and reference director $n_0 \in \mathbb{S}^2$ that is subject to a deformation $y^h \colon \Omega \to \mathbb{R}^3$ and deformed director $n^h \colon \Omega_h \to \mathbb{S}^2$. The free energy is given by

$$\mathcal{E}_{n_0}^h(y^h, n^h) := \int_\Omega \left(W^e(\nabla y^h, n^h, n_0) + \frac{\kappa}{2} |(\nabla n^h)(\operatorname{cof} \nabla y^h)^T|^2 \right) dx \tag{A.34}$$

where we assume the non-ideal parameter $\alpha = 0$ (recall the discussion in Chapter 2).

To derive the membrane theory, we rescale the deformation and director to study sequences on a fix domain Ω exactly as in Section 3.3, and we consider the energy

$$\tilde{\mathcal{I}}^h_{n_0}(w^h, m^h) = \begin{cases} \int_\Omega \left(W^e(\nabla_h w^h, m^h, n_0) + \frac{\kappa_h}{h^2} |(\nabla m^h)(\mathrm{cof}\nabla w^h)^T|^2 \right) dz & \text{if } (w^h, m^h) \in \mathcal{A} \\ +\infty & \text{else.} \end{cases} \tag{A.35}$$

Here, the admissible class $\mathcal{A}$ is given by

$$\begin{aligned} \mathcal{A} := \{ (w^h, m^h) \in W^{1,2}(\Omega, \mathbb{R}^3) \times W^{1,2}(\Omega, \mathbb{S}^2) \\ \text{such that} \quad (\nabla m^h)(\mathrm{cof}\nabla w^h)^T \in L^2(\Omega, \mathbb{R}^3) \Big\}. \end{aligned} \tag{A.36}$$

Finally, we study the functional defined on $W^{1,2}(\Omega, \mathbb{R}^3)$ given by

$$\mathcal{I}^h_{n_0}(w^h) := \inf \left\{ \tilde{\mathcal{I}}^h_{n_0}(w^h, m^h) \colon m^h \in W^{1,2}(\Omega, \mathbb{S}^2) \right\}. \tag{A.37}$$

Theorem A.2.1 *Let $r_f = r_0 = r$. Let $\mathcal{I}^h_{n_0}$ as above with $n_0 \in \mathbb{S}^2$ such that $n_0 \cdot e_3 = 0$, $\kappa_h \geq 0$ and $\kappa_h \to 0$ as $h \to 0$. Then in the weak topology of $W^{1,2}(\Omega, \mathbb{R}^3)$, $\mathcal{I}^h_{n_0}$ is equicoercive and Γ-converges to*

$$\mathcal{I}_{n_0}(y) := \begin{cases} \int_\omega W^{qc}_{2D}(\tilde{\nabla} y (\tilde{\ell}^*_{n_0})^{1/2}) d\tilde{z} & \text{if } \partial_3 y = 0 \text{ a.e.} \\ +\infty & \text{otherwise.} \end{cases} \tag{A.38}$$

Here, $(\tilde{\ell}^*_{n_0})^{1/2} = r^{-1/6}(I_{2\times 2} + (r^{1/2} - 1)\tilde{n}_0 \otimes \tilde{n}_0)$.

Proof. Compactness. Let $\{w^h\} \subset W^{1,2}(\Omega, \mathbb{R}^3)$ such that $\mathcal{I}^h_{n_0}(w^h) \leq C$ for some C independent of h. We let $\zeta = (\ell^*_{n_0})^{-1/2} z$ and defined for each w^h the function $w^h_{iso} \in W^{1,2}((\ell^*_{n_0})^{-1/2}\Omega, \mathbb{R}^3)$ given by

$$w^h_{iso}(\zeta) = w^h((\ell^*_{n_0})^{1/2}\zeta), \quad \zeta \in (\ell^*_{n_0})^{-1/2}\Omega \tag{A.39}$$

for $(\ell^*_{n_0})^{1/2} = r^{-1/6}(I_{3\times 3} + (r^{1/2} - 1)n_0 \otimes n_0)$. Hence, we observe via the chain rule

$$\begin{aligned} \nabla_h w^h_{iso}(\zeta) &= \left(\tilde{\nabla} w^h_{iso}(\zeta) | \frac{1}{h} \partial_3 w^h_{iso}(\zeta) \right) \\ &= \left(\nabla w^h((\ell^*_{n_0})^{1/2}\zeta) \left((\ell^*_{n_0})^{1/2} e_1 | (\ell^*_{n_0})^{1/2} e_2 \right) \middle| \frac{1}{h} \nabla w^h((\ell^*_{n_0})^{-1/2}\zeta) r^{1/6} e_3 \right) \\ &= \left(\tilde{\nabla} w^h((\ell^*_{n_0})^{1/2}\zeta)(\tilde{\ell}^*_{n_0})^{1/2} \middle| \frac{r^{-1/6}}{h} \partial_3 w^h((\ell^*_{n_0})^{-1/2}\zeta) \right) \\ &= \nabla_h w^h((\ell^*_{n_0})^{1/2}\zeta)(\ell^*_{n_0})^{1/2} \end{aligned} \tag{A.40}$$

almost everywhere. Here, we are using the fact that $n_0 \cdot e_3 = 0$. Hence,

$$\begin{aligned}
\mathcal{I}^h_{n_0}(w^h) &\geq \frac{1}{h}\int_\Omega \inf_{n\in\mathbb{S}^2} W^e(\nabla_h w^h(z), n, n_0)dz \\
&= \frac{1}{h}\int_{(\ell^*_{n_0})^{-1/2}\Omega} \inf_{n\in\mathbb{S}^2} W_{nH}\Big((\ell^*_n)^{-1/2}\nabla_h w^h((\ell^*_{n_0})^{1/2}\zeta)(\ell^*_{n_0})^{1/2}\Big)d\zeta \\
&= \frac{1}{h}\int_{(\ell^*_{n_0})^{-1/2}\Omega} \inf_{n\in\mathbb{S}^2} W_{nH}\Big((\ell^*_n)^{-1/2}\nabla_h w^h_{iso}(\zeta)\Big)d\zeta \\
&= \frac{1}{h}\int_{(\ell^*_{n_0})^{-1/2}\Omega} \inf_{n\in\mathbb{S}^2} W^e_{iso}(\nabla_h w^h_{iso}(\zeta), n)d\zeta = \mathcal{I}^h_{\kappa=0}(w^h_{iso}).
\end{aligned} \tag{A.41}$$

Thus, from the compactness result of Conti and Dozlmann [31], we conclude that there is a $y_{iso} \in W^{1,2}((\ell^*_{n_0})^{-1/2}\Omega, \mathbb{R}^3)$ indepedent of z_3 such that $(w^h_{iso} - \fint w^h_{iso}d\zeta) \rightharpoonup y_{iso}$ in $W^{1,2}((\ell^*_{n_0})^{-1/2}\Omega, \mathbb{R}^3)$. It follows that $(w^h - \fint w^h) \rightharpoonup y$ in $W^{1,2}(\Omega, \mathbb{R}^3)$ with

$$\tilde{\nabla} y(z) = \tilde{\nabla} y_{iso}((\ell^*_{n_0})^{-1/2}z)(\tilde{\ell}^*_{n_0})^{-1/2} \quad \text{a.e. } z \in \Omega, \tag{A.42}$$

and further that y is independent of z_3 since $n_0 \cdot e_3 = 0$.

Lower bound. We may assume $w^h \rightharpoonup y$ in $W^{1,2}(\Omega, \mathbb{R}^3)$ for some y independent of z_3. Set $w^h_{iso} \in W^{1,2}((\ell^*_{n_0})^{-1/2}\Omega, \mathbb{R}^3)$ as in (A.39). Since $n_0 \cdot e_3 = 0$, we have $w^h_{iso} \rightharpoonup y_{iso}$ in $W^{1,2}((\ell^*_{n_0})^{-1/2}\Omega, \mathbb{R}^3)$ where $y_{iso}(\zeta) = y((\ell^*_{n_0})^{1/2}\zeta)$ for a.e. ζ. (This is also independent of η_3 since $n_0 \cdot e_3 = 0$.) By the lower bound result of Conti and Dozlmann [31] and using the results above in (A.41), we have

$$\begin{aligned}
\liminf_{h\to 0} \mathcal{I}^h_{n_0}(w^h) &\geq \liminf_{h\to 0} \mathcal{I}^h_{\kappa=0}(w^h_{iso}) \\
&\geq \int_{(\ell^*_{n_0})^{-1/2}\Omega} W^{qc}_{2D}\Big(\tilde{\nabla} y_{iso}(\zeta)\Big)d\zeta = \int_\Omega W^{qc}_{2D}\Big(\tilde{\nabla} y_{iso}((\ell^*_{n_0})^{-1/2}z)\Big)dz \\
&= \int_\Omega W^{qc}_{2D}\Big(\tilde{\nabla} y(z)(\tilde{\ell}^*_{n_0})^{1/2}\Big)dz = \int_\omega W^{qc}_{2D}\Big(\tilde{\nabla} y(\tilde{z})(\tilde{\ell}^*_{n_0})^{1/2}\Big)d\tilde{z}.
\end{aligned} \tag{A.43}$$

The second to last equality uses (A.42) and the last uses that y is independent of z_3.

Upper bound. Let $y \in W^{1,2}(\Omega, \mathbb{R}^3)$ independent of z_3. We set $y_{iso}(\zeta) = y((\ell^*_{n_0})^{1/2}\zeta)$. This is independent of ζ_3 since $n_0 \cdot e_3 = 0$. Thus, there exists a sequence $\{(w^h_{iso}, m^h_{iso})\} \in C^\infty((\ell^*_{n_0})^{-1/2}\overline{\Omega}, \mathbb{R}^3) \times C^1((\ell^*_{n_0})^{-1/2}\overline{\Omega}, \mathbb{S}^2)$ as in Proposition 3.3.4. In particular, $w^h_{iso} \rightharpoonup y_{iso}$ in $W^{1,2}((\ell^*_{n_0})^{-1/2}\Omega, \mathbb{R}^3)$. Further, we set $w^h(z) =$

$w^h_{iso}((\ell^*_{n_0})^{-1/2}z)$ and $m^h(z) = m^h_{iso}((\ell^*_{n_0})^{-1/2}z)$ for each $z \in \Omega$, and find

$$\begin{aligned}
&\limsup_{h\to 0} \mathcal{I}^h_{n_0}(w^h, m^h) \\
&\quad = \limsup_{h\to 0} \left(\int_{(\ell^*_{n_0})^{-1/2}\Omega} \left(W^e_{iso}(\nabla_h w^h_{iso}, n^h_{iso}) + \frac{\kappa_h}{h^2} |(\nabla m^h_{iso})(\operatorname{cof} \nabla w^h_{iso})^T|^2 \right) d\zeta \right) \\
&\quad \leq \int_{(\ell^*_{n_0})^{-1/2}\Omega} W^{qc}_{2D}(\tilde{\nabla} y_{iso}) d\zeta = \int_{\omega} W^{qc}_{2D}(\tilde{\nabla} y (\tilde{\ell}^*_{n_0})^{1/2}) d\tilde{z}.
\end{aligned} \tag{A.44}$$

It is also easy to see that $w^h \rightharpoonup y$ in $W^{1,2}(\Omega, \mathbb{R}^3)$. This completes the proof. □

Remark A.2.2 *(i) Let us discuss some heuristics of this theory: Suppose we have a monodomain sample with the director $n_0 = e_1$, and we wish to stretch it along this direction. Before stretching $\tilde{\nabla} y = I_{3\times 2}$, but $W^{qc}_{2D}(\cdot)$ lies on the energy landscape at $(\lambda_M, \delta) = (r^{1/3}, r^{1/6})$ in Figure 3.2. Thus, if we stretch along the e_1 direction, we immediately belong in a regime of stress. In other words, this membrane is not exhibiting soft elasticity. This is exactly what one should expect since the director is already aligned with the direction of stretch, and since director reorientation is the cause of soft elasticity.*

(ii) The proof of this theorem relies on the ability for us to map the monodomain energy back to the isotropic energy in the Γ-convergence setting. In particular, it was important for the proof that $n_0 \cdot e_3 = 0$. Indeed, the $h-$dependence of the chain rule does not decouple nicely as in (A.40) if the director tilts out-of-plane, and our proof relied on this decoupling. To our knowledge, the effective membrane theory in the case where the director tilts is open.

(iii) A similar argument can be done for the Koiter theory. Working out the details, if we have an undeformed monodomain configuration Ω_h and an isotropic reference configuration $(\ell^*_{n_0})^{-1/2}\Omega_h$, we can repeat some of the arguments to derive the Koiter theory to obtain a deformation $y^h_k \colon (\ell^*_{n_0})^{-1/2}\Omega_h \to \mathbb{R}^3$ (deformed from the isotropic configuration) which satisfies

$$\begin{aligned}
\mathcal{E}^h_{3D}(y^h_k) &\approx \int_{(\ell^*_{n_0})^{-1/2}\Omega_h} \left(W_{ps}(\tilde{\nabla} y_k(\chi)) + 2\mu r^{1/3} \chi_3^2 |\operatorname{II}_{y_k}(\chi)|^2 \right) d\chi \\
&= \int_{\Omega_h} \left(W_{ps}(\tilde{\nabla} y_k((\ell^*_{n_0})^{-1/2}x)) + 2\mu r^{1/3} (r^{1/6}x_3)^2 |\operatorname{II}_{y_k}((\ell^*_{n_0})^{-1/2}x)|^2 \right) dx
\end{aligned} \tag{A.45}$$

for some tension wrinkling ansatz y_k independent of χ_3 which is a deformation from the isotropic reference midplane. Here, we have set $\chi = (\ell^*_{n_0})^{-1/2}x$. Now,

we let $y_k^m(x) = y_k((\ell_{n_0}^*)^{-1/2}x)$ *for all* $x \in \Omega_h$*, and we see that*

$$\begin{aligned}
&\tilde{\nabla} y_k((\ell_{n_0}^*)^{-1/2}x) = \tilde{\nabla} y_k^m(x)(\tilde{\ell}_{n_0}^*)^{1/2},\\
&\mathrm{II}_{y_k}\left((\ell_{n_0}^*)^{-1/2}x\right) = (\tilde{\nabla} y_k((\ell_{n_0}^*)^{-1/2}x))^T\tilde{\nabla}\left(\frac{\operatorname{adj}\tilde{\nabla} y_k((\ell_{n_0}^*)^{-1/2}x)}{|\operatorname{adj}\tilde{\nabla} y_k((\ell_{n_0}^*)^{-1/2}x)|}\right)\\
&\qquad = (\tilde{\ell}_{n_0}^*)^{1/2}(\tilde{\nabla} y_k^m(x))^T\tilde{\nabla}\left(\frac{\operatorname{adj}\tilde{\nabla} y_k^m(x)\det((\tilde{\ell}_{n_0}^*)^{1/2})}{|\operatorname{adj}\tilde{\nabla} y_k^m(x)\det((\tilde{\ell}_{n_0}^*)^{1/2})|}\right)\\
&\qquad = (\tilde{\ell}_{n_0}^*)^{1/2}\,\mathrm{II}_{y_k^m}(x).
\end{aligned} \tag{A.46}$$

Consequently, we have

$$\begin{aligned}
\mathcal{E}_{3D}^h(y_k^h) &\approx \int_{\Omega_h}\Big(W_{ps}(\tilde{\nabla} y_k^m(x)(\tilde{\ell}_{n_0}^*)^{1/2}) + \frac{\mu r^{2/3}}{2}x_3^2|(\tilde{\ell}_{n_0}^*)^{1/2}\,\mathrm{II}_{y_k^m}(x)|^2\Big)dx\\
&= h\int_{\omega}\Big(W_{ps}(\tilde{\nabla} y_k^m(\tilde{x})(\tilde{\ell}_{n_0}^*)^{1/2}) + \frac{\mu r^{2/3}}{6}|(\tilde{\ell}_{n_0}^*)^{1/2}\,\mathrm{II}_{y_k^m}(\tilde{x})|^2\Big)d\tilde{x},
\end{aligned} \tag{A.47}$$

where the equality uses that y_k^m *is independent of* x_3*. Finally, we can relate the deformation* y_k^h *back to a deformation deformed from the monodomain reference* Ω_h *via the identical change of variables. Hence,*

$$\mathcal{E}_{K,n_0}^h(y) := h\int_{\omega}\Big(W_{ps}(\tilde{\nabla} y(\tilde{\ell}_{n_0}^*)^{1/2}) + \frac{\mu r^{2/3}h^2}{6}|(\tilde{\ell}_{n_0}^*)^{1/2}\,\mathrm{II}_y\,|^2\Big)d\tilde{x} \tag{A.48}$$

is the appropriate Koiter theory for taut membranes using the undeformed monodomain sample as the reference as long as $n_0 \cdot e_3 = 0$*.*

A.3 Nonisometric origami: Three-faced interior junctions

On three-faced interior junctions (Formulation)

Let $\omega = B_1(0) \subset \mathbb{R}^2$ (i.e., the ball of radius 1 centered at the origin). For any vector $\tilde{t}_{\alpha\beta} \in \mathbb{S}^1$, we set $I_{\alpha\beta} := \{\delta\tilde{t}_{\alpha\beta} \in \mathbb{R}^2 \colon \delta \in [0,1]\}$, and define each $\omega_\alpha \subset \omega$ as

$$\begin{aligned}
\omega_1 &:= \text{sector between } \{I_{12}, I_{13}\} \text{ not containing } I_{23},\\
\omega_2 &:= \text{sector between } \{I_{12}, I_{23}\} \text{ not containing } I_{13},\\
\omega_3 &:= \text{sector between } \{I_{23}, I_{13}\} \text{ not containing } I_{12},
\end{aligned} \tag{A.49}$$

for some collection of distinct $\tilde{t}_{12}, \tilde{t}_{13}$ and $\tilde{t}_{23} \in \mathbb{S}^1$ (to be determined). Hence, (up to a set of measure zero), $\omega = \cup_{\alpha=1,2,3}\omega_\alpha = B_1(0)$ and each ω_α is non-empty with $\omega_\alpha \cap \omega_\beta = \emptyset$ for $\alpha \neq \beta$.

With the notation set, we envision that a fixed set of three distinct (and non-trivial) planar directors is used to program the sheet, i.e.,

$$\begin{aligned} \{n_{01}, n_{02}, n_{03}\} \equiv \{\tilde{n}_{01}, \tilde{n}_{02}, \tilde{n}_{03}\} \quad \text{is fixed} \\ \text{with} \quad n_{0\alpha} \neq \pm n_{0\beta} \quad \text{for all } \alpha \neq \beta. \end{aligned} \tag{A.50}$$

Here, each $n_{0\alpha}$ is programmed in the (to be determined) region ω_α. Hence, we are interested in identifying *all* possible compatible three-faced interior junctions that can be built from this set of directors. Note that from (4.203), we have a compatible junction if and only if there exist $\tilde{t}_{12}, \tilde{t}_{13}, \tilde{t}_{23} \in \mathbb{S}^1$ and $R_1, R_2, R_3 \in SO(3)$ such that

$$\begin{aligned} R_1(\ell^{1/2}_{n_{01}})_{3\times 2}\tilde{t}_{12} &= R_2(\ell^{1/2}_{n_{02}})_{3\times 2}\tilde{t}_{12}, \\ R_2(\ell^{1/2}_{n_{02}})_{3\times 2}\tilde{t}_{23} &= R_3(\ell^{1/2}_{n_{03}})_{3\times 2}\tilde{t}_{23}, \\ R_1(\ell^{1/2}_{n_{01}})_{3\times 2}\tilde{t}_{13} &= R_3(\ell^{1/2}_{n_{03}})_{3\times 2}\tilde{t}_{23}. \end{aligned} \tag{A.51}$$

Note further that the regions ω_1, ω_2 and ω_3 are set by the $g_{\alpha\beta}$'s procedurally by (A.49).

Now to classify all possible compatible three-faced junctions (up to a rigid body rotation of the entire junction and choice of coordinate frame), we are not required to consider all possible sets of directors as in (A.50). In fact:

Remark A.3.1 *(i) By choosing a coordinate frame, we may assume $n_{01} = e_1$.*

(ii) Since we are only interested in classification up to a rigid body rotation, we may assume $R_1 = I_{3\times 3}$.

(iii) Define $\theta_{12}, \theta_{13} \in (0, \pi)$ such that $n_{01} \cdot n_{02} = \cos(\theta_{12})$ and $n_{01} \cdot n_{03} = \cos(\theta_{13})$. We may assume that both of these angles are acute, i.e., $\theta_{12}, \theta_{13} \in (0, \pi/2]$.

(iv) Finally, we may assume $n_{02} = \cos(\theta_{12})e_1 + \sin(\theta_{12})e_2$ and $n_{03} = \cos(\theta_{13})e_1 - \sin(\theta_{13})e_2$.

In this remark, (i) and (ii) are immediate. For (iii):

Proof of Remark A.3.1(iii). Fix a set of directors as in (A.50) and suppose $n_{01} \cdot n_{02} = \cos(\theta_{12})$ for $\theta_{12} \in (\pi/2, \pi)$. Note that if there exist $\tilde{t}_{12}, \tilde{t}_{23}, \tilde{t}_{13} \in \mathbb{S}^1$ and $R_1, R_2, R_3 \in SO(3)$ such that (A.51) holds, then (A.51) also holds with the same set of interfaces and rotation if we replace n_{02} with $-n_{02}$ since $(\ell^{1/2}_{n_{02}})_{3\times 2} = (\ell^{1/2}_{-n_{02}})_{3\times 2}$. Thus for generating compatible geometries, the sets of directors $\{n_{01}, n_{02}, n_{03}\}$ and $\{n_{01}, -n_{02}, n_{03}\}$ are equivalent. The only difference in comparing the latter to the

former is that we have $n_{01} \cdot (-n_{02}) = -\cos(\theta_{12}) = \cos(\pi - \theta_{12})$ with $\pi - \theta_{12} \in (0, \pi/2)$. That is, for compatible geometries, we now have an equivalent set of directors where the angle between n_{01} and $-n_{02} = n_{02}^{eq} \equiv n_{02}$ is acute. The same argument works for n_{03}. □

Now, Remark A.3.1(iv) follows after (possibly/as needed) changing the coordinate frame and (possibly/as needed) relabeling the director fields (which implicitly relabels the interfaces, rotations and regions ω_α).

As a consequence of this remark, instead of considering an arbitrary set (A.50) and attempting to find all possible interfaces and rotations which satisfy (A.51), we may restrict our attention to the sets

$$\begin{aligned} &\{e_1, n_{02}, n_{03}\} \quad \text{where:} \\ &\quad n_{02} = \cos(\theta_{12})e_1 + \sin(\theta_{12})e_2 \quad \text{for some } \theta_{12} \in (0, \pi/2], \\ &\quad n_{03} = \cos(\theta_{13})e_1 - \sin(\theta_{13})e_2 \quad \text{for some } \theta_{13} \in (0, \pi/2). \end{aligned} \tag{A.52}$$

This set is parameterized by only two acute angles. Hence it remains to classify the $\tilde{t}_{12}, \tilde{t}_{23}, \tilde{t}_{13} \in \mathbb{S}^1$ and the $R_2, R_3 \in SO(3)$ such that

$$\begin{aligned} &(\ell^{1/2}_{e_1})_{3\times 2}\tilde{t}_{12} = R_2(\ell^{1/2}_{n_{02}})_{3\times 2}\tilde{t}_{12}, \\ &R_2(\ell^{1/2}_{n_{02}})_{3\times 2}\tilde{t}_{23} = R_3(\ell^{1/2}_{n_{03}})_{3\times 2}\tilde{t}_{23}, \\ &(\ell^{1/2}_{e_1})_{3\times 2}\tilde{t}_{13} = R_3(\ell^{1/2}_{n_{03}})_{3\times 2}\tilde{t}_{13} \end{aligned} \tag{A.53}$$

for any set as in (A.52).

On three-faced interior junctions (Necessary condition)

We turn now to the necessary condition (4.204). Suppose a set of directors as in (A.52). Then we need to ensure $\tilde{t}_{12}, \tilde{t}_{13}$ and $\tilde{t}_{23} \in \mathbb{S}^1$ satisfy

$$|\tilde{e}_1 \cdot \tilde{t}_{12}| = |\tilde{n}_{02} \cdot \tilde{t}_{12}|, \quad |\tilde{e}_1 \cdot \tilde{t}_{13}| = |\tilde{n}_{03} \cdot \tilde{t}_{13}|, \quad |\tilde{n}_{02} \cdot \tilde{t}_{23}| = |\tilde{n}_{03} \cdot \tilde{t}_{23}| \tag{A.54}$$

for a compatible three-faced junction. In this direction, we have that:

Proposition A.3.2 *$\tilde{t}_{12}, \tilde{t}_{13}$ and $\tilde{t}_{23} \in \mathbb{S}^1$ satisfy (A.54) if and only if $\tilde{t}_{12} \in \mathcal{G}_{12}$, $\tilde{t}_{13} \in \mathcal{G}_{13}$ and $\tilde{t}_{23} \in \mathcal{G}_{23}$, where*

$$\begin{aligned} \mathcal{G}_{12} &:= \Big\{ \frac{\tilde{e}_1 + \tilde{n}_{02}}{|\tilde{e}_1 + \tilde{n}_{02}|}, \frac{\tilde{e}_1 - \tilde{n}_{02}}{|\tilde{e}_1 - \tilde{n}_{02}|}, \frac{\tilde{n}_{02} - \tilde{e}_1}{|\tilde{e}_1 - \tilde{n}_{02}|}, \frac{-(\tilde{e}_1 + \tilde{n}_{02}}{|\tilde{e}_1 + \tilde{n}_{02}|} \Big\}, \\ \mathcal{G}_{13} &:= \Big\{ \frac{\tilde{e}_1 + \tilde{n}_{03}}{|\tilde{e}_1 + \tilde{n}_{03}|}, \frac{\tilde{e}_1 - \tilde{n}_{03}}{|\tilde{e}_1 - \tilde{n}_{03}|}, \frac{\tilde{n}_{03} - \tilde{e}_1}{|\tilde{e}_1 - \tilde{n}_{03}|}, \frac{-(\tilde{e}_1 + \tilde{n}_{03})}{|\tilde{e}_1 + \tilde{n}_{03}|} \Big\}, \\ \mathcal{G}_{23} &:= \Big\{ \frac{\tilde{n}_{02} + \tilde{n}_{03}}{|\tilde{n}_{02} + \tilde{n}_{03}|}, \frac{\tilde{n}_{02} - \tilde{n}_{03}}{|\tilde{n}_{02} - \tilde{n}_{03}|}, \frac{\tilde{n}_{03} - \tilde{n}_{02}}{|\tilde{n}_{02} - \tilde{n}_{03}|}, \frac{-(\tilde{n}_{02} + \tilde{n}_{03})}{|\tilde{n}_{02} + \tilde{n}_{03}|} \Big\}. \end{aligned} \tag{A.55}$$

Proof. Since $\{\tilde{e}_1, \tilde{n}_{02}\}$ are linearly independent by assumption, any $\tilde{t}_{12} \in \mathbb{R}^2$ can be written as $\tilde{t}_{12} = \kappa_1 e_1 + \kappa_2 n_{02}$. Observe then that $(\tilde{t}_{12} \cdot \tilde{e}_1)^2 = \kappa_1^2 + 2\kappa_1\kappa_2(\tilde{n}_{02} \cdot \tilde{e}_1) + \kappa_2^2(\tilde{n}_{02} \cdot \tilde{e}_1)^2$ and $(\tilde{t}_{12} \cdot \tilde{n}_{02})^2 = \kappa_1^2(\tilde{n}_{02} \cdot \tilde{e}_1)^2 + 2\kappa_1\kappa_2(\tilde{n}_{02} \cdot \tilde{e}_1) + \kappa_2^2$ since $\tilde{e}_1$ and $\tilde{n}_{02}$ are unit vectors. Thus,

$$(\tilde{t}_{12} \cdot \tilde{e}_1)^2 - (\tilde{t}_{12} \cdot \tilde{n}_{02})^2 = (\kappa_1^2 - \kappa_2^2)(1 - (\tilde{n}_{02} \cdot \tilde{e}_1)^2). \tag{A.56}$$

Further, $(\tilde{n}_{02} \cdot e_1)^2 = \cos(\theta_{12})^2 < 1$ by definition. Hence, $|\tilde{n}_{02} \cdot \tilde{t}_{12}| = |\tilde{e}_1 \cdot \tilde{t}_{12}|$ if and only if $\kappa_1^2 = \kappa_2^2$ from (A.56). Restricting $\tilde{t}_{12}$ to be a unit vector, we deduce that $|\tilde{n}_{02} \cdot \tilde{t}_{12}| = |\tilde{e}_1 \cdot \tilde{t}_{12}|$ if and only if $\tilde{t}_{12} \in \mathcal{G}_{12}$. We repeat this argument for the other relations. □

Remark A.3.3 *(i) (A generic redundancy.) This proposition provides that there are at most* 64 *possible compatible interfaces for the given collection (A.52). However, at least* 32 *are redundant in the following sense: Consider any set* $\{\tilde{t}_{12}, \tilde{t}_{13}, \tilde{t}_{23}\} \subset \mathcal{G}_{12} \times \mathcal{G}_{13} \times \mathcal{G}_{23}$*. Observe that,*

$$\tilde{R}_\pi \tilde{e}_1 = -\tilde{e}_1, \quad \tilde{R}_\pi \tilde{n}_{02} = -\tilde{n}_{02}, \quad \tilde{R}_\pi \tilde{n}_{03} = -\tilde{n}_{03}, \tag{A.57}$$

where $\tilde{R}_\pi \in SO(2)$ *denotes a rotation by* π*. Thus,*

$$\tilde{R}_\pi \tilde{t}_{12} \in \mathcal{G}_{12}, \quad \tilde{R}_\pi \tilde{t}_{13} \in \mathcal{G}_{13}, \quad \tilde{R}_\pi \tilde{t}_{23} \in \mathcal{G}_{23}. \tag{A.58}$$

Hence, by rigidly rotating our (possibly) compatible junction by π*, we obtain an identical junction using that the directors are invariant under a change of sign. We can eliminate this redundancy by replacing* $\mathcal{G}_{12}$ *with*

$$\mathcal{G}_{12}^* := \Big\{ \frac{\tilde{e}_1 + \tilde{n}_{02}}{|\tilde{e}_1 + \tilde{n}_{02}|}, \frac{\tilde{e}_1 - \tilde{n}_{02}}{|\tilde{e}_1 - \tilde{n}_{02}|} \Big\}. \tag{A.59}$$

(ii) (The case $\theta_{12} = \theta_{13}$*.) Of the* 64 *possible compatible junctions, in this case, only* 20 *are not redundant due to additional reflection reflection symmetry. Specifically, let* $\tilde{Q}^{ref} = diag(1, -1) \in O(2)$*, and notice that* $\tilde{Q}^{ref} \tilde{n}_{02} = \tilde{n}_{03}$*. Hence, if* $\{\tilde{t}_{12}, \tilde{t}_{13}, \tilde{t}_{23}\} \subset \mathcal{G}_{12} \times \mathcal{G}_{13} \times \mathcal{G}_{23}$ *in this case, then*

$$\tilde{Q}^{ref} \tilde{t}_{12} \in \mathcal{G}_{13}, \quad \tilde{Q}^{ref} \tilde{t}_{13} \in \mathcal{G}_{12}, \quad \tilde{Q}^{ref} \tilde{t}_{23} = \mathcal{G}_{23}. \tag{A.60}$$

Thus, we can simply take any (possibly) compatible junction and reflect it about e_1 *to obtain another (or maybe the same) compatible junction. This implies*

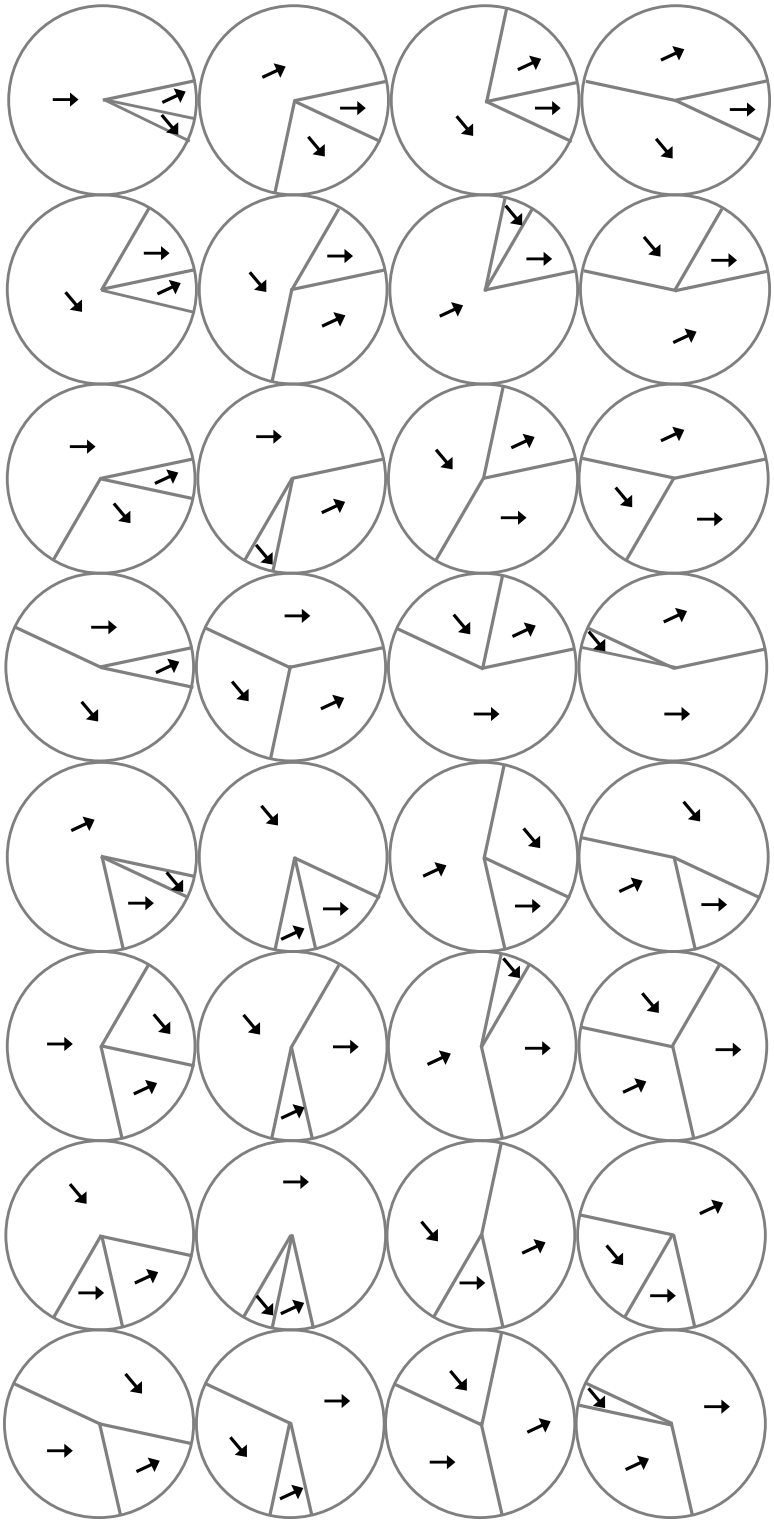

Figure A.1: For any fixed set of directors taken from the set (A.52), there are up to 32 non-trivial junctions which satisfy the necessary condition (A.54). Here is one such example with 32 non-trivial junctions. Note that the three directors are the same for each junction.

additional redundancies. In particular, cataloguing the set $\mathcal{G}_{12}^{*} \times \mathcal{G}_{13} \times \mathcal{G}_{23}$, *we have:*

$$\begin{aligned}
\left\{\tilde{t}_{12}^{++}, \tilde{t}_{13}^{++}, \tilde{t}_{23}^{+-}\right\} &\xmapsto{\tilde{Q}^{ref}} \left\{\tilde{t}_{12}^{++}, \tilde{t}_{13}^{++}, \tilde{t}_{23}^{-+}\right\}, \\
\left\{\tilde{t}_{12}^{++}, \tilde{t}_{13}^{+-}, \tilde{t}_{23}^{+-}\right\} &\xmapsto{\tilde{Q}^{ref}} \left\{\tilde{t}_{12}^{+-}, \tilde{t}_{13}^{++}, \tilde{t}_{23}^{-+}\right\}, \\
\left\{\tilde{t}_{12}^{++}, \tilde{t}_{13}^{-+}, \tilde{t}_{23}^{+-}\right\} &\xmapsto{\tilde{R}_{\pi}\tilde{Q}^{ref}} \left\{\tilde{t}_{12}^{+-}, \tilde{t}_{13}^{--}, \tilde{t}_{23}^{+-}\right\}, \\
\left\{\tilde{t}_{12}^{++}, \tilde{t}_{13}^{--}, \tilde{t}_{23}^{+-}\right\} &\xmapsto{\tilde{R}_{\pi}\tilde{Q}^{ref}} \textit{itself};
\end{aligned} \tag{A.61}$$

further,

$$\begin{aligned}
\left\{\tilde{t}_{12}^{+-}, \tilde{t}_{13}^{++}, \tilde{t}_{23}^{+-}\right\} &\xmapsto{\tilde{Q}^{ref}} \left\{\tilde{t}_{12}^{++}, \tilde{t}_{13}^{+-}, \tilde{t}_{23}^{-+}\right\}, \\
\left\{\tilde{t}_{12}^{+-}, \tilde{t}_{13}^{+-}, \tilde{t}_{23}^{+-}\right\} &\xmapsto{\tilde{Q}^{ref}} \left\{\tilde{t}_{12}^{+-}, \tilde{t}_{13}^{+-}, \tilde{t}_{23}^{-+}\right\}, \\
\left\{\tilde{t}_{12}^{+-}, \tilde{t}_{13}^{-+}, \tilde{t}_{23}^{+-}\right\} &\xmapsto{\tilde{R}_{\pi}\tilde{Q}^{ref}} \textit{itself};
\end{aligned} \tag{A.62}$$

further,

$$\begin{aligned}
\left\{\tilde{t}_{12}^{++}, \tilde{t}_{13}^{++}, \tilde{t}_{23}^{++}\right\} &\xmapsto{\tilde{Q}^{ref}} \textit{itself}, \\
\left\{\tilde{t}_{12}^{++}, \tilde{t}_{13}^{+-}, \tilde{t}_{23}^{++}\right\} &\xmapsto{\tilde{Q}^{ref}} \left\{\tilde{t}_{12}^{+-}, \tilde{t}_{13}^{++}, \tilde{t}_{23}^{++}\right\}, \\
\left\{\tilde{t}_{12}^{++}, \tilde{t}_{13}^{-+}, \tilde{t}_{23}^{++}\right\} &\xmapsto{\tilde{R}_{\pi}\tilde{Q}^{ref}} \left\{\tilde{t}_{12}^{+-}, \tilde{t}_{13}^{--}, \tilde{t}_{23}^{--}\right\}, \\
\left\{\tilde{t}_{12}^{++}, \tilde{t}_{13}^{--}, \tilde{t}_{23}^{++}\right\} &\xmapsto{\tilde{R}_{\pi}\tilde{Q}^{ref}} \left\{\tilde{t}_{12}^{++}, \tilde{t}_{13}^{--}, \tilde{t}_{23}^{--}\right\};
\end{aligned} \tag{A.63}$$

further,

$$\begin{aligned}
\left\{\tilde{t}_{12}^{+-}, \tilde{t}_{13}^{+-}, \tilde{t}_{23}^{++}\right\} &\xmapsto{\tilde{Q}^{ref}} \textit{itself}, \\
\left\{\tilde{t}_{12}^{+-}, \tilde{t}_{13}^{-+}, \tilde{t}_{23}^{++}\right\} &\xmapsto{\tilde{R}_{\pi}\tilde{Q}^{ref}} \left\{\tilde{t}_{12}^{+-}, \tilde{t}_{13}^{-+}, \tilde{t}_{23}^{--}\right\}, \\
\left\{\tilde{t}_{12}^{+-}, \tilde{t}_{13}^{--}, \tilde{t}_{23}^{++}\right\} &\xmapsto{\tilde{R}_{\pi}\tilde{Q}^{ref}} \left\{\tilde{t}_{12}^{++}, \tilde{t}_{13}^{-+}, \tilde{t}_{23}^{--}\right\};
\end{aligned} \tag{A.64}$$

further,

$$\begin{aligned}
\left\{\tilde{t}_{12}^{++}, \tilde{t}_{13}^{-+}, \tilde{t}_{23}^{-+}\right\} &\xmapsto{\tilde{R}_{\pi}\tilde{Q}^{ref}} \left\{\tilde{t}_{12}^{+-}, \tilde{t}_{13}^{--}, \tilde{t}_{23}^{-+}\right\}, \\
\left\{\tilde{t}_{12}^{++}, \tilde{t}_{13}^{+-}, \tilde{t}_{23}^{--}\right\} &\xmapsto{\tilde{Q}^{ref}} \left\{\tilde{t}_{12}^{+-}, \tilde{t}_{13}^{++}, \tilde{t}_{23}^{--}\right\};
\end{aligned} \tag{A.65}$$

further

$$\begin{aligned}
\left\{\tilde{t}_{12}^{++}, \tilde{t}_{13}^{--}, \tilde{t}_{23}^{-+}\right\} &\xmapsto{\tilde{R}_{\pi}\tilde{Q}^{ref}} \textit{itself}, \\
\left\{\tilde{t}_{12}^{+-}, \tilde{t}_{13}^{-+}, \tilde{t}_{23}^{-+}\right\} &\xmapsto{\tilde{R}_{\pi}\tilde{Q}^{ref}} \textit{itself}, \\
\left\{\tilde{t}_{12}^{+-}, \tilde{t}_{13}^{+-}, \tilde{t}_{23}^{--}\right\} &\xmapsto{\tilde{Q}^{ref}} \textit{itself}, \\
\left\{\tilde{t}_{12}^{++}, \tilde{t}_{13}^{++}, \tilde{t}_{23}^{--}\right\} &\xmapsto{\tilde{Q}^{ref}} \textit{itself}.
\end{aligned} \tag{A.66}$$

Here, we have used the notation $\tilde{t}^{+-}_{\alpha\beta} = (+n_{0\alpha} - n_{0\beta})/|(+n_{0\alpha} - n_{0\beta})|, \ldots$ *etc. This exhausts all* 32 *cases and shows that* 12 *can be obtained from reflection and then (possible/as needed) a rotation by* π *of one of the other cases. This leaves* 20 *non-redundant possibly compatible junctions.*

(iii) (The case $\theta_{12} = \theta_{13} = \pi/3$*.) Of the* 64 *possible compatible junction, in this case, only* 10 *are not redundant since there is an additional symmetry by rigidly rotating the possibly compatible junction by* $\pi/3$*. Specifically, notice that applying* $\tilde{R}_{\pi/3} \in SO(2)$ *to the directors in this case yields,*

$$\tilde{R}_{\pi/3}\tilde{e}_1 = \tilde{n}_{02}, \quad \tilde{R}_{\pi/3}\tilde{n}_{02} = -\tilde{n}_{03}, \quad \tilde{R}_{\pi/3}\tilde{n}_{03} = \tilde{e}_1. \tag{A.67}$$

As a consequence, for any $\{\tilde{t}_{12}, \tilde{t}_{13}, \tilde{t}_{23}\} \subset \mathcal{G}_{12} \times \mathcal{G}_{13} \times \mathcal{G}_{23}$*,*

$$\tilde{R}_{\pi/3}\tilde{t}_{12} \in \mathcal{G}_{23}, \quad \tilde{R}_{\pi/3}\tilde{t}_{13} \in \mathcal{G}_{12}, \quad \tilde{R}_{\pi/3}\tilde{t}_{23} \in \mathcal{G}_{13}. \tag{A.68}$$

Hence, in cataloguing the 20 *possibly compatible configurations from the previous case that are not redundant, we find:*

$$\begin{aligned}
\left\{\tilde{t}^{++}_{12}, \tilde{t}^{++}_{13}, \tilde{t}^{+-}_{23}\right\} &\xmapsto{\tilde{R}_{\pi/3}} \left\{\tilde{t}^{++}_{12}, \tilde{t}^{--}_{13}, \tilde{t}^{+-}_{23}\right\}, \\
&\xmapsto{\tilde{Q}^{ref}\tilde{R}_{-\pi/3}} \textit{itself}, \\
\left\{\tilde{t}^{++}_{12}, \tilde{t}^{+-}_{13}, \tilde{t}^{+-}_{23}\right\} &\xmapsto{\tilde{Q}^{ref}\tilde{R}_{\pi}\tilde{R}_{\pi/3}} \textit{itself}, \\
&\xmapsto{\tilde{R}_{-\pi/3}} \left\{\tilde{t}^{++}_{12}, \tilde{t}^{++}_{13}, \tilde{t}^{++}_{23}\right\}, \\
\left\{\tilde{t}^{++}_{12}, \tilde{t}^{-+}_{13}, \tilde{t}^{+-}_{23}\right\} &\xmapsto{\tilde{Q}^{ref}\tilde{R}_{\pi}\tilde{R}_{\pi/3}} \textit{itself}, \\
&\xmapsto{\tilde{R}_{-\pi/3}} \left\{\tilde{t}^{++}_{12}, \tilde{t}^{++}_{13}, \tilde{t}^{--}_{23}\right\};
\end{aligned} \tag{A.69}$$

further,

$$\begin{aligned}
\left\{\tilde{t}^{+-}_{12}, \tilde{t}^{++}_{13}, \tilde{t}^{+-}_{23}\right\} &\xmapsto{\tilde{R}_{\pi/3}} \left\{\tilde{t}^{++}_{12}, \tilde{t}^{--}_{13}, \tilde{t}^{++}_{23}\right\}, \\
&\xmapsto{\tilde{R}_{-\pi/3}} \left\{\tilde{t}^{++}_{12}, \tilde{t}^{-+}_{13}, \tilde{t}^{-+}_{23}\right\}, \\
\left\{\tilde{t}^{+-}_{12}, \tilde{t}^{+-}_{13}, \tilde{t}^{+-}_{23}\right\} &\xmapsto{\tilde{Q}^{ref}\tilde{R}_{\pi}\tilde{R}_{\pi/3}} \left\{\tilde{t}^{++}_{12}, \tilde{t}^{+-}_{13}, \tilde{t}^{--}_{23}\right\}, \\
&\xmapsto{\tilde{R}_{-\pi/3}} \left\{\tilde{t}^{++}_{12}, \tilde{t}^{-+}_{13}, \tilde{t}^{++}_{23}\right\}, \\
\left\{\tilde{t}^{+-}_{12}, \tilde{t}^{-+}_{13}, \tilde{t}^{+-}_{23}\right\} &\xmapsto{\tilde{R}_{\pi/3}} \left\{\tilde{t}^{+-}_{12}, \tilde{t}^{--}_{13}, \tilde{t}^{++}_{23}\right\}, \\
&\xmapsto{\tilde{Q}^{ref}\tilde{R}_{\pi}\tilde{R}_{-\pi/3}} \textit{excluded already};
\end{aligned} \tag{A.70}$$

further,

$$\begin{aligned}
\left\{\tilde{t}_{12}^{++},\tilde{t}_{13}^{+-},\tilde{t}_{23}^{++}\right\} &\xmapsto{\tilde{R}_\pi\tilde{R}_{\pi/3}} \left\{\tilde{t}_{12}^{+-},\tilde{t}_{13}^{-+},\tilde{t}_{23}^{-+}\right\},\\
&\xmapsto{\tilde{R}_\pi\tilde{R}_{-\pi/3}} \textit{itself}\,,\\
\left\{\tilde{t}_{12}^{+-},\tilde{t}_{13}^{+-},\tilde{t}_{23}^{++}\right\} &\xmapsto{\tilde{Q}^{ref}\tilde{R}_{\pi/3}} \left\{\tilde{t}_{12}^{+-},\tilde{t}_{13}^{-+},\tilde{t}_{23}^{++}\right\},\\
&\xmapsto{\tilde{R}_{-\pi/3}} \textit{excluded already}\,,\\
\left\{\tilde{t}_{12}^{++},\tilde{t}_{13}^{--},\tilde{t}_{23}^{-+}\right\} &\xmapsto{\tilde{Q}^{ref}\tilde{R}_{\pi/3}} \textit{itself},\\
&\xmapsto{\tilde{Q}^{ref}\tilde{R}_{-\pi/3}} \textit{itself},\\
\left\{\tilde{t}_{12}^{+-},\tilde{t}_{13}^{+-},\tilde{t}_{23}^{--}\right\} &\xmapsto{\tilde{R}_\pi\tilde{R}_{\pi/3}} \textit{itself},\\
&\xmapsto{\tilde{R}_\pi\tilde{R}_{-\pi/3}} \textit{itself}\,.
\end{aligned} \tag{A.71}$$

Here, we have used the notation as defined in (ii).

With this result, all possible compatible interfaces are defined now in terms of the angles $\theta_{12} \in (0, \pi/2]$ and $\theta_{13} \in (0, \pi/2)$.

On three-faced junctions (Sufficiency)

Now, we take as given some collection of directors in the set (A.52). Further, we assume $\tilde{t}_{12} \equiv \tilde{t}_{12}(\theta_{12}, \theta_{13})$ is taken from the set $\mathcal{G}_{12}^*$, $\tilde{t}_{13} \equiv \tilde{t}_{13}(\theta_{12}, \theta_{13})$ is taken from the set $\mathcal{G}_{13}$ and $\tilde{t}_{23} \equiv \tilde{t}_{23}(\theta_{12}, \theta_{13})$ is taken from the set $\mathcal{G}_{23}$. Hence, the necessary condition (A.54) holds, and for a compatible junction, it remains to determine if there exists an R_2 and $R_3 \in SO(3)$ such that (A.53) holds.

To make progress, let us suppose we are just interested in satisfying both the latter and former equations in (A.53) (we ignore the middle equation for now). For simplicity in the notation, we define

$$\begin{aligned}
f_1 &:= (\ell_{e_1}^{1/2})_{3\times 2}\tilde{t}_{12}, \quad f_2 := (\ell_{n_{02}}^{1/2})_{3\times 2}\tilde{t}_{12},\\
h_1 &:= (\ell_{e_1}^{1/2})_{3\times 2}\tilde{t}_{13}, \quad h_3 := (\ell_{n_{03}}^{1/2})_{3\times 2}\tilde{t}_{13}
\end{aligned} \tag{A.72}$$

(these quantities only depend on θ_{12} and θ_{13}). With this, we observe that to solve the latter and former equations in (A.53), we need an $R_2 \in SO(3)$ and an $R_3 \in SO(3)$ such that

$$f_1 = R_2 f_2, \quad h_1 = R_3 h_3. \tag{A.73}$$

Since $f_1, f_2, h_1, h_3 \cdot e_3 = 0$ and $|f_1| = |f_2|$,$|h_1| = |h_2|$ by the satisfaction of (A.54), we can solve this equation through the rotations $R_2 \equiv R_{e_3}(\phi_2)$ and $R_3 \equiv R_{e_3}(\phi_3)$ given by

$$\begin{aligned} R_{e_3}(\phi_2) &:= \cos(\phi_2)(e_1 \otimes e_1 + e_2 \otimes e_2) + \\ &\qquad \sigma(f_1, f_2)\sin(\phi_2)(e_1 \otimes e_2 - e_2 \otimes e_1) + e_3 \otimes e_3 \\ \phi_2 &= \arccos\Big(\frac{f_1 \cdot f_2}{|f_1|^2}\Big), \\ R_{e_3}(\phi_3) &:= \cos(\phi_3)(e_1 \otimes e_1 + e_2 \otimes e_2) + \\ &\qquad \sigma(h_1, h_3)\sin(\phi_2)(e_1 \otimes e_2 - e_2 \otimes e_1) + e_3 \otimes e_3, \\ \phi_3 &= \arccos\Big(\frac{h_1 \cdot h_3}{|h_1|^2}\Big). \end{aligned} \tag{A.74}$$

Here, $\sigma\colon \mathbb{R}^3 \times \mathbb{R}^3 \to \{1, 0, -1\}$ is given by

$$\sigma(a, b) := \operatorname{sign}\Big(e_3 \cdot (a \times b)\Big) \tag{A.75}$$

where $\operatorname{sign}(0) = 0$.

Note that $R_{e_3}(\phi_2) \equiv Q(\theta_{12}, \theta_{13}) \in SO(3)$ and similarly for $R_{e_3}(\phi_3)$ (that is, they are both completely determined for given θ_{12} and θ_{13}). However, notice that for $R_{f_1}(\eta_2) \in SO(3)$ such that $R_{f_1}(\eta_2)f_1 = f_1$ and for $R_{h_1}(\eta_3) \in SO(3)$ such that $R_{h_1}(\eta_3)h_1 = h_1$, we have

$$f_1 = R_{f_1}(\eta_2)R_{e_3}(\phi_2)f_2, \quad h_1 = R_{h_1}(\eta_3)R_{e_3}(\phi_3)h_3 \tag{A.76}$$

for any choice of η_2, η_3. That is, we satisfy two of our three compatibility equations with *two* free parameters to play with. For definiteness with these equations, we set

$$f_1^\perp := -(f_1 \cdot e_2)e_1 + (f_1 \cdot e_1)e_2, \quad h_1^\perp := -(h_1 \cdot e_2)e_1 + (h_1 \cdot e_1)e_2 \tag{A.77}$$

(since $f_1, h_1 \cdot e_3 = 0$), and define the rotation R_{f_1} and R_{h_1} as

$$\begin{aligned} R_{f_1}(\eta_2) &:= \cos(\eta_2)(|f_1|^{-2} f_1^\perp \otimes f_1^\perp + e_3 \otimes e_3) + \\ &\qquad \sin(\eta_2)|f_1|^{-1}(e_3 \otimes f_1^\perp - f_1^\perp \otimes e_3 -) + |f_1|^{-2} f_1 \otimes f_1, \\ R_{h_1}(\eta_3) &:= \cos(\eta_3)(|h_1|^{-2} h_1^\perp \otimes h_1^\perp + e_3 \otimes e_3) + \\ &\qquad \sin(\eta_3)|h_1|^{-1}(e_3 \otimes h_1^\perp - h_1^\perp \otimes e_3) + |h_1|^{-2} h_1 \otimes h_1 \end{aligned} \tag{A.78}$$

for $\eta_2, \eta_3 \in [-\pi, \pi]$ (these are, in fact, the desired rotations since $|f_1| = |f_1^\perp|$ and $|h_1| = |h_1^\perp|$).

So, do we have a compatible junction for the given θ_{12} and θ_{13}? In light of (A.76), it remains only to satisfy the middle equation in (A.53) for a compatible junction.

Specifically, this boils down to the question: does there exist $(\eta_2^*, \eta_3^*) \in [-\pi, \pi]^2$ such that

$$R_{f_1}(\eta_2^*)R_{e_3}(\phi_2)(\ell_{n_{02}}^{1/2})_{3\times 2}\tilde{t}_{23} = R_{h_1}(\eta_3^*)R_{e_3}(\phi_3)(\ell_{n_{03}}^{1/2})_{3\times 2}\tilde{t}_{23}? \tag{A.79}$$

This is actual not a good way of posing the question because the solutions have a transparent geometrical structure that is disguised in the above formulation. In fact, we only need to consider the problem associated with how these equations project onto the plane with normal e_3. To formulate this precisely and algebraically, we define

$$g_2 := R_{e_3}(\phi_2)(\ell_{n_{02}}^{1/2})_{3\times 2}\tilde{t}_{23}, \quad g_3 := R_{e_3}(\phi_3)(\ell_{n_{03}}^{1/2})_{3\times 2}\tilde{t}_{23}. \tag{A.80}$$

We have the following:

Proposition A.3.4 *Fix $\theta_{12} \in (0, \pi/2]$ and $\theta_{13} \in (0, \pi/2)$ and let all quantities be appropriately defined (as above) in terms of these quantities. Suppose there exist $\eta_2^*, \eta_3^* \in [-\pi, \pi]$ such that*

$$(I_{3\times 3} - e_3 \otimes e_3)R_{f_1}(\eta_2^*)g_2 = (I_{3\times 3} - e_3 \otimes e_3)R_{h_1}(\eta_3^*)g_3. \tag{A.81}$$

Then either

$$R_{f_1}(\eta_2^*)g_2 = R_{h_1}(\eta_3^*)g_3 \quad \text{or} \quad R_{f_1}(\eta_2^*)g_2 = R_{h_1}(-\eta_3^*)g_3. \tag{A.82}$$

Proof. Observe that

$$\begin{aligned} &|(I_{3\times 3} - e_3 \otimes e_3)R_{f_1}(\eta_2^*)g_2|^2 + (R_{f_1}(\eta_2^*)g_2 \cdot e_3)^2 = |g_2|^2 \\ &\quad = |g_3|^2 = |(I_{3\times 3} - e_3 \otimes e_3)R_{h_1}(\eta_3^*)g_3|^2 + (R_{h_1}(\eta_3^*)g_3 \cdot e_3)^2. \end{aligned} \tag{A.83}$$

Here, we have used the fact that $R_{f_1}, R_{h_1} \in SO(3)$ and that $|g_2| = |g_3|$ since (A.54) holds. Consequently, if (A.81) holds, then it must be that

$$R_{f_1}(\eta_2^*)g_2 \cdot e_3 = (+ \text{ or } -)R_{h_1}(\eta_3^*)g_3 \cdot e_3. \tag{A.84}$$

If the sign is +, then the result is proved with (η_2^*, η_3^*). Alternatively, since $g_2, g_3 \cdot e_3 = 0$, we see from (A.78) that (A.81) will hold if we replace η_3^* with $-\eta_3^*$. Moreover, this replacement flips the sign in (A.84). Thus, in the case the sign is −, the result is proved with $(\eta_2^*, -\eta_3^*)$. □

Given this proposition, most of the work to solve for η_2 and η_3 is done. Indeed, we define

$$y_2(\eta_2) := R_{f_1}(\eta_2)g_2, \quad y_3(\eta_3) := R_{h_1}(\eta_3)g_3 \tag{A.85}$$

and we notice that g_2 and g_3 can be rewritten as

$$\begin{aligned} g_2 &= \Big(\frac{g_2 \cdot f_1}{|f_1|^2}\Big) f_1 + \Big(\frac{g_2 \cdot f_1^\perp}{|f_1|^2}\Big) f_1^\perp, \\ g_3 &= \Big(\frac{g_2 \cdot h_1}{|h_1|^2}\Big) h_1 + \Big(\frac{g_2 \cdot h_1^\perp}{|h_1|^2}\Big) h_1^\perp \end{aligned} \tag{A.86}$$

since $g_2, g_3 \cdot e_3 = 0$. Hence, we see that the question posed in (A.79) is now (due to this proposition) equivalent to the question: does there exist $(\eta_2^*, \eta_3^*) \in [-\pi, \pi]^2$ such that

$$\begin{aligned} \tilde{y}_2(\eta_2^*) &\equiv (I_{3\times 3} - e_3 \otimes e_3) y_2(\eta_2^*) \\ &= (I_{3\times 3} - e_3 \otimes e_3) y_3(\eta_3^*) \equiv \tilde{y}_3(\eta_3^*), \end{aligned} \tag{A.87}$$

(that is, such that $\tilde{y}_2(\eta_2^*) = \tilde{y}_3(\eta_3^*)$). In this direction, we use the identities in (A.86) to observe that

$$\begin{aligned} \tilde{y}_2(\eta_2) &= \Big(\frac{\tilde{g}_2 \cdot \tilde{f}_1}{|\tilde{f}_1|^2}\Big) \tilde{f}_1 + \cos(\eta_2)\Big(\frac{\tilde{g}_2 \cdot \tilde{f}_1^\perp}{|\tilde{f}_1|^2}\Big) \tilde{f}_1^\perp, \\ \tilde{y}_3(\eta_3) &= \Big(\frac{\tilde{g}_3 \cdot \tilde{h}_1}{|\tilde{h}_1|^2}\Big) \tilde{h}_1 + \cos(\eta_3)\Big(\frac{\tilde{g}_3 \cdot \tilde{h}_1^\perp}{|\tilde{h}_1|^2}\Big) \tilde{h}_1^\perp. \end{aligned} \tag{A.88}$$

This observation motivates the following proposition:

Proposition A.3.5 *Fix $\theta_{12} \in (0, \pi/2]$ and $\theta_{13} \in (0, \pi/2)$ and let all quantities be appropriately defined (as above) in terms of these quantities. Let*

$$\begin{aligned} \tilde{a}(\alpha) &= \Big(\frac{\tilde{g}_2 \cdot \tilde{f}_1}{|\tilde{f}_1|^2}\Big) \tilde{f}_1 + \alpha\Big(\frac{\tilde{g}_2 \cdot \tilde{f}_1^\perp}{|\tilde{f}_1|^2}\Big) \tilde{f}_1^\perp, \quad \alpha \in \mathbb{R}, \\ \tilde{b}(\beta) &= \Big(\frac{\tilde{g}_3 \cdot \tilde{h}_1}{|\tilde{h}_1|^2}\Big) \tilde{h}_1 + \beta\Big(\frac{\tilde{g}_3 \cdot \tilde{h}_1^\perp}{|\tilde{h}_1|^2}\Big) \tilde{h}_1^\perp, \quad \beta \in \mathbb{R}. \end{aligned} \tag{A.89}$$

Then,

$$\begin{aligned} &\tilde{a}(\alpha) = \tilde{b}(\beta) \quad \Leftrightarrow \\ &\begin{pmatrix} \alpha \\ \beta \end{pmatrix} = \begin{pmatrix} \frac{(\tilde{g}_3 \cdot \tilde{h}_1)|\tilde{f}_1|^2 - (\tilde{h}_1 \cdot \tilde{f}_1)(\tilde{g}_2 \cdot \tilde{f}_1)}{(\tilde{h}_1 \cdot \tilde{f}_1^\perp)(\tilde{g}_2 \cdot \tilde{f}_1^\perp)} \\ \frac{(\tilde{g}_2 \cdot \tilde{f}_1)|\tilde{h}_1|^2 - (\tilde{h}_1 \cdot \tilde{f}_1)(\tilde{g}_3 \cdot \tilde{h}_1)}{(\tilde{f}_1 \cdot \tilde{h}_1^\perp)(\tilde{g}_3 \cdot \tilde{h}_1^\perp)} \end{pmatrix}. \end{aligned} \tag{A.90}$$

Proof. Observe that

$$\begin{aligned}&\tilde{a}(\alpha) = \tilde{b}(\beta) \quad \Leftrightarrow \\ &\left(\Big(\frac{\tilde{g}_2 \cdot \tilde{f}_1^{\perp}}{|\tilde{f}_1|^2}\Big)\tilde{f}_1^{\perp}\Big| - \Big(\frac{\tilde{g}_3 \cdot \tilde{h}_1^{\perp}}{|\tilde{h}_1|^2}\Big)\tilde{h}_1^{\perp}\right)\begin{pmatrix}\alpha\\ \beta\end{pmatrix} = \Big(\frac{\tilde{g}_3 \cdot \tilde{h}_1}{|\tilde{h}_1|^2}\Big)\tilde{h}_1 - \Big(\frac{\tilde{g}_2 \cdot \tilde{f}_1}{|\tilde{f}_1|^2}\Big)\tilde{f}_1,\end{aligned} \tag{A.91}$$

and further that

$$\left(\Big(\frac{\tilde{g}_2 \cdot \tilde{f}_1^{\perp}}{|\tilde{f}_1|^2}\Big)\tilde{f}_1^{\perp}\Big| - \Big(\frac{\tilde{g}_3 \cdot \tilde{h}_1^{\perp}}{|\tilde{h}_1|^2}\Big)\tilde{h}_1^{\perp}\right)^{-1} = \left(\frac{|\tilde{f}_1|^2\tilde{h}_1}{(\tilde{g}_2 \cdot \tilde{f}_1^{\perp})(\tilde{h}_1 \cdot \tilde{f}_1^{\perp})}\Big|\frac{-|\tilde{h}_1|^2\tilde{f}_1}{(\tilde{g}_3 \cdot \tilde{h}_1^{\perp})(\tilde{h}_1^{\perp} \cdot \tilde{f}_1)}\right)^T. \tag{A.92}$$

(Note, $(\tilde{g}_3 \cdot \tilde{h}_1^{\perp}), (\tilde{h}_1^{\perp} \cdot \tilde{f}_1) = -(\tilde{f}_1^{\perp} \cdot \tilde{h}_1), (\tilde{g}_2 \cdot \tilde{f}_1^{\perp}) \neq 0$ since each of these quantities depends on θ_{12} and θ_{13} as defined above. That is, the inverse exists as asserted.) Applying (A.92) to (A.91), we arrive at (A.90) after some manipulation. □

With this result, we can completely characterize *all* compatible three-faced interior junctions.

Main result (A complete characterization)

Theorem A.3.6 *Consider the case of three fixed planar directors:*

$$\begin{aligned}&\{e_1, n_{02}, n_{03}\} \quad \textit{where} \\ &\quad n_{02} = \cos(\theta_{12})e_1 + \sin(\theta_{12})e_2 \quad \textit{for some } \theta_{12} \in (0, \pi/2], \\ &\quad n_{03} = \cos(\theta_{13})e_1 - \sin(\theta_{13})e_2 \quad \textit{for some } \theta_{13} \in (0, \pi/2).\end{aligned} \tag{A.93}$$

(i) (Necessary.) There exist $\tilde{g}_{12}, \tilde{g}_{23}, \tilde{g}_{13} \in \mathbb{S}^1$ and $R_2, R_3 \in SO(3)$ such that

$$\begin{aligned}(\ell^{1/2}_{e_1})_{3\times 2}\tilde{g}_{12} &= R_2(\ell^{1/2}_{n_{02}})_{3\times 2}\tilde{g}_{12}, \\ R_2(\ell^{1/2}_{n_{02}})_{3\times 2}\tilde{g}_{23} &= R_3(\ell^{1/2}_{n_{03}})_{3\times 2}\tilde{g}_{23}, \\ (\ell^{1/2}_{e_1})_{3\times 2}\tilde{g}_{13} &= R_3(\ell^{1/2}_{n_{03}})_{3\times 2}\tilde{g}_{23}\end{aligned} \tag{A.94}$$

(i.e., there exists a compatible junction) only if $\{\tilde{g}_{12}, \tilde{g}_{13}, \tilde{g}_{23}\} \subset \mathcal{G}_{12}\times\mathcal{G}_{13}\times\mathcal{G}_{23}$, where:

$$\begin{aligned}\mathcal{G}_{12} &:= \Big\{\frac{\tilde{e}_1 + \tilde{n}_{02}}{|\tilde{e}_1 + \tilde{n}_{02}|}, \frac{\tilde{e}_1 - \tilde{n}_{02}}{|\tilde{e}_1 - \tilde{n}_{02}|}, \frac{\tilde{n}_{02} - \tilde{e}_1}{|\tilde{e}_1 - \tilde{n}_{02}|}, \frac{-(\tilde{e}_1 + \tilde{n}_{02}}{|\tilde{e}_1 + \tilde{n}_{02}|}\Big\}, \\ \mathcal{G}_{13} &:= \Big\{\frac{\tilde{e}_1 + \tilde{n}_{03}}{|\tilde{e}_1 + \tilde{n}_{03}|}, \frac{\tilde{e}_1 - \tilde{n}_{03}}{|\tilde{e}_1 - \tilde{n}_{03}|}, \frac{\tilde{n}_{03} - \tilde{e}_1}{|\tilde{e}_1 - \tilde{n}_{03}|}, \frac{-(\tilde{e}_1 + \tilde{n}_{03})}{|\tilde{e}_1 + \tilde{n}_{03}|}\Big\}, \\ \mathcal{G}_{23} &:= \Big\{\frac{\tilde{n}_{02} + \tilde{n}_{03}}{|\tilde{n}_{02} + \tilde{n}_{03}|}, \frac{\tilde{n}_{02} - \tilde{n}_{03}}{|\tilde{n}_{02} - \tilde{n}_{03}|}, \frac{\tilde{n}_{03} - \tilde{n}_{02}}{|\tilde{n}_{02} - \tilde{n}_{03}|}, \frac{-(\tilde{n}_{02} + \tilde{n}_{03})}{|\tilde{n}_{02} + \tilde{n}_{03}|}\Big\}.\end{aligned} \tag{A.95}$$

(ii) (Necessary and sufficient.) Let $\tilde{g}_{12} \equiv \tilde{g}_{12}(\theta_{12}, \theta_{23})$ *as in* $\mathcal{G}_{12}$*;* $\tilde{g}_{13} \equiv \tilde{g}_{13}(\theta_{12}, \theta_{23})$ *as in* $\mathcal{G}_{13}$*;* $\tilde{g}_{23} \equiv \tilde{g}_{23}(\theta_{12}, \theta_{23})$ *as in* $\mathcal{G}_{23}$*. Define:*

$$
\begin{aligned}
&f_1 \equiv f_1(\theta_{12}, \theta_{13}) := (\ell^{1/2}_{e_1})_{3\times 2}\tilde{g}_{12},\\
&f_1^{\perp} \equiv f_1^{\perp}(\theta_{12}, \theta_{13}) := -(f_1 \cdot e_2)e_1 + (f_1 \cdot e_1)e_2,\\
&f_2 \equiv f_2(\theta_{12}, \theta_{13}) := (\ell^{1/2}_{n_{02}})_{3\times 2}\tilde{g}_{12},\\
&h_1 \equiv h_1(\theta_{12}, \theta_{13}) := (\ell^{1/2}_{e_1})_{3\times 2}\tilde{g}_{13},\\
&h_1^{\perp} \equiv h_1(\theta_{12}, \theta_{13}) := -(h_1 \cdot e_2)e_1 + (h_1 \cdot e_1)e_2,\\
&h_3 \equiv h_3(\theta_{12}, \theta_{13}) := (\ell^{1/2}_{n_{03}})_{3\times 2}\tilde{g}_{13},\\
&R_{e_3}(\phi_2) \equiv R_{e_3}(\phi_3, \theta_{12}, \theta_{13}) := \cos(\phi_2)(e_1 \otimes e_1 + e_2 \otimes e_2) +\\
&\qquad sign(e_3 \cdot (f_1 \times f_2))\sin(\phi_2)(e_1 \otimes e_2 - e_2 \otimes e_1) + e_3 \otimes e_3,\\
&\quad \phi_2 \equiv \phi_2(\theta_{12}, \theta_{13}) = \arccos\Big(\frac{f_1 \cdot f_2}{|f_1|^2}\Big),\\
&R_{e_3}(\phi_3) \equiv R_{e_3}(\phi_3, \theta_{12}, \theta_{13}) := \cos(\phi_3)(e_1 \otimes e_1 + e_2 \otimes e_2) +\\
&\qquad sign(e_3 \cdot (h_1 \times h_3))\sin(\phi_2)(e_1 \otimes e_2 - e_2 \otimes e_1) + e_3 \otimes e_3,\\
&\quad \phi_3 \equiv \phi_3(\theta_{12}, \theta_{13}) = \arccos\Big(\frac{h_1 \cdot h_3}{|h_1|^2}\Big),\\
&g_2 \equiv g_2(\theta_{12}, \theta_{13}) := R_{e_3}(\phi_2)(\ell^{1/2}_{n_{02}})_{3\times 2}\tilde{g}_{23},\\
&g_3 \equiv g_3(\theta_{12}, \theta_{13}) := R_{e_3}(\phi_3)(\ell^{1/2}_{n_{03}})_{3\times 2}\tilde{g}_{23},\\
&\begin{pmatrix} \alpha \\ \beta \end{pmatrix} \equiv \begin{pmatrix} \alpha(\theta_{12}, \theta_{13}) \\ \beta(\theta_{12}, \theta_{13}) \end{pmatrix} := \begin{pmatrix} \frac{(\tilde{g}_3\cdot\tilde{h}_1)|\tilde{f}_1|^2 - (\tilde{h}_1\cdot\tilde{f}_1)(\tilde{g}_2\cdot\tilde{f}_1)}{(\tilde{h}_1\cdot\tilde{f}_1^{\perp})(\tilde{g}_2\cdot\tilde{f}_1^{\perp})} \\ \frac{(\tilde{g}_2\cdot\tilde{f}_1)|\tilde{h}_1|^2 - (\tilde{h}_1\cdot\tilde{f}_1)(\tilde{g}_3\cdot\tilde{h}_1)}{(\tilde{f}_1\cdot\tilde{h}_1^{\perp})(\tilde{g}_3\cdot\tilde{h}_1^{\perp})} \end{pmatrix}.
\end{aligned}
\tag{A.96}
$$

There exist $R_2, R_3 \in SO(3)$ *such that (A.94) holds if and only if* $\alpha \in [-1, 1]$ *and* $\beta \in [-1, 1]$*.*

(iii) (Explicit construction.) If $\alpha \equiv \alpha(\theta_{12}, \theta_{13}) \in [-1, 1]$ *and* $\beta \equiv \beta(\theta_{12}, \theta_{13}) \in [-1, 1]$*, then* R_2 *and* $R_3 \in SO(3)$ *from (ii) satisfy*

$$
\begin{aligned}
R_2 \equiv R_2(\eta_2, \theta_{12}, \theta_{13}) &= R_{f_1}(\eta_2)R_{e_3}(\phi_2),\\
R_3 \equiv R_3(\eta_3, \theta_{12}, \theta_{13}) &= R_{h_1}(\eta_3)R_{e_3}(\phi_3),
\end{aligned}
\tag{A.97}
$$

where

$$
\begin{aligned}
R_{f_1}(\eta_2) \equiv R_{f_1}(\eta_2, \theta_{12}, \theta_{13}) &:= \cos(\eta_2)(|f_1|^{-2}f_1^{\perp} \otimes f_1^{\perp} + e_3 \otimes e_3) +\\
&\quad \sin(\eta_2)|f_1|^{-1}(e_3 \otimes f_1^{\perp} - f_1^{\perp} \otimes e_3 -) + |f_1|^{-2}f_1 \otimes f_1,\\
R_{h_1}(\eta_3) \equiv R_{h_1}(\eta_3, \theta_{12}, \theta_{13}) &:= \cos(\eta_3)(|h_1|^{-2}h_1^{\perp} \otimes h_1^{\perp} + e_3 \otimes e_3) +\\
&\quad \sin(\eta_3)|h_1|^{-1}(e_3 \otimes h_1^{\perp} - h_1^{\perp} \otimes e_3) + |h_1|^{-2}h_1 \otimes h_1,
\end{aligned}
\tag{A.98}
$$

and $(\eta_2, \eta_3) \in [\pi, \pi]^2$ *satisfy*

$$\begin{aligned} &\cos(\eta_2) = \alpha, \quad \cos(\eta_3) = \beta, \\ &sign\Big((\tilde{g}_2 \cdot \tilde{f}_1^{\perp}) \sin(\eta_2)\Big) = sign\Big((\tilde{g}_3 \cdot \tilde{h}_1^{\perp}) \sin(\eta_3)\Big). \end{aligned} \tag{A.99}$$

Remark A.3.7 *(i) For each possibly compatible junction, there are are either two solutions (if* $\alpha, \beta \in [-1, 1]$*) for actuation or no solutions (if at least one is not). These are given by*

$$\begin{aligned} &\eta_2^+ = \arccos(\alpha), \quad \eta_3^+ = sign\Big((\tilde{g}_2 \cdot \tilde{f}_1^{\perp})(\tilde{g}_2 \cdot \tilde{h}_1^{\perp})\Big) \arccos(\beta) \\ &\eta_2^- = -\arccos(\alpha), \quad \eta_3^- = -sign\Big((\tilde{g}_2 \cdot \tilde{f}_1^{\perp})(\tilde{g}_2 \cdot \tilde{h}_1^{\perp})\Big) \arccos(\beta). \end{aligned} \tag{A.100}$$

The solutions are reflections of each other about the $\{e_1, e_2\}$ *plane.*

(ii) When the anisotropy parameter $\bar{r}$ *is equal to* 1*, the junction is compatible and flat. By explicit examination of various examples, it does appear that exactly half of all junctions which satisfy the necessary condition in (i) are compatible for heating and only heating (i.e,* $\bar{r} \in (0, 1]$*) with the other half compatible for cooling and only cooling (i.e.,* $\bar{r} \geq 1$*). We see this, for instance, in comparing the junction Figure 4.11, as the junction here is only compatible for cooling or heating (depending on the director program).*